

Towards understanding the mechanisms of the periplasmic pyoverdine maturation

Von der Naturwissenschaftlichen Fakultät
der Gottfried Wilhelm Leibniz Universität Hannover

zur Erlangung des Grades

Doktor der Naturwissenschaften (Dr. rer. nat.)

genehmigte Dissertation von

Michael-Frederick Sague, M.Sc.

2022

Referent: Prof. Dr. rer. nat. Thomas Brüser

Korreferent: Prof. Dr. rer. nat. Marcus Andreas Horn

Tag der Promotion: 18.03.2022

Abstract

Iron plays an essential role in the maintenance of various vital processes. Therefore, obtaining iron, especially under adverse conditions, is an elementary component for the survival of microorganisms. Bacteria produce so-called siderophores, which help to procure iron in iron-limiting environments. The siderophores of fluorescent pseudomonads are called pyoverdines. During this work, the enzymes involved in the periplasmic maturation of pyoverdines have been further characterized towards a better understanding of their respective mechanisms.

PvdM was shown to be essential for the activity of PvdP *in vivo*. The putative role of PvdM here could be either a kind of handover mechanism of the substrate ferribactin to PvdP. Alternatively, PvdM could be directly involved in the incorporation of copper by presenting copper on its surface to PvdP, which is essential for the reaction of the tyrosinase PvdP. Furthermore, it could be shown that PvdP appears not to be an enzyme liberated into the periplasm after the translocation as previously assumed, but to catalyse the oxidative cyclization of the chromophore as a membrane-bound protein. Responsible for this seems to be the signal peptide of PvdP, which appears to be one of only a few Tat-signal peptides known to date, that is not cleaved after translocation but rather involved in the integration of the protein into the cytoplasmic membrane. In parallel, the actual conversion of the N-terminal glutamic acid residue of pyoverdine by PvdN was demonstrated. Thereby, the role of PvdN in the periplasmic maturation process was finally confirmed. Furthermore, glutamine was identified as a new substrate, eliminating the need for the laborious purification of pyoverdine for future enzymatic studies of PvdN. This realisation will make conversion experiments and detection much easier and faster in the future. In addition, oxygen was shown to be indispensable for the catalytic reaction of PvdN, which supports the postulated unusual PLP-dependent oxidative decarboxylation under the retention of the amine (Ringel *et al.* 2016). Finally, it was demonstrated that growth is possible in medium depleted with the iron chelator EDDHA, even though pyoverdine synthesis is eliminated. In this context, a modified form of EDDHA was detected, which is dimethylated and thus probably facilitates the release of bound iron by having two out of six ligand sites modified.

Key words: pyoverdine, fluorescence, *Pseudomonas fluorescens* A506, iron stress, methylation

Zusammenfassung

Eisen spielt eine wesentliche Rolle bei der Erhaltung verschiedener Lebensprozesse. Daher ist die Gewinnung von Eisen, insbesondere unter widrigen Bedingungen, ein elementarer Bestandteil für das Überleben von Mikroorganismen. Bakterien produzieren sogenannte Siderophore, die bei der Eisenbeschaffung in eisenlimitierenden Umgebungen helfen. Die Siderophore der fluoreszierenden Pseudomonaden werden Pyoverdine genannt. Im Rahmen dieser Arbeit wurden die Enzyme, die an der periplasmatischen Maturierung der Pyoverdine beteiligt sind, weiter charakterisiert, um ihre jeweiligen Mechanismen besser zu verstehen.

Es wurde gezeigt, dass PvdM essenziell für die Aktivität der Tyrosinase PvdP *in vivo* ist. PvdM könnte hier in eine Art Übergabemechanismus des Substrats Ferribactin an PvdP involviert oder aber direkt am Einbau von Kupfer beteiligt sein, indem es Kupfer auf seiner Oberfläche an PvdP weitergibt, welches für dessen Reaktion unerlässlich ist. Darüber hinaus konnte gezeigt werden, dass PvdP nicht, wie bisher angenommen, nach der Translokation ins Periplasma entlassen wird, sondern wahrscheinlich als membrangebundenes Protein die oxidative Zyklisierung des Chromophors katalysiert. Verantwortlich dafür scheint das Signalpeptid von PvdP zu sein, das als eines der wenigen bisher bekannten Tat-Signalpeptide nicht abgespalten wird, sondern an der Integration des Proteins in die innere Membran beteiligt ist. Parallel dazu wurde die tatsächliche Umwandlung des N-terminalen Glutamatrestes von Pyoverdin durch PvdN nachgewiesen und die Rolle von PvdN im periplasmatischen Maturierungsprozess endgültig bestätigt. Darüber hinaus wurde Glutamin als neues Substrat identifiziert, wodurch die mühsame Reinigung von Pyoverdin für künftige enzymatische Untersuchungen von PvdN überflüssig wird. Experimente und Nachweise werden zukünftig wesentlich einfacher und schneller. Es konnte gezeigt werden, dass Sauerstoff für die Katalyse von PvdN unverzichtbar ist. Dies unterstützt die postulierte PLP-abhängige oxidative Decarboxylierung unter Erhaltung des Amins (Ringel *et al.* 2016). Schließlich konnte gezeigt werden, dass Wachstum in mit dem Eisenchelator EDDHA depletierten Medium möglich ist, obwohl die Pyoverdinsynthese unterbunden wird. In diesem Zusammenhang wurde eine modifizierte Form von EDDHA nachgewiesen, welche dimethyliert ist und somit wahrscheinlich die Freisetzung des gebundenen Eisens erleichtert.

Schlagwörter: Pyoverdin, Fluoreszenz, *Pseudomonas fluorescens* A506, Eisenstress, Methylierung

List of abbreviations

3-Oxo-C12-HSL	N-(3-oxododecanoyl)-L-homoserine lactone
ABC	ATP-binding-cassette
AHL	N-acyl homoserine lactone
amp/ampR	ampicillin, ampicillin resistance
AU	arbitrary units
BCCP	biotin carboxyl carrier protein
BSA	bovine serum albumin
C	cytoplasmic fraction
C4-HSL	N-butanoyl-L-homoserine lactone
CAA	casamino acids
CP	cytoplasm
CuP	copper(II) phenanthroline
CV	column volume
DA	Dalton
DDM	dodecyl- β -D-maltoside
DMSO	dimethyl sulfoxide
DNA	deoxyribonucleic acid
dNTP	deoxynucleotide triphosphate
DTT	dithiothreitol

List of abbreviations

E	elution fraction
EDDHA	ethylenediamine- <i>N,N'</i> -bis(2-hydroxyphenylacetic acid)
EDTA	ethylenediaminetetraacetic acid
FM	fluorescence microscopy
FPLC	fast protein liquid chromatography
FT	flow through
HEPES	4-(2-hydroxyethyl)-1-piperazineethanesulfonic acid
ICP-MS	inductively coupled plasma - mass spectrometry
IM	inner membrane
IPTG	isopropyl β -D-1 thiogalactopyranoside
kan/kanR	kanamycin/kanamycin resistance
kb	Kilobases
L-ASA	L-aspartate β -semialdehyde
LB	Luria Bertani
LC-MS	liquid chromatography–mass spectrometry
L-Dab	L-2,4-diaminobutyrate
L-fOHOrn	L-N5-formyl-N5-hydroxyornithine
M	membrane fraction
MC	membrane fraction after carbonate wash
MS	mass spectrometry
MW	molecular weight

List of abbreviations

NRPS	non-ribosomal peptide synthetase
NTA	nitrilotriacetic acid
NTN	N-terminal nucleophile
OD ₆₀₀	optical density at 600 nm
OM	outer membrane
Pa	Pascal
PAGE	polyacrylamide gel electrophoresis
PBS	phosphate buffered saline
PC	phase contrast microscopy
PCR	polymerase chain reaction
PfA506	<i>Pseudomonas fluorescens</i> A506
pH	<i>potentia hydrogenii</i>
PKS	polyketide synthetase
PLP	pyridoxal-5-phosphate
PMP	pyridoxamine-5-phosphate
PMSF	phenylmethanesulfonyl fluoride
P	periplasmic fraction
Psi	pounds per square inch
PVD	pyoverdine
RBS	ribosomal binding site
rpm	rotations per minute

List of abbreviations

RT	room temperature
SC	supernatant after carbonate wash
SOC	super optimal catabolite-repression
SDS	sodium dodecyl sulfate
SUMO	small ubiquitin like modifier
Tat	twin-arginine translocation
TEMED	N,N,N',N'-tetramethylethane-1,2-diamine
Tris	tris(hydroxymethyl)-aminomethane
TSS	transformation and storage solution
UV	ultra violet
UPLC	ultra performance liquid chromatography
v/v	volume per volume
W	washing fraction
w/v	weight per volume
wt	wild-type strain
xg	multitude of the acceleration of gravity ($g = 9.81 \text{ m/s}^2$)

Table of content

Abstract	I
Zusammenfassung	II
List of abbreviations	III
Table of content.....	VII
1. Introduction.....	1
1.1 The role of iron	1
1.2 Siderophores	2
1.3 Cytoplasmic biosynthesis of ferribactin	7
1.4 Periplasmic pyoverdine formation and maturation	10
1.5 Export, import and recycling of pyoverdine.....	14
1.6 Regulation of pyoverdine biosynthesis.....	15
1.7 Aims of this study.....	18
2 Material and Methods	19
2.1 Bacterial strains, plasmids and primers	19
2.2 Cultivation of bacteria	27
2.2.1 Media, antibiotics and solutions.....	27
2.3 Molecular methods	29
2.3.1 Preparation of plasmids	29
2.3.2 Preparation of genomic DNA.....	29
2.3.3 Polymerase chain reaction (PCR)	29

2.3.4	Restriction of DNA	32
2.3.5	Agarose gel electrophoresis	33
2.3.6	Purification of DNA fragments	34
2.3.7	Ligation of DNA	34
2.3.8	Production of competent <i>E. coli</i> cells.....	34
2.3.9	Transformation of <i>E. coli</i>	35
2.3.10	Fast transformation of <i>E. coli</i>	35
2.3.11	Electroporation of <i>P. fluorescens</i> A506	35
2.3.12	Genomic deletion in <i>P. fluorescens</i> A506.....	36
2.4	Biochemical methods	37
2.4.1	Isolation of periplasm, cytoplasm and total membrane fraction in <i>E. coli</i>	37
2.4.2	Isolation of periplasm, cytoplasm and total membrane fraction in <i>P. fluorescens</i>	37
2.4.3	Carbonate wash	38
2.4.4	Protease accessibility assay	38
2.4.5	Alkaline phosphatase (PhoA) activity assay	39
2.4.6	Recombinant protein production	40
2.4.7	Cell disruption	40
2.4.8	Immobilized Ni-NTA affinity chromatography	41
2.4.9	Size exclusion chromatography	41
2.4.10	Bradford assay	42

2.4.11	Cystein crosslinking	43
2.4.12	SDS-PAGE.....	43
2.4.13	Colloidal Coomassie staining.....	44
2.4.14	Silver staining.....	45
2.4.15	Western blot and protein detection.....	47
2.4.16	Complementation analysis	48
2.4.17	Growth curves	48
2.4.18	Extraction of pyoverdine	49
2.5	Analytical methods	49
2.5.1	Mass spectrometry for pyoverdine identification.....	49
2.5.2	Sample preparation for shotgun mass spectrometry	50
2.5.3	Shotgun mass spectrometry for anchorage site identification.....	50
2.5.4	Microscopy	51
2.5.5	Spectrophotometry	51
2.5.6	Gas chromatography	52
3	Results.....	53
3.1	Towards understanding the function of PvdM	53
3.1.1	PvdM is a membrane integrated protein with its globular domain facing the periplasm.....	54
3.1.2	PvdM is not involved in the regulation of pyoverdine biosynthesis as a peptidase	56

3.1.3	Substitution of conserved metal ligands of the human renal dipeptidase reveals no function in PvdM	58
3.1.4	The human renal dipeptidase inhibitor Cilastatin slightly effects PvdM.....	61
3.1.5	PvdM is required for the activity of PvdP <i>in vivo</i>	63
3.1.6	Copper cannot compensate for missing PvdM <i>in vivo</i>	65
3.1.7	PvdM possesses at least two membrane anchors	66
3.1.8	Identification of potential anchorage sites	69
3.2	Further analyses of PvdP	71
3.2.1	PvdP is a membrane bound tyrosinase	72
3.2.2	Analysis of the copper contained in PvdP as a function of PvdM	73
3.2.3	Cysteine crosslinking of PvdP.....	75
3.3	Enzymatic analysis of PvdN.....	77
3.3.1	PvdN requires molecular oxygen for conversion of glutamic acid to succinamide	77
3.3.2	PvdN accepts glutamine as a substrate.....	81
3.3.3	PvdN _{H260A} favours different hydrolyses of the glutamic acid variant of pyoverdine	84
3.4	Substrate analysis of PvdQ	86
3.4.1	A <i>P. fluorescens</i> A506 $\Delta pvdQ$ strain produces fluorescence.....	87
3.5	Additional growth studies of strains lacking pyoverdine on iron depleted medium .	91
3.5.1	Identification of an EDDHA derivate in the supernatant of a pyoverdine impaired strain	92

4	Discussion	98
4.1	Interaction of PvdM in the maturation process of pyoverdines.....	98
4.1.1	The N-terminus of PvdM mediates membrane integration	100
4.1.2	Additional integration into the membrane of PvdM	104
4.1.3	Two possible functions of PvdM	105
4.2	PvdN is an oxygen dependent enzyme	110
4.2.1	Alternative substrate of PvdN	112
4.3	PvdP possesses an unusual signal peptide.....	113
4.4	PvdQ deacylates ferribactin.....	116
4.5	Di-methylated EDDHA could facilitate iron release.....	118
4.6	Summary and Outlook.....	121
5	References.....	124
6	Supplement	151
7	Acknowledgements.....	154
8	Curriculum vitae	156
9	List of publications	157

1. Introduction

1.1 The role of iron

Iron is in many ways a highly interesting element. Like most of the elements in the universe, except for hydrogen, helium and lithium which formed during the big bang, iron emerged several billion years ago by the fusion of lighter elements such as helium and silicon under high pressure and temperatures of at least 200,000,000 °C in stellar interiors or supernova explosions (Wagoner *et al.* 1967). Through the so-called alpha process, elements ranging from elemental carbon to nickel are formed by the conversion of helium into heavier elements (Burbidge *et al.* 1957). Iron plays a special role in this process of elementary creation. On the one hand, elements heavier than iron are not fused by the normal nuclear fusion in stars, because the fusion process of iron with other elements is highly endothermic, absorbing more energy than it is releasing (Chaisson and McMillan 1999). Among other things, this is due to the fact that iron contains the highest binding energy per nucleon (Fewell 1995). On the other hand, the radioactive elements heavier than iron, such as nickel, which are naturally produced by the neutron capture, tend to decay further and further to iron, which is one of the most stable nuclei (Dyson 1979; Blean 2011). It will therefore not decay any longer. These two characteristics provide for the large abundance of iron in the universe and accordingly also on earth.

Although iron is, in terms of mass, the most abundant element in the earth's crust and ubiquitous in the biosphere, lithosphere and hydrosphere it is hardly bioavailable for bacteria and other organisms (Crichton and Charloreaux-Wauters 1987; Frey and Reed 2012). The low concentration of soluble bioavailable iron is often a limiting factor for growth and cellular processes (Behrenfeld and Kolber 1999). The reason for this is the oxidation state, in which iron is mainly found on earth (Morgan and Anders 1980). Iron is found either in its reduced form as ferrous iron (Fe^{2+}) or in its oxidized form as ferric iron (Fe^{3+}). Under oxic conditions, such as those usually found on earth, molecular iron is readily oxidized to rust, an insoluble ferric oxide, as a product of the reaction of iron and oxygen in the presence of water. Its insolubility makes this form of ferric iron scarcely bioavailable for microorganisms. With a few exceptions such as *Lactobacillus plantarum*, iron is an essential metal required by the majority of living organisms (Frawley and Fang 2014; Archibald 1983). As part of several co-factors for proteins such as the heme co-factor, iron sulfur clusters or the iron molybdenum co-factor, iron

is the most common redox active metal found in proteins (Andreini *et al.* 2008). It is a key element in various elementary cellular processes and metabolic pathways such as DNA replication, transcription, the electron transfer in the terminal electron transfer pathways and is even involved in the regulation of the life cycle of *Drosophila*, a genus of small flies of the family of *Drosophilidae*, by controlling the cell metabolism (Anraku 1988; Marelja *et al.* 2018; Ilbert and Bonnefoy 2013). Moreover, iron is a key element in the interplay between pathogens and plants or mammals by affecting the outcome of infections either in favour of the pathogen or the host organism (Nairz *et al.* 2010).

Having stated the importance of iron and its involvement in different elementary cellular processes, one comes to the understanding that microorganisms must adapt to and overcome the low bioavailability of iron especially in hosts environments.

1.2 Siderophores

To circumvent the low bioavailability of iron, microorganisms such as fungi and bacteria have evolved different mechanisms to sequester iron from their environment. These mechanisms include surface reductases and haemolysins, for example (Marvin *et al.* 2003). It could be shown that the opportunistic human pathogen *Listeria monocytogenes* is able to rapidly reduce ferric iron to ferrous iron using cell surface-associated ferric reductases systems involving bound flavin as a co-factor. It was also observed that *L. monocytogenes* was capable to reduce iron chelates such as haemoglobin and transferrin (Deneer *et al.* 1995; Jeeves *et al.* 2011). It has further been shown that the opportunistic fungal pathogen *Candida albicans* acquires iron via a highly conserved high affinity iron uptake system which includes cell-surface ferric reductases (Gerwien *et al.* 2017). The source for sequestering the essential iron are often host-iron complexes (Romero *et al.* 2021). The reduced and therefore soluble ferrous iron is then immediately taken up into the cell. A third mechanism to acquire iron from the environment is via siderophores. Siderophores, meaning iron carriers in Greek, are secondary metabolites of the cell and small water-soluble peptide molecules with extremely high affinities for iron (Hider and Kong 2010). They are secreted by bacteria, fungi and plants under iron depleted conditions and are able to bind Fe^{3+} from the insoluble iron oxides to form Fe^{3+} complexes. These soluble complexes are then able to be taken up by the respective organisms through selective uptake

systems (**Figure 1**). While all organisms are naturally capable of taking up their own siderophores, there are some microorganisms that possess uptake systems for foreign siderophores, and thus engage in siderophore piracy (Traxler *et al.* 2013; Grandchamp *et al.* 2017; Ye *et al.* 2014). Some pseudomonads species even have up to 15 different predicted TonB-dependent receptors that can recognise various ferri-pyoverdines and import and utilise them in the cells (Ye *et al.* 2014). This seemingly superfluous number of receptors for species foreign pyoverdines underlines the position pyoverdine occupies in iron stress situations.

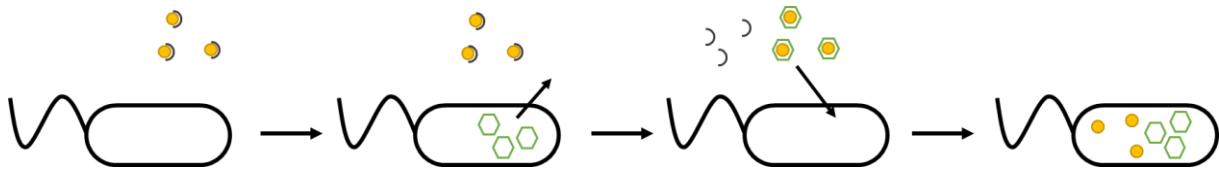


Figure 1: Schematic overview of the function of siderophores. When iron is deficient, organisms are able to produce siderophores and release them into the environment. There, the chelators sequester iron from the existing insoluble compounds. The soluble ferri-siderophores are then actively transported into the cell and the iron obtained can be used for essential functions.

Next to Fe^{3+} , siderophores are also capable of binding other metal ions such as divalent cations including Cd^{2+} , Cu^{2+} , Ni^{2+} , Pb^{2+} and Zn^{2+} and other trivalent cations such as Mn^{3+} , Co^{3+} and Al^{3+} (Nair *et al.* 2007; Hu and Boyer 1996). Although more than 100 different siderophores are known today, the majority of siderophores can be assigned to four different main categories: hydroxamate, catecholates, carboxylates and phenolates depending on the functional group responsible for the coordination of the Fe^{3+} -ion (Winkelmann 1991). Siderophores themselves are not rigid structures. It is the bond with the Fe^{3+} -ion that stabilizes their structure. Typically, three functional groups of the siderophore act as bidentate ligands to bind the iron at its six coordination sites and form a hexadentate structure. The stability of the ferri-siderophore is a result of the ligand denticity and the interactions between iron, a hard Lewis acid and oxygen, a hard Lewis base. Although each functional group involved in the coordination of iron usually donates two oxygen atoms for the complexation, some alternatives can occur where the functional oxide ions are substituted by nitrogen or sulfur. This substitution results in a weaker interaction between the siderophore and the Fe^{3+} -ion. Beside the above mentioned and clearly defined groups of hydroxamate-, catecholate-, carboxylate- and phenolate-siderophores like yersiniabactin, a siderophore produced by *Yersinia pestis*, the bacterium that causes the bubonic

and pneumonic plague, there are also mixed type siderophores with more than one functional group and some non-conventional siderophores (**Figure 2**).

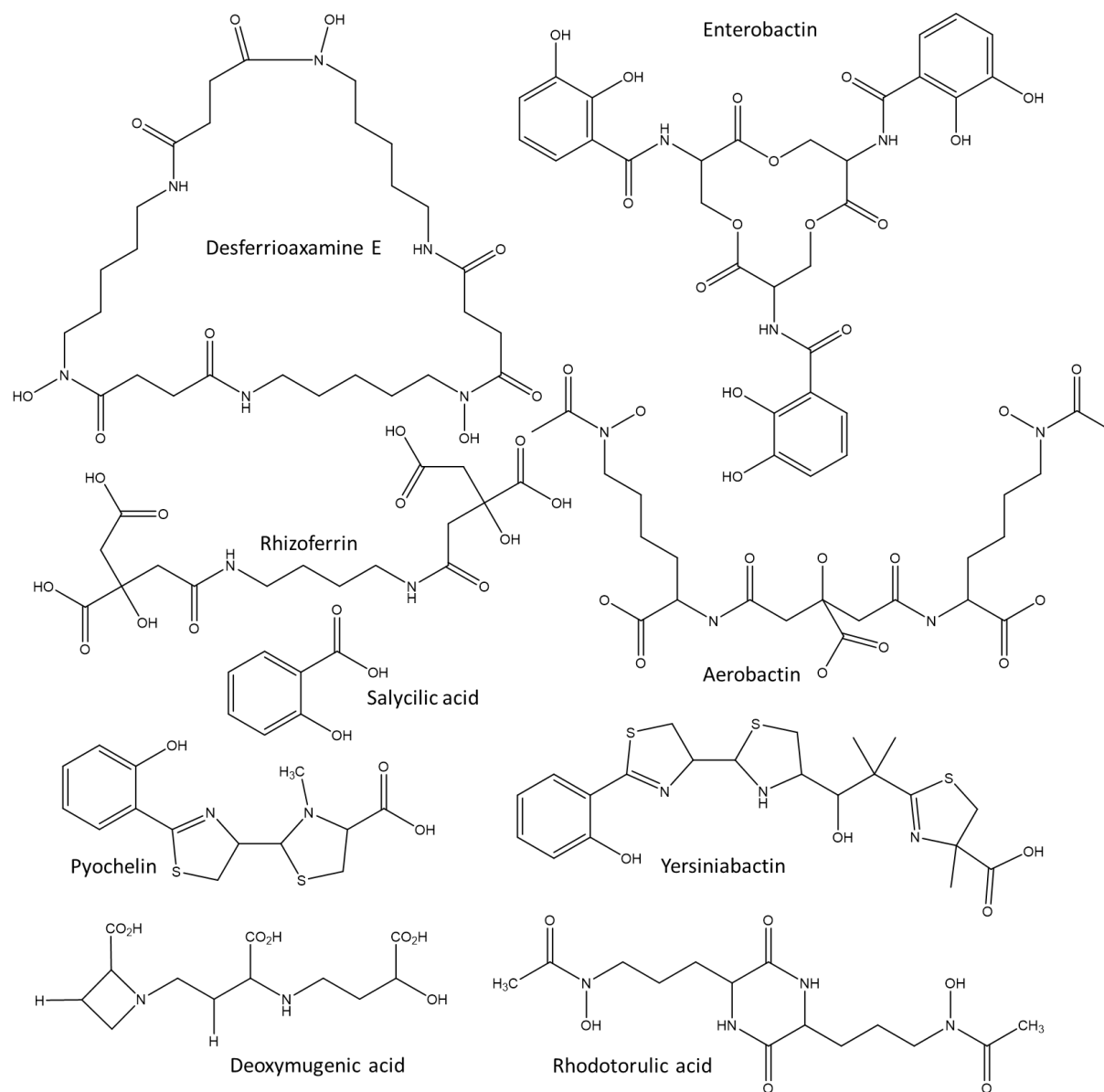


Figure 2: Different types of siderophore and phyto-siderophore structures. Structures of phenolate- (e.g., pyochelin, yersiniabactin), catecholate (e.g., enterobactin), carboxylate- (e.g., rhizoferrin), hydroxamate- (e.g., rhodotorulic acid, desferrioxamine E), phyto- (deoxymugenic acid) and mixed-type siderophores (e.g., aerobactin).

One of the many mixed-type siderophores is pyoverdine, the main siderophore of the fluorescent pseudomonads (**Figure 3**). Pyoverdines possess two hydroxamate groups and one catecholate group which are involved in the Fe^{3+} -ion complexation and are able to bind iron

with an affinity 10^{24} M^{-1} in an octahedral complex (Visca *et al.* 2007a). These functional groups are responsible for the extreme high affinity to ferric iron, allowing pyoverdine to sequester iron from iron complexes in the environment but also from host proteins such as transferrin and lactoferrin (Meyer *et al.* 1996; Xiao and Kisaalita 1997). The ferric iron in the ferri-pyoverdine is coordinated by the functional groups of the hydroxamate, namely the hydroxy and the carbonyl groups, and the hydroxy groups of the catechol. Pyoverdines in general consist of three main parts: (i) a strain specific peptide backbone that can vary in length and composition and consists of 6-14 residues, (ii) a 2,3-diamino-6,7-dihydroxyquinoline core, that is invariant amongst all pyoverdines and responsible for the characteristic fluorescence and (iii) a glutamic acid residue that can be modified to various acyl side chains. Next to its ability to chelate metal ions, pyoverdines can also act as a signalling molecule for the upregulation of pyoverdine production, but also for the expression of virulence factors by influencing the gene expression of virulence genes such as exotoxin A or the protease PrpL in *Pseudomonas aeruginosa* (Bonneau *et al.* 2020; Lamont *et al.* 2002; Visca *et al.* 2007a). This is one reason for the great interest in pyoverdines in medical research. Due to the fact that more and more clinically relevant bacterial strains such as *P. aeruginosa* are developing resistances to various antibiotics used in modern medicine, scientists are looking for other ways to combat these pathogenic strains (Kollef *et al.* 2017). A promising approach is not to target the growth capacity of bacteria directly with antibiotics, but to regulate the virulence factors in the cells (Kirienko *et al.* 2018). Pyoverdines are the main siderophores of pseudomonads and are responsible for iron acquisition in host environments. Since they also play a decisive role in the regulation of certain virulence factors, pyoverdines have been increasingly coming into focus as a possible starting point for combating *P. aeruginosa* infections (Kirienko *et al.* 2016). Finding a way to inhibit the production of pyoverdines in the opportunistic human pathogens would allow to drastically influence the growth of these bacteria.

Another interest is the potential use of pyoverdines in the uptake of antibiotics by a “Trojan horse” strategy, following the example of sideromycins (Mislin and Schalk 2014; González *et al.* 2021). Sideromycins are siderophores with a covalently linked antibiotic, which are produced by various microorganisms and actively transported into the cell (Bickel *et al.* 1960; Knüsel and Nüsch 1965; Braun *et al.* 2009). In the approach including pyoverdines, the antibiotic would be conjugated to a free amine of the pyoverdine, with a certain distance to the N-terminus in order not to interfere with the recognition of pyoverdine by its outer membrane receptor and importer FpvA (Greenwald *et al.* 2009; Shen *et al.* 2005). As the pyoverdines are recognized by outer membrane receptors and actively imported into the cell, the problem of low permeability of the outer membrane for certain drugs can be bypassed.

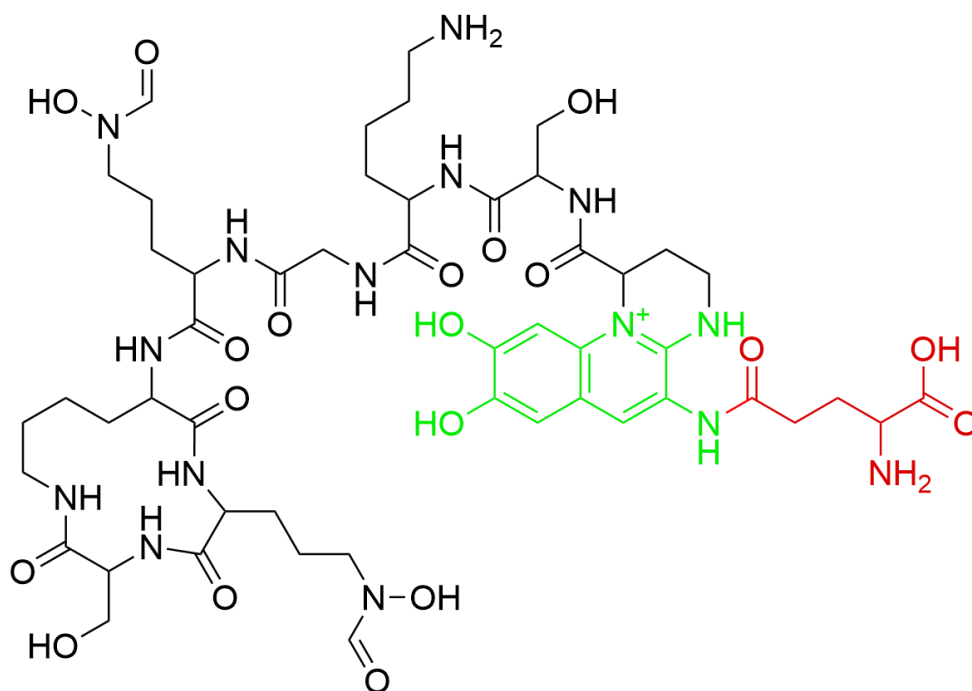


Figure 3: Structure of the fluorescent siderophore pyoverdine from *P. fluorescens* A506. The mixed type siderophore consists of three main parts, namely the modifiable side chain (highlighted in red), the invariable 2,3-diamino-6,7-dihydroxyquinoline core (highlighted in green) and the peptide backbone, which can vary depending on the species (in black). The ferric iron is being coordinated by the functional groups of the hydroxamate, namely the hydroxy and the carbonyl groups, and the hydroxy groups of the catechol.

1.3 Cytoplasmic biosynthesis of ferribactin

The production of pyoverdines can generally be divided into two major stages, the synthesis of a precursor in the cytoplasm and the maturation to the mature pyoverdine in the periplasm. The biosynthesis of pyoverdines starts in the cytoplasm by the assembly of an acylated ferribactin, the precursor of pyoverdine (**Figure 4**). These syntheses are usually catalysed by modular non-ribosomal peptide synthetases (NRPSs) or polyketide synthase (PKS) domains that cooperate with NRPS modules (Donadio *et al.* 2007). In pseudomonads, the condensation reactions of partly rather unusual amino acids such as β -hydroxy histidine, ornithine, cyclo- N_5 -hydroxy ornithine, L- N_5 -formyl- N_5 -hydroxyornithine (L-fOHOrn), N_5 -acetyl- N_5 -hydroxyornithine, β -hydroxy aspartic acid and N_5 -hydroxybutyryl- N_5 -hydroxyornithine are catalysed by the NRPS PvdL, PvdI and PvdD (Mossialos *et al.* 2002; Lehoux *et al.* 2000; Ackerley *et al.* 2003). The syntheses of the unusual non-canonical amino acids building blocks used for the formation of ferribactin are carried out by auxiliary enzymes such as PvdH, PvdF and PvdA (Vandenende *et al.* 2004; McMorran *et al.* 2001; Visca *et al.* 1994).

NRPSs in general are large enzymes that are build up modularly, with each module catalysing the incorporation of a single amino acid into the construct to be formed (Lautru and Challis 2004; Kleinkauf and Döhren 1996). The number of individual modules of a NRPS usually corresponds to the number of amino acids to be incorporated into the peptide chain by the respective NRPS. The enzymatic units of each module of the NRPS can be subdivided into domains, namely the A-domain, the PCP-domain and the N-terminal C-domain. These domains are responsible for the substrate recognition and activation as an amino acyl adenylate, covalent binding and the peptide bond formation (Schwarzer and Marahiel 2001). The adenylation domain (A-domain) is responsible for the recognition of the cognate amino acid and activates it as an amino acyl adenylate under the consumption of ATP. The activated amino acid is then covalently linked to the 4'phosphopantetheine co-factor of the peptidyl carrier protein (PCP-Domain) to form an activated thioester derivate (Stachelhaus and Marahiel 1995; Challis and Naismith 2004). The peptidyl carrier protein serves as a flexible structure that enables the transfer of the bound substrate to the catalytic centre of the next module (Mercer and Burkart 2007). The condensation domain (C-domain) catalyses the peptide bond formation between to amino acid building blocks. In this elongation reaction, the nascent peptidyl chain bound to the 4'phosphopantetheine co-factor of the upstream peptidyl carrier protein is, in a condensation

reaction, linked to the amino acid bound to the 4'phosphopantetheine co-factor of the downstream peptidyl carrier protein (Rausch *et al.* 2007; Lautru and Challis 2004).

Within the first steps of ferribactin synthesis, the within all fluorescent pseudomonads highly conserved NRPS PvdL first incorporates a 14-carbon fatty acid, which can be either a fully saturated myristic acid or a monounsaturated myristoleic acid. Subsequently, the three conserved amino acids L-glutamic acid, D-tyrosine and L-2,4-diaminobutyrate are linked to the fatty acid. These three amino acids are important for the reason that the chromophore formation to form the final fluorescent pyoverdine is executed by the oxidative cyclisation of D-tyrosine and L-2,4-diaminobutyrate (Nadal-Jimenez *et al.* 2014; Ringel *et al.* 2018). All enzymes involved in the process of ferribactin synthesis are believed to form a multi-enzyme complex which is called the siderosome (Imperi and Visca 2013). After the remaining amino acid building blocks are incorporated by the NRPSs PvdI and PvdD, and sometimes additional NRPSs depending on the strain, the acylated ferribactin is exported into the periplasm, most likely by the ATP-binding-cassette (ABC) transporter PvdE, for the conversion to pyoverdine and possible further maturation steps (McMorran *et al.* 1996; W Saurin *et al.* 1999)

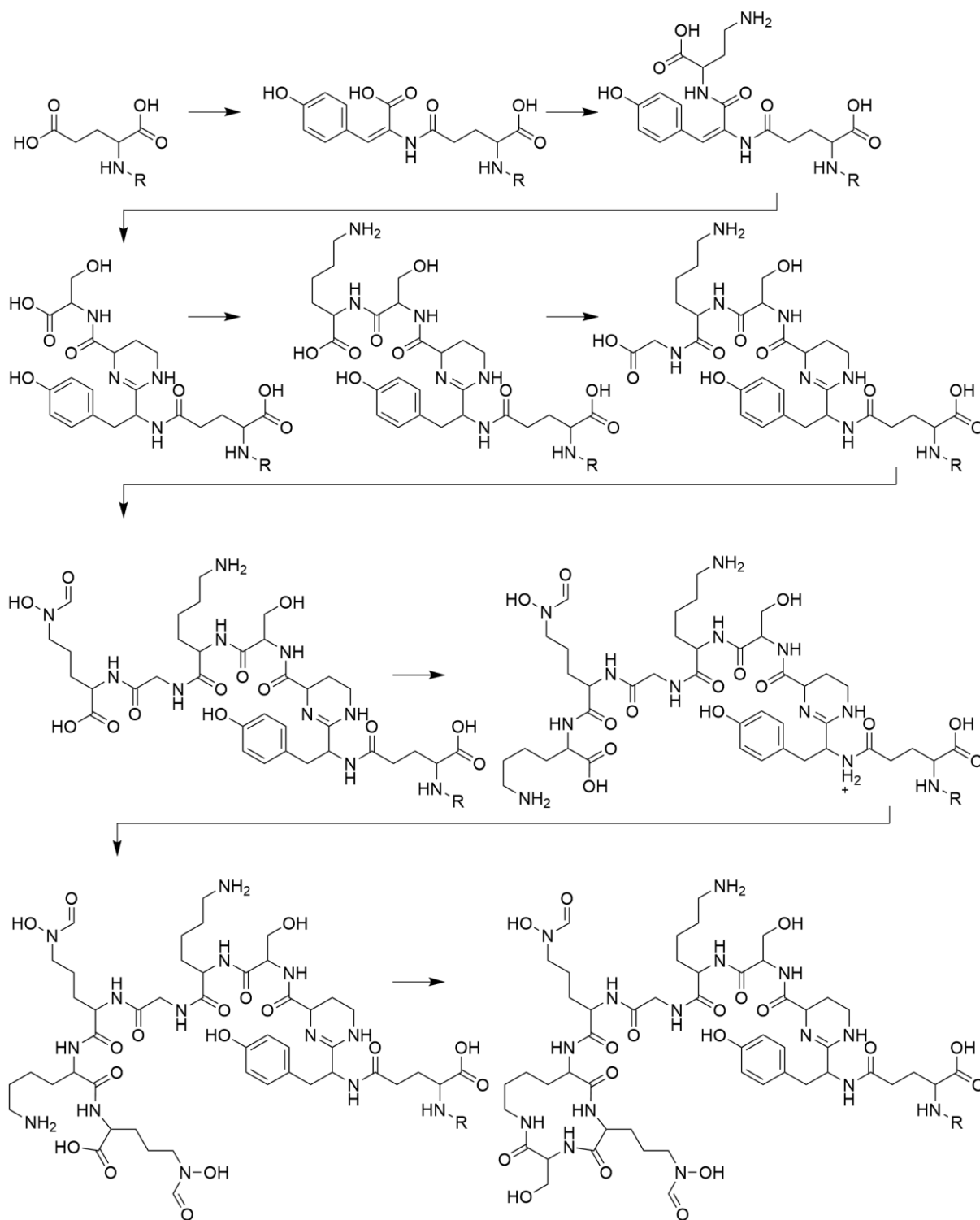


Figure 4: Overview of the ferribactin synthesis in *P. fluorescens* A506. The individual synthesis steps from the initial amino acid glutamate to the finished acylated ferribactin. The ten synthesis steps are being catalysed by the non-ribosomal peptide synthetases PvdL, PvdI and PvdD. The myristic acid or myristoleic acid residue incorporated by PvdL in the first synthesis step is represented by the R.

1.4 Periplasmic pyoverdine formation and maturation

Once exported into the periplasm, it is believed that the acylated ferribactin is immediately deacylated by the N-terminal nucleophile hydrolase (NTN)-type hydrolase PvdQ (Drake and Gulick 2011). First discovered as a quorum quencher by degrading long-chain N-acylhomoserine lactones (AHL), it was later shown that PvdQ has at least one additional function in the biosynthesis of pyoverdines (Hannauer *et al.* 2012). PvdQ is a typically $\alpha\beta\alpha$ -folded NTN-type hydrolase that is produced as a proenzyme and undergoes autoproteolytical posttranslational cleavage resulting in the formation of a 18 kDa α -chain and an enzymatically active 60 kDa β -chain (Bokhove *et al.* 2010). After the separation of the ferribactin from the fatty acid chain, the deacylated ferribactin is converted to pyoverdine in a cascade of oxidations (**Figure 5**). Unlike previously assumed to be carried out by only one enzyme, it has been shown that the complete conversion of ferribactin to pyoverdine is catalysed by two enzymes, namely PvdP and PvdO (Nadal-Jimenez *et al.* 2014; Ringel *et al.* 2018). PvdP belongs to the superfamily of tyrosinases and is believed to be located in the periplasm. It is being transported across the cytoplasmic membrane via the twin-arginine translocation (Tat) pathway, meaning that the folding of the protein is already happening in the cytoplasm prior to the translocation (Nadal-Jimenez *et al.* 2014; Brüser 2007). Tyrosinases are metal-containing enzymes, which catalyse the oxidation of phenols to the corresponding catechol by oxygen within the type-three dicopper (Cu^{2+}) containing active site of the enzyme (Poppe *et al.* 2018). In case of PvdP, the hydroxylation of the substrate ferribactin as a first catalytic step leads to a catechol, which is oxidized yielding a *o*-quinone. A nucleophilic addition to the electrophilic carbon of this intermediate and tautomerization, re-establishing the catechol, leads to the final product of PvdP, dihydropyoverdine (Dorrestein *et al.* 2003). In an immediately following reaction, PvdO catalyses the oxidation of dihydropyoverdine and the subsequent tautomerization, resulting in the mature fluorophore (Ringel *et al.* 2018).

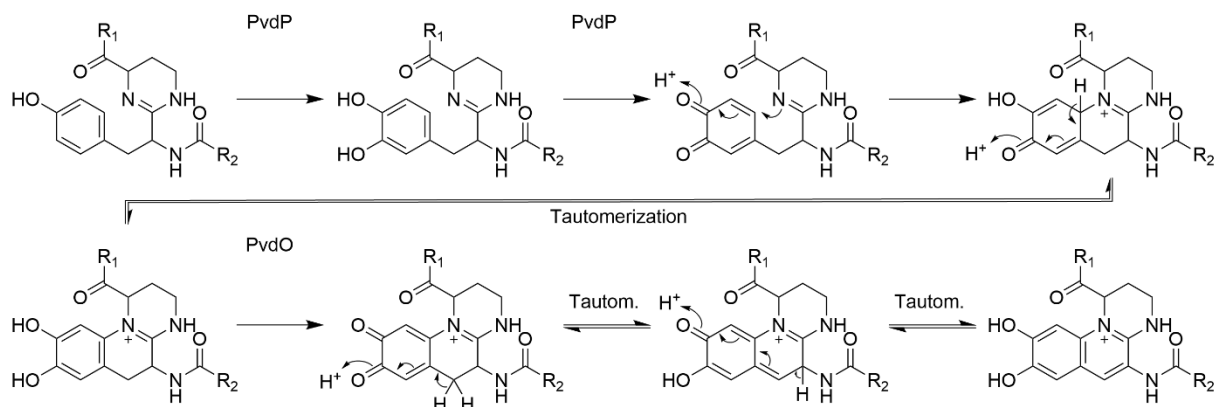


Figure 5: Oxidation mechanism of ferribactin to pyoverdine. Overview of oxidation of ferribactin to dihydropyoverdine and the subsequent oxidation to pyoverdine catalyse by PvdP and PvdO, respectively. R_1 represents the rest of the pyoverdine backbone, while R_2 represents the glutamic acid residue.

In a final maturation step, the N-terminal glutamic acid residue of the pyoverdine which has been incorporated by PvdL, the first module of the NRPS, can be processed by either one of two recently characterized periplasmic enzymes, namely PvdN or PtaA (Voulhoux *et al.* 2006; Ringel *et al.* 2016, 2017). In case of PvdN, the glutamic acid residue is converted into a succinamide residue in a postulated unique pyridoxal-5-phosphate (PLP)-dependent oxidative decarboxylation under the retention of an amine (**Figure 6**) (Ringel *et al.* 2016). Being transported across the cytoplasmic membrane via the Tat pathway, PvdN folds and integrates its indispensable PLP co-factor prior to its translocation. For the modification of the side chain of pyoverdine, a catalytic mechanism was proposed, in which the lysine at position 261, which is covalently bound to the PLP co-factor in the active site of PvdN, is replaced by the substrate, the chromophore coupled glutamic acid residue, to form Schiff base, more precisely an external aldimine. Subsequent decarboxylation would lead to a quinonoid intermediate. Addition of molecular oxygen with a simultaneous protonation, provided by a proximate base, would in turn lead to an unstable intermediate with a hydroperoxide group at the α -C atom. The base providing the proton is believed to be the neighbouring histidine at position 260. After subsequent electron shuffling and a dehydration reaction, the succinamide residue would be retained (Wang *et al.* 2016; Jansonius 1998; Sun *et al.* 1998; Ringel *et al.* 2016). After the succinamide residue has been released from the holoenzyme, the PLP co-factor would be regenerated by covalently binding to the amino group of the lysine at position 261 in PvdN, which allows for a new cycle of conversion.

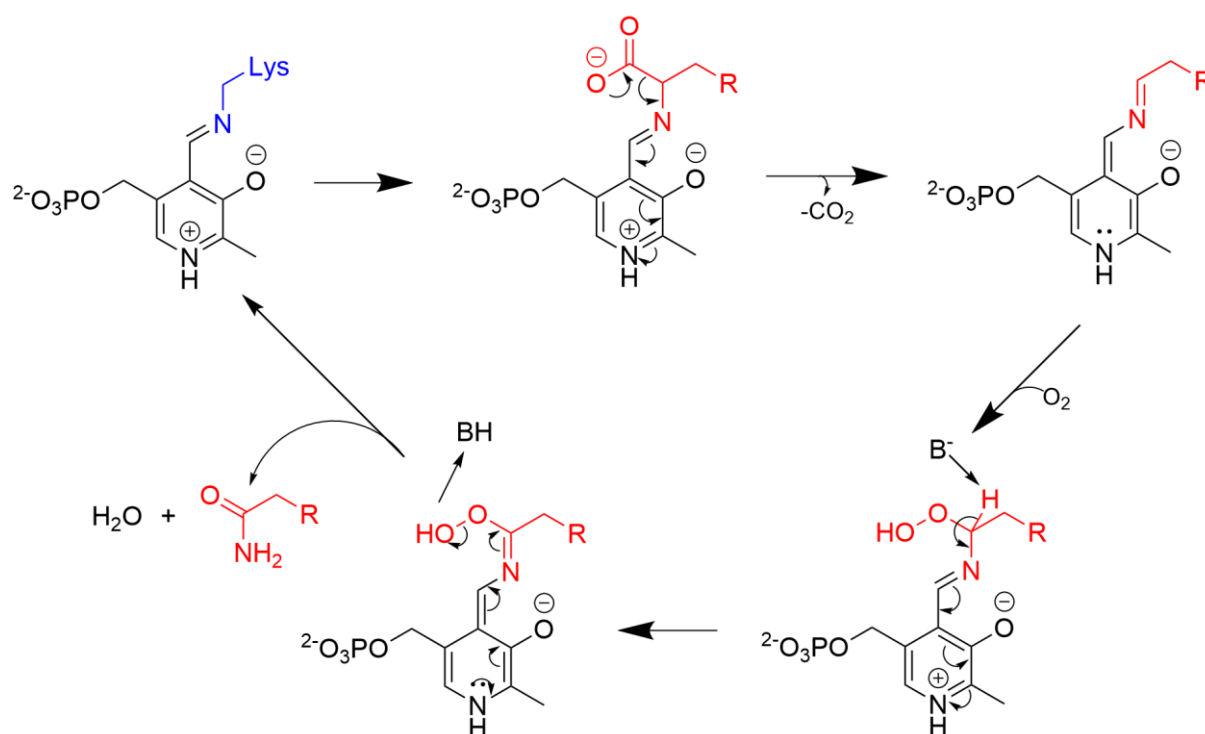


Figure 6: Postulated catalytic mechanism of PvdN. A possible mechanism for the conversion of the N-terminally bound glutamic acid residue of the pyoverdine to succinamide with the respective intermediates. After binding of the glutamic acid residue of the pyoverdine to the PLP co-factor, an external aldimine is formed. Subsequent decarboxylation and the formation of a quinonoid intermediate, addition of molecular oxygen and deprotonation by a base mediate the forming a rather reactive hydroperoxide intermediate. After a dehydration step, succinamide is formed and released while PLP is regenerated. The lysine residue is coloured in blue. The substrate residue and its intermediates throughout the reaction are coloured in red.

In a parallel enzymatic reaction competing for the substrate with PvdN, the homodimeric periplasmic transaminase PtaA catalyses the conversion of the glutamic acid residue to α -ketoglutarate (**Figure 7**). Just like PvdN, PtaA is a PLP containing enzyme and is translocated into the periplasm via the Tat-pathway. In contrast to the unusual reaction catalysed by PvdN, this reaction mechanism can be explained by standard PLP chemistry (Ringel *et al.* 2017). In a first transamination step, the lysine residue at the PLP co-factor is displaced by the N-terminal glutamic acid residue of the pyoverdine forming an internal aldimine. This aldimine undergoes deprotonation, subsequent electron shuffling and immediate reprotonation, leading to a carbanionic intermediate with a shifted imine. Hydrolysis of the imine bond yields the α -ketoglutaric acid variant of the pyoverdine sidechain and a pyridoxamine phosphate (PMP)

(Toney 2014; Toney and Kirsch 1993). The amino group of the PMP is then transferred to a yet unknown amino accepting carbonyl compound for regeneration of the PLP co-factor (Ringel *et al.* 2017).

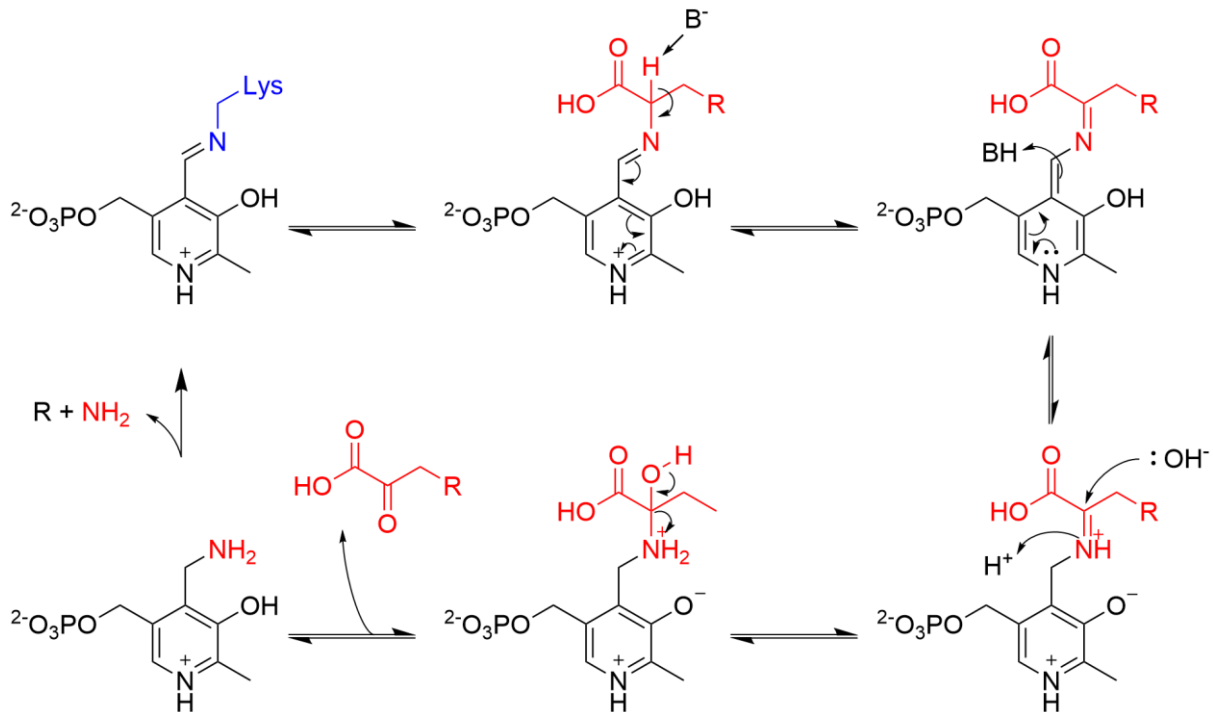


Figure 7: Catalytic mechanism of PtaA. After transimination of the lysine residue by the glutamic acid residue an internal aldimine is formed. This intermediate is deprotonated, and after electron shuffling and subsequent reprotonation, the carbonic intermediate with the shifted imine is retained. The imine bond is hydrolysed and the pyoverdine with the N-terminal α -ketoglutaric acid is released from the PLP co-factor. The remaining amino group is transferred to an unknown carbonyl compound, represented by the black “R”, in order for the PLP co-factor to be regenerated.

The N-terminally modified forms of pyoverdine, namely the succinamide and the α -ketoglutarate variants, have not shown any major advantages nor disadvantages in terms of iron scavenging or otherwise compared to the glutamic acid variant of pyoverdine. Thus, the exact function and reason for the bacteria's modifications remain unclear and have not yet been elucidated (Ringel *et al.* 2016).

After the chromophore formation in the periplasm by PvdP and PvdO is completed and the modification of the N-terminal glutamic acid residue by either PvdN or PtaA has been carried out, the mature pyoverdine is exported into the extracellular environment for the acquisition of iron and other essential metals.

1.5 Export, import and recycling of pyoverdine

The export into the extracellular space, the import of the ferri-bound pyoverdine and the recycling is a complex interplay of various different enzymes (**Figure 8**). Once the mature pyoverdine has been synthesized and modified, it is exported into the extracellular environment by different efflux systems. While the efflux pump consisting of the three proteins PvdR, PvdT and OpmQ is believed to be the main exporter of pyoverdines, it has been shown that a deletion of this system did not lead to a complete abolishment of pyoverdine export, but rather to a reduction by 30 % of exported pyoverdine in the environment (Hannauer *et al.* 2010). A second efflux system, namely MexABC-OprM, which belongs to the resistance nodulation cell division (RND) family, has been suggested to act as a transporter for the secretion of pyoverdines. However, an involvement of this efflux system in the export of pyoverdine has been refuted in a later study (Poole *et al.* 1993a; Imperi *et al.* 2009). Another export system, encoded by the genes *mdtA*, *mdtB*, *mdtC* and *opmB*, has also been investigated as for its involvement in the periplasmic export of pyoverdines. While a deletion of this transporter did not have any effects on growth, a deletion of both efflux systems, PvdRT-OpmQ and MdtABC-OpmB, did show great impact on growth and the export of pyoverdines. However, the strain with the deletion of these two efflux systems was still able to excrete pyoverdine in a not insignificant amount. Accordingly, at least one other unknown exporter must be involved in the export of pyoverdine. (Henríquez *et al.* 2019).

Once exported, the apo-pyoverdine chelates metal and binds to the outer membrane receptor FpvA in its metal-bound state (Poole *et al.* 1993b). FpvA is a TonB-dependent transporter not only responsible for the specific recognition of the ferri-pyoverdine, but also for the import of the complex into the periplasm (Shen *et al.* 2005; Adams *et al.* 2006). With the binding site located at the extracellular space, FpvA has been shown to not only bind and import ferri-pyoverdine, but also pyoverdine complexes involving the divalent cations Cu^{2+} , Co^{2+} , Cd^{2+} , Mn^{2+} , and Ni^{2+} and the trivalent cations Al^{3+} and Ga^{3+} . Import of these alternative metals, however, was only verified for Cu^{2+} , Mn^{2+} , and Ni^{2+} and Ga^{3+} , but with a reduced uptake rate compared to that of ferri-pyoverdine (Clément *et al.* 2004; Braud *et al.* 2009). The import of bound ferri-pyoverdine is facilitated by an interaction of FpvA with the TonB-ExbB-ExbD-complex and the transduction of energy generated by the protonmotive force (Schalk *et al.* 1999; Clément *et al.* 2004; Noinaj *et al.* 2010). In the periplasm, the ferri-pyoverdine is

recognised by FpvF and FpvC, two proteins which catalyse the reduction of the ferric iron to ferrous iron and the liberation of the ion from the pyoverdine into the periplasm. The liberated iron is then taken up into the cytoplasm by FpvDE, a membrane traversing transporter located in the cytoplasmic membrane (Brillet *et al.* 2012). After the processing by the two PvdE associated proteins FpvA and FpvC, the recycled pyoverdine is released again into the extracellular environment for a new cycle of metal chelation (Greenwald *et al.* 2007; Imperi *et al.* 2009).

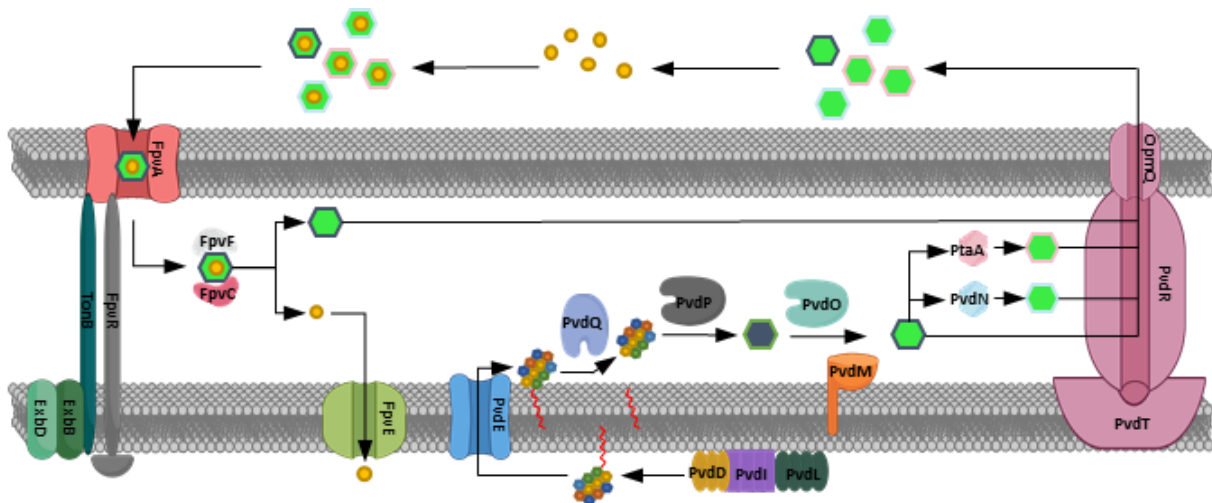


Figure 8: Overview of the biosynthesis of pyoverdine and the cycle of iron sequestering. Synthesis starts in the periplasm by the formation of an acylated precursor ferribactin by the NRPSs PvdL, PvdI, PvdD. Subsequently, the acylated ferribactin is exported into the periplasm by the ABC transporter PvdE and deacylated by PvdQ. The deacylated ferribactin is then oxidized by PvdP and PvdO to pyoverdine, forming the fluorescent chromophore. In additional modifications, the glutamic acid side chain can be modified by either PvdN or PtaA. The mature pyoverdine is then exported into the extracellular medium by PvdRTOPmQ and other unidentified transport systems. Once the ferri-pyoverdine interacts with the outer membrane importer FpvA, it is actively imported into the periplasm by the interaction of FpvA and the TonB-ExbB-ExbD-complex. Inside the periplasm, the iron is disassociated from the pyoverdine while at the same time being reduced to Fe^{2+} . The ferrous iron is then imported into the cytoplasm by FpvE while the pyoverdine is being regenerated and exported for another cycle of iron chelation.

1.6 Regulation of pyoverdine biosynthesis

As the above-described mechanisms, including the synthesis of various proteins and pyoverdines themselves, are highly energy consuming processes for the cell and too high a concentration of iron can be toxic due to the formation of reactive oxygen species by Fenton chemistry, the biosynthesis of pyoverdines in fluorescent pseudomonads is tightly regulated (Dixon and Stockwell 2014; Visca *et al.* 2007b; Ringel and Brüser 2018).

As for many other species as well, the transcription, or more precisely the repression of iron uptake related genes in pseudomonads is controlled by the master regulator of iron homeostasis, the Ferric uptake regulator Fur (Kaushik *et al.* 2016). Fur is a DNA binding protein and forms complexes with Fe^{2+} -ions, interacting with DNA depending on the intracellular Fe^{2+} concentration (Bagg and Neilands 1987). In the regulation of the pyoverdine biosynthesis in fluorescent pseudomonads, the Fur-complex represses the transcription of *fpvI*, *fpvR* and *pvdS* by binding to the so called Fur boxes, palindromic adenosine and thymine rich sequences in the promotor regions of the respective genes (Troxell and Hassan 2013).

Since the transcription of all pyoverdine related genes, except for *fpvI*, *fpvR* and *pvdS*, is dependent on the activation by the alternative sigma factor PvdS, the expression of *pvdS* in the presence of an adequate iron concentration in the cell is repressed by the transcriptional regulator Fur in complex with Fe^{2+} (Ochsner *et al.* 1995). FpvI is an alternative sigma factor that activates the expression of the genes encoding for the outer membrane receptor and importer FpvA (Visca 2004; R dly and Poole 2003). To activate the biosynthesis of pyoverdine, an interaction of ferri-pyoverdine bound FpvA and TonB-ExbBD complex is needed, ultimately leading to cleavage of FpvR (Beare *et al.* 2003). FpvR is an anti-sigma factor, that spans the periplasm and is responsible for the binding of the two alternative sigma factors FpvI and PvdS on its cytoplasmic domain, thereby impeding their function as activators (Lamont *et al.* 2002; Beare *et al.* 2003). FpvR undergoes autoproteolytical cleavage in the periplasm but the cleaved parts reassociate immediately after separation. After interaction of a ferri-pyoverdine bound FpvA and the TonB-ExbBD complex, FpvR undergoes a confirmation change, allowing it to be cleaved by a yet unknown site 1-like peptidase and the zinc metalloprotease RseP in the periplasm, which in turn leads to the liberation of PvdS and FpvI in the cytoplasm (R dly and Poole 2005). Presumably, the residues of FpvR are still separated from the alternative sigma factors PvdS and FpvI in the cytoplasm by an unknown peptidase, so that they can pursue their task in the synthesis of pyoverdine. Once liberated, the alternative sigma factors activate the expression of the genes in the *pvdS-regulon*, containing genes directly involved in the biosynthesis of pyoverdine such as *pvdM*, *pvdO* and *pvdP* and virulence genes and the expression of *fpvA* (**Figure 9**). Production of these alternative sigma factors can lead to an upregulation of all genes involved in the biosynthesis and uptake of pyoverdines (Swingle *et al.* 2008; Ochsner *et al.* 1996; Vasil *et al.* 1998; Wilderman *et al.* 2001; Wilson and Lamont 2000; Cunliffe *et al.* 1995).

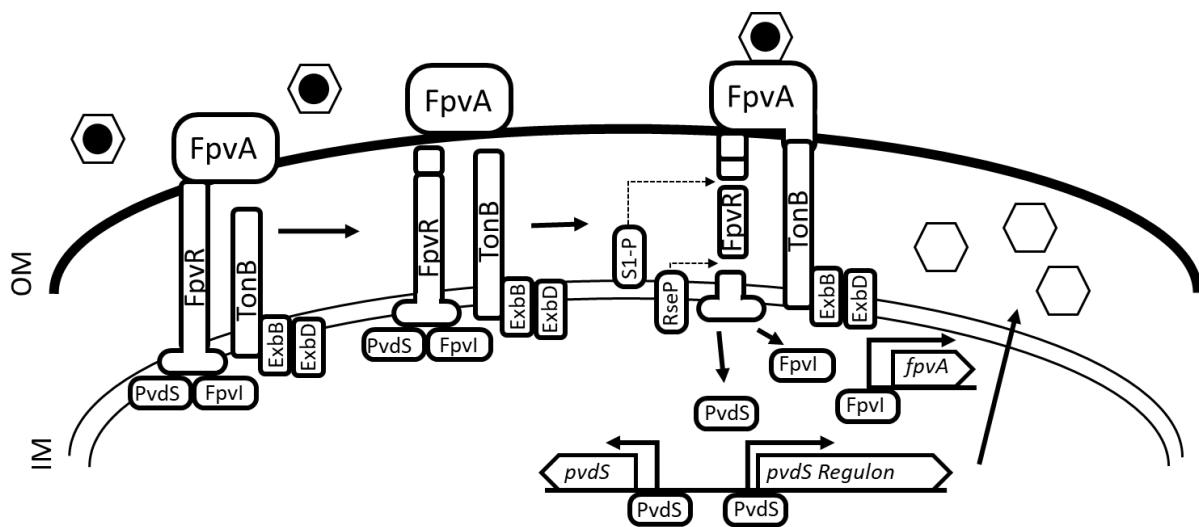


Figure 9: Scheme of initiation of pyoverdine biosynthesis. Overview of interactions involved in the upregulation of pyoverdines starting with the autoproteolysis of FpvR and subsequent self-assembly. Following an interaction of ferri-bound FpvA and the TonB-ExbBD complex, the truncation of FpvR is shown. This leads to the liberation of the alternative sigma factors PvdS and FpvI and the subsequent production of proteins involved in the pyoverdine synthesis. Dotted lines indicate truncation of FpvR by the respective protein.

If the TonB-ExbBD complex cannot interact with FpvA in a ferri-pyoverdine bound state because there is no more iron to sequester from the environment, FpvR does not undergo the conformational change after the autoproteolytic cleavage process in the periplasm with subsequent reassociation of the cleaved fragments. It therefore remains inaccessible to the cleavage of both, the yet unknown site 1-like peptidase and RseP, thereby not releasing the alternative sigma factors FpvI and PvdS bound at the cytoplasmic domain. This, in consequence, ends the upregulation of the genes involved in the synthesis of pyoverdines (Bishop *et al.* 2017; Minandri *et al.* 2016). Additionally, if the intercellular iron concentration is high enough for transcriptional regulator Fur to bind free iron, the complex binds to the Fur boxes upstream of the pyoverdine synthesis genes and inhibits their transcription. Thus, the expression of these genes is at its highest under iron starvation conditions and in turn, is strongly down regulated in the presence of free Fe^{2+} -ions in the cell (Cunliffe *et al.* 1995). For this mechanism and the activation cascade to work, it is crucial that there is always a basal level of the alternative sigma factors FpvI and PvdS present in the cytoplasm. This results in a minimal production of pyoverdines in order to start the activation cascade in case of iron starvation.

1.7 Aims of this study

In previous work by Michael Ringel, the exact role of three important proteins in the maturation of pyoverdines in the model organism *Pseudomonas fluorescens* A506 was identified, which allows for a nearly complete understanding of the processes involved. In this context, a novel reaction mechanism for one of these newly identified proteins, PvdN, which catalyses the modification of the side chain of the pyoverdine, was also postulated.

In this work, this novel reaction and its mechanism should be investigated in more detail and the actual modification should be verified *in vitro*.

Additionally, the subcellular orientation and the site of action of the essential maturation PvdM should be determined. Furthermore, it should be investigated whether PvdM is involved in the regulation of pyoverdine production or in the maturation of pyoverdines. Moreover, the actual task of PvdM in the process of pyoverdine synthesis should be elucidated.

Furthermore, the sequence of the individual maturation steps was investigated, focusing on deacylation by PvdQ, the timing and substrate of which have not yet been clearly defined due to contradictory results.

2 Material and Methods

2.1 Bacterial strains, plasmids and primers

Table 1: List of strains.

Strain	Genotype	Reference
<i>Escherichia coli</i>		
DH5 α	F ⁻ Φ 80 <i>lacZ</i> Δ M15 Δ (<i>lacZY A-argF</i>) U169 <i>recA1</i> <i>endA1</i> <i>hsdR17</i> (rk ⁻ , mk ⁺) <i>phoA</i> <i>supE44</i> λ ⁻ <i>thi-1</i> <i>gyrA96</i> <i>relA1</i>	Invitrogen
BL21 (DE3)	F ⁻ <i>ompT</i> <i>hsdS_B</i> (r _B ⁻ , m _B ⁻) <i>gal dcm</i> (DE3)	Agilent
XL1-Blue	<i>recA1</i> <i>endA1</i> <i>gyrA96</i> <i>thi-1</i> <i>hsdR17</i> <i>supE44</i> <i>relA1</i> <i>lac</i> [F' <i>proAB</i> <i>lacI^q</i> Z <i>ΔM15</i> Tn10 (Tetr)]	Agilent
MC4100	F ⁻ [<i>araD139</i>]B/r Δ (<i>argF-lac</i>)169* λ ⁻ e14 ⁻ <i>flhD5301</i> Δ (<i>fruK-yeiR</i>)725 (<i>fruA25</i>) \ddagger <i>relA1</i> <i>rpsL150</i> (strR) <i>rbsR22</i> Δ (<i>fimB-fimE</i>)632(::IS1) <i>deoC1</i>	(Casabadian 1976)
<i>Pseudomonas fluorescens</i>		
A506	wild-type	(Loper <i>et al.</i> 2012)

Table 2: Used oligonucleotides.

Name	Sequence	Use
<i>pvdN</i> -H260A for	CATCGCTGGCACCCGCCAAGTG GATGTTTCG	QuikChange primer for substitution of H260A in <i>pvdN</i>
<i>pvdN</i> -H260A rev	CGAACATCCACTTGGCGGTGC CAGCGATG	QuikChange primer for substitution of H260A in <i>pvdN</i>
NdeI- <i>pvdP</i> - XbaI-HindIII - for	CCACATATGACAATCTCTCGA CGTGGGTTTCATCGCAGGCC	Amplification of <i>pvdP</i> and insertion of a C-terminal XbaI and HindIII restriction site
NdeI- <i>pvdP</i> - XbaI-HindIII- rev	GCGAAGCTTGCGTCTAGACCA AAGCGTGTGCGTGACC	Amplification of <i>pvdP</i> and insertion of a C-terminal XbaI and HindIII restriction site
XhoI-RBS- <i>pvdN</i> -for-MS	CTTGCTCGAGGTTTAACTTTAA GAAGGAGATATACATATGACC GACCGCCGTACATTTTC	Amplification of <i>pvdN</i> and insertion of an N-terminal XhoI restriction site
<i>pvdN</i> -XbaI- HindIII-rev-MS	TCTAAGCTTGTCCGCTCTAGAT CTAACCGCTGGCTCAGCAGGG TCATGAAGCG	Amplification of <i>pvdN</i> and insertion of a N-terminal XbaI and HindIII restriction site
KpnI-RBS- <i>pvdM</i> -for-MS	CTTGGGTACCGTTTAACTTTAA GAAGGAGATATACATATGACA AAATCACGTTTCG	Amplification of <i>pvdM</i> and insertion of a N-terminal KpnI restriction site for cloning into pME6010
<i>pvdM</i> -XbaI- HindIII-rev- mod-MS	TCTAAGCTTGTCCGCTCTAGA ATGCGGTTGGCCAAGGGTTTG GC	Amplification of <i>pvdM</i> and insertion of a C-terminal XbaI and HindIII restriction site for cloning into pME6010
<i>pvdM</i> -M246A- for-MS	CGTGTCGCAGGCGTCGACCAA GG	QuikChange prime for substitution of M246A in <i>pvdM</i>
<i>pvdM</i> -M246A- rev-MS	TCGATGATCACCCCCAGG	QuikChange prime for substitution of M246A in <i>pvdM</i>
<i>pvdM</i> -H266A- for-MS	GGTGGCGTCCGCCTCGGCGCC TC	QuikChange prime for substitution of H266A in <i>pvdM</i>
<i>pvdM</i> -H266A- rev-MS	ATCGGCGTGCGGCTCAAC	QuikChange prime for substitution of H266A in <i>pvdM</i>
SpeI-RBS- <i>pvdM</i> -for-MS	CTTGACTAGTGTTTAACTTTAA GAAGGAGATATACATATGACA AAATCACGTTTCG	Amplification of <i>pvdM</i> and insertion of a N-terminal SpeI restriction site for cloning into pUCP20-ANT2-MCS
SpeI-RBS- <i>pvdP</i> - for-MS	CTTGACTAGTGTTTAACTTTAA GAAGGAGATATACATATGACA ATCTCTCGACGTGGG	Amplification of <i>pvdP</i> and insertion of a N-terminal SpeI restriction site for cloning into pUCP20-ANT2-MCS

KpnI-RBS- <i>pvdO</i> -for-MS	CTTGGGTACCGTTTAACTTTAA GAAGGAGATATACATATGACG CCATCCCGACTCAAAC	Amplification of <i>pvdO</i> signal sequence with overlapping sequence of mature <i>pvdM</i>
<i>pvdOSP</i> -rev-MS	CCAGCAAGCCGGCATGGGCCA GGCCGGGC	Amplification of <i>pvdO</i> signal sequence with overlapping sequence of mature <i>pvdM</i>
mat <i>pvdM</i> -for- MS	CGCAAGCTTTTACTTTTTCGAAC TGCGGGTGGCTCCAGC	Amplification of mature <i>pvdM</i> with overlapping of <i>pvdO</i> signal sequence
SP <i>pvdM</i> - mat <i>phoA</i> -rev- MS	CTGGTGTCCGCAGCAAGCCAG CCCCGGCGCCG	Amplification of <i>pvdM</i> signal sequence with overlapping sequence of mature <i>phoA</i>
mat <i>phoA</i> -for-MS	GCTGGCTTGCTGCGGACACCA GAAATGCCTG	Amplification of mature <i>phoA</i> with overlapping sequence of <i>pvdM</i> signal sequence
mat <i>phoA</i> -Strep- MfeI-rev-MS	GAGCAATTGTTACTTTTTCGAA CTGCGGGTGGCTCCATTTTCAG CCCCAGAGCGGC	Amplification of mature <i>phoA</i> with overlapping sequence of <i>pvdM</i> signal sequence and insertion of C-terminal Strep tag
His-SP <i>pvdM</i> - for-MS	GATATACATATGACACACCAT CACCATCACCATAAATCACGT TCGAAAAAGGCGCTG	Amplification of <i>pvdM</i> and insertion of a N-terminal His-tag.
His-SP <i>pvdO</i> -for- MS	GATATACATATGACGCACCAT CACCATCACCATCCATCCCGA CTCAAACCGCTCACCG	Amplification of <i>pvdO</i> and insertion of a N-terminal His-tag.
Strep-XbaI-rev- MS	CAAGTTCTAGATTATCATTACT TTTCGAACTGCGGGTGGCTCC A	Amplification of Strep-tag and insertion of a C-terminal XbaI restriction site.
pEXPT7-Strep- term-rev-MS	CCCTAAGCTTGAATTCAAAAA AAACCCCGCCCTGTCAGGGGC GGGGTTTTTTTTTTCATTACTT TTCGAACTGCGGGTGGCTCC	Amplification of Strep-tag and the following terminator sequence
SpeI-His- SP <i>pvdP</i> -for-MS	GATCAAAGTAGTAGGAGATAT ACATATGACACACCATCACCA TCACCATATCTCTCGACGTGG GTTTCATCG	Amplification of <i>pvdP</i> with a N-terminal His-tag and insertion of a N-terminal SpeI restriction site for cloning into pUCP20- ANT2-MCS
<i>pvdP</i> -XbaI-rev- MS	GCTTGTCCGCTCTAGAATTCAT TAAAGCGTGTGCGTGACC	Amplification of <i>pvdP</i> and insertion of a C-terminal XbaI restriction site for cloning into pUCP20-ANT2-MCS
SpeI-SP <i>pvdP</i> - for-MS	GATCAAAGTAGTAGGAGATAT ACATATGACAATCTCTCGACG TGGGTTTCATCGC	Amplification of <i>pvdP</i> and insertion of a N-terminal SpeI restriction site for cloning into pUCP20-ANT2-MCS

<i>pvdP</i> -His-XbaI-rev-MS	GCAGGTCTGACTCTAGAATTCA TTAATGGTGATGGTGATGGTG AAGCGTGTGCGTGACCTTCAA ATGTCGG	Amplification of <i>pvdP</i> with a C-terminal His-tag and insertion of a C-terminal XbaI restriction site for cloning into pUCP20-ANT2-MCS
<i>pvdP</i> -Strep-XbaI-rev-MS	GCAGGTCTGACTCTAGAATTCA TTACTTTTCGAACTGCGGGTG GCTCCAAAGCGTGTGCGTGAC CTTCAAATGTCGG	Amplification of <i>pvdP</i> with a C-terminal Strep-tag and insertion of a C-terminal XbaI restriction site for cloning into pUCP20-ANT2-MCS
<i>pvdP</i> -A22C-for-MS	GCGGTGCCTGCGTGCTTTTATG CCC	QuikChange primer for substitution of A22C in <i>pvdP</i>
<i>pvdP</i> -A22C-rev-MS	GGGCATAAAAGCACGCAGGC ACCGC	QuikChange primer for substitution of A22C in <i>pvdP</i>
<i>pvdP</i> -A25C-for-MS	GCCTTTTATTGCCATCGCGAGT TGACG	QuikChange primer for substitution of A25C in <i>pvdP</i>
<i>pvdP</i> -A25C-rev-MS	CGTCAACTCGCGATGGCAATA AAAGGC	QuikChange primer for substitution of A25C in <i>pvdP</i>
<i>pvdP</i> -H26C-for-MS	CCTTTTATGCCTGCCGCGAGTT GACG	QuikChange primer for substitution of H26C in <i>pvdP</i>
<i>pvdP</i> -H26C-rev-MS	CGTCAACTCGCGGCAGGCATA AAAGG	QuikChange primer for substitution of H26C in <i>pvdP</i>
<i>pvdP</i> -R27C-for-MS	GCCTTTTATGCCATTGCGAGT TGACGCGGG	QuikChange primer for substitution of R27C in <i>pvdP</i>
<i>pvdP</i> -R27C-rev-MS	CCCGCGTCAACTCGCAATGGG CATAAAAGGC	QuikChange primer for substitution of R27C in <i>pvdP</i>
<i>pvdP</i> -E28C-for-MS	GCCTTTTATGCCATCGCTGCT TGACGCGGG	QuikChange primer for substitution of E28C in <i>pvdP</i>
<i>pvdP</i> -E28C-rev-MS	CCCGCGTCAAGCAGCGATGGG CATAAAAGGC	QuikChange primer for substitution of E28C in <i>pvdP</i>
<i>pvdP</i> -F35C-for-MS	GGAAGACGAGTGCCCCATCAC CCCCGG	QuikChange primer for substitution of F35C in <i>pvdP</i>
<i>pvdP</i> -F35C-rev-MS	CCGGGGGTGATGGGGCACTCG TCTTCC	QuikChange primer for substitution of F35C in <i>pvdP</i>
<i>pvdP</i> -NdeI-deletion-1-for-MS	CTTCATGCACCGCCACATGCTT GGCACCGC	QuikChange primer for deletion of internal NdeI restriction site in <i>pvdP</i>
<i>pvdP</i> -NdeI-deletion-1-rev-MS	GCGGTGCCAAGCATGTGGCGG TGCATGAAG	QuikChange primer for deletion of internal NdeI restriction site in <i>pvdP</i>
<i>pvdP</i> -NdeI-deletion-2-for-MS	ACGACTGGCTGCACATGCGTT GGGCC	QuikChange primer for deletion of internal NdeI restriction site in <i>pvdP</i>

<i>pvdP</i> -NdeI-deletion-2-rev-MS	GGCCCAACGCATGTGCAGCCA GTCGT	QuikChange primer for deletion of internal NdeI restriction site in <i>pvdP</i>
pEX-tac-HindIII-for-MS	CGTTCATAAGCTTATCGATGA TAAGCTGTCAAACATGAGAAT TCTTGAAG	Primer for amplification of pEX-tac backbone and substituting XbaI restriction site by SpeI restriction site
pEX-tac-SpeI-rev-MS	CAGTACTAGTGTGAAATTGTT ATCCGCTCACAATTCACACA TTATACGA	Primer for amplification of pEX-tac backbone and substituting XbaI restriction site by SpeI restriction site
PfA506- <i>fpvR</i> -F1-MS	TCAAGAATTCCGATGAACTCA CCGCCCCAGCTTGACCGGTC CGAACTCCATGCG	Primer for left flanking region of <i>fpvR</i>
PfA506- <i>fpvR</i> -R1-MS	CTTTTCGCTCATTA ACTCATCC TGATTCCCACATTCTAACCTC CCAAGGTGG	Primer for left flanking region of <i>fpvR</i>
PfA506- <i>fpvR</i> -F2-MS	GTTAATGAGCGAAAAGCGTAA AGCCCCAAGGGCTGAGCCCG CTCGCACGAAGCG	Primer for right flanking region of <i>fpvR</i>
PfA506- <i>fpvR</i> -R2-MS	ATTCAAGCTTACCGGCGGCCT GGTTGATCGACAGCACGCCGT CGTATTGCTGGCCGCTGTG	Primer for right flanking region of <i>fpvR</i>

Table 3: Used primers for sequencing.

Name	Sequence	Use
pUCP20-seq-for-MS	CACCGCATCGCAGCCGC TTAATG	For pUCP20-ANT2-MCS constructs; binds upstream of MCS
pUCP20-seq-rev-MS	CGACGTTGTAAAACGAC GGCCAGTGCC	For pUCP20-ANT2-MCS constructs; binds downstream of terminator
<i>pvdP</i> -seq-for-MS	GACTTGCCGTCCTGGCC GCAATTTCCC	For <i>pvdP</i> ; binds within <i>pvdP</i>
PfA506- <i>fpvR</i> -DF-MS	GAACTGCCGCCGCAACG TTGCGCAATTTGCTGTA C	For genomic deletion of <i>fpvR</i> , binds upstream of deleted region
PfA506- <i>fpvR</i> -DR-MS	GCTGTCTCAGCCATGTA ACACTGCCTGTGACAGA ACCATGAATCCGC	For genomic deletion of <i>fpvR</i> , binds downstream of deleted region

Table 4: Used plasmids.

Plasmid	Description	Reference
pME6010	Small shuttle vector for constitutive expression in pseudomonads, tet ^R	(Heeb <i>et al.</i> 2000)
pME6010-RBS- <i>matpvdM</i> -Strep-term	Derivative of pME6010 for constitutive production of mature PvdM in <i>P. fluorescens</i> A506, tet ^R	This work
pEX-H5-tac	pEXH5 derivate with a <i>tac</i> -promotor, amp ^R	(Richter and Brüser 2005)
pEX- <i>pvdP</i> -His-term-tac	Derivative of pEX-H5-tac for constitutive production of PvdP in <i>E. coli</i> BL21 (DE3), amp ^R	This work
pEX- <i>pvdM</i> -Strep-tac	Derivative of pEX-H5-tac for constitutive production of PvdM in <i>E. coli</i> BL21 (DE3), amp ^R	This work
pEXPT7	Expression vector with T7-promotor, amp ^R	Michael Ringel, unpublished
pEXPT7- <i>pvdN</i> -Strep	Derivative of pEXPT7 for production of Strep-tagged PvdN in <i>E. coli</i> BL21 (DE3), amp ^R	Michael Ringel, unpublished
pCA528	pET24a containing SMT3 from yeast (His6-SUMO), kan ^R	(Andréasson <i>et al.</i> 2008)
pCA528- <i>matpvdN</i>	Derivative of pCA528 for production of SUMO-tagged PvdN in <i>E. coli</i> BL21 (DE3), kan ^R	Ali Burdur, unpublished
pCA528- <i>matpvdN</i> _{H260A}	Derivative of pCA528 for production of SUMO-tagged PvdN _{H260A} in <i>E. coli</i> BL21 (DE3), kan ^R	This work
pMK-RQ- <i>pvdM</i> -ASA	pMK-RQ derivate with synthesized fragment of <i>pvdM</i> containing ASA cutting site, kan ^R	This work
pUCP20-ANT2-MCS	Anthranilate-inducible expression vector for pseudomonads, kan ^R	(Hoffmann <i>et al.</i> 2021)

pUCP20-ANT2-MCS- His- <i>pvdM</i> -Strep-term	Derivative of pUCP20-ANT2-MCS for production of PvdM in <i>P. fluorescens</i> A506, kan ^R	This work
pUCP20-ANT2-MCS- <i>pvdM</i> -ASA-Strep-term	Derivative of pUCP20-ANT2-MCS for production of PvdM with inserted ASA-cutting site in <i>P. fluorescens</i> A506, kan ^R	This work
pUCP20-ANT2-MCS- <i>pvdM</i> -M246A-Strep-term	Derivative of pUCP20-ANT2-MCS for production of PvdM _{H246A} in <i>P. fluorescens</i> A506, kan ^R	This work
pUCP20-ANT2-MCS- His- <i>pvdM</i> -H266A- Strep-term	Derivative of pUCP20-ANT2-MCS for production of PvdM _{H266A} in <i>P. fluorescens</i> A506, kan ^R	This work
pUCP20-ANT2-MCS- His-SP <i>pvdO</i> - <i>matpvdM</i> - Strep-term	Derivative of pUCP20-ANT2-MCS for production of mature PvdM fused to PvdO-signal peptide in <i>P. fluorescens</i> A506, kan ^R	This work
pUCP20-ANT2-MCS- <i>phoA</i> -Strep-term	Derivative of pUCP20-ANT2-MCS for production of PhoA in <i>P. fluorescens</i> A506, kan ^R	This work
pUCP20-ANT2-MCS- <i>matphoA</i> -Strep-term	Derivative of pUCP20-ANT2-MCS for production of mature PhoA in <i>P. fluorescens</i> A506, kan ^R	This work
pUCP20-ANT2-MCS- His-SP <i>pvdM</i> - <i>matphoA</i> - Strep-term	Derivative of pUCP20-ANT2-MCS for production of mature PhoA fused to PvdM-signal peptide in <i>P. fluorescens</i> A506, kan ^R	This work
pUCP20-ANT2-MCS- His-SP <i>pvdO</i> - <i>matpvdM</i> -Strep-term	Derivative of pUCP20-ANT2-MCS for production of mature PhoA fused to PvdO-signal peptide in <i>P. fluorescens</i> A506, kan ^R	This work
pUCP20-ANT2-MCS- His- <i>pvdP</i> -term	Derivative of pUCP20-ANT2-MCS for production of PvdP in <i>P. fluorescens</i> A506, kan ^R	This work

pUCP20-ANT2-MCS- <i>pvdP</i> -His-term	Derivative of pUCP20-ANT2-MCS for production of PvdP in <i>P. fluorescens</i> A506, kan ^R	This work
pUCP20-ANT2-MCS- <i>pvdP</i> -Strep-term	Derivative of pUCP20-ANT2-MCS for production of PvdP in <i>P. fluorescens</i> A506, kan ^R	This work
pUCP20-ANT2-MCS- <i>pvdP</i> -A22C-His-term	Derivative of pUCP20-ANT2-MCS for production of PvdP _{A22C} in <i>P. fluorescens</i> A506, kan ^R	This work
pUCP20-ANT2-MCS- <i>pvdP</i> -A25C-His-term	Derivative of pUCP20-ANT2-MCS for production of PvdP _{A25C} in <i>P. fluorescens</i> A506, kan ^R	This work
pUCP20-ANT2-MCS- <i>pvdP</i> -H26C-His-term	Derivative of pUCP20-ANT2-MCS for production of PvdP _{A26C} in <i>P. fluorescens</i> A506, kan ^R	This work
pUCP20-ANT2-MCS- <i>pvdP</i> -R27C-His-term	Derivative of pUCP20-ANT2-MCS for production of PvdP _{R27C} in <i>P. fluorescens</i> A506, kan ^R	This work
pUCP20-ANT2-MCS- <i>pvdP</i> -E28C-His-term	Derivative of pUCP20-ANT2-MCS for production of PvdP _{E28C} in <i>P. fluorescens</i> A506, kan ^R	This work
pUCP20-ANT2-MCS- <i>pvdP</i> -F35C-His-term	Derivative of pUCP20-ANT2-MCS for production of PvdP _{E35C} in <i>P. fluorescens</i> A506, kan ^R	This work
pK18 <i>mobsacB</i>	Derivative of pK18 with mob region of RP4 and a modified <i>sacB</i> of <i>Bacillus subtilis</i>	(Schäfer <i>et al.</i> 1994)
pK18 <i>mobsacB</i> - Δ <i>fpvR</i>	Derivate of pK18 <i>mobsacB</i> for scarless in frame deletion of <i>fpvR</i> in <i>P. fluorescens</i> A506	This work

2.2 Cultivation of bacteria

2.2.1 Media, antibiotics and solutions

All media used in this work was autoclaved for 20 min at 120 °C and 1 bar gauge pressure before use (Systec VX-150 or Systec DE-23, Systec, Linden). Heat sensitive components such as antibiotics and sugars were sterile filtered using a Filtropur S sterile filter with a pore size of 0.2 µM (Sarstedt, Nümbrecht) and added after autoclaving. Incubation in liquid medium was performed aerobically at 180 rpm and at 30°C for *Pseudomonas fluorescens* A506 and 37°C for *Escherichia coli* strains, respectively.

If the medium was to be used as a solid medium, 1.5 % (w/v) agar was added before autoclaving.

Table 5: Composition of Luria Bertani (LB) medium.

Ingredient	Concentration
Tryptone	1 % (w/v)
NaCl	1 % (w/v)
Yeast extract	0.5 % (w/v)

Table 6: Composition of super optimal broth medium supplemented with glucose.

Ingredient	Concentration
Tryptone	2 % (w/v)
Yeast extract	0.5 % (w/v)
NaCl	10 mM
KCl	2.5 mM
MgCl ₂	10 mM
MgSO ₄	10 mM
Glucose	20 mM

Table 7: Composition of Casamino acids (CAA) medium.

Ingredient	Concentration
Casamino acids	0.5 % (w/v)
K ₂ HPO ₄	5 mM
MgSO ₄	1 mM
EDDHA	1.38 mM

Table 8. Composition of M9 salt solution (5X).

Ingredient	Concentration
Na ₂ HPO ₄	30 g/l
KH ₂ PO ₄	15 g/l
NH ₄ Cl	5 g/l
NaCl	2.5 g/l
H ₂ O	-

Table 9: Composition of M9 mineral medium.

Ingredient	Concentration
5 x M9 Salze	200 ml/l
Phosphate buffer (pH 7.0)	50 mM
MgSO ₄	1 mM
Glucose	0.4 %
CaCl	0.1 mM
FeCl ₃	1 μM
H ₂ O	-

Table 10: List of used antibiotics.

Antibiotic	Stock solution	Final concentration
Ampicillin	100 mg/ml	100 µg/ml
Chloramphenicol	25 mg/ml	25 µg/ml
Kanamycin	50 mg/ml	50 µg/ml
Tetracycline	12.5 mg/ml	12.5 µg/ml for <i>E. coli</i> ; 25 µg/ml for <i>P. fluorescens</i>

2.3 Molecular methods

2.3.1 Preparation of plasmids

For the extraction of pure plasmid DNA, the peqGOLD Plasmid Miniprep Kit I (peqlab/VWR, Erlangen) was used according to the manufacturers protocol. The obtained DNA was eluted in 50 µl distilled H₂O and, before being stored away at -20 °C for further experiments, the concentration of DNA was determined using Nanodrop2000 spectrophotometer (Thermo Scientific, Dreieich).

2.3.2 Preparation of genomic DNA

Pure genomic DNA was extracted using Monarch[®] Genomic DNA Purification Kit (New England Biolabs, Frankfurt), according to the manufacturers protocol. The genomic DNA bound to the silica membrane was eluted using 100 µl nuclease-free water.

2.3.3 Polymerase chain reaction (PCR)

A polymerase chain reaction was carried out for various purposes, either for the amplification of a DNA fragment via standard PCR, the verification of a deletion via colony PCR, the substitution of bases by site-directed-mutagenesis via QuikChange[®] PCR (Agilent, Waldbronn) or the fusion of two DNA fragments by fusion PCR. For all different PCR approaches, the Phusion[®] High-Fidelity DNA Polymerase or the Q5[®] High-Fidelity DNA Polymerase (New England Biolabs, Frankfurt am Main) were always used. To perform the various PCR runs, the FlexCycler2 PCR Thermal Cycler (Analytik Jena, Jena) was used.

In case of the standard PCR, two oligonucleotide primers flanking the region of interest were designed and used for the amplification of the DNA fragment (Biomers, Ulm). The oligonucleotide primers were dissolved in nuclease free water according to the manufacturer's instructions resulting in stock solution with a concentration of 100 pmol/ μ l. This stock solution was diluted 1:10 resulting in a working solution with a concentration of 10 pmol/ μ l. The final concentration of the oligonucleotide primers in the reaction mix was 25 pmol/ μ l. The standard annealing temperature was set at 55 °C, but could be changed to a higher temperature depending on the outcome of the PCR. The elongation time was set depending on the size of the fragment that was to be amplified (30 sec per kb).

Table 11: Pipetting scheme for a standard PCR.

Ingredient	Volume
Template DNA (10-100 ng/ μ l)	1 μ l
Forward Primer (10 pmol/ μ l)	2.5 μ l
Reverse Primer (10 pmol/ μ l)	2.5 μ l
dNTPs (10 pmol/ μ l)	1 μ l
Polymerase	0.5 μ l
5 X Phusion HF or GC Buffer/5X Q5	10 μ l
Reaction Buffer	
DMSO (optional)	1.5 μ l
Nuclease free water	to 50 μ l

Table 12: Thermal profile for a standard PCR.

Step	Temperature	Duration
1. Initial Denaturation	96-98 °C	3 min
2. Denaturation	96-98 °C	45 sec
3. Primer annealing	55 °C	30 sec
4. Elongation	68-72 °C	30 sec/kb
5. Final Extension	68-72 °C	30 sec/kb
6. Storing	16 °C	∞

For the verification of a genomic deletion, a colony PCR was performed by setting up the standard PCR reaction mix with all the ingredients except the template DNA. Next, a colony was picked from an agar plate using a sterile toothpick. The cells attached to the toothpick were added to the reaction mix by holding the tip of the toothpick in the reaction mix and moving it back and forth. Subsequently, an amplification of the desired fragment was carried out using the standard protocol.

For a site-directed-mutagenesis via QuikChange[®] PCR (Agilent, Waldbronn), a complement oligonucleotide primer pair was designed, that contained the desired exchanges in the middle of the primer. The exchanges in the oligonucleotide primers were flanked by approximately 25 bases to ensure specific binding to the template DNA. After the amplification of the DNA with the insertion of the desired mutation using the standard PCR protocol, the template DNA was degraded by adding 1 µl DpnI to the reaction mix and incubating the reaction mix for 3 h at 37 °C.

For the fusion of two DNA fragments, a two-step PCR set up was performed. In a first PCR cycle, the fragments with an overlapping 5' end of at least 15 bp and all necessary ingredients excluding primers were added to a reaction mix and incubated using the standard PCR protocol. With no primers in the reaction mix, the two overlapping fragments served each other as primers. The PCR run was stopped after 10 reaction cycles and 2.5 µl of the forward primer of fragment one and the reverse primer of fragment two, respectively, were added before starting a new PCR run according to the standard PCR protocol.

Table 13: Pipetting scheme for a fusion PCR.

Ingredient	Volume
DNA Fragments (10-100 ng/ μ l)	1 μ l
Forward Primer (10 pmol/ μ l)	2.5 μ l
Reverse Primer (10 pmol/ μ l)	2.5 μ l
dNTPs (10 pmol/ μ l)	1 μ l
Polymerase	0.5 μ l
5 X Phusion HF or GC Buffer/5X Q5 Reaction Buffer	10 μ l
DMSO (optional)	1.5 μ l
Nuclease free water	to 50 μ l

Table 14: Thermal profile for a fusion PCR.

Step	Temperature	Duration
1. Initial Denaturation	96-98 °C	3 min
2. Denaturation	96-98 °C	45 sec
3. Primer annealing	55 °C	30 sec
4. Elongation	68-72 °C	30 sec/kb
5. Addition of Primers	-	-
6. Initial Denaturation	96-98°C	3 min
7. Denaturation	96-98 °C	45 sec
8. Primer annealing	55 °C	30 sec
9. Elongation	68-72 °C	30 sec/kb
10. Final Extension	68-72 °C	30 sec/kb
11. Storing	16 °C	∞

2.3.4 Restriction of DNA

The restriction of DNA was carried out preparing a reaction mix and incubating the contained DNA and the added restriction endonucleases (New England Biolabs, Frankfurt) for 1 h at

37 °C using the thermo cell mixing block MB-102 (Bioer, Hangzhou, China). If High-Fidelity (HF[®]) restriction endonucleases were used (New England Biolabs, Frankfurt), the incubation time was reduced to 15 min. If the restriction endonucleases NdeI or DpnI were used, the incubation time was prolonged to 3 h.

Table 15: Pipetting scheme for a standard DNA restriction.

Ingredient	Volume
DNA	25 µl
10 x CutSmart [®] buffer	5 µl
restriction endonucleases	1 µl per restriction endonucleases
H ₂ O	Ad 50 µl

2.3.5 Agarose gel electrophoresis

For the separation of DNA fragments according to their size-depending negative charge, an agarose gel electrophoresis approach was used. A final concentration of 1.5 % agarose was dissolved in TAE-Puffer [40 mM Tris, 20 mM acetate, 1 mM EDTA] by heating up the solution. The liquid agarose was then cooled down and 4-6 µl HD-Green+ DNA Stain (Intas, Göttingen) were added. After stirring the solution for a uniform mixing, the solution was poured into agarose gel chambers Perfect Blue[™] gel system Mini S, Mini M or Mini L (peqlab/VWR, Erlangen), depending on the total amount of samples. Before loading the samples onto the agarose gels, 1/6 of the total volume of loading dye was added [50 % (w/v) glycerine, 200 mM EDTA, 0.2 % (w/v) xylene cyanole or bromphenole blue]. For the separation of the DNA fragments in the gel, a voltage of 100-120 volt was applied for 30-60 min by the Power Pac 300 power supply (Biorad, Feldkirchen). As a standard, the markers SERVA FastLoad 100 bp DNA Ladder or SERVA FastLoad 1 kb DNA Ladder (SERVA, Heidelberg) were used. The detection of the separated DNA fragments was carried out under UV light using the UV-system Gel Stick Imager (Intas, Göttingen).

2.3.6 Purification of DNA fragments

For the purification and elution of DNA fragments from a separation via agarose gel electrophoresis or a restriction set up, the NucleoSpin Gel and PCR Clean-up Mini kit (Macherey-Nagel, Düren) was used according to the manufacturer's protocol. The DNA fragments bound to the silica membrane were eluted in 30 µl nuclease-free water.

2.3.7 Ligation of DNA

For the ligation of multiple linearised DNA fragments or a QuikChange PCR reaction set-up, purified DNA was used. 0.02 pmol of each DNA fragment were used in a reaction mix with 2 µl T4-DNA Ligation buffer and 1 µl T4 DNA Ligase (New England Biolabs, Frankfurt) with a total volume of 20 µl. The ratio of backbone DNA and insert DNA was 1:5, meaning that the concentration of the backbone DNA was 0.02 pmol and the concentration of the insert was 0.1 pmol. The reaction mix was incubated overnight at 16 °C using the thermo cell mixing block MB-102 (Bioer, Hangzhou, China). 10 µl of the reaction set up were used for transformation.

2.3.8 Production of competent *E. coli* cells

For the production of competent *E. coli* cells, an overnight culture, which was incubated at 37 °C and 180 rpm, was used to inoculate 25 ml LB medium. This culture was then incubated at 37 °C and 180 rpm until an OD₆₀₀ of 0.6 was reached. The cells were then cooled on ice for 20 min before being centrifuged for 10 min at 6,800 xg and 4 °C. The supernatant was discarded and the cell pellet was resuspended in 7.5 ml transformation buffer [10 mM PIPES (pH 6.7), 55 mM MnCl₂, 15 mM CaCl₂, 250 mM KCl]. The suspension was again incubated on ice for 45 min prior to a second centrifugation step of 10 min at 6,800 xg and 4 °C. The supernatant was again discarded and the resulting pellet was resuspended in 2.5 ml transformation buffer and incubated on ice for another 45 min. After adding 160 µl DMSO and mixing the suspension vigorously, the cells were incubated for a last time on ice for 10 min and aliquoted. The aliquots were frozen in liquid nitrogen and stored away at -80 °C.

2.3.9 Transformation of *E. coli*

For the transformation of *E. coli*, 100 µl competent cells were thawed on ice and mixed with DNA. After an incubation on ice for 15 min, a heat shock at 42 °C for 1 min was applied before the cells were shifted on ice for another incubation of 15 min. Subsequently, 1 ml SOC medium [2 % (w/v) tryptone, 0,5 % (w/v), yeast extract, 10 mM NaCl, 2,5 mM KCl, 10 mM MgCl₂, 10 mM MgSO₄, 20 mM glucose] were added to the cells and the suspension was incubated for one hour at 37 °C and 600 rpm. Finally, the cells were centrifuged for 5 min at 8000 rpm, the supernatant was discarded and the resulting pellet was resuspended in 50 µl LB medium. The cells were then plated on LB agar plates with the appropriate antibiotic and incubated overnight at 37 °C.

2.3.10 Fast transformation of *E. coli*

For the fast transformation of *E. coli* strains, which were not in stock as competent cells, a main culture of 5 ml LB medium was inoculated with 100 µl of an overnight culture, which has been incubated at 37 °C and 180 rpm. The main culture was incubated at 37 °C and 180 rpm until an OD₆₀₀ of 0.3-0.4 was reached. The cells were then cooled on ice for 30 min and 1 ml of the main culture was centrifuged for 5 min at 6,800 xg. The supernatant was discarded and the resulting pellet was resuspended in 100 µl TSS buffer [LB medium (pH 6.5), 10 % (w/v) PEG 6000, 5 % (v/v) DMSO, 33 mM MgSO₄]. After addition of the DNA, the cells were incubated on ice for 30 min and 1 ml of SOC medium was added. The cell suspension was then incubated for one hour at 37 °C and 600 rpm before being centrifuged for 5 min at 8,000 rpm. The supernatant was again discarded and the resulting pellet was resuspended in 50 µl LB medium and cells were plated on LB agar plates with the appropriate antibiotic and incubated overnight at 37 °C and checked the next day for growth of colonies.

2.3.11 Electroporation of *P. fluorescens* A506

For the electroporation of *P. fluorescens* A506, 1.5 ml of an overnight culture, which has been incubated at 30 °C and 180 rpm, was centrifuged for 3 min and 7,000 rpm. The resulting pellet was washed three times with 1 ml of sucrose [300 mM]. After the last washing step, the

supernatant was discarded and the pellet was resuspended in 100 μ l sucrose [300 mM]. The DNA, that was to be transformed into the strain, was mixed with the suspended cells and electroporated, using a cuvette with a width of 2 mm and an exponential decay pulse at 200 μ F, 200 Ω and 2,500 V applied by the Gene Pulser Xcell Electroporation System (Biorad, Feldkirchen). After addition of 1 ml LB medium to the electroporated cells, the suspension was incubated for 2 h at 30 °C and 600 rpm before being plated on LB agar plates with the appropriate antibiotic. The plated cells were then incubated overnight at 30 °C and checked the next day for growth of colonies.

2.3.12 Genomic deletion in *P. fluorescens* A506

For constructing scarless deletion mutants of *P. fluorescens* A506, a protocol established by Michael Ringel was used (Ringel 2018). Left and right flanking regions of the gene, which was to be deleted were cloned into the plasmid pK18mobSacB by fusion PCR and transformed into *P. fluorescens* A506 by electroporation. The transformants were plated onto kanamycin containing LB agar plates and incubated. Kanamycin containing LB medium was inoculated with colonies grown on the agar plate and incubated overnight, before being diluted 1:1,000 and 50 μ l of each picked colony were plated onto a 10 % sucrose containing LB agar plate and incubated overnight. Colonies grown on 10 % sucrose containing LB agar plate were picked and patched onto a new 10 % sucrose containing LB agar plate and a kanamycin containing agar plate. After incubation overnight, colonies that were able to grow on the 10 % sucrose containing LB agar plate but not on the LB-agar plate containing kanamycin, were picked and incubated in 5 ml LB medium. With genomic DNA extracted from the selected colonies, a PCR was run amplifying the region of interest with primers binding outside of the flanking regions cloned into the plasmid pK18mobSacB in the beginning. The obtained PCR product was purified and sequenced for verification of the intended deletion.

2.4 Biochemical methods

2.4.1 Isolation of periplasm, cytoplasm and total membrane fraction in *E. coli*

For the subcellular fractionation of *E. coli*, 50 ml LB medium were inoculated with 2 ml of an overnight culture and incubated at 37 °C and 180 rpm. After 3 h, the cells were harvested by centrifugation for 10 min at 4,500 rpm and 4 °C. The resulting pellet was resuspended in 20 ml TES buffer [10 mM Tris-HCl pH 8.0; 20 % (w/v) sucrose] and incubated for 10 min at room temperature, before being pelleted again. The supernatant was discarded and the pellet was resuspended in 1 ml ice-cold MgSO₄ [5 mM] and incubated on ice. After 20 min, the cells were once again centrifuged for 10 min at 13000 rpm and 4 °C using a Heraeus Megafuge 8R benchtop centrifuge (Thermo Scientific, Dreieich). The resulting supernatant was collected as the periplasmic fraction. The pellet was resuspended in 1 ml ice-cold 5 mM MgSO₄ and the cells were disrupted by 3 cycles of sonication, each cycle consisting of 30 seconds intervals with 50 % duty cycle and intensity level 3, applied by ultrasonic homogenizer Branson 250 Sonifier (Branson, Saint Louis, USA). The disrupted cells were centrifuged for 15 min at 13,000 rpm and 4 °C, sedimenting intact cells and cell debris. The supernatant was removed and centrifuged for 45 min at 130,000 xg and 4 °C. The supernatant was kept as a cytoplasmic fraction and the resulting pellet was resuspended in ice-cold 5 mM MgSO₄ according to the total sample volume.

2.4.2 Isolation of periplasm, cytoplasm and total membrane fraction in *P. fluorescens*

The subcellular fractionation of *P. fluorescens* was based on a protocol by Izé *et al.* (Izé *et al.* 2014). Cells corresponding to 100 ml of an OD₆₀₀ of 1 were harvested by centrifuging 15 min at 4,500 xg and 4 °C using Heraeus Megafuge 8R benchtop centrifuge (Thermo Scientific, Dreieich). The received pellet was washed once in 1 ml buffer A [50 mM Tris-HCl (pH 7.6)] and resuspended in 1 ml buffer B [200 mM MgCl₂, 50 mM Tris-HCl (pH 7.6)]. The cell suspension was first incubated for 30 min at 30 °C and 500 rpm, then put on ice for 5 min and finally incubated for 15 min at room temperature. After that, the cells were centrifuged for 10 min at 8,000 xg and 4 °C and the supernatant was taken as a periplasmic fraction. The remaining cells were once again washed in 1 ml buffer A and resuspended in 1 ml buffer A, before being disrupted via 3 cycles of sonication, each cycle consisting of 30 seconds intervals at 50 % duty

cycle and intensity level 3 using the ultrasonic homogenizer Branson 250 Sonifier (Branson, Saint Louis, USA). The disrupted cells were centrifuged for 15 min at 13,000 xg and 4 °C to remove cell debris using a Heraeus Megafuge 8R benchtop centrifuge (Thermo Scientific, Dreieich). 750 µl of the supernatant containing the cytoplasm and the membrane, was ultracentrifuged for 45 min at 130,000 xg and 4 °C using the Sorvall Discovery M120SE (Thermo Scientific, Dreieich). The supernatant was collected as the cytoplasmic fraction and the pellet containing the membrane was resuspended in 750 µl buffer A.

2.4.3 Carbonate wash

To verify that a protein is indeed membrane integrated and not only loosely attached to the membrane, the fractions obtained in the subcellular fractionation (chapter 2.4.2) were treated with carbonate buffer. For that purpose, the fraction containing both the cytoplasm and the membrane fraction after cell sonication was split into two parts. One sample was treated according to the protocol described above, the other sample was ultracentrifuged for 45 min at 130,000 xg and 4 °C, the supernatant was discarded and the obtained membrane pellet was resuspended in 375 µl ice-cold 100 mM Na₂CO₃. The resuspended membrane was again ultracentrifuged for 45 min at 130,000 xg and 4 °C. The supernatant was kept as part of the carbonate wash fraction and the pellet was again resuspended in 375 µl ice-cold 100 mM Na₂CO₃.

2.4.4 Protease accessibility assay

For protease accessibility assays, an established protocol was used (Porcelli *et al.* 2002). A cell pellet corresponding to 100 ml of an OD₆₀₀ of 1 was resuspended in 2.5 ml permeabilization buffer [33 mM Tris-HCl (pH 8.0), 40 % sucrose, 5 mM Na₂EDTA] and incubated for 30 min at 4 °C. The suspended cells were centrifuged for 15 min at 7,000 xg and the cells were resuspended in 1 ml stabilization buffer [33 mM Tris-HCl (pH 8.0) and 40 % sucrose], keeping the cells and the buffers constantly on ice. The permeabilized cells were then aliquoted into working samples of 200 µl. These samples were then incubated for 30 min at 25 °C in the presence of 0.5 mg/ml proteinase K with and without 2 % (v/v) Triton X-100, respectively.

2.4.5 Alkaline phosphatase (PhoA) activity assay

To test the activity of the alkaline phosphatase (PhoA), an enzyme assay was performed with whole cells. The assay is based on the removal of the phosphate group (PO_4^{3-}) from the colourless substrate *p*-nitrophenyl phosphate (pNPP) retaining the yellow-coloured *p*-nitrophenol (pNP) and a phosphate. For this, LB medium was inoculated with 125 μl of an overnight culture and incubated to an OD_{600} of 0.8 - 1.0 at the temperature corresponding to the growth optimum of the respective cells. The cultures were then chilled on ice for 20 min before 500 μl of cell culture were sedimented for 10 min at 13,000 $\times g$ and 4 °C using a Heraeus Megafuge 8R benchtop centrifuge (Thermo Scientific, Dreieich). The obtained cell pellet was then resuspended in 2 ml Tris-HCl (pH 8.0). OD_{600} was determined with 1 ml of this suspension. To the remaining 1 ml, 100 μl PNPP solution [0.4 % (w/v) pNPP in 1 M Tris-HCl, pH 8] was added and incubated until a distinct yellow colouration was visible, but for no longer than 10 min. The reaction was then stopped by adding 100 μl 1M K_2HPO_4 . The reaction mixture was then centrifuged at 13,000 $\times g$ and 4 °C for 2 min. Finally, the absorbance at 420 nm was measured from the obtained supernatant using the DS-11 UV-Vis Spectrophotometer (DeNovix, Wilmington) and the activity was calculated using the following formula:

$$Activity = \frac{1000 \times E_{420}}{reaction\ time\ [min] \times 1\ ml \times OD_{600}}$$

Since alkaline phosphatase (PhoA) is normally only active in the periplasm, this enzyme assay can be used to investigate the correct translocation of proteins from the cytoplasm into the periplasm (Brickman and Beckwith 1975; Manoil and Beckwith 1986; Manoil 1991).

2.4.6 Recombinant protein production

For the production of recombinant proteins in *E. coli*, the strain *E. coli* BL21 (DE3) was used. After inoculation of the main culture with an overnight culture to an OD₆₀₀ of 0.1, the cells were incubated at 37 °C and 180 rpm until they reached an OD₆₀₀ of 0.5-0.7. By adding 1 mM IPTG, overexpression was started and the cells were incubated overnight at a lowered temperature of 22 °C and 180 rpm. For the production of recombinant proteins in *P. fluorescens*, the strain *P. fluorescens* A506 was used. After the main culture has been inoculated with an overnight culture to an OD₆₀₀ of 0.1, the cells were incubated at 30 °C and 180 rpm until they reached an OD₆₀₀ of 0.5. By adding 0.1 mM anthranilic acid, overexpression was started and the cells were incubated for another 3 h at 30 °C. For harvesting the cells, the cell suspension was centrifuged for 15 min at 6,000 xg and 4 °C in a Sorvall Lynx 4000 superspeed centrifuge (Thermo Scientific, Dreieich). The cell pellet was resuspended in Tris-HCl buffer and centrifuged for another 15 min at 4,500 xg at 4 °C using a benchtop centrifuge 5804 R (Eppendorf, Hamburg). The obtained cell pellet was frozen in liquid nitrogen and stored at -20 °C.

2.4.7 Cell disruption

For cell disruption on a large scale, namely culture volume of more than 100 ml, the French press French Pressure Cell Press Model FA-078 (SLM Aminco, Urbana, USA) or the LV1 Low Volume Microfluidizer[®] Homogenizer (Microfluidics, Westwood, USA) were used. In both cases, the pellet was resuspended in 10 times the pellet volume (for example 5 ml pellet volume were resuspended in a total volume of 50 ml) with the appropriate buffer on ice with the addition of 100 µl (10 mg/ml) DNase I and 2 mM PMSF. If using the French press, the cell disruption was performed by three passages at a pressure of 18,000 psi. All portable parts of the French press were cooled and stored at 4 °C prior to use. When using the Low Volume Microfluidizer, cells were disrupted by one passage at 30,000 psi cooling the suction loop with ice.

Cells harvested from a culture volume of less than 100 ml were disrupted using the ultrasonic homogenizer Branson 250 Sonifier (Branson, Saint Louis, USA). If not stated otherwise, cells were disrupted by 3 cycles of sonication, each cycle consisting of 30 seconds intervals at 50 % duty cycle and an intensity level of 3. During the entire disruption, cells were cooled on ice.

After disruption of the cells, the suspension was centrifuged for 15 min at 4,500 xg and 4 °C using a benchtop centrifuge Megafuge 8R (Thermo Scientific, Dreieich) to get rid of intact cells and cell debris. The obtained supernatant was then ultracentrifuged for 45 min at 130,000 xg and 4 °C using either the Sorvall Discovery M120SE (Thermo Scientific, Dreieich) or Optima L-80 XP (Beckman Coulter, Krefeld). Depending on the protein, either the supernatant or the pellet was used for further purification steps.

2.4.8 Immobilized Ni-NTA affinity chromatography

For purification of produced hexahistidine (H6)-tagged proteins, an immobilized metal ion affinity chromatography (Ni-IMAC) was performed using a fast protein liquid chromatography system consisting of two Pump P-500 modules and a gradient programmer GP-250 (Pharmacia Biotech). The column XK 15 (Pharmacia Biotech) was loaded with 4.6 ml Protino Ni-NTA Agarose (Macherey-Nagel, Düren) and the protein was washed and eluted from the beaded agarose matrix according to the manufacturers protocol, using washing and elution buffers.

Table 16: Buffer for immobilized Ni-NTA affinity chromatography.

Ingredient	Washing buffer	Elution buffer
HEPES	50 mM	50 mM
KCl	150 mM	150 mM
Imidazole	20 mM	250 mM
PLP	1 mM	1 mM
H ₂ O		

2.4.9 Size exclusion chromatography

For further purification of proteins via size exclusion chromatography, an ÄKTA FPLC system (GE Healthcare, Solingen) with a Superdex 200 10/300 GL column (GE Healthcare, Solingen) and a column volume of 1 ml and a flow rate of 0.5 ml/min was used at 4 °C. The elution fractions, selected via SDS-gel before the size exclusion chromatography (chapter 2.4.12), were pooled and have been concentrated to a volume of 500 µl using a Vivaspin 10,000 MWCO polyethersulfone concentrator (Sartorius, Göttingen). The elution was always performed in the

identical buffer the protein has been dissolved in. All used buffers were degassed and sterile filtered prior to use. The pressure limit on the ÄKTA was set to 1,500 Pa and the samples were analysed at 280 nm, 400 nm and 420 nm using a UV-900 UV detector and a pH/C-900 monitor for pH and conductivity (GE Healthcare, Solingen). The column was equilibrated with 5 CV of buffer before purifying the protein. The protein was eluted in 1.5 CV and fractioned in volumes of 0.5 ml using a Frac-950 fractionation system (GE Healthcare, Solingen).

2.4.10 Bradford assay

For the photometric determination of protein concentration in solutions or suspensions, the Bradford test was performed (Bradford 1976). The test is based on a shift of the absorption maximum of Coomassie brilliant blue from 470 nm to 595 nm due to the stabilisation of the unprotonated dye anion. In acidic solution, the red triphenylmethane dye Coomassie-Brilliant-Blue G-250 forms complexes with both cationic and nonpolar, hydrophobic side chains of proteins. This complexation stabilises the dye in its blue, anionic sulphonate form and shifts the absorption maximum to a wavelength of 595 nm, with a higher absorption corresponding to a higher concentration of proteins in the sample. For each determination, a calibration line was measured in duplicates to guarantee the reliability of the test. For this purpose, dilutions with concentrations of 0, 0.125, 0.25, 0.5, 0.75, 1.0, 1.5 and 2 mg/ml were prepared from a stock solution of BSA (0.1 mg/ml). The samples to be measured were diluted so that they fell within the range of the calibration line. 10 µl of the dilutions of the calibration line and the samples to be analysed pipetted into a microplate and mixed with 200 µl 1x ROTI[®]Quant Bradford reagent (Carl Roth, Karlsruhe). After an incubation time of 2 min, the absorbance at 595 nm was measured with SpectraMax iD3 microplate reader (Molecular Devices, San Jose, USA). The concentrations of the respective samples were calculated by the software of the SpectraMax iD3 microplate reader. First, the dilution factor was calculated from the given values and then the mean values were formed.

2.4.11 Cystein crosslinking

In vitro crosslinking of cysteines was performed as previously described, with minor modifications (Lee *et al.* 2006). The cells with the protein of interest were incubated and a subcellular fractionation was subsequently carried out (chapter 2.4.2). The fractions to be analysed were incubated at room temperature for 1 h with a final concentration of 2 mM copper phenanthroline. After that, the samples were mixed in a ratio of 1:1 with two-fold concentrated non-reducing SDS sample buffer [100 mM Tris-HCl, pH 6.8, 2 % SDS, 10 % glycerol, 0.2 % bromophenol blue]. The samples were then incubated for 5 min at 95 °C before being analysed via electrophoresis.

If crosslinking experiments were carried out *in vivo*, the cells were incubated to an OD₆₀₀ of 0.7. When they reached the desired OD, a final concentration of 10 mM copper phenanthroline was added to the medium and the cells were incubated for another 90 minutes at the respective temperature. The cells were subsequently harvested and a subcellular fractionation was performed, mixing the fractions to be analysed in a 1:1 ratio with two-fold concentrated non-reducing SDS sample buffer [100 mM Tris-HCl, pH 6.8, 2 % SDS, 10 % glycerol, 0.2 % bromophenol blue]. Finally, the samples were incubated for 5 min at 95 °C and subsequently analysed via electrophoresis.

2.4.12 SDS-PAGE

The SDS polyacrylamide gel electrophoresis (SDS-PAGE) was performed according to the established protocol by Laemmli (Laemmli 1970). Samples were mixed in a ratio of 1:1 with two-fold concentrated reducing SDS sample buffer [100 mM Tris-HCl (pH 6.8), 20 % (v/v) glycerol, 4 % (w/v) SDS, 0.2 % (w/v) bromophenol blue, 200 mM DTT]. The mixtures were then incubated for 5 min at 95 °C and 12 µl of sample were loaded onto the gel. For these protein electrophoreses, the PageRuler™ Prestained Protein Ladder was used as a size standard (Thermo Scientific, Dreieich).

The proteins in the sample were separated using a voltage of 100 V, until the running band reached the resolving gel. Subsequently, the voltage was increased to 120 V. The protein electrophoresis was carried out in Minigel-Twin electrophoresis systems (Analytik Jena, Jena).

Table 17: Ingredients for denaturing SDS gel.

Ingredient	Stacking gel		Resolving gel	
	4 %	10 %	15 %	
Acrylamide/bisacrylamide solution (30 % (w/v), 2.6 % C)	630 μ l	2.5 ml	3.75 ml	
0.5 M Tris-HCl (pH 6.8)	950 μ l	-	-	
1.5 M Tris-HCl (pH 8.8)	-	1.88 ml	1.88 ml	
H ₂ O	2.13 ml	3 ml	1.72 ml	
10 % SDS	37.5 μ l	75 μ l	75 μ l	
TEMED	37.5 μ l	75 μ l	75 μ l	
10 % APS	5 μ l	10 μ l	10 μ l	

2.4.13 Colloidal Coomassie staining

The purified proteins that were separated via protein electrophoresis were detected via Coomassie staining. The Coomassie dye binds to the hydrophobic amino acids of the proteins in the gel and subsequently changes colour to an intense blue that is detectable.

First, the SDS gel was washed in distilled water for 5 min to remove excess electrophoresis buffers from the gel matrix. In a second step, the gel was incubated overnight in staining solution. In a last step, the staining solution was discarded and the gel was incubated in 20 ml of destaining solution until bands that could be clearly separated from the background became visible. The destained gels were then scanned and documented using the Perfection V850 Pro Scanners (Epson, Meerbusch).

Table 18: Staining solution for SDS-gels.

Ingredient	Concentration
Ethanol	50 % (v/v)
Acidic acid	5 % (v/v)
Coomassie Brilliant Blue G 250	0.24 % (w/v)

Table 19: Destainig solution for SDS-gels.

Ingredient	Concentration
Ethanol	10 % (v/v)
Acidic acid	7 % (v/v)

2.4.14 Silver staining

For a more sensitive colorimetric detection of proteins, silver staining was applied. In this method, silver ions in the staining solution interact with the functional groups of the proteins, namely carboxylic acid groups, imidazole, amines and sulfhydryls. In this multi-step staining protocol, the gel was first fixed for one hour using solution I to limit diffusion of protein bands from the gel matrix. Subsequently, the gel was washed 40 min in solution II and 20 min in solution III, respectively. After incubation for 1 min in solution IV, the gel was washed three time in distilled water and then incubated for 20 min in solution V before being washed again twice for 30 sec in water. Development of the gel is done by incubating the gel for 60 min in solution VI, resulting in the reduction of the silver ions to metallic silver. After a washing the gel twice in distilled water for 2 min, the stained protein bands are fixed by incubating the gel for 15 min in solution VII. The silver-stained gels were then scanned and documented using the Perfection V850 Pro Scanners (Epson, Meerbusch).

Table 20: Solutions for silver staining

Ingridient	Concentration
Solution I	
Ethanol	50 % (v/v)
Acetic acid	12 % (v/v)
Formaldehyde	0.05 % (v/v)
Solution II	
Ethanol	50 % (v/v)
Solution III	
Ethanol	30 % (v/v)
Solution IV	
Sodium thiosulfate	0.02% (w/v)
Solution V	
Silver nitrate	0.2 % (w/v)
Formaldehyde	0.075 % (v/v)
Solution VI	
Sodium carbonate	6 % (v/v)
Sodium thiosulfate	0.0004 % (w/v)
Formaldehyde	0.05 % (v/v)
Solution VII	
Methanol	10 % (v/v)
Acetic acid	12 % (v/v)

2.4.15 Western blot and protein detection

Western blotting was carried out according to an established protocol (Towbin *et al.* 1979; Burnette 1981). For detection of proteins by antibody interaction, the proteins needed to be transferred onto a nitrocellulose membrane using the semi dry method. For this purpose, the Amersham Protran 0.2 NC nitrocellulose Western blotting membranes (GE Healthcare, Freiburg) and Whatman Cellulose chromatography papers (GE Healthcare, Freiburg) were soaked in Towbin buffer [25 mM Tris, 192 mM glycine, 20 % (v/v) methanol]. The excess buffer was discarded and three chromatography papers, the nitrocellulose Western blotting membrane, the SDS gel and finally three more chromatography papers were stacked in that precise order on a Rapid Semi-Dry Transfer system Fastblot B44 (Analytik Jena, Jena). The transfer of the proteins was carried out by applying a current of 0.7 mA/cm² of gel for 1 h.

The detection of proteins was carried out by incubating the blotted membrane with the corresponding antibodies. To do so, the membrane was first blocked by incubating the membrane over night at 4 °C in 5 % (w/v) skim milk powder dissolved in PBS [4 mM Na₂HPO₄, 2 mM KH₂PO₄, 13.7 mM NaCl, 3 mM KCl]. Subsequently, the membrane was washed three times for 5 min each in PBS, before being incubating for 1 h with the primary antibody. After incubation with the first antibody, the membrane was again washed three times for 5 min each in PBS, before being incubating for 1 h with the secondary antibody. In a last washing step, the membrane was washed three times for 5 min each in PBS and subsequently incubated in a solution for analysis via enhanced chemiluminescence [100 mM Tris-HCl (pH 8.0), 1.25 mM Luminol, 0.225 mM p-Coumaric acid]. The chemiluminescent reaction of luminol was started by adding 5 µl 30 % (v/v) hydrogen peroxide to the solution. The emerging signals were recorded using the chemiluminescence imager ChemoStar 6.0 ECL (Intas, Göttingen).

Table 21: List of used antibodies.

Antibody	Type	Dilution	Source
α -His	Maus-IgG monoclonal	1:5,000	QIAGEN (Hilden)
Goat-anti-mouse- HRP-Konjugat	Goat-IgG polyclonal	1:5,000	Carl Roth (Karlsruhe)
Strep-Tactin [®] -HRP-Konjugat	recombinant	1:4,000	IBA (Göttingen)

2.4.16 Complementation analysis

For complementation analysis, the strains that were to be examined were grown over night in 5 ml LB medium with the appropriate antibiotics. With 5 μ l of that overnight culture, 5 ml CAA medium were inoculated and incubated overnight at 30 °C and 180 rpm. To ensure comparability among each other, the cells corresponding to 1 ml of an OD₆₀₀ of 1 were pelleted and washed three times with sterile saline (0.9 % NaCl (w/v)) and ultimately resuspended in 1 ml saline. For the complementation analysis via droplet assay, 5 μ l of each strain was pipetted onto a CAA agar plate and incubated for 36 h at 30 °C.

2.4.17 Growth curves

To investigate the effects of certain modifications in the genomic on the growth of the bacteria, growth curves were recorded. For this purpose, an overnight culture was normalised to an OD₆₀₀ of 1.0 and washed three times with sterile saline (0.9 % NaCl (w/v)). Afterwards, 2 μ l of the cell suspension was pipetted into each well of a 96-well micro test plate (Sarstedt, Nümbrecht) and filled with 198 μ l of the medium to be used supplemented with the corresponding antibiotics, whereby the outer wells were filled with 200 μ l of water to minimise a possible evaporation effect in the wells to be measured. The growth curves were recorded using the SpectraMax iD3 microplate reader (Molecular Devices, San Jose, USA) while taking measures every 15 min.

2.4.18 Extraction of pyoverdine

The extraction of pyoverdine was performed using a slightly modified protocol based on Meyer *et al.* (Meyer *et al.* 1997). 5 µl of an overnight culture were used to inoculate 5 ml of CAA medium and incubated overnight at 30 °C and 180 rpm. Of that new overnight culture, 1 ml was used to inoculate 1 l of CAA medium. This main culture was incubated for 72 h at 30 °C and 180 rpm before the cells were pelleted by centrifugation for 30 min at 20,000 xg and 4 °C using a Sorvall Lynx 4000 superspeed centrifuge (Thermo Scientific, Dreieich). The supernatant was sterile filtered using the sterile filter system Filtropur V50 (Sarstedt, Nümbrecht) with a pore size of 0.2 µm. After the pH was adjusted to pH 6.0 using 8 M HCl, 20 g/l XAD-4 resin was added and incubated under constant stirring for 3 h at 4 °C. The resin was filtered using a vacuum pump and the flowthrough was discarded, as the pyoverdine was now bound to the XAD-4. After resuspending the resin in 500 ml of distilled water and incubating the suspension for another 60 min at 4 °C, the resin was again filtered and resuspended in 200 ml 15 % methanol. After a short incubation step of 15 min at 4 °C, the resin was filtered and resuspended in 150 ml 50 % methanol. After incubation for 1 h at 4 °C, the resin was filtered and discarded as the flow through was kept, containing the released pyoverdines. The methanol-water mixture was removed using the rotary evaporator Rotavapor R-124 (Büchi, Essen) and the Waterbath B-480 (Büchi, Essen), keeping the solution constant at 30 °C. The resulting pyoverdine was resuspended in 1 ml of distilled water and sterile filtered using a Filtropur S sterile filter (Sarstedt, Nümbrecht) for further use.

2.5 Analytical methods

2.5.1 Mass spectrometry for pyoverdine identification

Mass spectra of pyoverdines and intermediates were obtained as previously described (Ringel *et al.* 2016). In detail, a Q-ToF Premier mass spectrometer (Waters, Eschborn) in electro spray ionisation mode (3 kV, 250 °C nitrogen gas flowing at 650 l/h) equipped with a LockSpray unit and an ACQUITY UPLC (Waters) were used. The separation of masses was performed using a Waters ACQUITY UPLC HSS T3 1.8 µm column. The solvents used in this setup were solvent A [0.1 % (v/v) formic acid] and solvent B [acetonitrile with 0.1 % (v/v) formic acid]. The flow rate was 0.4 ml/min with a gradient of 0 % B (0 min), 90 % B (10.00 min), 90 % B

(13.00 min), 10 % B (13.10 min), 10 % B (15.00 min). The detected Ion mass signals (m/z) in this work are reported as values in atomic mass units.

2.5.2 Sample preparation for shotgun mass spectrometry

Sample preparation for shotgun analysis of PvdM via tandem mass spectrometry (MS/MS) was performed as previously described (Fromm *et al.* 2016). In summary, PvdM was separated from other protein via SDS gel and the band containing PvdM was precisely excised to avoid protein contamination (chapter 2.4.12). The gel fragment was then cut into cubes with a length of approximately 1 mm and dried *in vacuo* in a centrifuge. The dried gel pieces were then rehydrated for 30 min at 56 °C in 200 µl reduction solution [20 mM DTT, 100 mM ammonium bicarbonate]. The rehydrated gel cubes were then dehydrated again by adding 200 µl acetonitrile and incubating the mixture for 10 min. The supernatant was removed and the gel pieces were incubated in the dark for 30 min in 200 µl alkylation solution (55 mM iodoacetamide, 100 mM ammonium bicarbonate). Dehydration with acetonitrile for another 10 min was followed by rehydration with 100 mM ammonium bicarbonate for 15 min. The supernatant was discarded again and the gel cubes were dehydrated a final time with acetonitrile and then dried for 20 min in a centrifuge *in vacuo*. Subsequently, the gel pieces were treated with trypsin (Promega, Mannheim) according to the manufacturer's instructions, whereby the samples were incubated overnight in 80 µl at 37 °C. For the extraction of the peptide fragments, 40 µl each of extraction solution I [50 % (v/v) acetonitrile, 5 % (v/v) formic acid], extraction solution II [50 % (v/v) acetonitrile, 1 % (v/v) formic acid] and solution III [100 % (v/v) formic acid] were added to the samples and incubated for 30 min each at 37 °C and 800 rpm. Between each incubation step with a new extraction solution, the supernatant was removed completely. The collected supernatants were pooled and dried at 30 °C for 30 min in a centrifuge *in vacuo*.

2.5.3 Shotgun mass spectrometry for anchorage site identification

Protein identification via shotgun mass spectrometry was performed as previously described (Thal *et al.* 2018). In summary, a Q-Exactive mass spectrometer (Thermo Scientific, Dreieich), which was used in positive electro spray ionisation mode (2.2 kV, capillary temperature 275 °C, S-lens RF level to 50 %), was coupled to an Ultimate 3000 UPLC (Thermo Scientific,

Dreieich). 2.5-5 μ l of a sample solution were used per run and injected at a rate of 4 μ l/min into a 2 cm, C18, 5 μ m, Acclaim PepMap100 reverse phase trapping column (Thermo Scientific, Dreieich). The peptides were separated on a 50 cm, C18, 3 μ m, Acclaim PepMap100 reverse phase analytical column (Thermo Scientific, Dreieich) and eluted in a non-linear acetonitrile gradient of 5-30 % (v/v) in 0.1 % (v/v) formic acid at a flow rate of 300 nl/min at 35 °C.

2.5.4 Microscopy

Microscopic images of bacteria were acquired using the Leica DMI8 automated inverted phase contrast fluorescence microscope (Leica Microsystems, Wetzlar) and the microscope camera sCMOS camera Leica DFC9000 (Leica Microsystems, Wetzlar) using a 100-x oil objective. Bacteria were washed three times with sterile saline (0.9 % NaCl (w/v)) prior to being fixed on agar slides containing 1 % (w/v) agar in saline for immobilization. For phase contrast microscopy, standard settings were used. For fluorescence imaging microscopy, the channel 390 LED was used with an excitation spectrum of 376-407 nm and an emission spectrum of 420-450 nm. For fluorescence microscopy of standard fluorescent proteins such as mCherry or GFP, common mCherry or gfp filters were used. The acquisition and the editing of the pictures has been carried out using the Leica software LAS X and the optimization tool Thunder.

2.5.5 Spectrophotometry

For determining the excitation maximum of a sample by the change in absorbance of different wavelengths of incident light, an absorbance spectrum between 190 nm and 840 nm was recorded using the DS-11 UV-Vis Spectrophotometer (DeNovix, Wilmington).

For measuring the characteristic fluorescence emission spectra of pyoverdine, the change of the intensity of fluorescence dependent on the wavelength of the emitted light at an excitation wavelength set at 400 nm was recorded. The measurement was performed using the Jasco FP-6500 spectrofluorometer (Jasco, Pfungstadt) while keeping the sample constantly at a temperature of 25 °C using the Julabo F 25 water pump (Jasco, Pfungstadt).

2.5.6 Gas chromatography

To separate and analyse single gaseous compounds from a mixture, gas chromatography was used as previously described with minor modifications (Zaman *et al.* 2021). 100 μ l of the sample were taken by a PAL Combi-xt autosampler (CTC Analytics, Zwingen, Switzerland) and injected into a 7890B gas chromatograph system (Agilent, Waldbronn), equipped with a split/splitless injector with the micro-packed column Shin Carbon ST 80/100, 2 m, 0.5 mm (Restek Corporation, Bellefonte, USA) and the capillary column RT-Molecular Sieve 5A, 30 m, 0.53 mm (Restek Corporation, Bellefonte, USA). Whereas the pulsed discharge helium ionization detector V1D-3-I-HP-220 (Valco Instruments Company Inc. VICI AG International, Houston, USA) was attached to the outlet of the Shin Carbon column acting as a molecular sieve especially for the separation of CO₂ and N₂O, the thermal conductivity detector G3440B (Agilent, Waldbronn) was coupled to the outlet of the capillary molecular sieve column. The gas chromatograph itself was operated with helium 6.0 as the carrier gas that was purified prior to use by two sequential helium purifiers V1HPM-220 (Valco Instruments Company Inc. VICI AG International, Houston, USA). In a first step, the samples were heated to 90 °C and remained at that temperature. After 2 min, the temperature shifted to 120 °C with a temperature rise of 50 °C min⁻¹. The gases to be analysed were held at that temperature for 2.1 min before being shifted to 200 °C. The analysing column was baked out for 2 min. For the detection of O₂ and N₂, the thermal conductivity detector was used, for the detection of CO₂ the pulsed discharge ionization detector was used.

3 Results

3.1 Towards understanding the function of PvdM

PvdM is the last enzyme involved in the periplasmic maturation of pyoverdine in fluorescent pseudomonads, that has not yet been assigned a function. It is essential for the maturation of pyoverdines since a *pvdM* knockout strain is neither able to form fluorescent pyoverdine nor to grow on iron depleted medium. A sequence alignment predicts PvdM to be a metal dependant peptidase of the metal hydrolase superfamily with the human renal dipeptidase as its closest homologue. The human renal dipeptidase is a membrane-bound glycoprotein, shown to be catalysing the hydrolysis of dipeptides exclusively (Campbell *et al.* 1966; Adachi *et al.* 1990b; Nitanaï *et al.* 2002). This homodimeric enzyme possesses two zinc ions per subunit and is also involved in the hydrolysis of penem and carbapenem β -lactam antibiotics (Kahan *et al.* 1983; Kim and Campbell 1982; Liao *et al.* 2010; Nitanaï *et al.* 2002). Although PvdM has been shown to be a membrane-associated protein, the subcellular orientation and the specific function are still unknown (Ringel 2018). PvdM could be involved in the regulation of pyoverdine synthesis by being the yet unidentified peptidase responsible for the initial cleavage of FpvR, ultimately resulting in an upregulation of essential genes involved in pyoverdine synthesis. Alternatively, in addition to the already known enzymes, PvdM may also be directly involved in the actual maturation of pyoverdines in the periplasm in a yet unknown way. In addition, PvdM may also be indirectly involved in maturation process by interacting essentially with one of the maturation proteins (**Figure 10**). Since there are still mechanisms unaccounted for in the biosynthesis of pyoverdine, especially in terms of regulation, it was investigated if and how PvdM is involved in the biosynthesis of pyoverdine and if PvdM was indeed one of the searched for unknown regulatory enzymes.

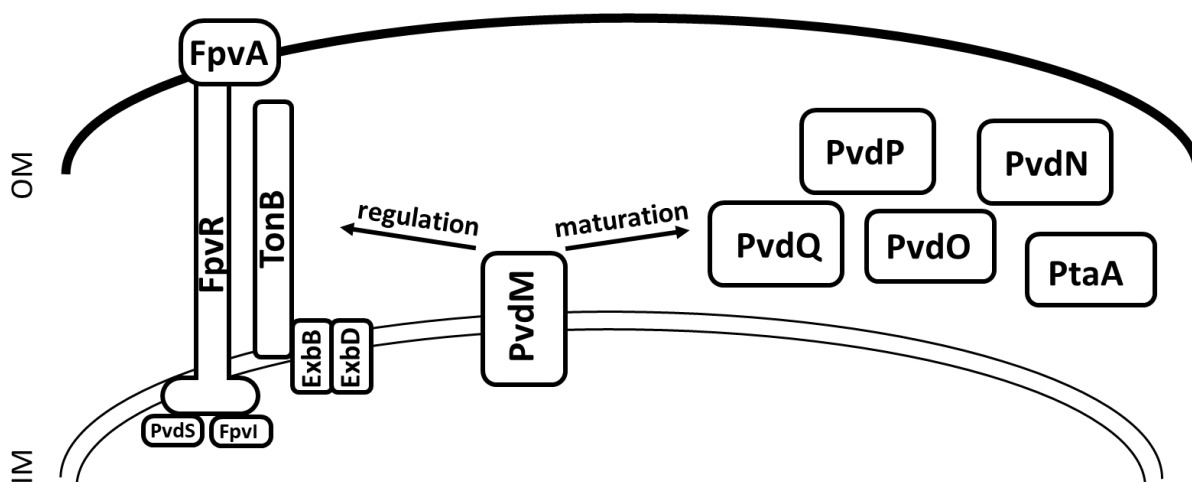


Figure 10: Schematic overview of possible involvements of PvdM in the biosynthesis of pyoverdines in PfA506. PvdM could be either involved in regulation of pyoverdine synthesis as an unknown peptidase or directly or indirectly involved in the maturation of pyoverdines.

3.1.1 PvdM is a membrane integrated protein with its globular domain facing the periplasm

In order to determine the topological orientation of PvdM, a subcellular fractionation was carried out first. Strep-tagged PvdM was produced in a *P. fluorescens* A506 $\Delta pvdM$ strain and the obtained cytoplasm, membrane and periplasm fractions were analysed after SDS-PAGE and western blotting. Membrane fractions were additionally treated with carbonate buffer. For the verification of the $\Delta pvdM$ phenotype, additional growth assays were performed, in which the growth of *pvdM* knockout strains complemented with different PvdM variants were compared on a variety of media. Furthermore, PvdM was produced as a recombinant Strep-tagged protein in *E. coli* and examined for accessibility for degradation after permeabilization of the cells. For the production of PvdM in *P. fluorescens* A506, the anthranilate tunable expression vector pUCP20-ANT2-MCS was used (Hoffmann *et al.* 2021).

As can be seen in the western blot of the subcellular fraction and the carbonate wash, PvdM is truly a membrane integrated protein. The interaction with the membrane could not be dissolved by a carbonate wash of the membrane fraction (**Figure 11 A**). Furthermore, as shown by the protease accessibility assay, the globular domain of PvdM was degraded by protease K, demonstrating that PvdM is membrane integrated with its globular domain facing the periplasm. As the naturally occurring biotin carboxyl carrier protein (BCCP) only occurs in the cytoplasm of *E. coli*, BCCP serves as a control for an intact cytoplasmic membrane. If the inner membrane was permeabilized unintentionally by the treatment, BCCP would have been degraded by protease K. Once Triton X-100, a detergent known to destabilize the membrane, was added to the sample both PvdM and BCCP were degraded by protease K (**Figure 11 B**).

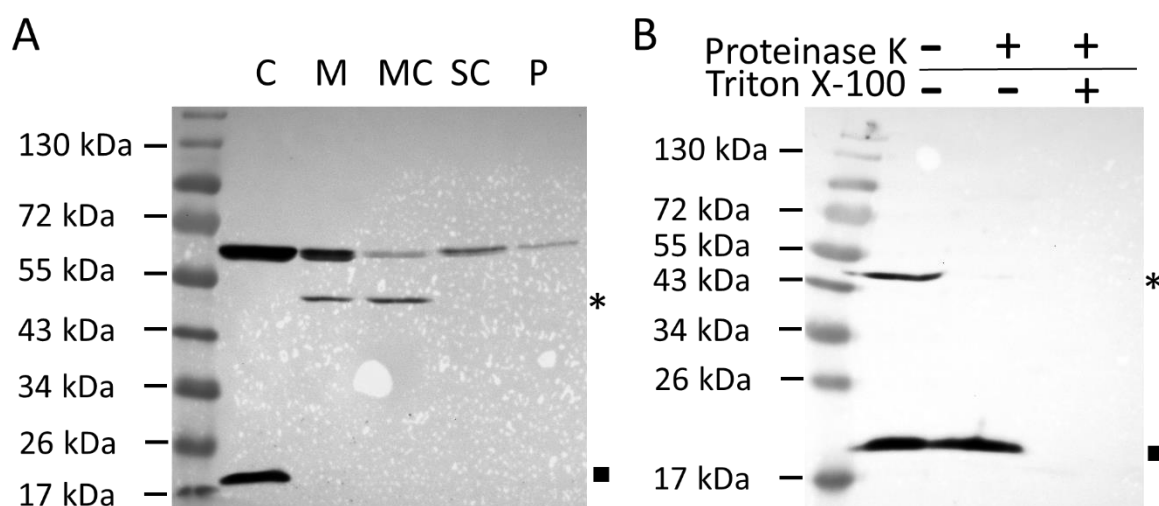


Figure 11: PvdM is a membrane integrated enzyme. (A) Western blot analysis of a subcellular fractionation of a PfA506 Δ pvdM strain complemented with Strep-tagged PvdM encoded on the plasmid pUCP20 ANT2 MCS His-pvdM-Strep. The membrane fraction was additionally treated with carbonate buffer. (B) Production of a Strep-tagged PvdM variant encoded on the plasmid pEX pvdM Strep-tac in *E. coli* BL21 and subsequent permeabilization of the outer membrane show the degradation of PvdM without and with the addition of protease K and/or Triton X-100 to the reaction set up. PvdM is marked by an asterisk (*). Naturally occurring BCCP serves as a control for cytoplasmic proteins (■). C: cytoplasm; M: membrane, MC: membrane after carbonate wash, SC: supernatant after carbonate wash, P: periplasm.

3.1.2 PvdM is not involved in the regulation of pyoverdine biosynthesis as a peptidase

As the function of PvdM within the tightly regulated biosynthesis pathway of pyoverdines still remains unclear, it was tested if PvdM, due to its predicted similarity with the renal dipeptidase, was the searched for site 1-like peptidase. This unidentified protein is responsible for the initially cleavage of the anti-sigma factor FpvR in the periplasm which leads to the release of the alternative sigma factors PvdS and FpvI (**Figure 9**). A deletion of FpvR should lead to a constant production of pyoverdine due to the fact that FpvR could not sequester the alternative sigma factors PvdS and FpvI in the cytoplasm. The liberated alternative sigma factors in turn would lead to an expression of *pvdS*, the *pvdS*-regulon and *fpvA*, the gene coding for outer membrane receptor of pyoverdines. Since FpvR would no longer have to be processed by PvdM, if PvdM were to be the unknown site 1-like peptidase, the absence of PvdM in the double knockout strain *P. fluorescens* A506 $\Delta fpvR\Delta pvdM$ should also lead to a constant production of pyoverdine. Consequently, the $\Delta fpvR\Delta pvdM$ knockout strain should be capable of growing on iron depleted medium.

To test the potential site 1-like dipeptidase function of PvdM, the described strain *P. fluorescens* A506 $\Delta fpvR\Delta pvdM$ was created and incubated on CAA agar plates and those to which EDDHA has been added for iron depletion. Additionally, the strain was incubated in CAA medium and the corresponding supernatant was checked for pyoverdine production by spectrophotometry. The pyoverdine production was then compared to that of a wild-type strain.

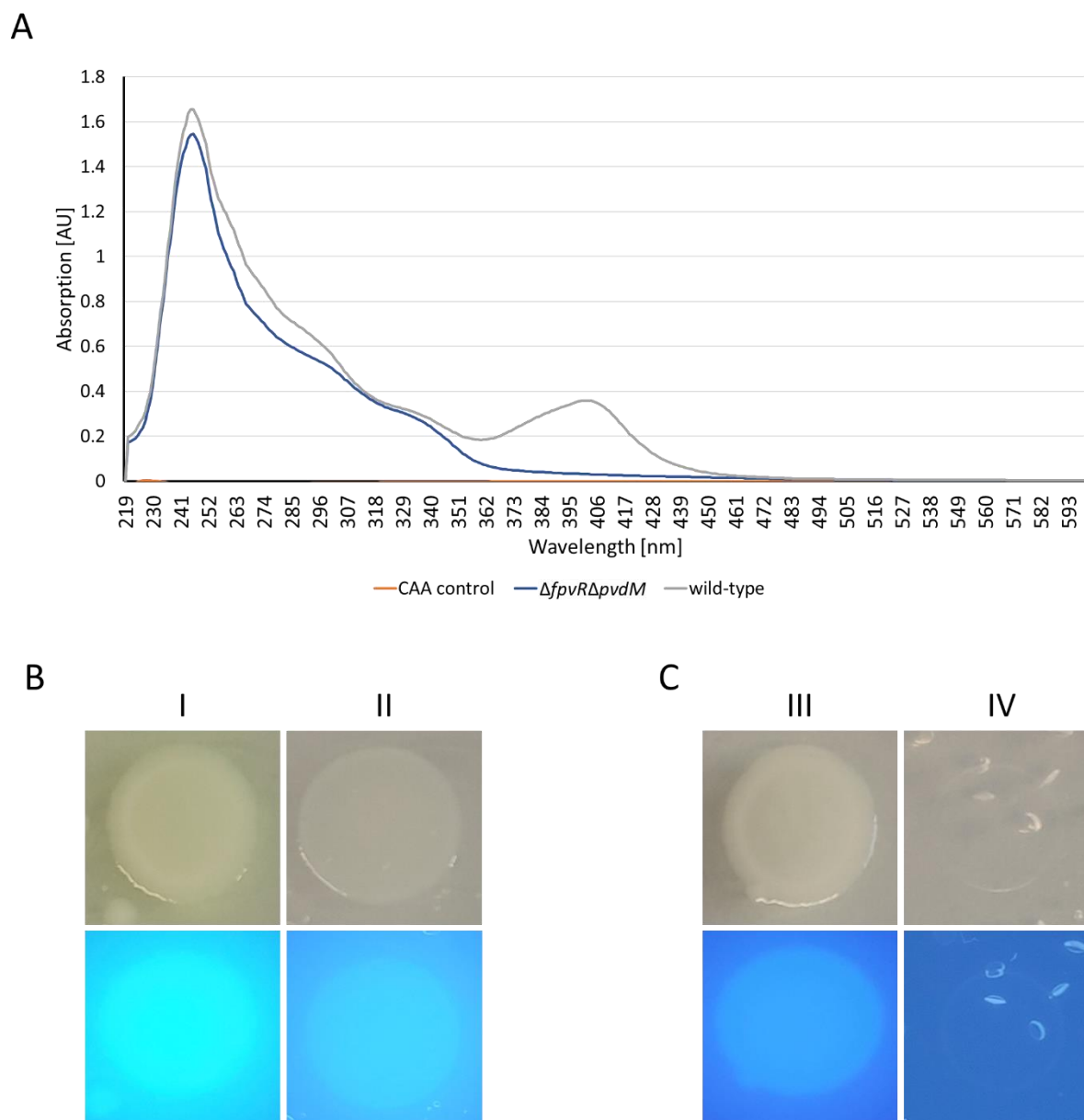


Figure 12: PvdM is not involved in the regulation of pyoverdine synthesis. (A) Absorption spectrum of the medium supernatant of the PfA506 wild-type strain and the PfA506 $\Delta fvpR\Delta pvdM$ strain in the range of 220-600 nm. (B) Growth of the PfA506 wild-type strain CAA medium (I) and CAA Medium depleted with EDDHA (II) and check for pyoverdine production under UV light. (C) Growth of the PfA506 $\Delta fvpR\Delta pvdM$ strain on CAA medium (I) and CAA Medium depleted with EDDHA (II) and check for pyoverdine production under UV light.

While the *P. fluorescens* A506 wild-type produces is a distinct peak with an absorbance maximum at around 400 nm, typical for that of pyoverdine, there is no significant absorbance at around 400 nm in case of the double knockout $\Delta fvpR\Delta pvdM$ (Figure 12 A). Accordingly,

the complementation experiments show a similar result. The $\Delta fpvR\Delta pvdM$ knockout strain was able to grow on normal CAA agar plates, but the formed colonies did not show any fluorescence under UV light. On CAA agar plates supplemented with EDDHA, however, the double knockout strain, in contrast to the wild-type, was not able to grow at all (**Figure 12 C**). The wild-type did not only form colonies, but also showed strong fluorescence under UV light on both CAA agar plates (**Figure 12 B**). These results lead to the conclusion that the created strain *P. fluorescens* A506 $\Delta fpvR\Delta pvdM$ did not produce any pyoverdine. Going further, this means that PvdM is not the unknown site 1-like peptidase, responsible for the periplasmic cleavage of FpvR and therefore not involved in the regulation of the pyoverdine biosynthesis pathway.

3.1.3 Substitution of conserved metal ligands of the human renal dipeptidase reveals no function in PvdM

Based on the similarity of PvdM to the dimeric human renal dipeptidase, a sequence comparison of the two proteins was conducted. The human renal dipeptidase was scanned for amino acids involved in the coordination of the two Zn^{2+} -ions, that were also conserved in PvdM. The metal centre in each monomer of the active site of the human renal dipeptidase consists of two Zn^{2+} -ions. The alpha- Zn^{2+} -ion is coordinated by His-20 and Asp-22 whereas the beta- Zn^{2+} -ion is coordinated by His-198 and His-219 (**Figure 13 A**). Both Zn^{2+} -ions are additionally bridged by water molecules and the side chain carboxylate of Glu-125 (Cummings *et al.* 2010; Nitanaï *et al.* 2002).

While the histidine at position 219 of the human renal dipeptidase is strictly conserved as His-266 in PvdM of *P. fluorescens* A506, the other amino acids involved in the coordination of the Zn^{2+} -ions are not conserved. Nevertheless, in the direct vicinity of His-266, there is a conserved methionine at position 246 in PvdM (**Figure 13 B**). While zinc ions are usually coordinated by histidine, it has been shown that glutamic acid, aspartic acid and cysteine, methionine are also capable of ligating zinc (Auld 2001; McAuliffe *et al.* 1966).

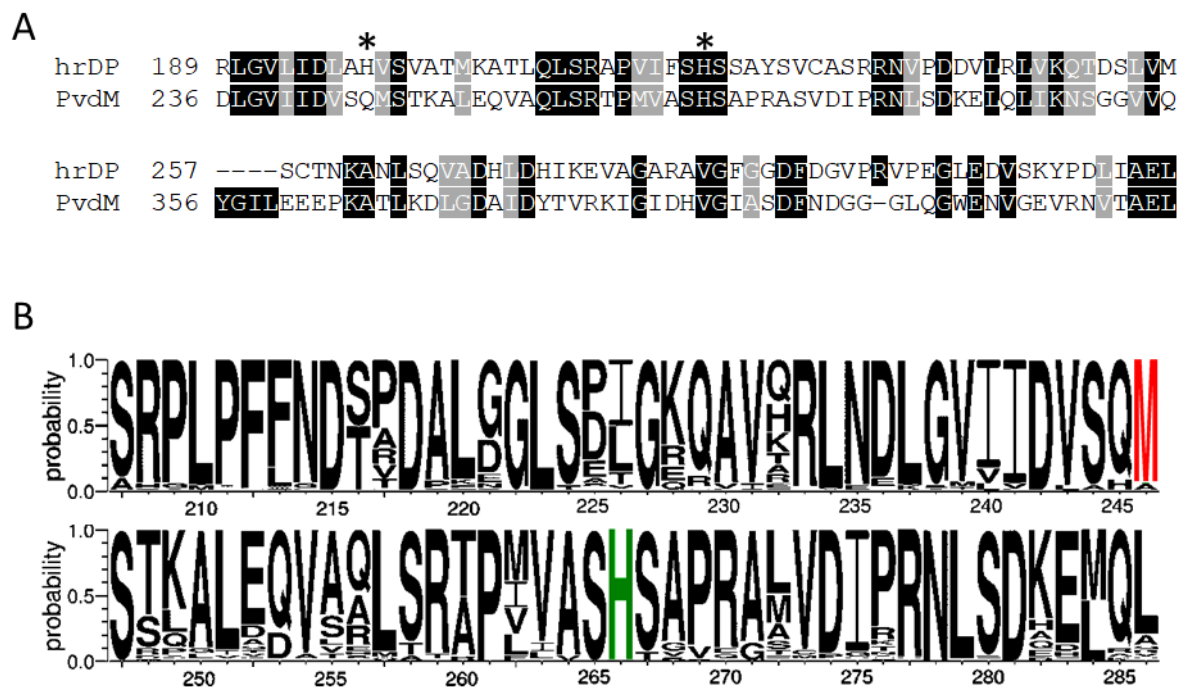


Figure 13: Sequence alignments of PvdM and hrDP. (A) Section of the sequence alignment of human renal dipeptidase and PvdM. The histidine responsible for the coordination of the beta zinc atom in hrDP are marked with an asterisk (*). (B) Sequence logo for the section with the amino acids involved in the possible coordination of a zinc ion in PvdM. The amino acid residues methionine and histidine identified for this purpose are highlighted in red and green, respectively. The numbers indicate the position in the amino acid sequence of PvdM from *P. fluorescens* A506

With these two amino acids His-266 and Met-246, PvdM would be able to coordinate a Zn^{2+} -ion corresponding the beta- Zn^{2+} -ion in the human renal dipeptidase. In order to test the influence of these two potentially coordinating amino acid residues on the function of PvdM, the mentioned amino acids were respectively substituted by alanine. For this purpose, the respective PvdM variants were produced in a *P. fluorescens* A506 $\Delta pvdM$ strain and a subcellular fractionation was carried out. At the same time, complementation experiments were conducted to determine whether the respective variants could complement the missing wild-type PvdM, in which the strains were incubated on CAA medium supplemented with EDDHA.

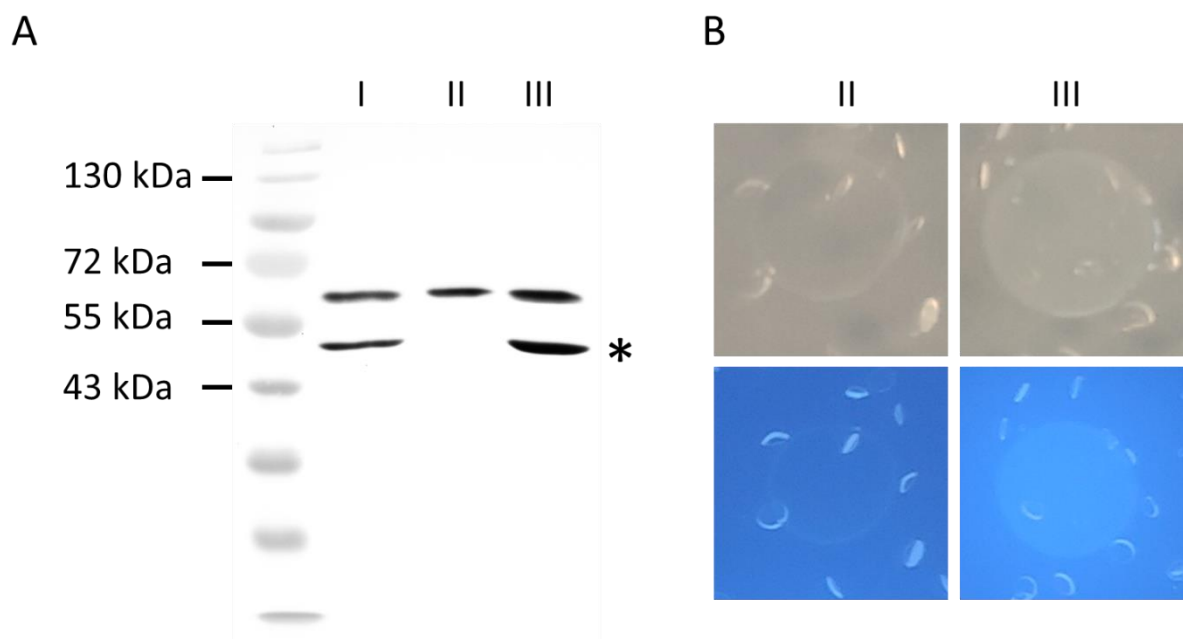


Figure 14: Conserved zinc binding sites are not necessary for the function of PvdM. Analysis of potential zinc ligands in PvdM. (A) Western blot analysis of the membrane fractions of subcellular fractionations of the PvdM variants produced in $\Delta pvdM$ strains. Membrane fraction of wild-type PvdM encoded on the plasmid pUCP20-ANT2-MCS-*His-pvdM*-Strep (I), a PvdM_{M246A} variant encoded on plasmid pUCP20-ANT2-MCS-*His-pvdM-M246A*-Strep (II) and a PvdM_{H266A} variant encoded on plasmid pUCP20-ANT2-MCS-*His-pvdM-H266A*-Strep (III). PvdM variants are marked by an asterisk (*). (B) The analysis of the respective strains and their complementation ability was tested on CAA medium supplemented with EDDHA. The growth was of the strains was documented under normal light (upper row), production of pyoverdine was checked under UV light (lower row).

As seen in the western blot, the substitution of methionine at position 246 by alanine resulted in a complete degradation of PvdM_{M246A} (Figure 14 A). This lack of functional PvdM resulted in the abolishment of pyoverdine production. Furthermore, a *P. fluorescens* A056 $\Delta pvdM$ strain complemented with the PvdM_{M246A} variant was no longer able to grow on iron depleted medium such as CAA supplemented with EDDHA (Figure 14 B). The second variant however, PvdM_{H266A}, did not show any effects on pyoverdine production. The *P. fluorescens* A506 $\Delta pvdM$ strain complemented with the PvdM_{H266A} variant was capable of growing on iron depleted medium (Figure 14 B). Additionally, the PvdM_{H266A} variant was detectable in the membrane fraction of the subcellular fractionation via western blots (Figure 14 A). These results indicate that the strictly conserved Met-246 is crucial for the stability of PvdM, and that the potential involvement of His-266 in the coordination of the beta-Zn²⁺-ion does not play a decisive role in the possible function of PvdM. Moreover, it can be concluded from the results that the conserved zinc coordinating amino acids residues

corresponding to the active site of the human renal dipeptidase are not necessarily needed for functional PvdM.

3.1.4 The human renal dipeptidase inhibitor Cilastatin slightly effects PvdM

The human renal dipeptidase (hrDP), identified as the closest homologue to PvdM, has been the target of many studies so far (Campbell *et al.* 1988; Adachi *et al.* 1990a; Hooper *et al.* 1990; Kropp *et al.* 1982). During these studies, it has been shown that the hrDP is a glycosyl phosphatidylinositol-anchored protein involved in the *in vivo* metabolism of glutathione and the hydrolysis of β -lactam antibiotics like penem and carbapenem (Adachi *et al.* 1990b; Kim and Campbell 1982; Campbell *et al.* 1984). Furthermore, Cilastatin was identified as a compound capable of reversibly inhibiting the hrDP (**Figure 15**) (Campbell *et al.* 1988).

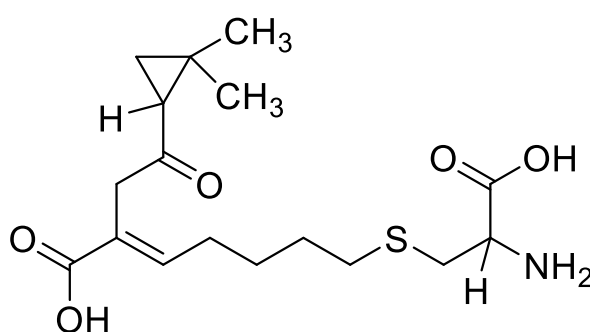


Figure 15: Structure of Cilastatin.

The inhibition by Cilastatin is due to the fact that the dipeptidyl inhibitor fits into the active site of the hrDP and interacts with not only the zinc ions, but also with amino acid residues on the surface of the active site's sidewall. The confirmation of Cilastatin within the active site of the hrDP seems to displace atoms important for the reaction just slightly away from the optimum location, preventing a hydrolysis of Cilastatin (Nitanai *et al.* 2002). This leads to a blockage of the active site for other possible substrates and therefore a reversible inhibition of the hrDP. Due to the similarity of hrDP and PvdM, it was investigated whether Cilastatin is also capable of inhibiting PvdM. For this purpose, two different strains, namely *P. fluorescens* A506 $\Delta pvdM$

and *P. fluorescens* A506 wild-type were incubated in iron-depleted medium supplemented with EDDHA and the growth of these two strains was compared. Additionally, droplet assays were performed to assess the pyoverdine production under the influence of Cilastatin.

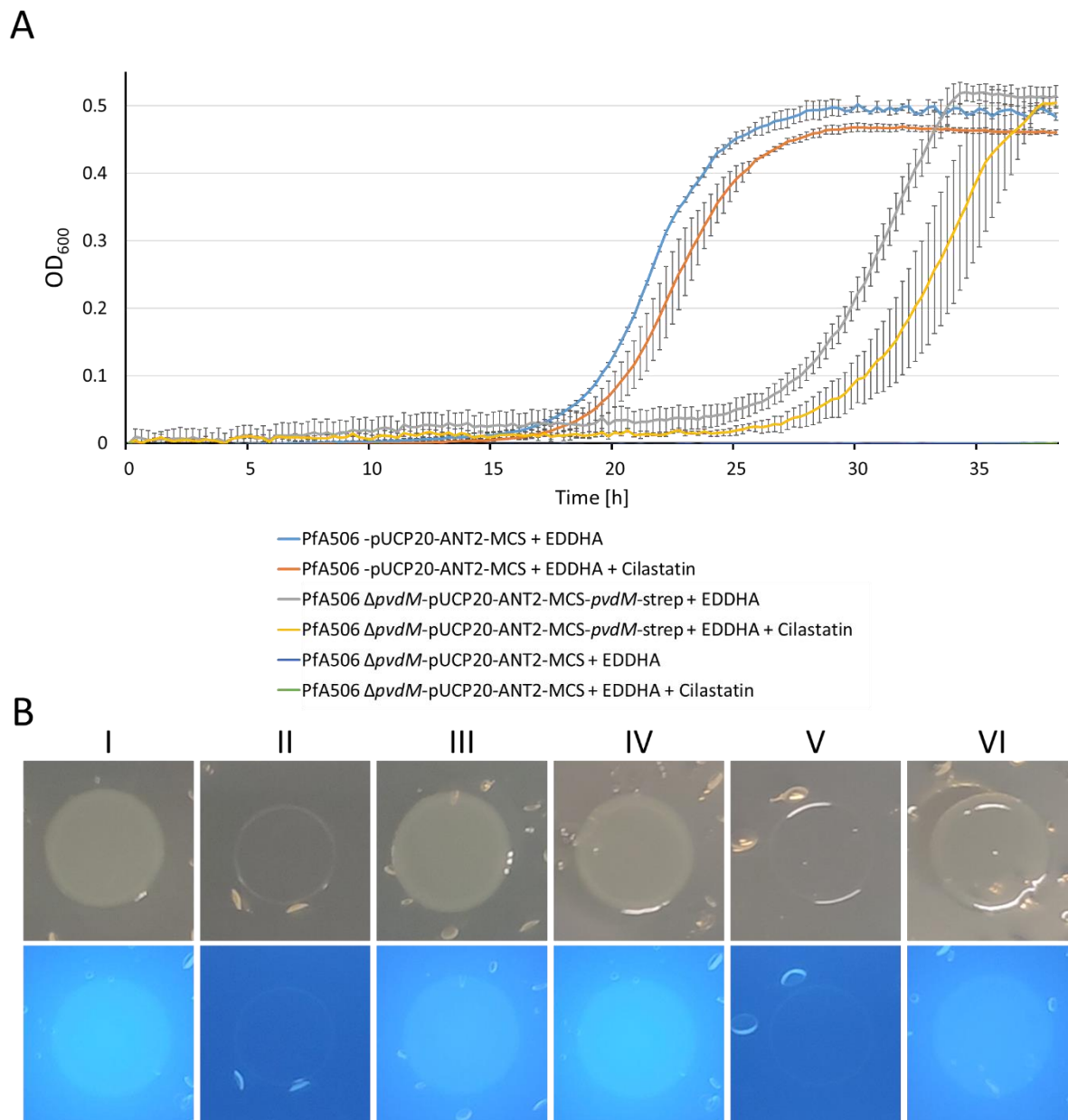


Figure 16: Cilastatin slightly affects the growth of *P. fluorescens* A506. Analysis of the effect of Cilastatin on the growth of *P. fluorescens* A506. (A) Comparison of growth of a PfA506 wild-type strain, a PfA506 $\Delta pvdM$ strain and a PfA506 $\Delta pvdM$ strain complemented with Strep-tagged PvdM encoded on the anthranilate inducible plasmid pUCP20-ANT2-MCS-His-*pvdM*-Strep in M9 medium supplemented with EDDHA with or without the presence of Cilastatin. Error bars display standard deviation of triplicates. (B) The growth of the strains was also assessed in droplet assay using iron depleted medium in absence (I, II, III) and in presence (IV, V, VI) of 10 mM Cilastatin. The growth of a PfA506 wild-type strain (I, IV), a PfA506 $\Delta pvdM$ strain (II, V) and a PfA506 $\Delta pvdM$ strain complemented with Strep-tagged PvdM (III, VI) was documented under normal light (upper row), production of pyoverdine was checked under UV light (lower row).

As seen in the growth curve data, Cilastatin does not only slightly affect the growth of the $\Delta pvdM$ strain complemented with PvdM, but also the growth of the wild-type strain. While the wild-type strain enters the exponential growth phase after approximately 18 h in medium without Cilastatin, reaching of this phase is delayed by approximately 2 h in presence of Cilastatin. In case of the complemented $\Delta pvdM$ strain, the strain reaches the exponential phase even later, only after approximately 26 h. If Cilastatin was added to the medium, this phase is reached after additional 4 h. As can also be seen from the graph, the addition of cilastatin has no polar effects on the growth of the control strain PfA506 $\Delta pvdM$, which was unable to grow on CAA medium supplemented with EDDHA in both the absence and presence of cilastatin (**Figure 16 A**). The evaluation of the droplet assay shows that pyoverdine production was only marginally influenced by Cilastatin in a comparison fluorescence after 36 h. Both, the wild type and the $\Delta pvdM$ strain complemented with *pvdM* were able to grow on the EDDHA-depleted medium and produce pyoverdine, as shown by the colonies glowing under UV light. However, it can be seen here that the PvdM-complementation strain produced slightly less pyoverdine than the wild type (**Figure 16 B**). In summary, these experiments show that Cilastatin appears to have only a slight effect on PvdM in terms of growth and pyoverdine production but does not appear to have the same inhibiting effect on PvdM as has previously been shown for the human renal dipeptidase.

3.1.5 PvdM is required for the activity of PvdP *in vivo*

As an involvement of PvdM in the regulation of pyoverdine biosynthesis as the unknown site 1-like peptidase, responsible for the periplasmic cleavage of FpvR, has been ruled out, we asked the question of the timepoint PvdM is possibly involved in the maturation of pyoverdines. Since each step in the maturation of pyoverdine is accounted for by the maturation enzymes PvdN, PvdO, PvdP, PvdQ and PtaA and an intermediate of the pyoverdine biosynthesis has never been shown in a *P. fluorescens* A506 $\Delta pvdM$ strain, it was investigated if a variant of pyoverdine or ferribactin was detectable in the aforementioned strain. With the potential identification of ferribactin or an intermediate of pyoverdine, a conclusion could be drawn as to when PvdM interacts in the known order of maturation. For this experiment, a *P. fluorescens* A506 $\Delta pvdM$ strain was incubated in CAA medium and the supernatant was analysed via UPLC-MS.

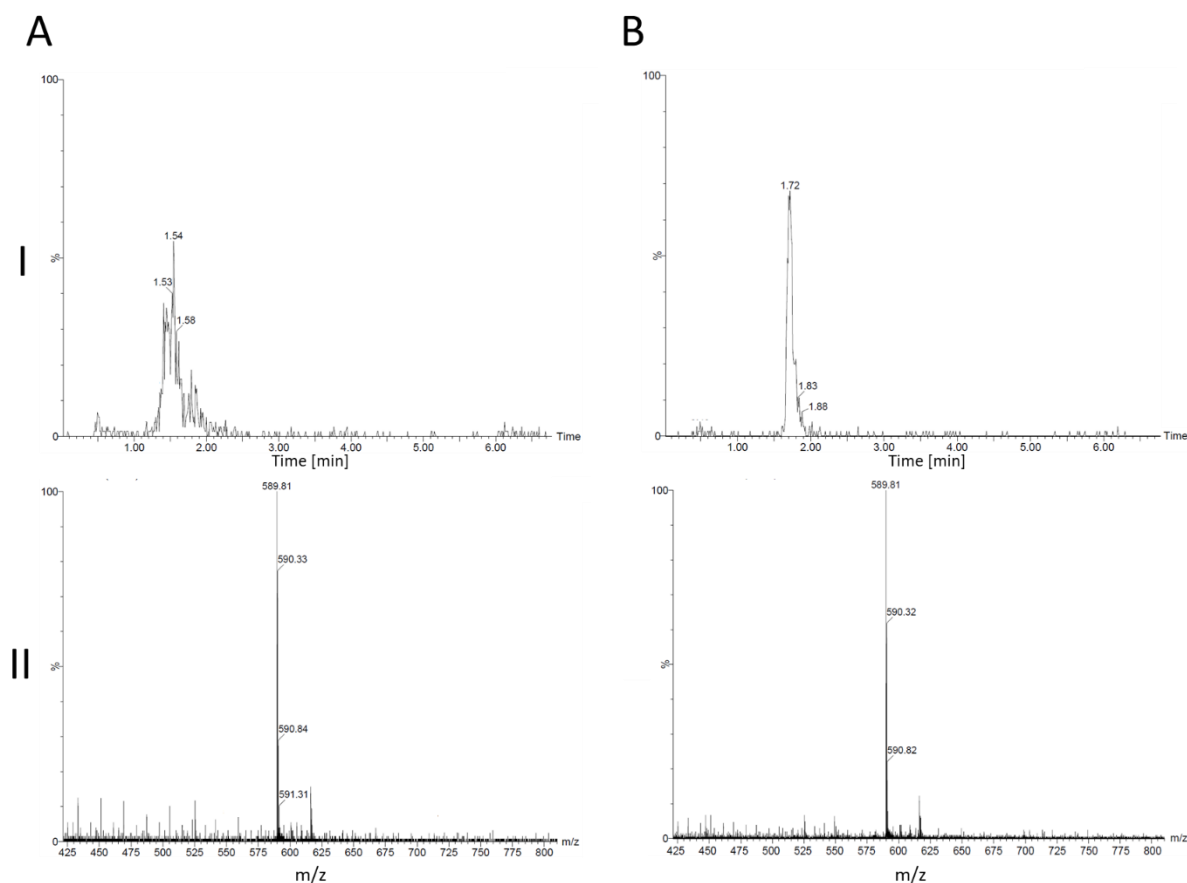


Figure 17: Detection of ferribactin in the supernatant of *P. fluorescens* A506 $\Delta pvdM$ and *P. fluorescens* A506 $\Delta pvdP$. (A) Chromatogram (I), and spectrum (II) of the UPLC-MS analysis of the medium supernatant of a *P. fluorescens* A506 $\Delta pvdM$ strain grown in CAA medium supplemented in EDDH. (B) Chromatogram (I), and spectrum (II) of the UPLC-MS analysis of the medium supernatant of a *P. fluorescens* A506 $\Delta pvdP$ strain grown in CAA medium supplemented in EDDHA.

Surprisingly, as shown by the UPLC-MS data (**Figure 17 A**), deacylated ferribactin, with a mass of 1178.62 Da was detected as the only intermediate of the pyoverdine biosynthesis pathway. This result shows that PvdM is involved in the maturation step between the export of ferribactin into the periplasm by PvdE and the oxidative cyclisation to dihydropyoverdine by PvdP. To verify that *P. fluorescens* A506 $\Delta pvdP$ strain indeed only produces ferribactin, said strain was incubated in CAA medium and the supernatant was analysed in the same manner as before. As expected in a *P. fluorescens* A506 $\Delta pvdP$ strain, the only intermediate of the pyoverdine biosynthesis pathway was indeed the deacylated ferribactin, as all following maturation reactions are not feasible without the oxidative cyclisation to dihydropyoverdine (**Figure 17 B**). This shows that PvdM is necessary for the activity of PvdP *in vivo*.

3.1.6 Copper cannot compensate for missing PvdM *in vivo*

Since PvdM has been shown to be essential for the activity of PvdP *in vivo* and previous experiments with PvdP required an unusually high copper concentration, it was investigated whether the lack of PvdM could be compensated with an increased copper concentration (Nadal-Jimenez *et al.* 2014; Wibowo *et al.* 2020). For this purpose, $\Delta pvdM$ strains were incubated with different concentrations of added copper(II) sulfate and checked whether growth, which has not been possible before, could now be restored.

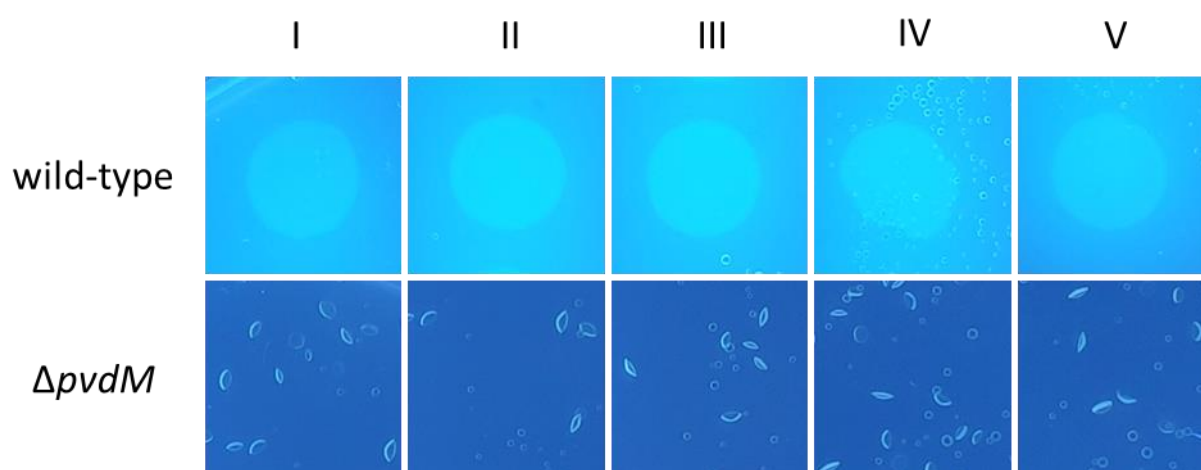


Figure 18: Copper does not restore a *P. fluorescens* A506 $\Delta pvdM$ phenotype. Evaluation and comparison of growth and pyoverdine production between the *P. fluorescens* A506 wild-type and a $\Delta pvdM$ deletion strain with 0 μM (I), 5 μM (II), 10 μM (III), 50 μM (IV) and 100 μM (V) of added copper(II) sulfate.

As can be seen from the growth experiments, the external addition of copper at concentrations up to 100 μM did not cause the *P. fluorescens* A506 $\Delta pvdM$ strain to grow on iron-depleted CAA medium, let alone to form pyoverdine. At the same time, the addition of up to 100 μM copper showed no effects on the wild type in terms of both growth and pyoverdine production, and thus served as a useful control (**Figure 18**).

3.1.7 PvdM possesses at least two membrane anchors

In the results presented previously, it has been shown that PvdM is a membrane integrated protein with the globular domain facing the periplasm. Although it has been postulated that the membrane anchor of PvdM is required for its activity, this observation was only based on the observation that a PvdM variant missing its membrane anchor was not capable of complementing a $\Delta pvdM$ phenotype (Ringel 2018). In this attempt, it was tested, whether the insertion of cleavage site and the release of the PvdM variant into the periplasm as a soluble protein after its translocation would affect the function of PvdM in any way. To address this question, an AXA signal peptidase cleavage site, more precisely Ala-Ser-Ala, was inserted into the end of the predicted trans-membrane domain region substituting the last hydrophobic amino acids leucine, valine and tryptophan. A *P. fluorescens* A506 $\Delta pvdM$ strain was complemented with the PvdM-ASA variant encoded on the anthranilate inducible vector pUCP20-ANT2-MCS-*pvdM*-ASA-Strep and its effects and location were analysed via growth experiments and western blot analyses of subcellular fractionations.

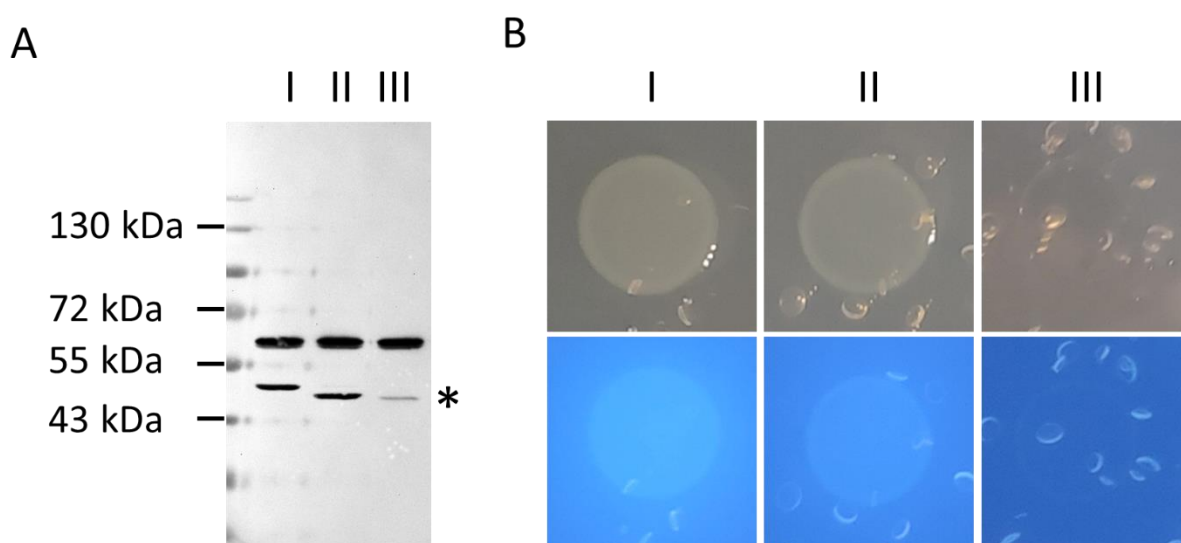


Figure 19: PvdM variant analyses of their localisation and ability to complement a *pvdM* deletion. (A) Western blot analysis of the membrane fractions of subcellular fractionations of the PvdM variants produced in $\Delta pvdM$ strains. Membrane fraction of wild-type PvdM encoded on the plasmid pUCP20-ANT2-MCS-His-*pvdM*-Strep (I), a PvdM variant with the signal peptide substituted by that of PvdO encoded on plasmid pUCP20-ANT2-MCS-His-*SPpvdO-pvdM*-Strep (II) and a PvdM variant with an insertion of an ASA cleavage site encoded on the plasmid pUCP20-ANT2-MCS-His-*pvdM*-ASA-Strep (III). PvdM variants are marked by an asterisk (*). (B) The analysis of the respective strains and their complementation ability was tested on CAA medium supplemented with EDDHA. The growth was of the strains was documented under normal light (upper row), production of pyoverdine was checked under UV light (lower row).

The western blot analysis of the membrane fractions of the PvdM variants produced in $\Delta pvdM$ strains shows differences in processing. The PvdM-ASA variant was indeed processed but unexpectedly, remained in the membrane fraction. Furthermore, a degradation of the PvdM-ASA variant can be observed (**Figure 19 A**). As the growth experiments on CAA agar plates supplemented with EDDHA show, the PvdM-ASA variant was not able to complement a $\Delta pvdM$ phenotype and was therefore inactive (**Figure 19 B**).

In a second approach, an attempt was made to circumvent the degradation problem by retaining the end of the transmembrane domain at the mature PvdM. The amino acid residues 1-24 of PvdM were exchanged by the proper Sec signal peptide of PvdO, a protein shown to be soluble in the periplasm. With the retention of the last five amino acids glycine, leucine, leucine, valine and tryptophan attached to the N-terminus of the mature protein, a stable and soluble periplasmic protein was expected.

As expected, the construct of the signal peptide of PvdO fused to the end of the N-terminal signal peptide of PvdM was indeed processed. This is shown by the reduced molecular weight of the PvdM detected in the western Blot. Most surprisingly, the mature PvdM remained attached to the membrane even after processing of the signal peptide and could not be detached from it by carbonate washes (**Figure 19 A**). In contrast to the construct with the inserted ASA cleavage site, this construct was active and was able to complement a $\Delta pvdM$ phenotype on iron depleted CAA agar plates (**Figure 19 B**).

To verify that the signal peptide of PvdM actually also functions as a membrane anchor for the protein, further protein constructs were made. It was checked how the subcellular localisation of the periplasmic phosphatase PhoA changes after replacement of the signal peptide by that of membrane integrated PvdM or the proper translocated PvdO, respectively. For this purpose, the mature PhoA from *E. coli* MC4100 was fused with the respective signal peptides and produced in *P. fluorescens* A506. The subcellular fractions were then analysed for the presence of the respective Strep-tagged protein.

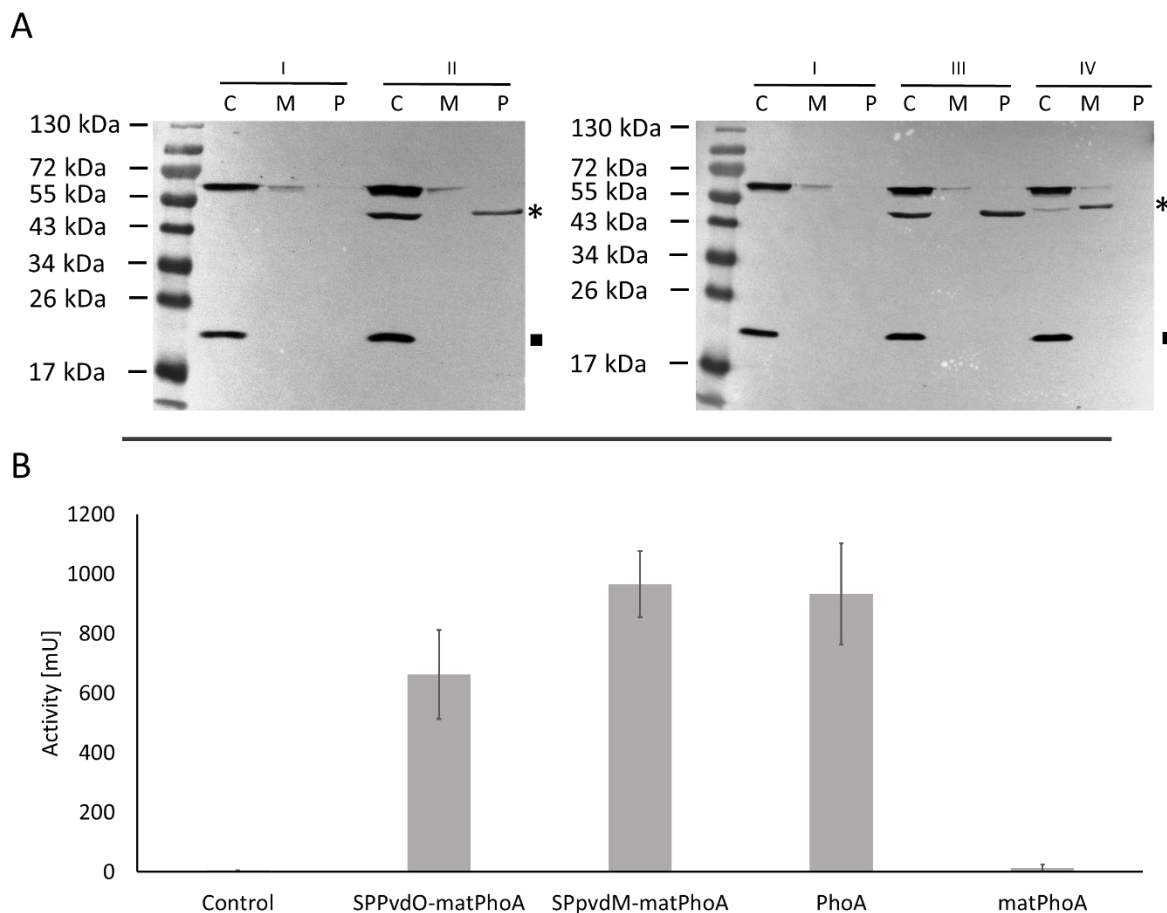


Figure 20: PvdM signal peptide causes anchoring in cytoplasmic membrane. Analysis of subcellular localisation of different PhoA variants produced in Pfa506. **(A)** Western blot analysis of Pfa506 wild-type with the plasmid pUCP20-ANT2-MCS (I), wild type PhoA encoded on the plasmid pUCP20-ANT2-MCS-*phoA*-Strep (II), the PhoA variant with the signal peptide of PvdO encoded on the plasmid pUCP20-ANT2-MCS-*SPPvdO-phoA*-Strep (III) and the PhoA variant that has the signal peptide substituted by that of PvdM, encoded on the plasmid pUCP20-ANT2-MCS-*SPPvdM-phoA*-Strep (IV). C: cytoplasm; M: membrane, P: periplasm. PhoA variants are marked by an asterisk (*). Naturally occurring BCCP serves as a control for cytoplasmic proteins (■). **(B)** Measured activity of different PhoA variants in *P. fluorescens* A506. Error bars display standard deviation of triplicates

As seen in the western blot of the respective fractionations, wild-type PhoA is found equally distributed in the cytoplasm and in the periplasm (**Figure 20 A**). PhoA, which has been produced but not yet translocated into the periplasm is therefore found in the cytoplasmic fraction. As the signal peptide is substituted by that of PvdO, the same distribution pattern can be observed and the overall distribution of the protein does not change. However, with the PhoA signal peptide substituted by that of PvdM, PhoA is predominantly found in the membrane fraction, with no PhoA liberated into the periplasm. Furthermore, this construct seems to have

a slightly higher molecular mass, which could be due to the uncut signal peptide of PvdM. These data show, that the signal peptide of PvdM indeed provides membrane anchoring.

Additionally, it could be shown that PhoA variants with the substituted signal peptide with that of PvdM and PvdO, respectively, were indeed transported into the periplasm by the performance of an alkaline phosphatase assay. As seen in the graph, the measured activity of the control, both a PfA506 wild-type strain carrying an empty pUCP20-ANT2-MCS vector and the mature PhoA was virtually non-existent. The measured activity of the remaining PhoA variants, i.e., the two already mentioned variants with the signal peptide exchanges and the wild-type PhoA, however, was 600-1,000 times stronger (**Figure 20 B**).

With these experiments it could be shown that the last amino acid residues of the transmembrane domain of PvdM are equally important for its stability and activity. Furthermore, it could be proven that the complete transmembrane domain is not required for a functional PvdM. Finally, it was elucidated that PvdM has at least one membrane anchorage besides the N-terminal transmembrane domain, which is involved in the integration of the protein into the cytoplasmic membrane.

3.1.8 Identification of potential anchorage sites

Since the membrane integrity of PvdM has been verified and it has been shown, that PvdM possesses at least two anchorage sites for the integration into the cytoplasmic membrane, this additional membrane integration site was further analysed. In a next approach, Strep-tagged PvdM was produced in *E. coli* BL21 and solubilised. After subsequent Strep-Tactin gravity-flow purification, PvdM was concentrated using Vivaspin columns and isolated via a SDS gel electrophoresis (**Figure 21**). The corresponding band on the gel containing PvdM was cut out and then in-gel tryptically digested. The mass of the individual peptide fragments was compared with the previously calculated expected masses of PvdM after trypsin digestion and examined for possible post-translational modifications.

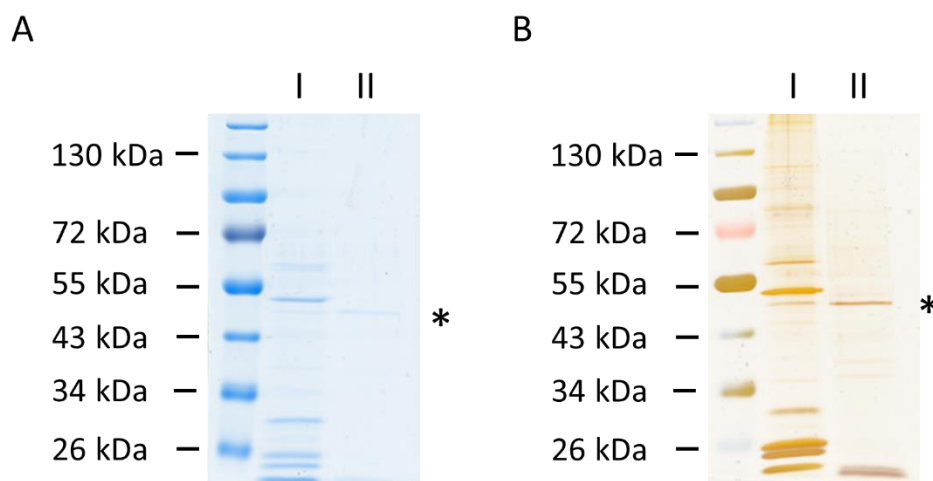


Figure 21: SDS-Gel of PvdM as purified from *P. fluorescens* A506. (A) Coomassie stained SDS gel of the membrane pellet after solubilisation of PvdM (I) and concentrated supernatant of the solubilisation after Strep-Tactin gravity-flow purification (II). (B) Silver stained SDS gel of the membrane pellet after solubilisation of PvdM (I) and concentrated supernatant of the solubilisation after Strep-Tactin gravity-flow purification for better visualisation (II). PvdM is marked by an asterisk (*)

While various modifications were presented after the analyses of the peptide fragments, only putative peptide modifications that possessed an increase in mass in comparison to the unmodified peptide fragment were considered. Since no fragment could be identified to harbour a post-translationally added membrane anchor, the identified fragments were compared with the original sequence of PvdM. After having covered 70 % of the sequence with fragments found in analysis of the tryptic in-gel digestion, six amino acids were identified, that could possibly be modified. Out of these six amino acids, only two amino acids were at the surface, namely serine at position 272 and serine at position 419 (**Figure 22**). While the modification of PvdM responsible for the integration into the cytoplasmic membrane despite the lack of the membrane peptide has not been identified, two possible modification sites positioned at the surface of the protein have been isolated.

MTKRSRKKALYIGLPLALAIAGAGALLVWDQWFKGNAGYPLEVIKQANEMQERLLSFDSHITLPL
 DFGTAGNEADKDGSGQFDLAKAARGRLSGAALTIFGWPEIWNGDNAPHKPTDGFVEEARHEHE
 VRYKIISGMVRDFPNQVGIAYTPDDMRRLHGEKGFAIFISMLNAYPLGNDLNQLDLWAARGMR
 MFGFSYIGNNAWSDSSRPLPFNDSPDALEGLSPIGQQAVHRLNDLGVIIDVSQMSTKALEQVA
 QLSRTPMVASHSAPRASVDIPRNLSDKELQLIKNSGGVVQVVGFPAYLRPLSQPTQDKLNTLRARF
 DLPPLPNLAMALMPGDAAIAAWPEQRFQYASALYGILEEPEKATLKDLGDAIDYTVRKIGIDHVGI
 ASDFNDGGGLQGWENVGEVRNVTAELIQRGYSEADIAKLWGGNFLRVWDQVQKAAKPLANR

Figure 22: Coverage of PvdM by found peptide fragments. Overview of the covered sequences of PvdM by detected unmodified peptide fragments highlighted in green. Amino acid residues that may be modified are highlighted in blue and red, with the red amino acid residues located on the surface of PvdM.

3.2 Further analyses of PvdP

As described above, PvdP is responsible for catalysing the oxidative cyclization of ferribactin to pyoverdine in periplasm. As a member of the tyrosinases, PvdP is equipped with a type-three dicopper Cu^{2+} active site in its catalytic centre (**Figure 23**). As shown in the previous results, the membrane bound PvdM is required for the catalysation of the oxidative cyclisation of ferribactin to pyoverdine by PvdP *in vivo*. Given these facts, we decided to investigate the exact subcellular localisation of PvdP, which was stated to be transported via the Tat-pathway and liberated into the periplasm as a soluble protein after its translocation (Nadal-Jimenez *et al.* 2014).

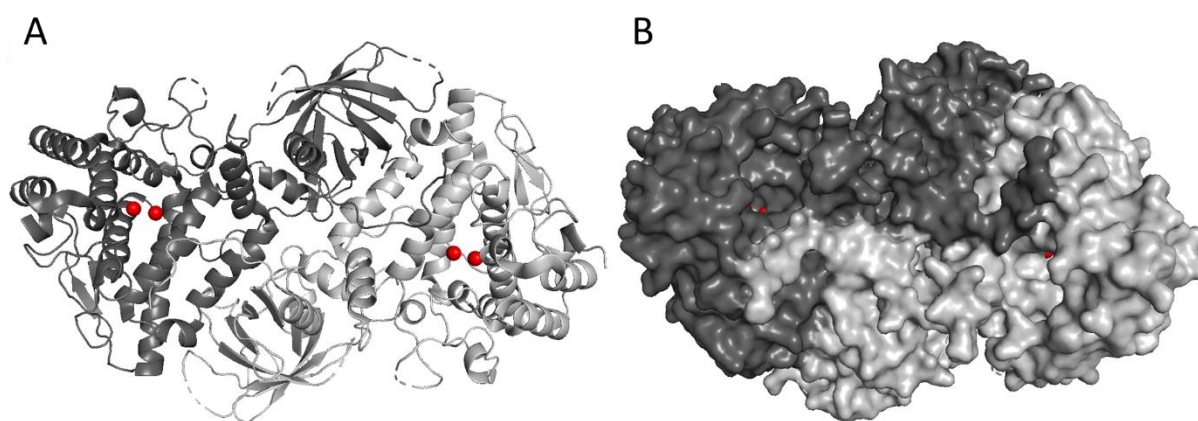


Figure 23: Model of PvdP from *P. aeruginosa*. (A) Model of PvdP from *P. aeruginosa* show the type-three copper ions highlighted in red coordinated within the structure of PvdP. (B) A model with a visualised surface of the protein shows the cavity of the active site with highlighted copper ions at the inside of the tunnel. These models were created using PyMol based on the crystal structure of PvdP from *P. aeruginosa* (Schrödinger and DeLano 2020; Poppe *et al.* 2018).

3.2.1 PvdP is a membrane bound tyrosinase

The confirmation of the subcellular localisation of PvdP has only ever been done in *E. coli* with a PvdP variant missing the N-terminal 25 amino acids including its complete signal peptide (Nadal-Jimenez *et al.* 2014). Analysis of the Tat signal peptide of PvdP however, revealed an unusual property with the lack of a distinct cleavage site, doubting that the signal peptide is cleaved at all. Therefore, in this work an approach was chosen to revise whether a full-length PvdP with its Tat signal peptide in its original host strain *P. fluorescens* A506 is still found as a liberated periplasmic protein. For that experiment, N-terminally His-tagged *pvdP* was cloned into the expression vector pUCP20-ANT2-MCS (Hoffmann *et al.* 2021). The anthranilate inducible vector was transformed into a *P. fluorescens* A506 $\Delta pvdP$ strain and a subcellular fractionation was performed after the production of His-PvdP. The obtained fractions were analysed via western blot for the detection of PvdP. The membrane fraction was additionally treated with carbonate buffer for the detachment of weakly associated proteins.

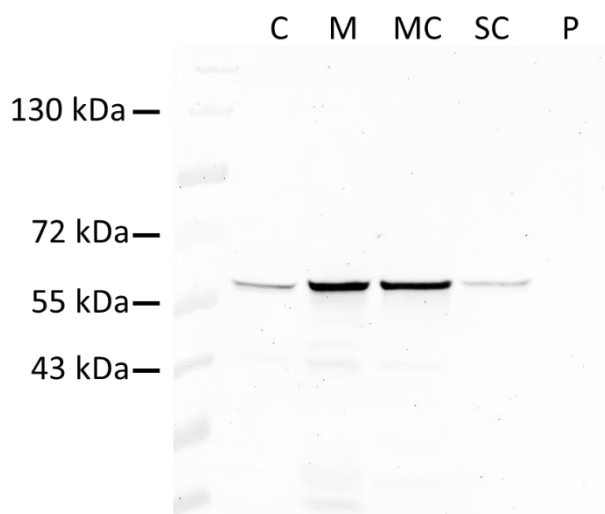


Figure 24: PvdP is localised in the cytoplasmic membrane. Western blot of a subcellular fractionation of a PfA506 $\Delta pvdP$ strain complemented with His-tagged PvdP encoded on the plasmid pUCP20-ANT2-MCS-His-*pvdP* and subsequent carbonate wash of the membrane fraction.

Surprisingly and contrary to the previously published data, the majority of PvdP was detected in the membrane fraction of *P. fluorescens* A506 and could hardly be detached from the

membrane by a carbonate wash. A small amount was also detectable in the cytoplasm. However, this is due to PvdP that has been produced in the cytoplasm, but has not yet been translocated into the periplasm. No PvdP, was found in periplasm, the fraction in which PvdP is found according to previous publications (**Figure 24**). As the N-terminal histidine-tag is still detectable, the signal peptide does not seem to be cleaved off after the translocation.

3.2.2 Analysis of the copper contained in PvdP as a function of PvdM

Since it has been elucidated that PvdM is indispensable for the activity of PvdP *in vivo*, it was investigated how PvdM could interact with PvdP to provide for its activity. As Tat substrates are folded prior to their translocation across the cytoplasmic membrane, incorporation of possible co-factors must already occur in the cytoplasm, otherwise proteins are not transported (Berks 1996; Berks *et al.* 2000). While this is the case for most of the known Tat substrates, it has been shown that the incorporation of copper must occur after the translocation into the periplasm (Stolle *et al.* 2016). As PvdP contains a type-three dicopper active site, PvdM may be involved in the incorporation of copper into the folded PvdP. To test this hypothesis, the copper content of PvdP produced under two different conditions was compared. On the one hand, PvdP was produced in a *P. fluorescens* A506 strain that contained PvdM and could therefore incorporate copper, if PvdM was indeed responsible for the copper incorporation; on the other hand, PvdP was produced in a *pvdM* deletion strain. The produced PvdP was enriched and analysed for their nickel, copper and zinc concentration via inductively coupled plasma - mass spectrometry (ICP-MS) (**Figure 25**).

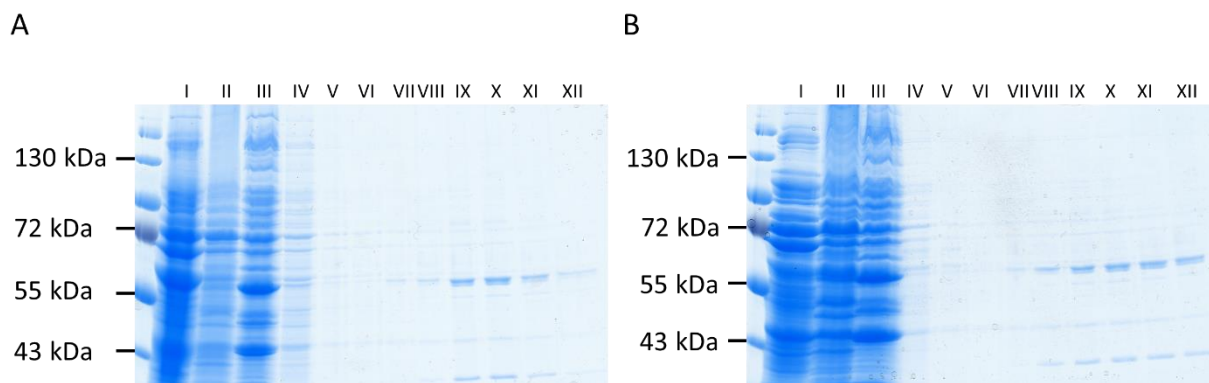


Figure 25: Production and enrichment of PvdP for copper analysis. Comparison SDS-gels of the production, purification and enrichment of His-tagged PvdP encoded on the plasmid pUCP20-ANT2-MCS-*pvdP*-His in a (A) PfA506 $\Delta pvdM$ strain and (B) a PfA506 wild-type strain. **I**: soluble proteins; **II**: solubilised proteins; **III**: membrane pellet after solubilisation; **IV**: flowthrough fraction, **V**: wash fraction; **VI-XII**: elution fractions 4-8.

Table 22: Inductively coupled plasma - mass spectrometry measurements of two PvdP variants.

PvdP variant	Nickel concentration	Copper concentration	Zinc concentration
PvdP ($\Delta pvdM$)	0.16 $\mu\text{g/ml}$	0.017 $\mu\text{g/ml}$	0.07 $\mu\text{g/ml}$
PvdP (WT)	0.20 $\mu\text{g/ml}$	0.049 $\mu\text{g/ml}$	0.08 $\mu\text{g/ml}$

Measuring the band intensity of the PvdP band and bringing it in relation to the rest of the proteins in the lanes resulted in concentration of 5.3 % for PvdP produced in the *P. fluorescens* A506 $\Delta pvdM$ strain and 8.5 % for PvdP produced in the *P. fluorescens* A506 wild-type strain (**Table 23**).

Table 23: Calculation of the relative PvdP content in the protein mixture.

PvdP variant	[c] Protein	[M] Protein	% PvdP	[M] PvdP
PvdP ($\Delta pvdM$)	600 $\mu\text{g/ml}$	9.55 μM	5.3 %	0.50 μM
PvdP (WT)	500 $\mu\text{g/ml}$	7.96 μM	8.5 %	0.67 μM

Combined with the measured protein concentration 0.6 mg/ml and 0.5 mg/ml for PvdP produced in the $\Delta pvdM$ strain and in the wild-type strain, respectively, the expected overall molarity of copper in the samples could be calculated.

Table 24: Comparison of expected and actually measured copper concentrations.

PvdP variant	[M] PvdP	[M]Copper expected	[M]Copper detected	Ratio
PvdP ($\Delta pvdM$)	0.50 μ M	1.00 μ M	0.27 μ M	27.0 %
PvdP (WT)	0.67 μ M	1.34 μ M	0.78 μ M	58.2 %

As seen in the tables, fewer copper than expected was detected in both samples. Because PvdP possesses two copper ions per subunit, the expected copper concentration in the samples is twice as high as the concentration of PvdP. While a copper concentration of 1 μ M was expected for the sample containing PvdP produced in the $\Delta pvdM$ strain, only 0.27 μ M copper was detected via ICP-MS. As for the PvdP variant produced in the wild-type strain, 0.78 μ M of copper were detected as opposed to the expected 1.34 μ M (**Table 22**). This means, that only 27.0 % and 58.2 % of the expected copper was detected in the two samples, respectively (**Table 24**). Although the copper values detected do not correspond to expectations, it can be seen that more than twice as much copper was detected in sample containing PvdP produced in the wild-type strain as in sample containing PvdP produced in the $\Delta pvdM$ strain. The simultaneously detected concentrations of nickel and zinc serve here as a control and show that the concentration of these metals, in contrast to copper, is independent of the presence of PvdM.

3.2.3 Cysteine crosslinking of PvdP

In a next step, the dimeric PvdP was examined for potential interactions of the signal peptides of the respective monomers. Posttranslational modifications in form of disulfide cross-linking were carried out to identify possible interactions. In this reaction the two adjacent sulfhydryl groups of the thiol residues are oxidized and form a disulfide bridge (Fass and Thorpe 2018). To do so, various amino acids within the signal peptide of PvdP, which has been shown not to be cleaved off after translocation into the periplasm, have been substituted by cysteine. With four consecutive amino acids being substituted by cysteine, a complete alpha helix turn was

covered. In this way, it was possible to ensure that, if an interaction between the signal peptides takes place, a cysteine is definitely present at the right position for disulfide crosslinking to occur.

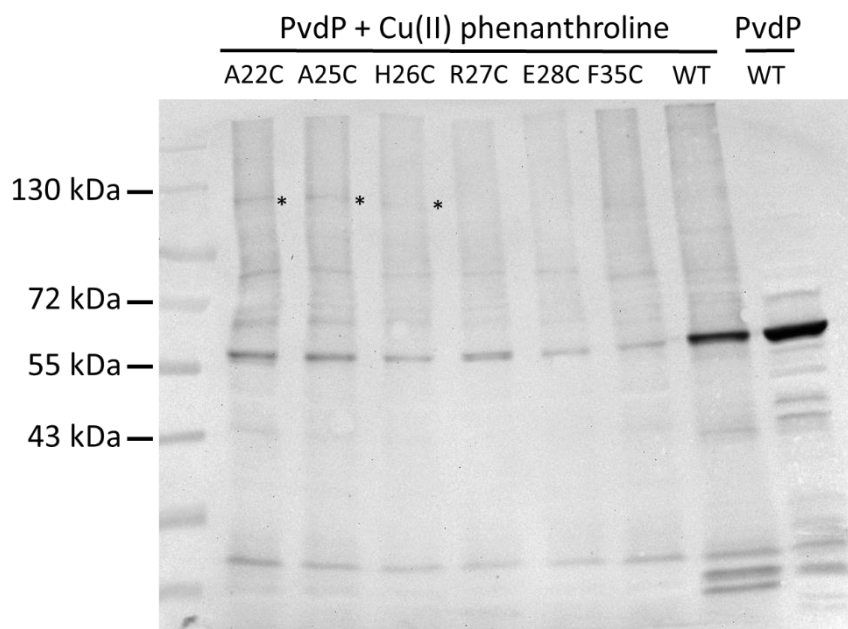


Figure 26: Signal peptides of PvdP monomers are in spatial proximity to interact with one another. Western blot of the membrane fractions containing unmodified PvdP and PvdP variants with various amino acids in the signal peptide replaced by cysteine. The proteins were produced in PfA506 $\Delta pvdP$ strains that were complemented with the respective PvdP variant encoded on the plasmid pUCP20-ANT2-MCS. Incubation of these fractions with Cu(II) phenanthroline and subsequent western blot analysis under non-oxidising conditions show a formation of a band at approximately 120 kDa when alanine at position 22 or 25 or histidine at position 26 are substituted by cysteine, respectively. The new formed bands are marked with a (*) for better visualisation.

As can be seen in the western blot, clearly visible bands in the higher kDa range are formed compared to the negative control untreated with CuP in the last lane. Since entire membrane fractions, which contain several other proteins in addition to PvdP, were treated with CuP, many bands are to be attributed to interactions between these proteins, that are either unspecific membrane associated or membrane integrated. However, it is clearly visible in that in the first three lanes a band with a molecular weight of approximately 120 kDa is formed when the membrane fractions of PvdP variants A22C, A25C and H26C are incubated with CuP, respectively. These emerging bands are not visible when the membrane fraction containing the unmodified PvdP is treated with CuP, as seen in the penultimate lane of the western blot, and correspond approximately to the molecular weight of a PvdP dimer of 116.66 kDa. While this

band can only be seen in the lanes of the first three PvdP variants, the other tested PvdP variants and the included wild type as a negative control do not have a specific band in this range of molecular weight, indicating that no interaction detectable by disulfide crosslinking occurred (**Figure 26**). These data show that it is sterically possible for the signal peptides of the respective PvdP monomers to interact with each other and possibly serve as a membrane anchor for the PvdP dimer on the periplasmic surface of the cytoplasmic membrane.

3.3 Enzymatic analysis of PvdN

As previously described, pyoverdine with a succinamide residue was not detectable anymore in a *pvdN* knockout strain. It was therefore concluded that PvdN is most likely responsible for catalysing the conversion of the N-terminal glutamic acid residue of pyoverdines to a succinamide residue via an unusual PLP-dependent oxidative decarboxylation reaction in the periplasm (Ringel *et al.* 2016). Since the established hypothesis of the reaction mechanism is only based on the missing succinamide variant of pyoverdine in the $\Delta pvdN$ strain, the actual verification of the catalytic conversion by the purified enzyme has not yet been presented.

3.3.1 PvdN requires molecular oxygen for conversion of glutamic acid to succinamide

In order to demonstrate that PvdN indeed catalyses the conversion of the N-terminal glutamic acid residue of pyoverdine, PvdN had to be overproduced and purified first. For this purpose, His-SUMO-tagged PvdN was heterologously overproduced in *E. coli* BL21 (DE3) and purified via nickel affinity chromatography. The resulting fractions were pooled and incubated overnight with Ulp-protease at 4 °C to cleave of the His-SUMO-tag and purified again using nickel affinity chromatography. The tag-less protein was flowing through while the His-SUMO-tag remained bound the Ni-NTA agarose matrix (**Figure 27 A**). To increase the purity level, PvdN was further isolated from the obtained fractions via an ÄKTA protein purification system-controlled size exclusion chromatography (**Figure 27 B**). The obtained fractions containing purified PvdN were further concentrated using a Vivaspin concentrator with a cut-off of 10 kDa. For stabilization of PvdN during these purification steps, 1 mM PLP was added to all buffers.

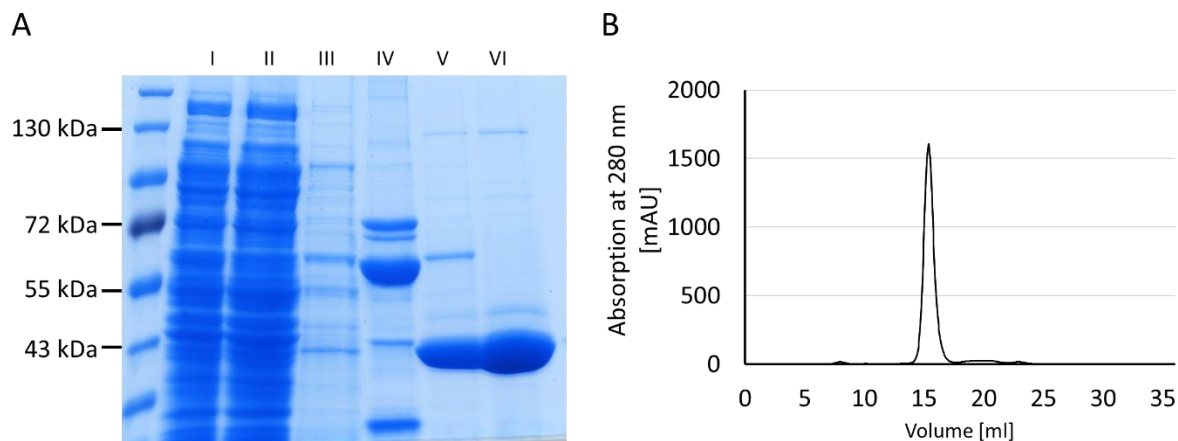


Figure 27: SDS-gel of PvdN purification steps. (A) Strep tagged PvdN, which was encoded on the plasmid pCA528-mat-*pvdN*, was produced in the expression strain *E. coli* BL21. Shown are the fractions after ultracentrifugation (I), the flow through of the His-column (II), the washing fraction (III), the pooled elution fraction (IV), the eluted fraction after restriction by Ulp1 (V), and the concentrated fraction after final purification by size exclusion chromatography (VI). (B) Absorption of PvdN at 280 nm during size exclusion chromatography using an ÄKTA protein purification system.

The purified enzyme was then used for testing the enzymatic conversion of the glutamic acid residue of pyoverdine in dependence on PvdN. The setup reactions were stopped after 15 min, 30 min, 45 min and 60 min, respectively. The supernatants of the reaction mixes were then analyzed via mass spectrometry to detect the N-terminal succinamide variant of pyoverdine.

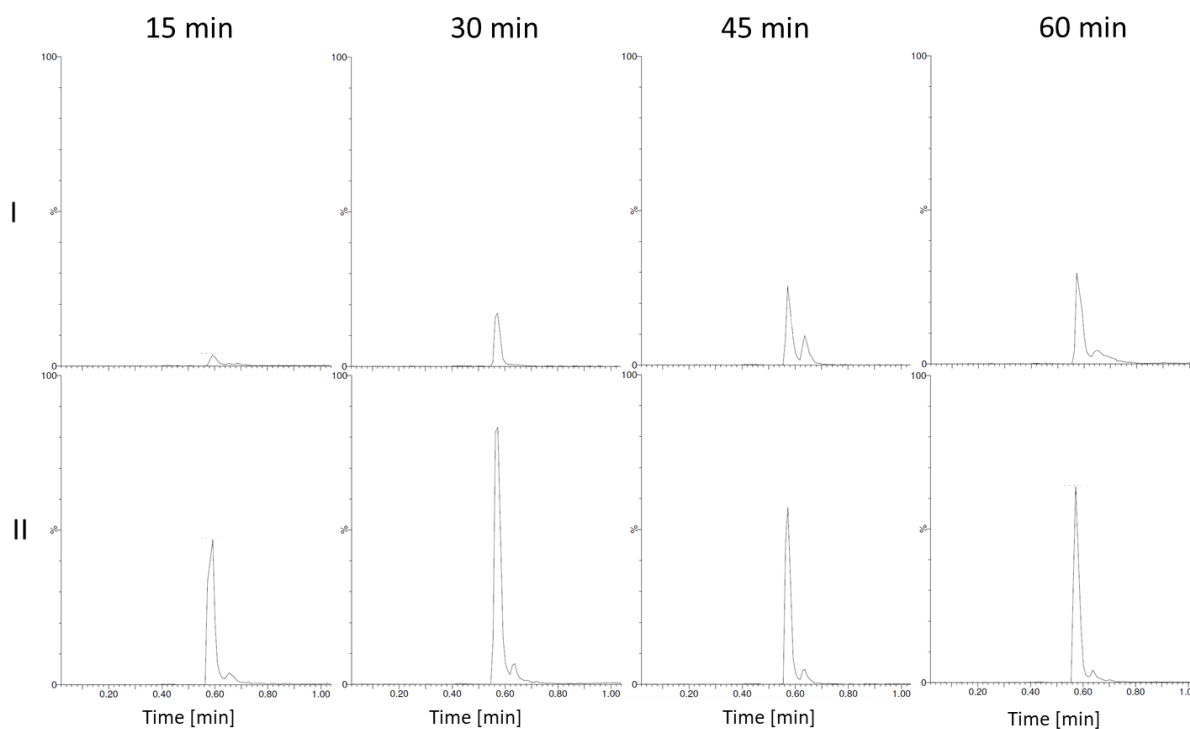


Figure 28: PvdN catalyses the conversion of the glutamic acid to the succinamide variant of pyoverdine. Chromatograms of the reaction of PvdN and the glutamic acid variant of pyoverdine stopped at different time points demonstrate a conversion of the glutamic acid residue to succinamide, clearly visible by the formation and accumulation of the succinamide variant of pyoverdine with a mass of $1160.6 \text{ Da} \pm 0.1 \text{ Da}$ over time span of 60 minutes (**I**). In parallel, the chromatogram of pyoverdine with the glutamic acid residue with a mass of $1190.6 \text{ Da} \pm 0.1 \text{ Da}$ is also shown (**II**). The comparison of the two peaks at the respective times shows that the ratio of the succinamide variant to the glutamate variant steadily increases.

As seen in the chromatograms, when purified PvdN was added to the reaction mix, a compound with the mass with 1160.6 Da is detectable, corresponding to the mass of pyoverdine with a succinamide residue. In contrast to the negative control, lacking PvdN in the reaction mix, no succinamide variant of pyoverdine was detectable. As the reaction continues over time, the amount of the detectable succinamide variant of pyoverdine increases (**Figure 28**). This shows clearly, that PvdN is responsible for the conversion of the glutamic acid residue of pyoverdine to the succinamide residue.

The purified PvdN was also used to perform enzymatic experiments investigating the dependence of the reaction on molecular oxygen. For these experiments, all used ingredients such as buffers, water, enzyme and substrate were gased with nitrogen for 15 min in order to displace oxygen from the samples. The individual compounds of the reaction were then

transferred into vials that had previously been flushed with nitrogen. To start a reaction, 2 ml of molecular oxygen were added to the reaction mix and the relative amount of oxygen, nitrogen and carbon dioxide was determined via gas chromatography.

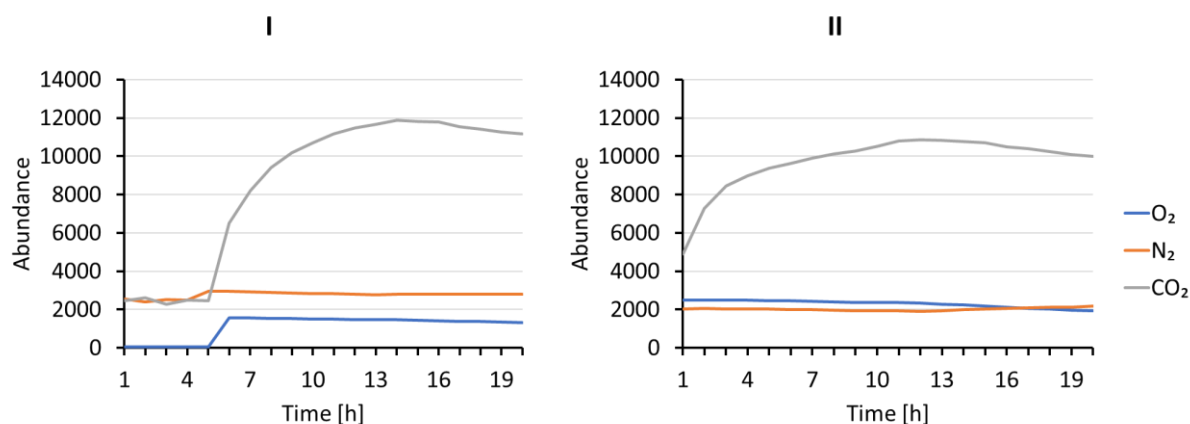


Figure 29: Catalytic activity of PvdN is dependent on molecular oxygen. Gas chromatography analysis of the gaseous phase of a PvdN reaction mix in the absence and presence of oxygen. Measurements of the abundance of nitrogen, oxygen and carbon dioxide over a period of 20 hours. In the first approach, the oxygen-free reaction mixture was spiked with molecular oxygen only after a 5-hour incubation period (I); in the other approach, oxygen was added directly at the beginning (II).

As can be seen from the measurements of the gas chromatograph, the conversion of the N-terminal glutamic acid residue to the succinamide residue is an oxygen-dependent reaction that produces carbon dioxide. Since oxygen was added to the first reaction mix only after 5 h of incubation, no drastic change in the ratio of the gases to each other can be seen at the beginning. Only after the addition of molecular oxygen does the concentration of carbon dioxide increase sharply. In the second approach, oxygen is present in the reaction from the beginning, as can be seen from the strong increase of carbon dioxide already in the first hours (**Figure 29**). In both samples a slight, but clear decrease of molecular oxygen can be observed over the whole measuring period of 20 h, while the measured nitrogen hardly changes noticeably.

3.3.2 PvdN accepts glutamine as a substrate

In search of alternative substrates to pyoverdine, the two most obvious alternatives to the original substrate, which is pyoverdine with a glutamic acid side chain, were first investigated. It was tested if PvdN was able to convert pure glutamic acid or glutamine without the extension of the pyoverdine. Therefore, a reaction setup similar to the one previously described was prepared with the substitution of pyoverdine as a substrate by either glutamic acid or glutamine. The reaction was incubated for 60 min and stopped by the addition of 3 volumes of pure ethanol. The supernatant of that reaction mix was analysed via UPLC-MS.

Interestingly, it could be shown that PvdN is not able to convert free glutamic acid to succinic acid, but was able to convert glutamine to succinamide (**Figure 30**).

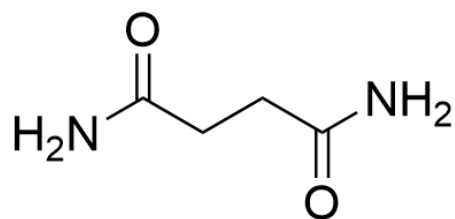


Figure 30: Structure of succinamide.

The UPCL-MS analysis of the supernatant of the preparation with glutamate and PvdN shows no changes compared to the preparation without PvdN and also no substrate peak that has the sought mass of 118.06 Da. The ratios of the measured masses also hardly change noticeably. However, in the reaction mixture in which the conversion of glutamine was investigated, a clear peak with a mass of 117.06 Da is detected, which elutes from the column after 0.86 min. This mass is also clearly detectable in the mass spectrum. At the same time, compared to the approach without PvdN, it can be seen that the relative abundance of glutamine has decreased significantly by approximately the amount that now corresponds to that of the newly formed succinamide peak (**Figure 31**).

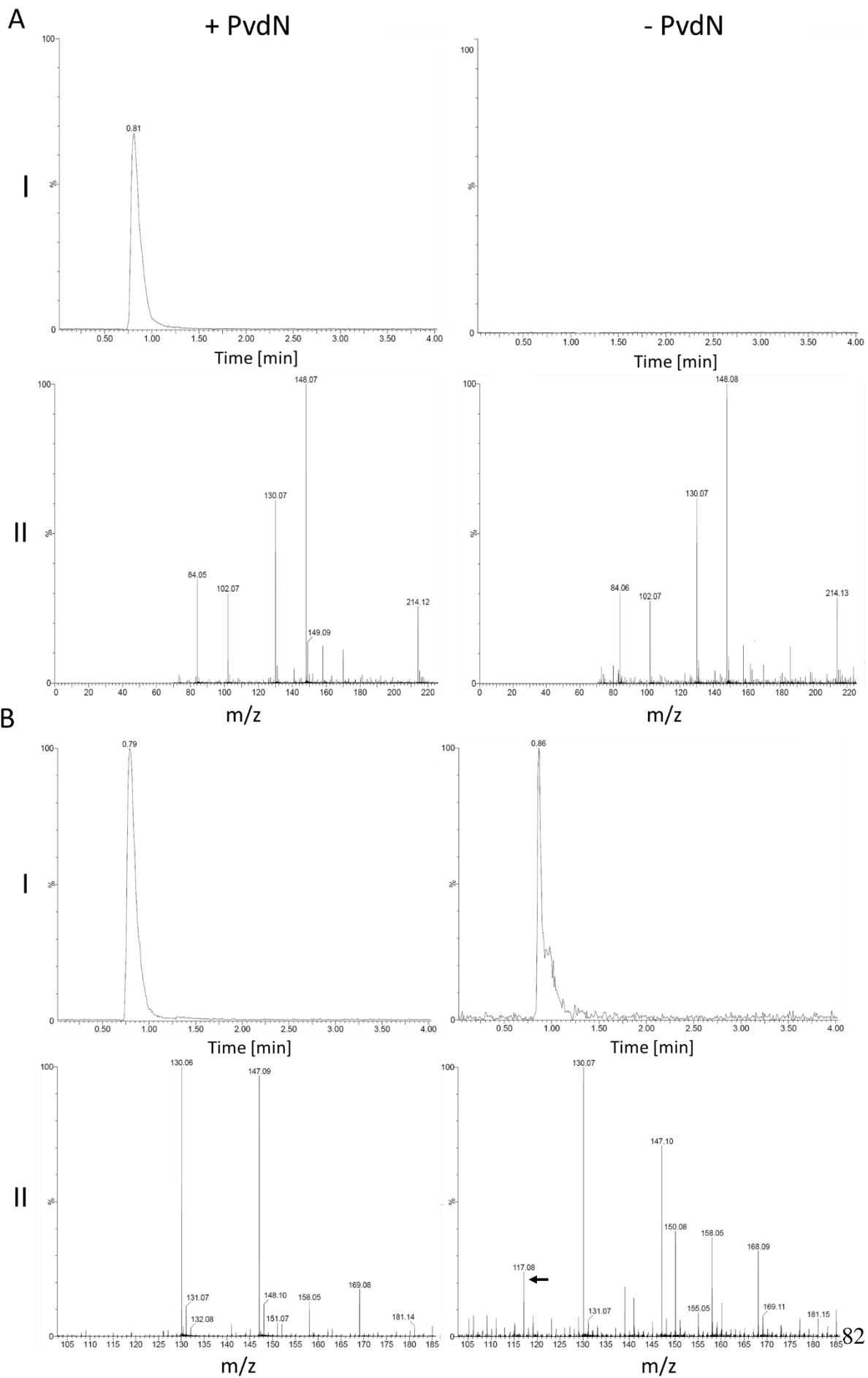


Figure 31: PvdN converts glutamine to succinamide. UPLC-MS analysis of the conversion of glutamate and glutamine by PvdN. (A) Conversion experiments with glutamic acid and the respective chromatograms (I) and spectra (II) with and without the addition of purified PvdN to the reaction setup. (B) Conversion experiments with glutamine and the respective chromatograms (I) and spectra (II) with and without the addition of purified PvdN to the reaction setup. The arrow indicates a newly eluting compound with a mass of 117.08 Da.

In a subsequent experiment, it was tested if the conversion of free glutamine to succinamide was as well dependent on the presence of molecular oxygen. A reaction mix comparable to the one previously described was set up and the emitted CO₂ was detected via gas chromatography.

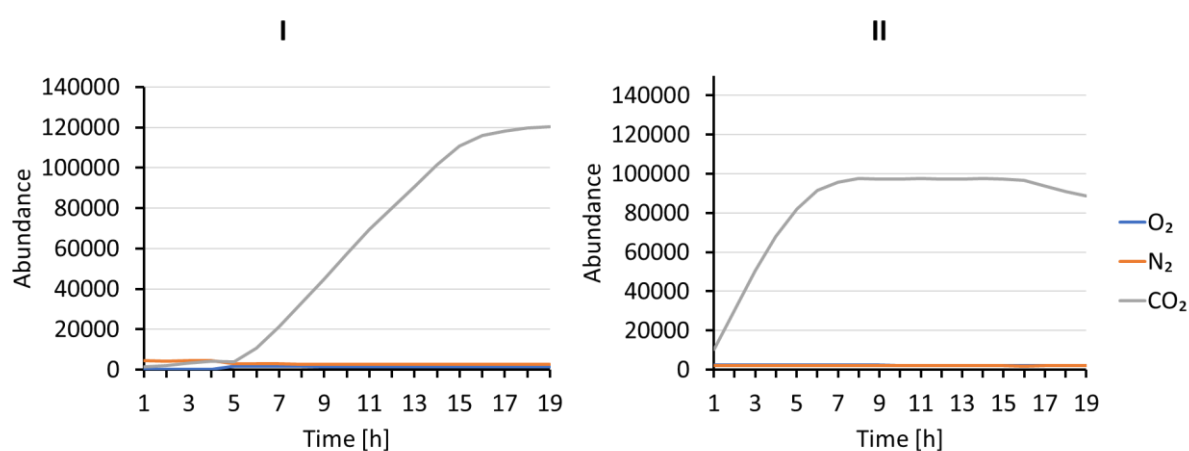


Figure 32: Gas chromatography analysis of the gaseous phase of PvdN converting glutamine in the absence and presence of oxygen. Measurements of the abundance of nitrogen, oxygen and carbon dioxide over a period of 19 hours. In the first approach, the oxygen-free reaction mixture was spiked with molecular oxygen only after a 5-hour incubation period (I); in the other approach, oxygen was added directly at the beginning (II).

Measurements of the abundance of CO₂, oxygen and nitrogen in the gas phase of the reaction mix in which glutamine is converted to succinamide by PvdN showed a significant increase in CO₂ when molecular oxygen was added to the reaction mixture after 5 h. The CO₂ content of the reaction mixture increased significantly. In contrast, during the time when the reaction mix was incubated without oxygen, only an irrelevant increase in CO₂ concentration was measured. At the same time, in the reaction mix in which molecular oxygen was added directly at the beginning of the measurement, a strong increase in the measured CO₂ can be observed immediately (**Figure 32**). At the same time, the N₂ measured in both reaction sets for control purposes remains at a constant level over the course of the measurement.

3.3.3 PvdN_{H260A} favours different hydrolyses of the glutamic acid variant of pyoverdine

To further analyse the reaction mechanism, a variant of PvdN has been created and tested. The basic amino acid histidine at position 260 plays a crucial role in the postulated PLP-involving reaction mechanism of PvdN, as it serves as a proton donor for the addition of molecular oxygen and the retention of a hydroperoxide. A substitution of this histidine by alanine should not result in a complete inactivation of PvdN, but rather a PvdN variant that stops its conversion of the glutamic acid residue after forming the quinoid intermediate. Additionally, the reaction in this variant should be stopped after half a cycle of a full conversion to succinamide, since the intermediate would still be bound to the PLP co-factor (**Figure 33 A**). Because this quinonoid intermediate could not be released, there would be no way for the PLP co-factor to be regenerated and to be bound to the lysine at position 261. The produced variant PvdN_{H260A} was incubated with the glutamic acid variant of pyoverdine extracted from a *P. fluorescens* A506 Δ *ptaA* Δ *pvdN* strain and the formed intermediates were analysed via UPLC-MS.

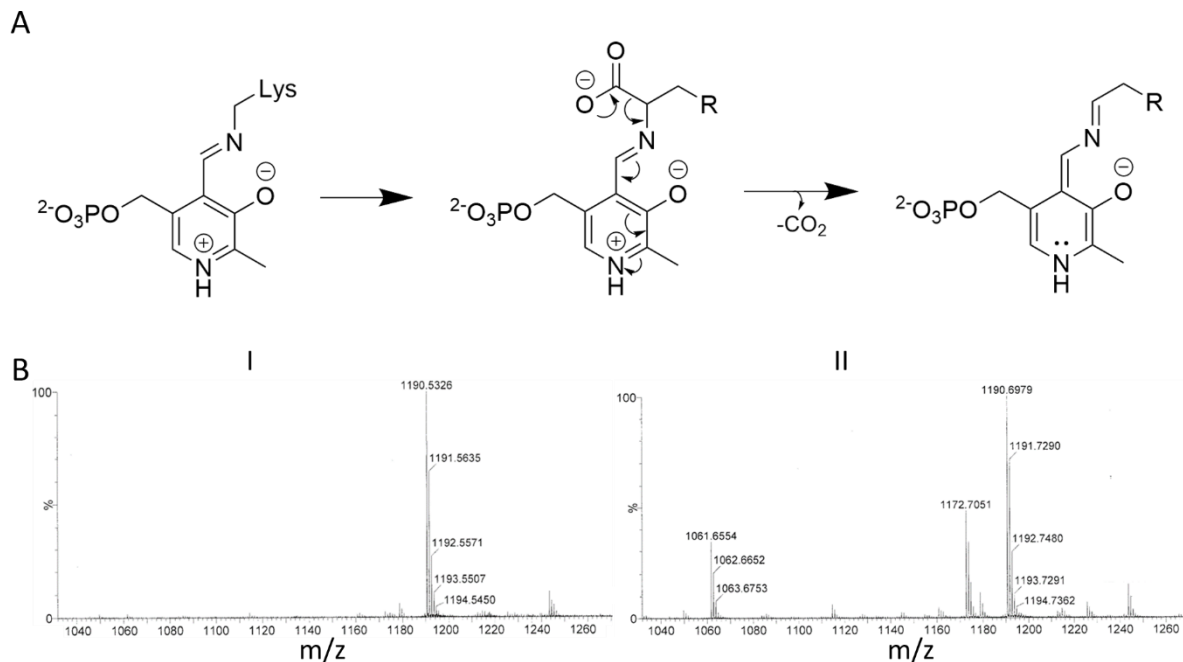


Figure 33: Mass spectrometric Analysis of the intermediates of the PvdN_{H260A} variant. (A) Expected intermediate and reaction mechanism that can occur if the intermediate is not protonated. (B) Detected masses in of pyoverdine in the absence (I) and the presence (II) of PvdN_{H260A}.

Interestingly, the detected masses did not correspond to the expected the mass of 1357.57 Da, which would be in accordance with the mass of decarboxylated glutamic acid variant bound to the PLP co-factor. Instead, two rather distinct peaks were detected with the masses of 1172.71 Da and 1061.66 Da, indicating that two unpredicted variants of pyoverdine have been formed in the reaction catalysed by the PvdN_{H260A} variant (**Figure 33 B**). The first of these two variants, shows an intramolecular cyclization of the hydroxy group of the glutamic acid residue to the amino group of L-2,4-diaminobutyrate with a simultaneous dehydration. The dehydration reaction of the amino group to the hydroxy group and the resulting loss of a water molecule explains the mass difference of 17.83 Da, as compared to the mass of 1190.54 Da for the unmodified glutamic acid residue variant of pyoverdine (**Figure 34 A**). The second variant of the formed pyoverdine displays a hydrolysis reaction at the N-terminal amino group of the glutamic side chain. As a result of this reaction, the complete side chain is split off, resulting in the mass difference of 128.88 Da, compared to the unmodified glutamic acid residue variant of pyoverdine (**Figure 34 B**).

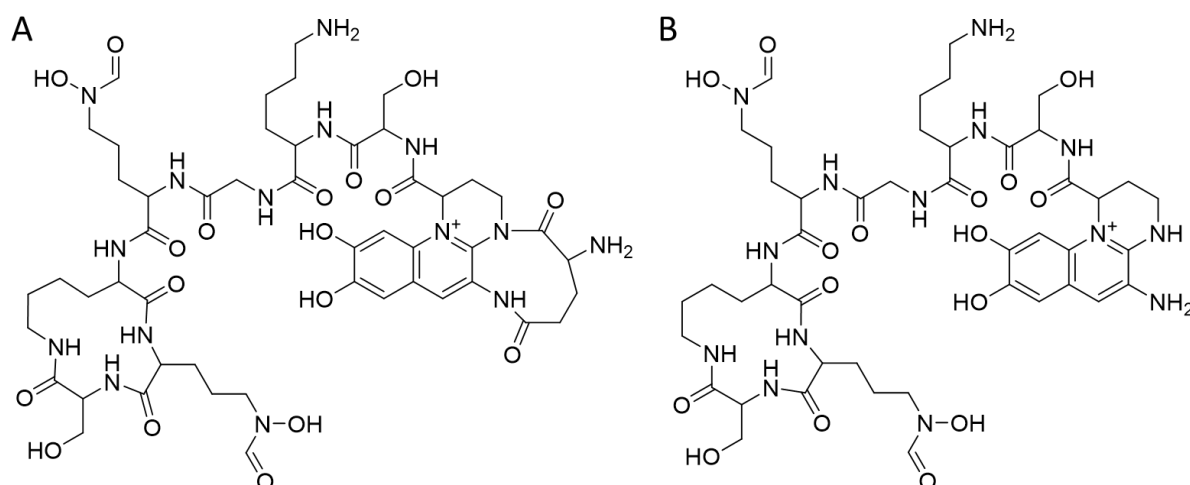


Figure 34: Structures of the detected pyoverdines. (A) Structure of pyoverdine with an intramolecular cyclization of the hydroxy group of the glutamic acid residue to the amino group of L-2,4-diaminobutyrate and a calculated mass of 1172.25 Da. (B) Structure of pyoverdine with the rest of a hydrolysed glutamic side chain at the N-terminal amino group and a calculated mass of 1061.50 Da.

3.4 Substrate analysis of PvdQ

PvdQ serves two different functions in pseudomonads. On the one hand, PvdQ is responsible for a decrease in virulence factors as a quorum sensing quencher (Nadal Jimenez *et al.* 2010; Huang *et al.* 2003). On the other hand, PvdQ is directly involved in the maturation process of pyoverdines with its function as NTN hydrolase (Bokhove *et al.* 2010). In this process of pyoverdine maturation, PvdQ is responsible for the deacylation of the acyl chain, which is believed to be either the unsaturated myristic acid or the monosaturated myristoleic acid (**Figure 35**) (Hannauer *et al.* 2012; Poppe *et al.* 2018; Clevenger *et al.* 2017). Although it has been stated in many publications that the processes of pyoverdine maturation after the export from the cytoplasm into the periplasm is initiated with the deacetylation of ferribactin by PvdQ, there are different views on whether PvdQ really deacylates ferribactin or has acylated pyoverdine as a substrate (Drake and Gulick 2011; Hannauer *et al.* 2012; Schalk and Guillon 2013; Nadal-Jimenez *et al.* 2014; Bonneau *et al.* 2020).

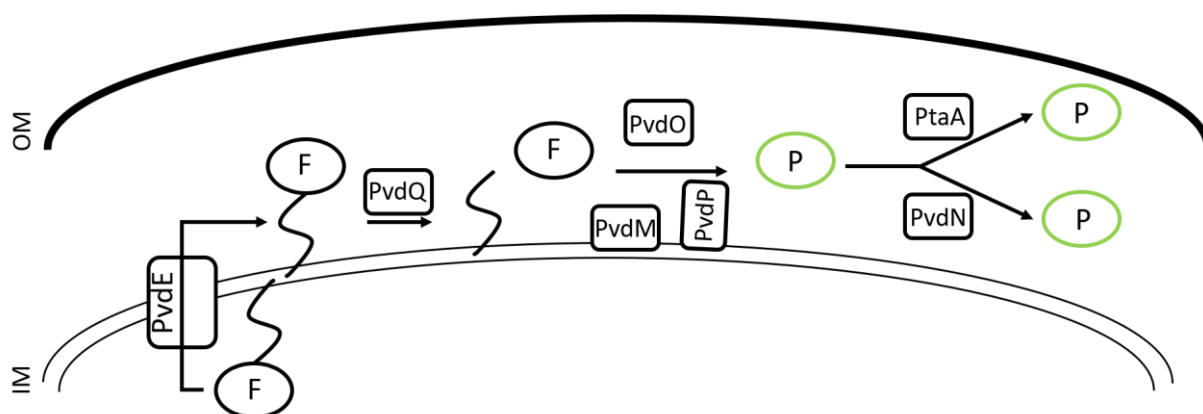


Figure 35: Schematic overview of the maturation of pyoverdines in *P. fluorescens* A506. Schematic overview of the export of ferribactin (F) into the periplasm by PvdE and the deacylation and maturation to pyoverdine (P) by different maturation proteins.

3.4.1 A *P. fluorescens* A506 $\Delta pvdQ$ strain produces fluorescence

In this work, the task was taken up to determine at what timepoint in the maturation process of pyoverdines PvdQ actually fulfils its task of deacylation and whether or not any pyoverdine intermediates of a *P. fluorescens* A506 $\Delta pvdQ$ strain would be detectable via UPLC-MS. For this purpose, a *P. fluorescens* A506 $\Delta pvdQ$, a *P. fluorescens* A506 $\Delta pvdL$, a *P. fluorescens* A506 $\Delta pvdM$ and the *P. fluorescens* A506 wild-type strain were grown in iron-limited CAA medium and compared with each other via phase contrast microscopy (PC) and fluorescence microscopy (FM).

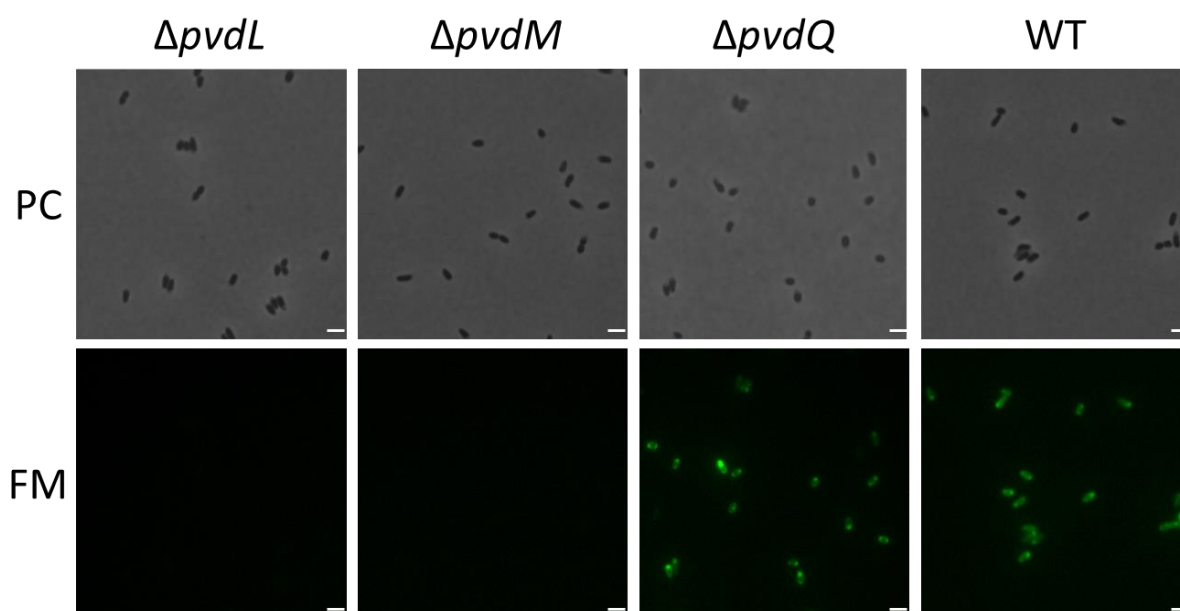


Figure 36: Pyoverdine deficient $\Delta pvdQ$ strain fluoresces. Phase contrast microscopy (PC) and fluorescence microscopy (FM) of *P. fluorescens* A506 $\Delta pvdL$, *P. fluorescens* A506 $\Delta pvdM$, *P. fluorescens* A506 $\Delta pvdQ$ and a *P. fluorescens* A506 wild-type strain. Scale bar: 2 μ m.

Since PvdM, a protein essential for maturation of pyoverdine, is needed for catalytic oxidative cyclisation of ferribactin to pyoverdine by pvdP *in vivo* and PvdL is the first the NRPS involved in the synthesis of ferribactin, pyoverdine cannot be produced in strains missing the genes encoding for these essential proteins. As expected, the $\Delta pvdM$ and $\Delta pvdL$ strains showed no signs of fluorescence, confirming the lack of pyoverdine in these strains. The detected

fluorescence in wild type however was expected due to the formation of pyoverdine in the iron limited medium. Surprisingly enough and in contrast to the previously described pyoverdine maturation process, the $\Delta pvdQ$ strain showed a clear fluorescence (**Figure 36**). This shows that pyoverdine production is possible even in the absence of PvdQ, which would imply that at least the chromophore formation, catalysed by PvdP, is also possible with an acylated form of ferribactin.

The cells that were observed under the fluorescence microscope were subsequently analysed for a subcellular localisation of the fluorescence in a spectrofluorometer. For that, the cells were disrupted via sonication and ultracentrifuged. A sample resulting supernatant and a sample of the resuspended pellet were taken and analysed. The remainder of the supernatant was centrifuged again. The supernatant of the second centrifugation and the resuspended pellet were also analysed via fluorescence spectroscopy. The medium of the respective cell culture was sterile filtered and additionally analysed for traces of fluorescence.

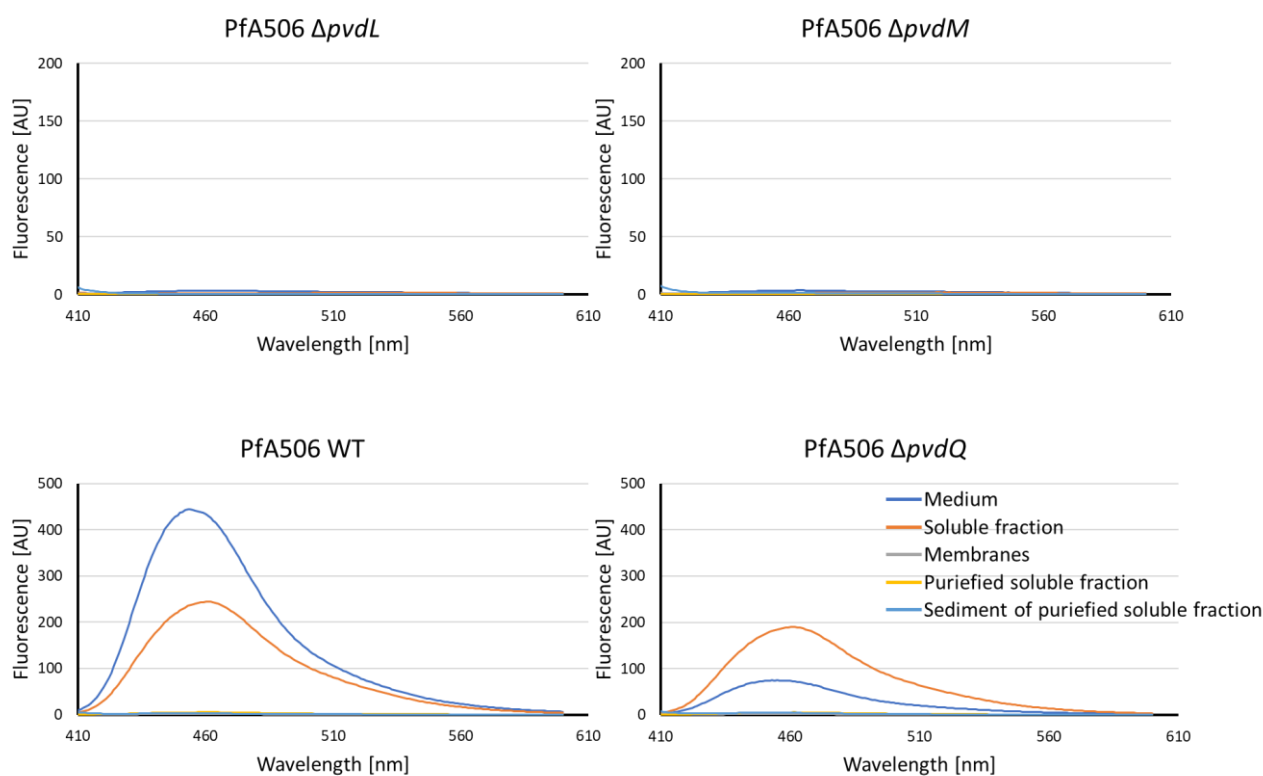


Figure 37: Fluorescence spectra of the different subcellular fractions. Indicated strains of *P. fluorescens* A506 were grown under iron-limiting conditions in CAA medium, and fluorescence spectra were recorded of the medium (culture supernatant after cell harvest), the soluble fraction (after cell disruption and ultracentrifugation), membranes (ultracentrifugation pellet), purified soluble fraction (after a second ultracentrifugation), and the resuspended sediment of the second ultracentrifugation. Shown are emission spectra with an excitation wavelength of 400 nm. Note that the membrane fraction still contains cell debris.

As seen in the fluorescence spectroscopy data, confirming the obtained results from the microscopy, fluorescence was indeed demonstrated only for the wild type strain and the $\Delta pvdQ$ strain (**Figure 37**). Whereas the highest amount fluorescence in the wild type could be detected in the medium and approximately half the value was detected in the supernatant after the first centrifugation (supernatant 1), the opposite was the case for the $\Delta pvdQ$ strain. Here, the highest fluorescence was measured in the supernatant 1 fraction, and a little less than half of the fluorescence detected in this supernatant was detected in the medium. Furthermore, the highest fluorescence measured in the $\Delta pvdQ$ strain was only half as high as in the wild type. Moreover, although a $\Delta pvdQ$ strain lacks the ability for the deacylation of the siderophore, no fluorescence was detected in either of the pellets after the two sonication and centrifugation cycles. Interestingly, the fluorescence in the supernatant 1 fraction after the first centrifugation was not detectable in any fractions obtained after the second centrifugation, neither in the wild type strain nor in the $\Delta pvdQ$ strain. Interestingly, a shift in the fluorescence maxima can be seen in both samples. While the measured maximum fluorescence in the sterile-filtered medium supernatant is 454 nm in the wild-type and 455 nm in the $pvdQ$ knockout strain, the measured fluorescence maxima of the supernatant after the first ultracentrifugation step is 461 nm in the wild-type strain and 462 nm in the $\Delta pvdQ$ strain, respectively (**Figure 37**).

In order to clarify the cause of the deviation in the fluorescence maximum of 6 nm between the samples of the medium and the supernatant after the first centrifugation (supernatant 1), it was investigated whether the difference in the pH value of the medium and the buffer is responsible for the observed shift. For this purpose, the media supernatant after growth, which contained secreted pyoverdine, was diluted in 50 mM Tris-buffer adjusted to different pH values and the fluorescence of pyoverdine was recorded at an excitation of 400 nm.

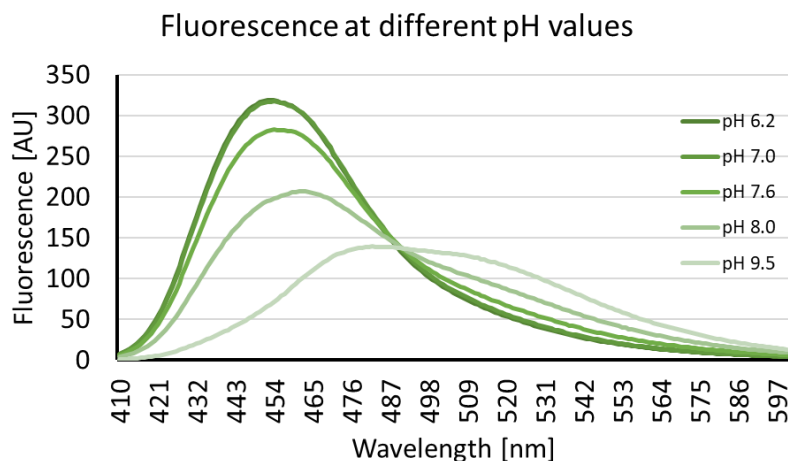


Figure 38: Fluorescence of pyoverdine shifts with an increase of the pH value. Fluorescence spectra of pyoverdine containing medium diluted with 50 mM Tris-buffer which has been adjusted to pH 6.2, 7.0, 7.6, 8.0 and 9.5 respectively upon excitation with light of a wavelength of 400 nm. The maximum fluorescence of pyoverdine depends on the pH of the buffer or medium in which it is dissolved.

As can be seen from the fluorescence spectra, the fluorescence shifted with increasing pH value. While at a pH value of 6.2 the maximum is at 452 nm, at a pH value of 7.0 and 7.6 it is at 454 nm. If the fluorescence is measured at pH 8.0, the maximum is 461 nm and at pH 9.5 even 482 nm. At the same time, the measured intensity decreases with increasing pH value, although all samples contain the same ratio of pyoverdine-containing medium and buffer. While the graph for values below pH 8.0 drops off again relatively quickly after reaching the maximum, a somewhat broader peak can already be seen at pH 8.0, which becomes a clear plateau at pH 9.0 (**Figure 38**). The shift of the fluorescence maximum between the different samples of the same culture can be explained by the different pH value of the medium after growth, which had a value of approximately pH 8.0 and the buffer in which the fluorescence of the pyoverdine was measured, which normally has a pH value of 7.6.

Since the analysis via fluorescence spectroscopy only allows for the identification of fluorescence, but not for the identification of the fluorescent compound, the respective medium, in which all four strains have been incubated, were analysed via UPLC-MS.

As expected for the non-fluorescent strains *P. fluorescens* A506 $\Delta pvdL$ and *P. fluorescens* A506 $\Delta pvdM$, there was no fluorescent pyoverdine detectable in the medium. In case of *P. fluorescens* A506 $\Delta pvdM$ though, deacylated ferribactin with a mass of 1179.59 Da was detected (**Supplement Figure S1**). In the medium of the wild-type strain, only the succinamide variant of pyoverdine with a mass of 1160.53 Da and the alpha-ketoglutarate variant with a molecular mass of 1189.51 Da were detected, which shows that the ferribactin was completely converted to pyoverdine and therefore ferribactin was not secreted into the medium. In the $\Delta pvdQ$ strain however, the precursors of pyoverdine, ferribactin with a myristic acid acylation and a mass of 1389.81 Da and ferribactin with a myristoleic acid acylation and a mass 1387.77 Da were detected, respectively. Additionally, a peak with the mass of 1360,86 Da was detected, indicating a myristic acid acylated ferribactin missing a formyl group. No acylated or deacylated form of pyoverdine was detectable in the medium (**Supplement Figure S2**). While this specific strain did show fluorescence under the microscope when excited with light between 375 nm and 407 nm and fluorescence was detected via fluorescence spectrometry, no compound in context of pyoverdine could be detected and hold responsible for this fluorescence via UPLC-MS.

3.5 Additional growth studies of strains lacking pyoverdine on iron depleted medium

In order to have as little iron as possible in the medium, a minimal medium was used which, apart from casamino acids, only contained K_2HPO_4 and $MgSO_4$. To make even the last free iron in the medium not easily available to the microorganisms, the chelator ethylenediamine-*N,N'*-bis(2-hydroxyphenylacetic acid) (EDDHA) was added. Just like pyoverdine, EDDHA binds metal ions with a high affinity. EDDHA can come in three different regioisomeric substitution patterns, as (i) *ortho, ortho* [*o,o*], (ii) *ortho, para* [*o,p*], and (iii) *para, para* [*p,p*], describing the position of the substituents and the hydroxy group of the phenyl ring in relation to each other (Klem-Marciniak *et al.* 2021). While the steric hindrance of the [*p,p*]-form of EDDHA does not allow any iron complexation, the [*o,p*]- and [*o,o*]-form of EDDHA are able to bind iron with five and six binding sites, respectively (Gómez-Gallego *et al.* 2002; Schenkeveld *et al.* 2007). As the isomer with the highest affinity to iron, [*o,o*]-EDDHA is a hexadentate ligand, that coordinates the bound metal with two amines, two carboxylates and

two phenolates (**Figure 39**). Strains with the ability to form siderophores, for example pyoverdines, are able to sequester the ferric iron from the [*o,o*]-EDDHA and grow in this iron depleted medium. Strains, however, who lack the ability of siderophore production cannot grow on under these conditions.

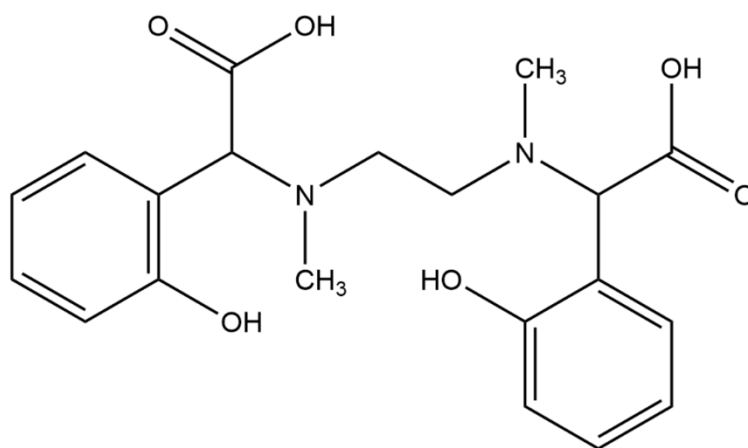


Figure 39: Structure of [*o,o*]-ethylenediamine-*N,N'*-bis(2-hydroxyphenylacetic acid).

3.5.1 Identification of an EDDHA derivate in the supernatant of a pyoverdine impaired strain

During experiments with impaired strains, as far as the synthesis of pyoverdines is concerned, and the analyses of the growth curves, an interesting growth behaviour of the cells was noticed. Whereas *P. fluorescens* A506 strains with gene deletions encoding for essential pyoverdine production proteins such as PvdL did not grow on iron depleted medium at first, they unexpectedly started to grow after a certain time being incubated at 30 °C on M9 medium supplemented with EDDHA (**Figure 40**). Although the growth of these strains, which lack pyoverdine, was normally only observed after 24 h, they nevertheless achieved an optical density comparable to that of a normally growing culture under these conditions.

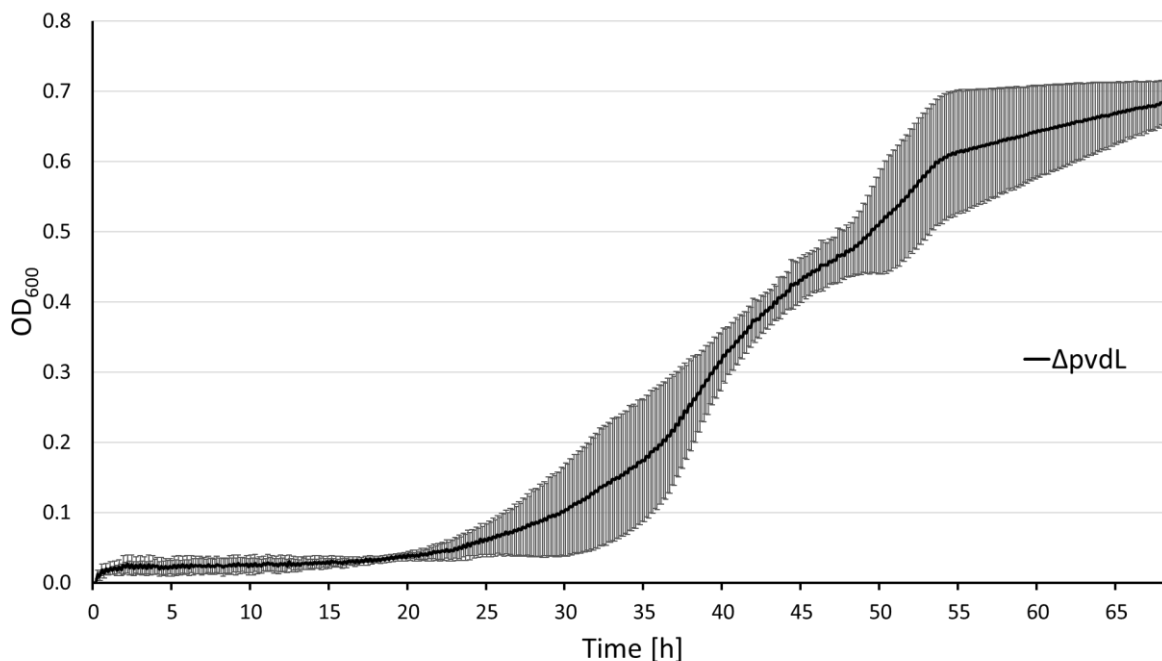


Figure 40: Pyoverdine deficient $\Delta pvdL$ strain grows in iron depleted medium. Growth curve of the pyoverdine impaired strain *P. fluorescens* A506 $\Delta pvdL$ in M9 medium supplemented with EDDHA over a period of 72 h. Error bars display standard deviation of triplicates.

To check whether a previously unknown siderophore was produced which allows the bacteria to grow in iron-depleted medium despite the lack of pyoverdine, a new growth experiment was designed. For this purpose, the medium in which the cells could grow notwithstanding the lack of pyoverdines was removed and sterile filtered. The carbon source in that medium, in this case sucrose, was then replenished and the regenerated medium was inoculated with a fresh culture of cells that are not able to produce pyoverdine. If an unknown siderophore was indeed secreted into the medium, the new cells should be able to use the unidentified iron chelator for sequestering and importing iron. These cells should therefore grow much faster in comparison to cells growing in an unused medium.

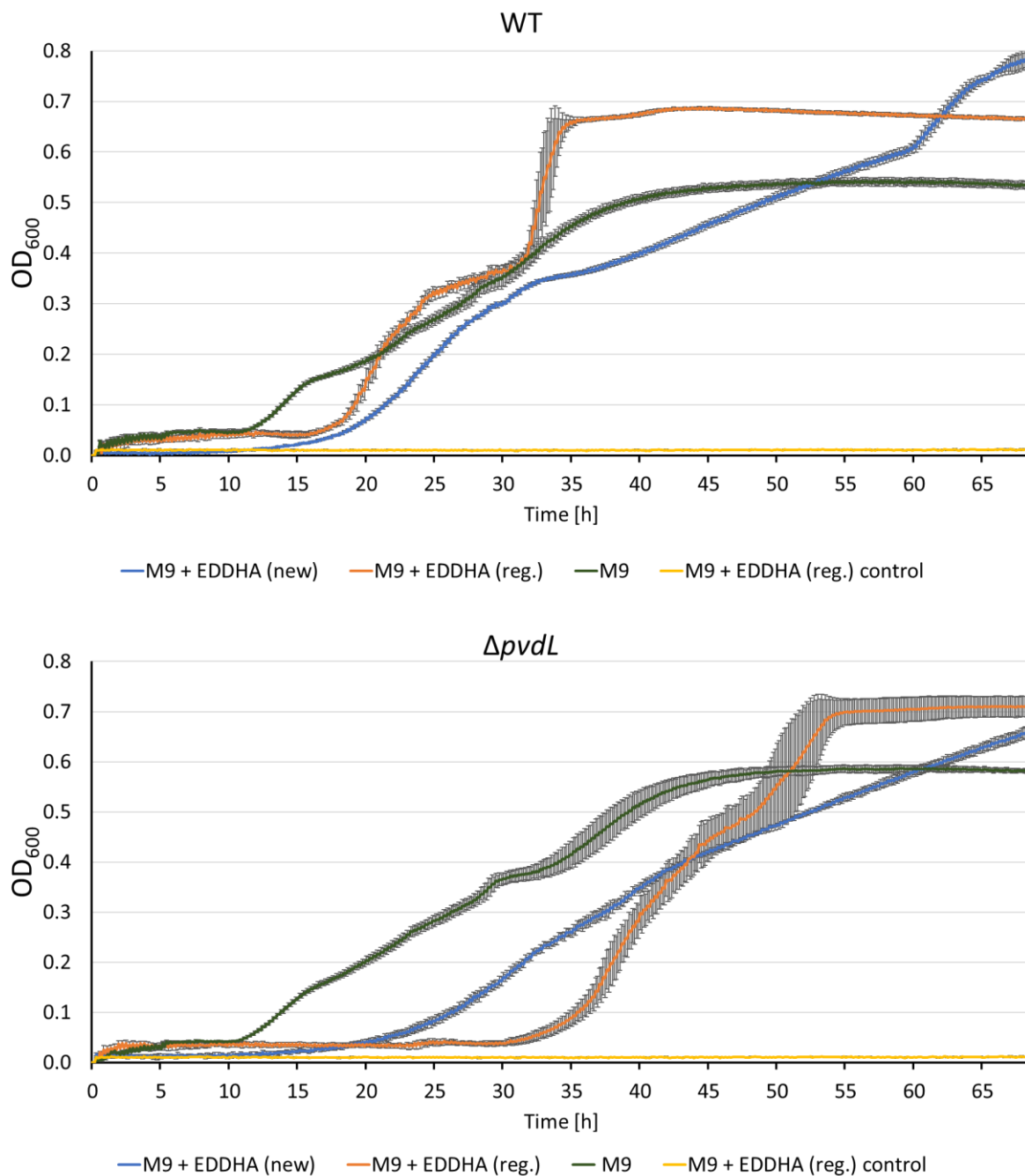


Figure 41: Growth of a PfA506 wild-type and a PfA506 $\Delta pvdL$ strain in different M9 media. Growth curve of a *P. fluorescens* A506 wild-type strain and *P. fluorescens* A506 $\Delta pvdL$ mutants in normal M9 medium, M9 medium supplemented with EDDHA and M9 medium sterile filtered and regenerated after growth of the $\Delta pvdL$ strain. Error bars display standard deviation of triplicates.

The effect of the regenerated medium supernatant of a PfA506 $\Delta pvdL$ culture on growth of a PfA506 wild-type strain and a PfA506 $\Delta pvdL$ strain is not concise. While there is no difference in the initial growth phase of the wild-type strain, growth in the regenerated medium shows a more pronounced biphasic growth than in the other two media. In contrast, there is a clear delay in growth of the $\Delta pvdL$ strain in the regenerated medium compared to the new medium (**Figure 41**). The PfA506 $\Delta pvdL$ strain did start to grow after 24 h in the new medium, while it took the same strain nearly 36 h to show the same growth in the regenerated medium (**Figure 41**). In both cases, growth in regenerated medium does not lead to faster growth compared to growth in new medium. Overall, there is no growth advantage that the regenerated medium could have given to the growing cells compared to a fresh medium. In both cases, the two compared strains did start to grow first in M9 medium, that was not depleted with EDDHA.

These results can indicate two different possibilities. Either the cells need some time to adapt to the iron limitation in the medium and to activate the corresponding systems for the uptake and production of the unknown siderophore, or the cells have a second, yet unknown way apart from pyoverdine to sequester iron from the Fe^{3+} -EDDHA complex and to use it for the cell's own processes. To identify a possible new siderophore, the overgrown medium was removed, the cells were centrifuged and the sterile filtered supernatant was analysed by UPLC-MS.



Figure 42: Medium supernatant of *P. fluorescens* $\Delta pvdL$ contains modified EDDHA. (A) Chromatogram (I) and spectrum (II) of the UPLC-MS analysis of the medium supernatant of *P. fluorescens* A506 $\Delta pvdL$ strain grown in M9 medium supplemented in EDDHA (I, II). (B) Chromatogram (I) and spectrum (II) of the UPLC-MS analysis of M9 medium supplemented with EDDHA. (C) structure of an [*o,o*]-EDDHA derivative, which has been methylated at both amino groups.

Interestingly enough, a distinct peak with the mass of 389.14 Da was detected in the medium supernatant in which the cells lacking pyoverdine were growing (**Figure 42 A**). In the control, incubated but unvegetated M9 medium, no retention time for a compound with the mass of 389.14 Da could be detected, only the unmodified EDDHA was detected in the spectrum of eluting fractions (**Figure 42 B**). Additionally, the modified EDDHA was only present in the medium supernatant, but was neither detectable in the cytoplasmic fractions of the cells nor in the periplasmic fractions (**Supplement Figure S3**). While the exact structure of this newly detected compound is not resolvable with the applied method, its mass corresponds to a modified variant of EDDHA, more precisely an EDDHA derivate methylated at both amino groups (**Figure 42 C**).

4 Discussion

4.1 Interaction of PvdM in the maturation process of pyoverdines

The discovery of pyoverdine dates back more than one hundred years. Since then, not only the main task of pyoverdines, iron acquisition in iron-deficient environments has been discovered, but also the role as a signalling molecule and the resulting involvement in the production of various virulence factors has been revealed. While in the course of time primarily the function itself and the effects on other living organisms were studied extensively, the first steps of pyoverdine synthesis in the cytoplasm and the maturation of pyoverdines in the periplasm has been elucidated more and more in recent years. The complete elucidation of the individual steps of pyoverdine synthesis and the processes involved is of essential importance for the development of possible drugs that can both inhibit the synthesis itself and thereby also prevent the activation of other virulence factors (Kang *et al.* 2019; Kang *et al.* 2021). Based on previous work, it has been possible to assign a corresponding catalysing enzyme to each step of pyoverdine synthesis. For example, in the near past it was possible to assign the oxidation and chromophore formation of the precursor ferribactin to the proteins PvdP and PvdO. PvdN, previously thought to be essential, was assigned to a non-essential modification of the side chain (Ringel *et al.* 2018, 2016).

The only crystal structure of PvdM comes from the model organism *P. aeruginosa* from the year 2007 and is as yet unpublished, but can be found in the publicly accessible protein data base PDB (Bonanno *et al.* 2007). However, the first 37 amino acid residues are not included in the crystal structure. Based on this template, the structure of PvdM from *P. fluorescens* A506 was modelled, which has a sequence identity of 76.1 % with that of PvdM from *P. aeruginosa*. To visualise the complete protein, the whole sequence including the N-terminus was analysed with the novel online bioinformatic tool RoseTTAFold and structurally predicted using deep learning (Baek *et al.* 2021).

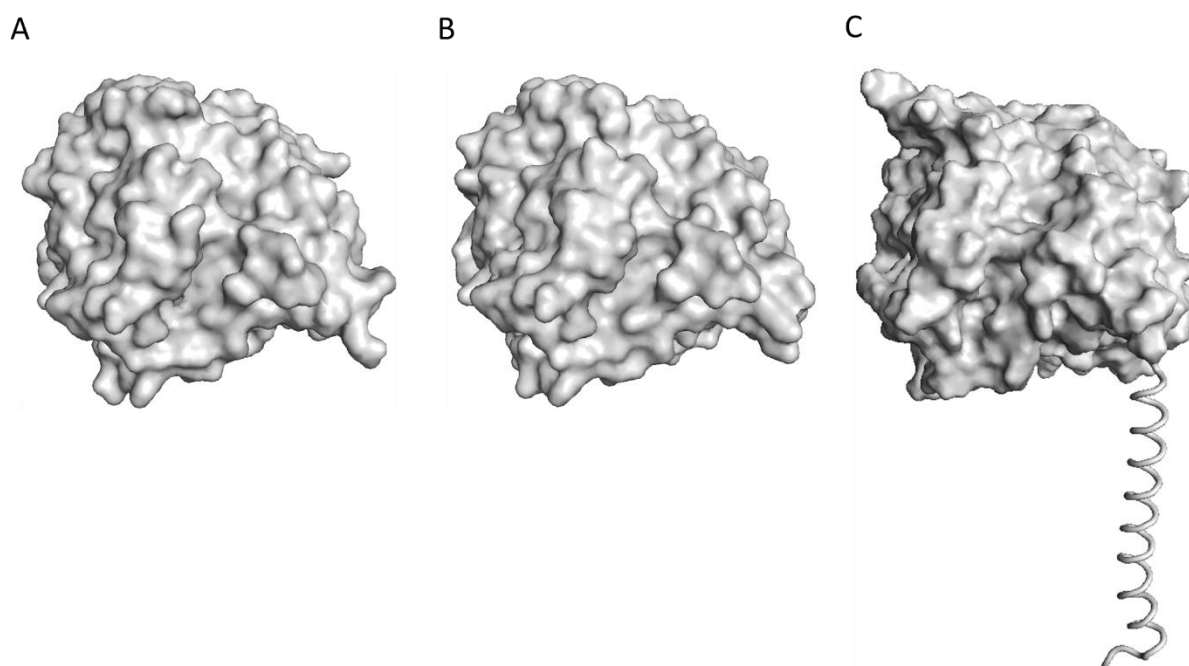


Figure 43: Models of PvdM using different methods. (A) Visualised surface of the crystal structure of PvdM from *P. aeruginosa* (Bonanno *et al.* 2007). (B) Visualised surface of a model of PvdM from *P. fluorescens* A506 using the crystal structure of PvdM from *P. aeruginosa* as a template. (C) Visualised surface of a predicted structure of PvdM from *P. fluorescens* A506 including the N-terminus using a deep learning-based method. For better visual understanding, the predicted N-terminus was displayed differently from the rest of the protein. These models were created using PyMol (Schrödinger and DeLano 2020).

As can be seen from the modelled PvdM, which was structurally predicted using a novel deep learning approach, the N-terminus, which was always absent in the previous models, is recognised as an alpha helix and modelled accordingly (**Figure 43**).

Despite the numerous advances in the elucidation of pyoverdine synthesis, some questions such as the not yet completely clarified export mechanisms, the exact regulation of pyoverdine synthesis itself and the involvement of PvdM in the process of pyoverdine biogenesis remain unclear. In the context of this work, the exact localisation and the task of PvdM, a protein essential for pyoverdine synthesis, was investigated in more detail.

4.1.1 The N-terminus of PvdM mediates membrane integration

Little attention has been paid to PvdM in the studies of the proteins involved in the maturation of pyoverdine. Although it has been confirmed to be a protein integrated into the cytoplasmic membrane, neither its function nor its subcellular orientation has been revealed (Ringel 2018). In this work, the subcellular localisation in the cytoplasmic membrane was confirmed. At the same time, it could be shown that pvdM is not only associated to the membrane, but is properly integrated by treating the membrane fraction with carbonate buffer. Due to the alkaline pH of the buffer, noncovalent protein-protein interactions are decreased, releasing loosely attached peripheral membrane proteins (Kim *et al.* 2015). By producing the full length PvdM in *E. coli* BL21 and permeabilising the outer membrane, followed by incubation with the serine protease Proteinase K, it was shown that PvdM has its globular domain in periplasm, suggesting a function in the periplasm.

While the PvdM variants with the inserted ASA signal peptidase cleavage site and the signal peptide replaced by the signal peptide of PvdO were expected to be transported and released into the periplasm after processing of the signal peptide, both PvdM variants were still tightly integrated into the cytoplasmic membrane and could not be liberated by a carbonate wash. Nevertheless, the recognisable shift of the band in the Western blot shows that the signal peptide was processed in both variants in contrast to the wild-type PvdM. Furthermore, a degradation of the PvdM-ASA variant could be observed, indicating that the lack of the first N-terminal amino acids including end of the trans-membrane domain is increasing the sensitivity for protease degradation in a dramatic manner. Thereafter, as the growth experiments on CAA agar plates supplemented with EDDHA show, the PvdM-ASA variant was not able to complement a $\Delta pvdM$ phenotype and was therefore inactive.

Although the aspartic acid at the N-terminus after processing of the signal peptide is not a destabilising amino acid in the classical sense to which ClpS binds, which in turn serves as an adaptor protein for the energy-dependent AAA+ protease ClpAP, the absence of the first amino acids may well have an effect on the folding behaviour of the protein (Tobias *et al.* 1991; Erbse *et al.* 2006; Schuenemann *et al.* 2009). The unfolded and misfolded proteins can interact with one another and form aggregates (Schramm *et al.* 2020). The abundance of these aggregates can lead to the recognition by ATP-dependent AAA+ proteases such as ClpXP, ClpAP and

ClpCP, that carry out the regulated proteolysis in bacteria (Gur *et al.* 2011; Olivares *et al.* 2016; Mahmoud and Chien 2018). This could mean that the detected PvdM-ASA variant was misfolding and interacting with other PvdM amino acids residues and was being partially degraded, which in turn would explain why the corresponding PvdM variant was detectable in the western blot, but not able to complement the $\Delta pvdM$ mutant.

In contrast, the PvdM variant integrated into the membrane despite a processed signal peptide, namely that of PvdO, was stable and was not degraded. In addition, this variant was able to complement a $\Delta pvdM$ strain making it possible to grow on iron depleted medium and to produce pyoverdines, as the fluorescence under UV light shows. This demonstrates the activity of this variant. Compared to the N-terminus of the PvdM-ASA construct, five additional amino acid residues of the hydrophobic transmembrane domain, namely Gly-Leu-Leu-Val-Trp were preserved. Since these five amino acid residues are part of the transmembrane helix which is integrated into the cytoplasmic membrane, they cannot be of importance for the catalytic function of PvdM. Still, the retention of these amino acids unmistakably prevents the degradation of the mature protein and whilst being crucial for the stability of PvdM.

In addition to the studies in which the signal peptide of the mature PvdM was exchanged, experiments were also carried out in which different signal peptides, including that of PvdM, were fused to the mature periplasmic PhoA. The aim was to experimentally investigate whether the bioinformatic predictions about the signal peptide of PvdM are indeed correct and whether it is an integral transmembrane helix, since it was shown that the mature PvdM is also tightly associated to the membrane without the original signal peptide. As shown in the results, the PhoA variant with the signal peptide of PvdM was found in the membrane fraction. Since the alkaline phosphatase PhoA is only active in the periplasm, this means that the globular domain of PhoA must have been transported into the periplasm. This shows that the N-terminus of PvdM is indeed a Sec signal peptide, which mediates integration into the cytoplasmic membrane after transport of the protein across it.

The translocation of proteins across the cytoplasmic membrane in bacteria is normally mediated by an interaction of the N-terminal signal sequence with the protein secretion system. A basic distinction is made between two different transport pathways through which proteins can be transported across the cytoplasmic membrane, namely the Sec-system (general secretion

pathway) or the Tat-system (twin-arginine translocation pathway) (Manting and Driessen 2000; Berks *et al.* 2000). In the Sec-pathway, unfolded proteins are transported across the membrane and subsequently integrated into or liberated from the membrane (Mori and Ito 2001). To prevent folding before the translocation, proteins are often bound to by the cytoplasmic chaperone SecB (Driessen 2001). In contrast to the mechanism of the Sec-pathway, in the Tat translocation pathway, folded proteins and cofactor-bound enzymes are transported across the cytoplasmic membrane (Berks *et al.* 2005). For the transport of proteins by either system, a signal peptide is required. The signal peptide of both transportation systems consists of three important regions, namely a positively charged n-region, a hydrophobic h-region and a hydrophilic carboxyterminal c-region. The last region typically also contains a conserved sequence at which the signal peptide is proteolytically removed by a leader peptidase located in the periplasm (Paetzel *et al.* 2002; Dalbey and Kuhn 2000). In addition, the Tat signal peptide also contains a name-giving and highly conserved twin arginine motif that is located in the transition zone between the n-region and the h-region (Berks 1996). Furthermore, the Tat signal peptide differs from the Sec signal peptide in that it has a h-region that is a little less hydrophobic and some positive charges in the n-region, which ensure that the protein is not transported via the Sec-pathway, the so called Sec avoidance motif (Cristóbal *et al.* 1999; Blaudeck *et al.* 2003).

The comparison of the N-terminus of PvdM with a standard signal peptide shows that there are some similarities. For example, in addition to a positively charged n-region, a hydrophobic h-region can also be assigned to the N-terminus of PvdM. But neither a hydrophilic c-region nor a proper cleavage site for a leader peptidase are found.

Further analyses of the N-terminus of PvdM with the bioinformatic online web service SignalP 5.0, which predicts the presence of signal peptides and the position of the putative cleavage site, only partly confirms the assessments and gives a probability of about 13 % that the N-terminus is a Sec signal peptide (Almagro Armenteros *et al.* 2019). This is due to the missing dipeptidase cleavage site at the end of the signal peptide. As can be seen, the probability of the N-terminus being transported via the Sec pathway increases to almost 100 % once a proper dipeptidase cleavage site, in this case the ASA motif, has been inserted into the sequence. If the complete Sec signal peptide of PvdO is fused to the mature PvdM, the analysis shows that the probability of the N-terminus of the protein being a Sec signal peptide increases to almost 90 %

(**Figure 44 A**). Additional analyses of the N-terminus of the unmodified PvdM for the prediction of transmembrane domains via the bioinformatic online tool TMHMM Server v. 2.0 give a similarly clear picture (Sonnhammer *et al.* 1998; Krogh *et al.* 2001). Here, for the first eight amino acids, i.e., precisely for the rather positively charged n-region, a localisation "inside", the cytoplasm, is predicted. For the amino acids from alanine at position 9 to tryptophan at position 29, i.e., precisely the hydrophobic h-region, a transmembrane helix is predicted. For the remaining part of PvdM, a localisation outside, here the periplasm, is predicted (**Figure 44 B**).

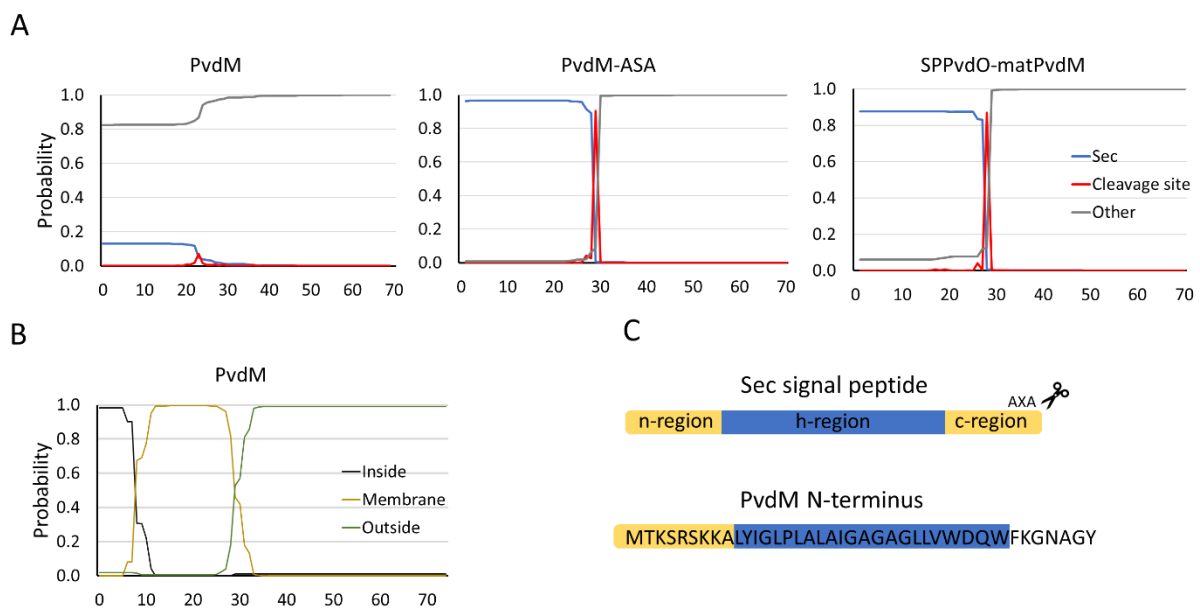


Figure 44: Prediction of cleavage sites of the protein of different PvdM variants and subcellular localisation prediction. (A) SignalP prediction of the cleavage site for the wildtype PvdM, the PvdM variant with the inserted ASA motif and the PvdM variant with the signal peptide substituted by that of PvdO. (B) Analysis of transmembrane helices by the online tool TMHMM. (C) Schematic structure of a sec signal peptide (top) and comparison with the sequence of the N-terminus of PvdM (bottom).

An integration of proteins into the membrane with the help of a transmembrane helix is possible via different types of helices. A distinction is made here between an α -, a 3_{10} - and a π -helix. In nature, however, 3_{10} -helices only make up about 10 % of all helical residues. π -helices occur in only 15 % of the helices and are mostly found either at the end of an α -helix or flanked by two α -helices (Crisma *et al.* 2007; Cooley *et al.* 2010). For the integration into the membrane with a transmembrane α -helix, the most frequently occurring type of helices, an average of 20 amino acids is required (Papaloukas *et al.* 2008). Therefore, with a length of 21 amino acids, which

are contained in the hydrophobic h-region in the N-terminus of PvdM, enough amino acids would be available.

4.1.2 Additional integration into the membrane of PvdM

The evaluation of the translocation results of the different PvdM variants has shown that, contrary to bioinformatic predictions, the PvdM signal peptide is a Sec signal peptide that also mediates integration into the membrane using a predicted hydrophobic transmembrane helix. Nevertheless, it was observed that the PvdM variants with processed signal peptides were so tightly associated with the membrane that they could not be detached even with a carbonate wash. A conserved serine at the C-terminus of the protein for the addition of a glycosylphosphatidylinositol anchor, as in the closest homolog of PvdM, human renal dipeptidase, is firstly not present in PvdM, and secondly, this type of posttranslational modification is also only found in eukaryotes (Adachi *et al.* 1990a; Paulick and Bertozzi 2008).

In the course of analysing the peptide fragments of tryptically digested PvdM, it was demonstrated that no post-translational modifications were present for most of the PvdM protein sequence except for a few subsections. Of the amino acids that were not covered by the detected peptide fragments, six amino acids which are often post-translationally modified, namely serine and threonine have been identified. But only two of these six possible modification sites are located on the surface of the folded protein. Since individual post-translational modifications can only be carried out on certain amino acid residues, the possibility of modifications is limited here. A *S*-palmitoylation can be excluded due to missing cysteines in the sequence of PvdM. The somewhat less frequent *O*-palmitoylation, however, can also be carried out on free serines or threonines. This modification is usually performed on membrane proteins, where the addition of palmitic acid increases the hydrophobicity, which contributes to the association to the membrane. Myristoylation is a translational modification that is carried out on an N-terminal glycine of a protein. Theoretically, the mature PvdM of the variant with the signal peptide of PvdO would have this very glycine at the N-terminus. But because this modification already occurs co-translational or post-translational in the cytoplasm, where the signal peptide is not yet processed, the potential modification site is blocked and is thus not available for a putative modification.

A straightforward way to further investigate the incorporation of PvdM into the cytoplasmic membrane would be to replace the aforementioned amino acid residues and thus ensure that the possible post-translational modifications can no longer be carried out and to test whether the subcellular localisation of the mature PvdM changes as a result.

Another possible explanation for the retention of PvdM in the membrane despite the absence of a membrane anchor could be the interaction of PvdM in a protein complex firmly anchored in the cytoplasmic membrane. This complex could next to PvdM also involve PvdP. These proteins could be interacting together in a tight complex to catalyse an essential step of pyoverdine maturation. As has been shown in other protein complexes, the distribution of proteins in a complex is not random but purposeful. It is more common for either mainly essential proteins to join together in a complex or for mainly nonessential proteins to form a complex (Ryan *et al.* 2013). In addition to these two proteins, PvdE may also be involved as a possible exporter of ferribactin into the periplasm. In the case of PvdM and PvdP, it would be a complex of essential proteins, without which pyoverdine synthesis cannot take place. To test the association of PvdM with PvdP to form a protein complex, one could produce PvdM with a signal peptide that is processed in a $\Delta pvdP$ strain. If PvdM is indeed detectable as a soluble protein in the periplasmic fraction, this strongly suggests an interaction with PvdP to form the protein complex.

4.1.3 Two possible functions of PvdM

The crystal structure of PvdM from *P. aeruginosa* reveals a total of five interactions with different metals, namely calcium, magnesium and cadmium. While the interactions with the hard alkaline earth metals calcium and magnesium are not of interest here, the interaction sites with cadmium were further investigated, of which there are a total of two on the surface of PvdM (Bonanno *et al.* 2007). The first cadmium ion is coordinated by the amino acid residues of two glutamates and an arginine while the second cadmium ion is coordinated by the amino acid residues of lysine, aspartate and histidine. While the first binding site is not particularly conserved, the second binding site exhibits a high degree of conservation (**Figure 45**). Since the heavy metal cadmium is highly toxic to living organisms in general, it could be possible that these binding sites were occupied by cadmium due to the crystallisation process and are

occupied by other metals such as copper in a physiological environment. (Begg *et al.* 2015; Trakhanov *et al.* 1998).

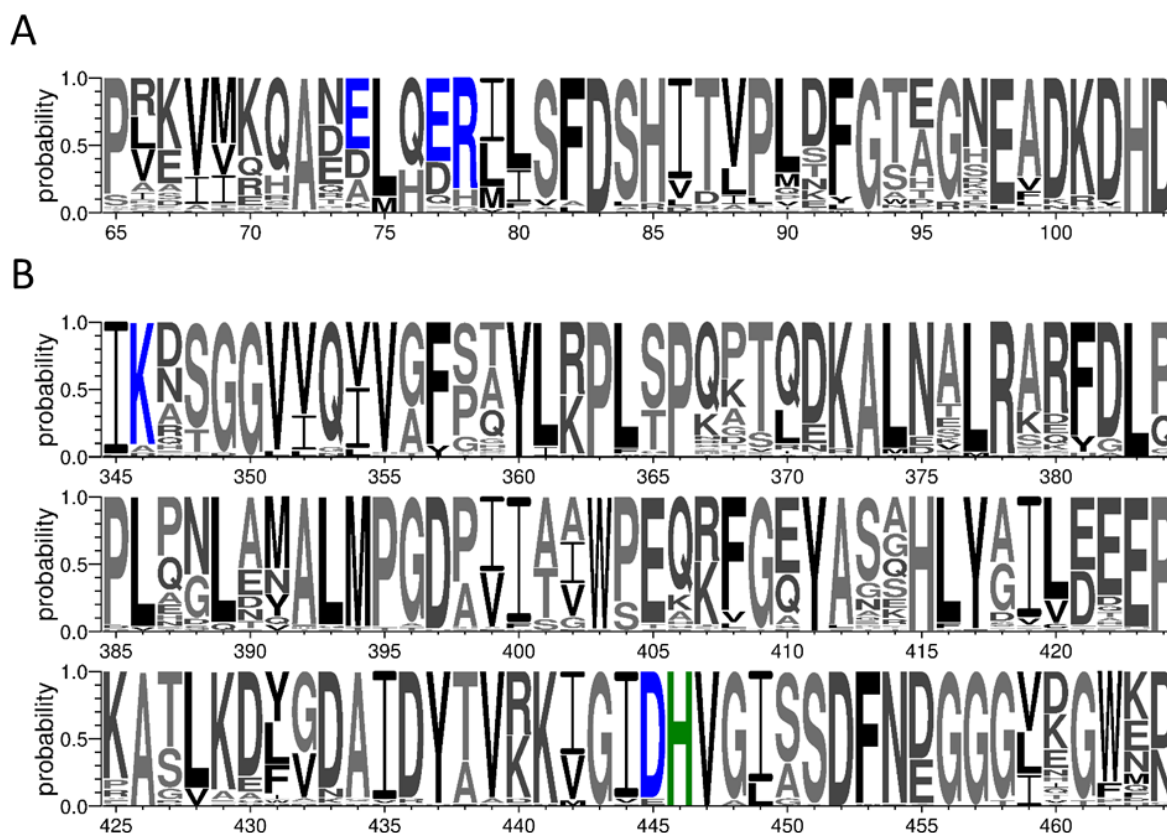


Figure 45: Sequence logo of the sections of PvdM that coordinate cadmium. (A, B) Conservation of the amino acids each responsible for the coordination of a cadmium ion on the surface of PvdM. The involved amino acid residues are highlighted in blue and green, respectively.

The detection of ferribactin as the only intermediate of the pyoverdine biosynthesis pathway in both the *P. fluorescens* A506 $\Delta pvdM$ strain and *P. fluorescens* A506 $\Delta pvdP$ strain and the demonstrated activity of purified PvdP *in vitro* clearly indicates that PvdM is essential for the activity of PvdP *in vivo*. This is initially in contrast to the previously published results that PvdP can oxidise ferribactin to dihydropyoverdine in the absence of PvdM *in vitro* (Nadal-Jimenez *et al.* 2014). A possible explanation for this contradiction would be the interaction of PvdM and PvdP and the task of PvdM as a potential auxiliary enzyme to facilitate the incorporation of copper.

Since the incorporation of copper, unlike the incorporation of other cofactors normally found in Tat-substrates, cannot occur in the cytoplasm but only in periplasm and since high concentrations of copper were not able to compensate the missing PvdM, it may have a role here as a copper chaperone for PvdP (Palmer *et al.* 2005; Stolle *et al.* 2016). This interplay has already been described for various *Streptomyces* species, including *S. antibioticus* and *S. lavendulae*, for example (Claus and Decker 2006). In these strains, upstream of *melC2*, which codes for the tyrosinase MelC2, lies *melC1*, a gene that codes for MelC1 (Huber *et al.* 1985). It was shown that MelC1 is a small chaperone-like protein, which, among other things, is responsible for the incorporation of copper into MelC2 and without which MelC2 is not active (Lee *et al.* 1988; Chen *et al.* 1992). In pseudomonads, the *pvdMNO* operon is usually encoded adjacent to the *pvdP* gene and the expression of these genes are all controlled by the alternative sigma-factor PvdS (**Figure 46**). That means that the expression of the genes is up- or down-regulated together and PvdM is always produced when PvdP is produced.

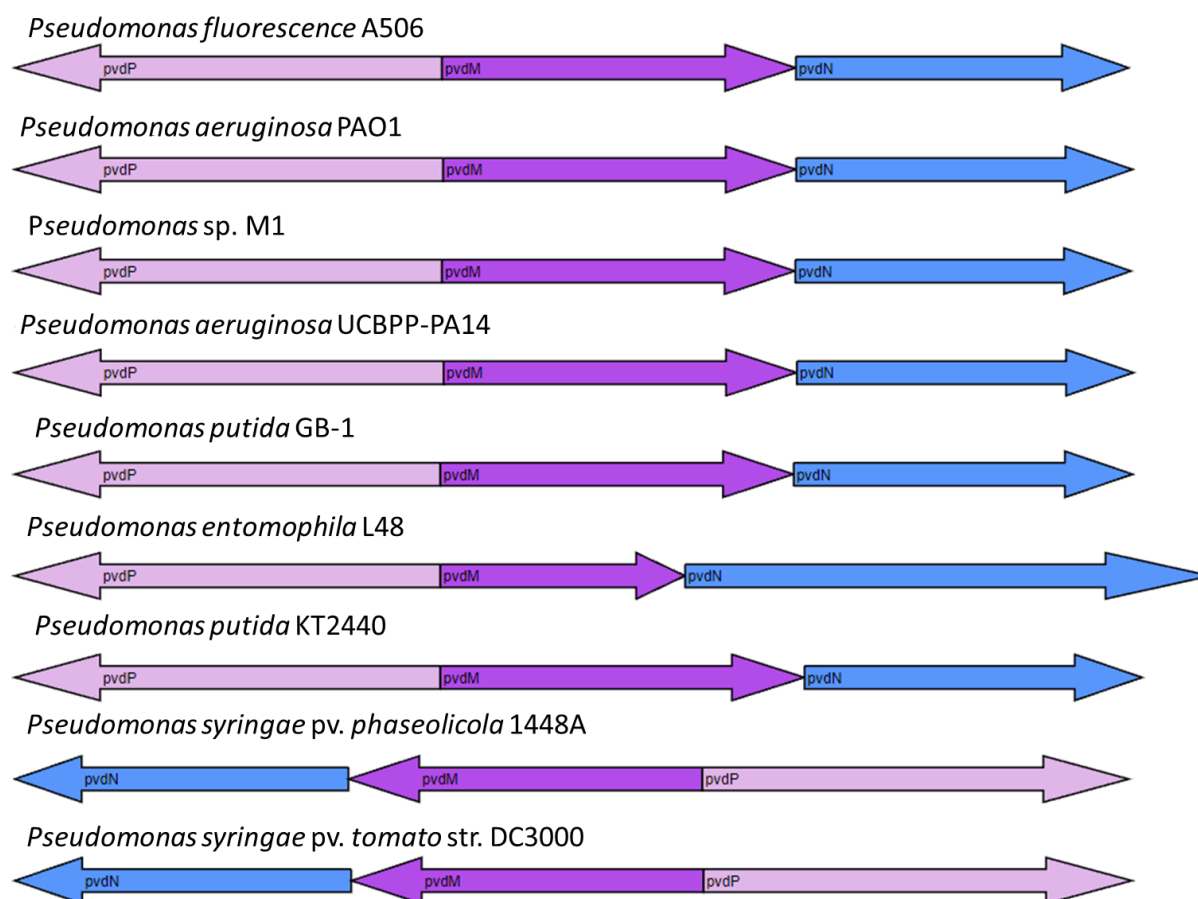


Figure 46: Comparison of *pvdP* and *pvdM* co-occurrence in representative *Pseudomonas* genomes. Comparison of the genomic co-occurrence of *pvdP* (shown in pink), *pvdM* (shown in purple) and *PvdN* (shown in blue) in representative pseudomonas strains. The comparison was visualised using Gene Graphics (Harrison *et al.* 2018).

A second indication, besides the non-existent conversion of ferribactin to dihydropyoverdine by PvdP without PvdM *in vivo*, is the excessive amount of copper needed for experiments involving PvdP *in vitro*. On one hand 250 μM copper needed to be added to the reaction mix for the demonstration of the catalytic activity of PvdP, on the other hand, 500 μM of copper had to be used for copper reconstitution in crystallisation studies of PvdP (Nadal-Jimenez *et al.* 2014; Wibowo *et al.* 2020) These high copper concentrations are already significantly above the toxic threshold for the cell under physiological conditions. Indeed, copper is an essential trace element and an important co-factor for many different redox reactions, but in its free form it is also an extremely toxic metal (Rensing and Grass 2003). It is capable of generating reactive oxidative species such as superoxides and hydroxyl radicals via Fenton-chemistry that can

damage proteins and other cofactors (Haber and Weiss 1934; Valko *et al.* 2007). The fact that PvdP has not been active without the amount of 250 μM copper in the reaction setup suggests that the copper cannot be trivially inserted in PvdP. Thus, a high concentration of copper must be chosen to increase the likelihood that copper ions will bind to the active sites of PvdP even without the potential copper chaperone PvdM

A third indication is provided by the analysis of the copper concentrations in PvdP variants produced in dependence of PvdM. The determination of the various metal concentrations in the two PvdP variants produced under different conditions also shows a variation of copper concentration in the PvdP produced in the presence of PvdM compared to the PvdP produced in the absence of PvdM. As the measurements of nickel, zinc and copper in the respective samples show, the concentrations of nickel and zinc do not change significantly, whereas the concentration of copper in the two samples differs significantly. Thus, only 27.0 % of the expected copper concentration was measured in the PvdP variant produced in the absence of PvdM. At the same time, 58.2 % of the expected copper concentration was detected in the PvdP variant produced in the presence of PvdM. Even though significantly less copper than expected was detected in both samples, relatively speaking, the variant produced without PvdM contained less than half as much copper as the variant produced under normal conditions. These generally low concentrations of all three metals in both protein samples are due to the low concentration of protein in the contained sample and the small proportion of PvdP in the total protein occurrence of the respective samples.

Although the data shown here should be taken with caution and determination of the incorporated copper of PvdP should be repeated with a more purified sample, they do show a trend from which a possible relationship between the incorporation of copper into PvdP and the presence of PvdM can be inferred. Following the results of these first preliminary experiments, and in order to complement the results presented here, further experiments can be carried out in which the activity of purified PvdP can be measured *in vitro* in dependence of the addition of PvdM.

A second possible role of PvdM in the interaction of PvdP could be to serve as a shuttle in a kind of handover mechanism for the deacylated ferribactin. Since PvdP seems to be a membrane-bound protein, the ferribactin needed for the conversion to pyoverdine must be kept

at the membrane after it has been deacylated by PvdQ, following the transport into the periplasm. Of the seven amino acid residues involved in binding the peptide backbone in hrDP, three amino acids, namely arginine at position 276, tyrosine at position 302 and aspartic acid at position 391 are conserved in PvdM (Nitanai *et al.* 2002). In this scenario, the deacylated ferribactin could be attached to the aforementioned amino acid residues of PvdM in order to present the N-terminus of the ferribactin to PvdP for the first oxidation step, resulting in dihydropyoverdine. One way to investigate this would be to exchange the amino acids that are involved and to examine whether PvdM is still active, or whether PvdP can still carry out the oxidation of ferribactin to dihydropyoverdine despite the amino acid exchanges.

4.2 PvdN is an oxygen dependent enzyme

Although much has been found out about PvdN and its role in the maturation of pyoverdines in general, in this work, PvdN was investigated in more detail. In the course of this work, the use of purified PvdN in *in vitro* enzyme assays and the analysis of the respective reaction products without doubt showed that PvdN is indeed responsible for the conversion of the glutamic acid residue to the succinamide residue at the N-terminus of pyoverdine, as previously stated (Ringel *et al.* 2016). Furthermore, it could be shown that the reaction is dependent on molecular oxygen, as conversion by PvdN did not occur when molecular oxygen was withheld in the reaction setup. This supports the postulated reaction mechanism of a oxidative decarboxylation under the retention of the amine (Ringel *et al.* 2016). While this unusual reaction mechanism was a novelty for PvdN as a PLP-dependent enzyme, another enzyme has since been discovered, Cap15, which uses a similar reaction and acts as a monooxygenase, and refers to the proposed reaction of PvdN. However, while the paper still mentioned the lack of evidence for the actual activity of PvdN *in vitro*, it has now been definitively shown that PvdN catalyses the predicted conversion (Huang *et al.* 2018).

In additional experiments, the amino acid histidine at position 260, which was mentioned in the postulated reaction mechanism as an essential proton donor, was exchanged for an alanine in an attempt to detect an intermediate with a covalent bound PLP co-factor (**Figure 33**). Alanine as a substituent was chosen to minimise adverse steric contacts and avoid novel charge interactions or hydrogen bonds. However, not the expected intermediate was detected, but two

individually modified pyoverdines. One pyoverdine variant showed a cyclisation of the glutamine residue to the nitrogen of the L-2,4-diaminobutyric acid with simultaneous elimination of the hydroxy group of the carbonyl group. In the other variant, the complete glutamic acid residue was cleaved from the chromophore, resulting in a pyoverdine without side chain as a product (**Figure 34**).

Since the histidine, which is responsible for the deprotonation in the postulated reaction mechanism in the wild-type PvdN, was no longer present due to the exchange with alanine, another amino acid with a basic residue was searched for that could carry out this reaction. The amino acid arginine at position 267 was identified in the immediate vicinity of the active centre (**Figure 47**). In a possible chain of reactions in wild-type PvdN, arginine could initiate the deprotonation of histidine, which in turn would cause the deprotonation of the glutamic acid residue in the conversion to succinamide. Since histidine is no longer available as an amino acid to be deprotonated, two different scenarios are possible leading to the formation of the detected modified pyoverdine. In a first reaction, the basic amino acid arginine could directly interact with the terminal carboxyl group of the side chain. This would lead to a hydrolysis and a simultaneous ring closure of the α -carbon of the glutamic acid residue and the nitrogen at the γ -carbon of the L-2,4-diaminobutyrate forming a carboxamide, which would result in the first detected variant of the pyoverdine. A second possibility could be that an activated water molecule attacks the peptide bond and causes hydrolysis of the side chain, resulting in the pyoverdine variant with the missing side chain (Min *et al.* 2008). Since the proteolysis of peptide bonds by the nucleophilic attack of water is very slow, this reaction must necessarily be catalysed by this PvdN variant (Raju 2019). The activation of the water to the reactive hydroxide ion could occur here through a deprotonation of the same and simultaneous protonation of the nearby arginine. In both reactions, arginine at position 267 would be involved as the amino acid required for the initial deprotonation. Although the cyclized succinic acid variant of pyoverdine was previously detected in minute amounts in a Δ *ptaA* strain, this variant of the protein appears to favour the conversion of the glutamic acid residue to the two detected pyoverdine variants (Ringel *et al.* 2017).

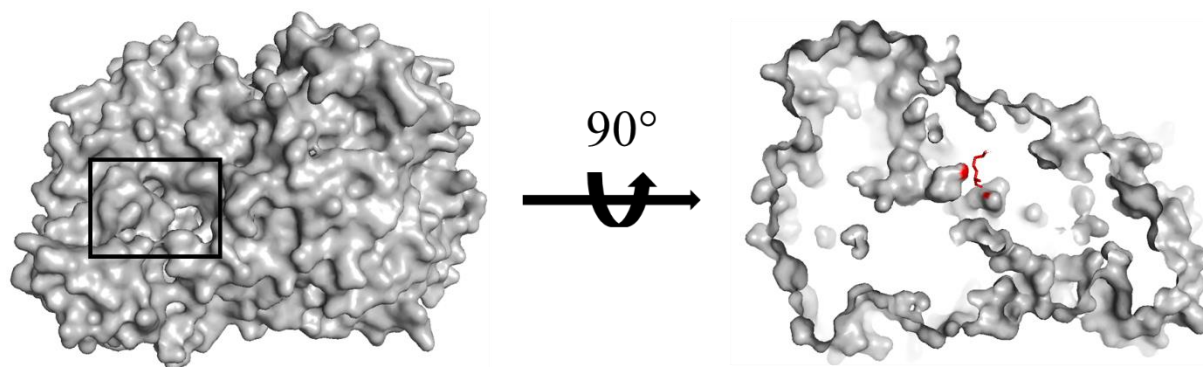


Figure 47: Model of the tunnels of PvdM and the neighbouring arginine. Model of PvdN with the tunnel entrance/exit marked by the black box. Rotation by 90 degrees and a look inside the structure reveal the tunnel and the arginine that potentially starts all reactions, which is marked in red in the immediate vicinity of the active centre.

In order to be able to detect the quinoid intermediate covalently bound to the PLP, one could also replace the arginine with alanine in addition to the essential histidine in future experiments. This could prevent the formation of the intermediates detected here, should arginine indeed be responsible for the initial deprotonation, and the reaction could actually be interrupted at the step where the PLP co-factor is bound to the quinoid intermediate. The detection of this intermediate would provide experimental evidence for the postulated reaction pathway.

4.2.1 Alternative substrate of PvdN

In parallel experiments, it was also investigated whether, in addition to the natural substrate pyoverdine with a glutamic acid side residue, other substances can be converted by PvdN that are easier to handle and, in contrast to pyoverdine, do not require complex purification. It was shown that PvdN accepts glutamine as a substrate, which is converted to succinamide, but does not accept glutamic acid as a substrate. This property can be explained by the structure of the different molecules (**Figure 48**). During the formation of the peptide bond of glutamic acid with tyrosine during the biosynthesis of ferribactin and the concomitant dehydration reaction, glutamic acid loses its hydroxyl group at the ϵ -carbon (Mossialos *et al.* 2002). Due to this process, the glutamic acid residue linked to an amino group of the pyoverdine has a greater similarity to free glutamine than to the original glutamic acid. The reason for not accepting the free glutamic acid as a substrate must therefore be the hydroxy group at the ϵ -carbon which has

to sterically prevent the correct positioning of the molecule in the active centre of PvdN, since it is the only different between glutamine and glutamic acid.

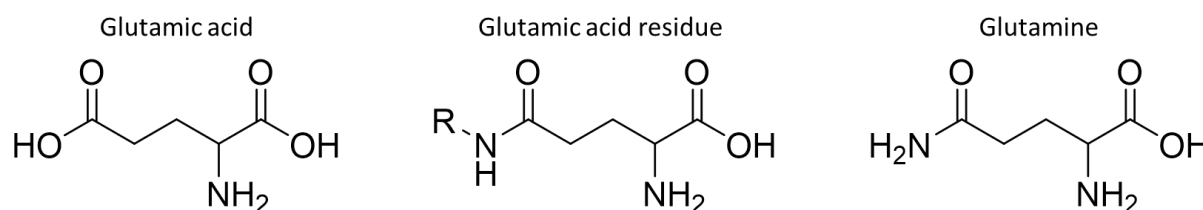


Figure 48: Comparison of glutamic acid, the glutamic acid residue and glutamine. Comparison of the structures of glutamic acid, the glutamic acid residue of pyoverdine (the R represents the pyoverdine residue) and glutamine. As can be seen, glutamine has a higher similarity to the glutamic acid residue of pyoverdine than pure glutamic acid.

4.3 PvdP possesses an unusual signal peptide

Since the role of PvdM was investigated in the context of this work and an essential role for the function of PvdP *in vivo* could be established, PvdP as a very likely interaction partner of PvdM was also investigated in more detail. For this purpose, PvdP was first produced in its natural organism *P. fluorescens* A506 and the subcellular localisation was determined. In contrast to previous publications, in which only a PvdP variant was investigated that did not possess a signal peptide and which has only been produced in *E. coli*, it was demonstrated here that, when produced as a full-length protein in its organism of origin, PvdP is not released into the periplasm after translocation across the cytoplasmic membrane. (Nadal-Jimenez *et al.* 2014). It is rather found in the membrane fraction of the subcellular fractionation.

The unusual localisation of the full-length PvdP in the membrane fraction allows for various conclusions to be drawn. Firstly, PvdP may be another of the few yet known Tat substrates that retains its signal peptide after translocation across the inner membrane. Thus, the signal peptide of PvdP would not only be responsible for the correct translocation from the cytoplasm into the periplasm, but also for the integration of PvdP into the cytoplasmic membrane. Although most Tat substrates are soluble proteins, which are released after translocation, there are some exceptions (Fröbel *et al.* 2012a; Fröbel *et al.* 2012b). One of these exceptions is the Rieske protein, an essential iron-sulfur containing subunit of the ubiquinol-cytochrome-c reductase in the respiratory chains of bacteria (Berks 1996; Rieske *et al.* 1964). It is, unlike most of the known Tat substrates, not released after translocation across the inner membrane, but inserted

into the cytoplasmic membrane (Bachmann *et al.* 2006). Analysis of the Tat signal peptide of PvdP revealed an unusual property with the lack of a distinct cleavage site similar to the signal peptide of the Rieske protein (**Figure 49**).

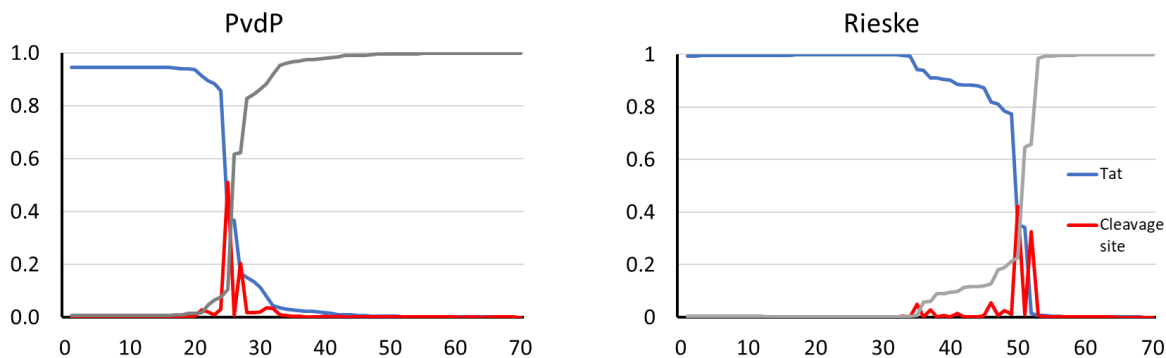


Figure 49: The prediction of the signal sequence cleavage site of PvdP is similar to that of the Rieske protein. Comparison of the signal sequences of PvdP and the Rieske subunit of the cytochrome bc_1 complex. Both signal peptides show a clear Tat sequence but only an inferior cleavage site.

The cysteine crosslinking experiments also show that the signal peptides of PvdP are at least spatially close to each other, so that an interaction between them is possible and an integration into the membrane is an option (**Figure 50**).

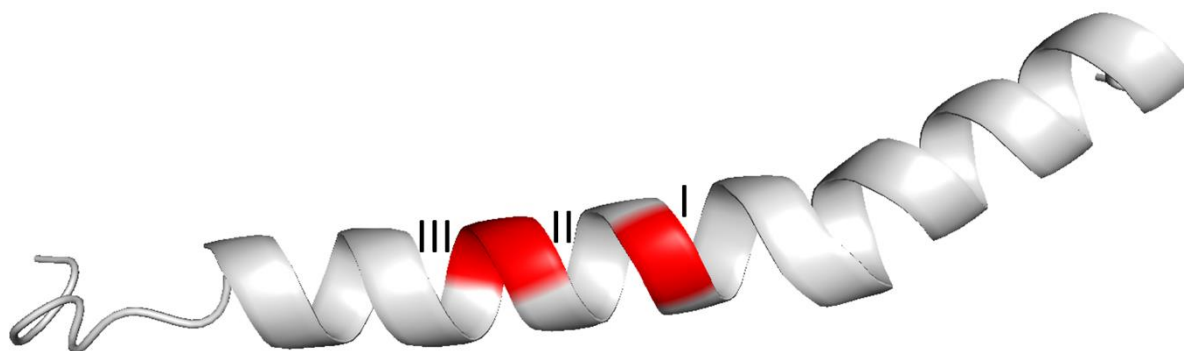


Figure 50: Cystein exchanges that formed a PvdP dimer. Predicted N-terminal signal peptide of PvdP with the highlighted amino acid exchanges A22C (I), A25C (II) and H26C (III) that respectively formed a dimer in cysteine crosslinking experiments.

However, the question arises why PvdP, although produced in large quantities and clearly detectable in the membrane fraction, could not be solubilised and liberated from the membrane

with the use of 2 % of the non-ionic detergent dodecyl- β -D-maltoside (DDM). During the solubilization of the membrane, detergents in general disintegrate the lipid bilayer and form lipid-detergent mixed micelles on the one hand, and protein-detergent complexes on the other hand, while the hydrophobic areas of the protein are covered by the detergent. If PvdP were present as a normal membrane-integrated protein, just like most proteins integrated into the membrane, PvdP would have been solubilised by the treatment of the membrane with DDM.

A second possibility for the remaining of PvdP in the membrane fraction after the treatment with DDM would be the formation of micro aggregates, which can occur when a protein is produced in large quantities in the cell. Usually, the formation of micro aggregates *in vivo* occurs because of the interaction of highly hydrophobic proteins, which have been expressed at high levels (Singh and Panda 2005). In case of PvdP, the hydrophobic signal peptides of the unfolded peptide chains could interact with one another which would condition the aggregation and the formation of micro aggregates in the cytoplasm. When separating the different fractions by subcellular fractionation, these micro aggregates would be pelleted down into the non-soluble pellet that contains, for example, cell wall fragments, simply due to their physical properties such as size and weight. However, since these microaggregates can be carried on by accident during subcellular fractionation, they may be found in the membrane fraction in the course of fractionation. On one hand, this would explain why PvdP was detected in the membrane fractions, on the other hand, it would explain why PvdP could not be detected as a soluble protein in the fractionation supernatant even after treatment with different detergents such as DDM or Triton X-100, since the micro aggregates can withstand concentrations of Triton X-100 up to 5 % (Palmer and Wingfield 2004) . This would mean that the interpretation of the fractionation results might lead to a misinterpretation of the subcellular localisation of PvdP and that it might not be a protein bound to the membrane in the periplasm, but actually a protein that occurs freely in the periplasm.

If this were the case, a way to verify the hypothesis would be an isolation and preparation of the potential micro aggregates a subsequent refolding of possibly contained PvdP. In addition, the membrane fraction could also be subjected to a gradient ultracentrifugation in which the different components of the fraction are separated with respect to their density (Brakke 1951). In this way, one could separate the proteins from the membrane components and identify PvdP, which possibly has been falsely assigned to the membrane fraction.

4.4 PvdQ deacylates ferribactin

During growth studies with different knockout strains, the strain *P. fluorescens* A506 $\Delta pvdQ$ showed a characteristic fluorescence despite the absence of an enzyme, which is believed to be essential for the maturation of pyoverdine. Since the pyoverdine precursor isolated from a $\Delta pvdQ$ strain was initially characterised as fluorescent in a publication, although this was revoked in a subsequent publication, and since there exist different opinions on whether PvdQ uses ferribactin or pyoverdine as a substrate, in the course of this work, an attempt was made to elucidate between which steps in the maturation process of pyoverdine PvdQ acts as deacylating enzyme (Yeterian *et al.* 2010; Drake and Gulick 2011; Hannauer *et al.* 2012). The detected fluorescence indicated a new order of the maturation sequence, in which the deacylation of ferribactin does not necessarily occur immediately after transport into the periplasm, but in principle could be preceded by oxidation to pyoverdine (**Figure 51**). Thus, an effort was made to detect the fluorescent intermediates in a *P. fluorescens* A506 $\Delta pvdQ$.

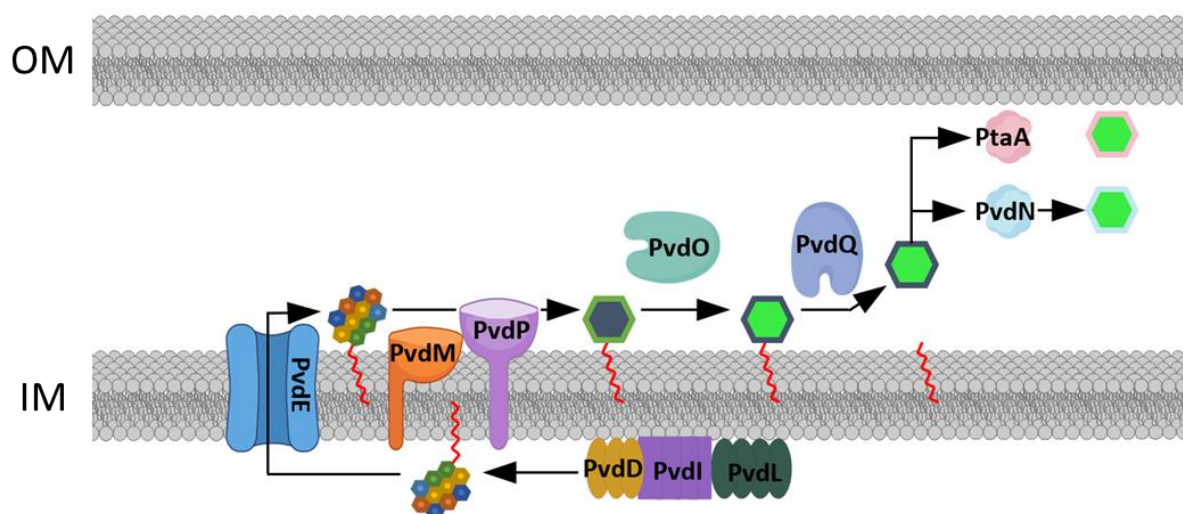


Figure 51: Possible new order of maturation. Postulated new sequence of pyoverdine maturation based on the detected fluorescence in a $\Delta pvdQ$ strain. Ferribactin, exported by PvdE, is first oxidised to dihydropyoverdine by the two membrane-bound proteins PvdM and PvdP and subsequently oxidised by PvdO to pyoverdine. Only after complete oxidation is the mature and fluorescent pyoverdine deacylated by PvdQ and can subsequently be modified by PtaA or PvdN.

Interestingly enough, no pyoverdine variants explaining the fluorescence could be detected by analysis of the supernatant via UPLC-MS. Instead, various ferribactin variants were detected, which can be explained by the absence of PvdQ in the mutant. On the one hand, masses corresponding to acylated ferribactin with myristic or myristoleic acid were detected. On the other hand, a mass which corresponds to a ferribactin acylated with myristic acid a formyl group at the peptide backbone was detected. This latter mass has also been detected in earlier studies on PvdQ (Drake and Gulick 2011).

Since neither pyoverdine in deacylated form nor pyoverdine variants in acylated form could be detected, these unusual results lead to the conclusion that the fluorescence may actually not be caused by pyoverdine, but is produced by another metabolite which is produced instead of pyoverdine, as previously proposed (Hannauer *et al.* 2012). Since most of the fluorescence was measured in the medium and in the supernatant fraction after the first disruption of the cells, these fractions should be pooled and concentrated for future determination of the fluorescent compound. It may also be possible to visualise the unknown fluorescent substance via in-gel fluorescence and to isolate and purify it for mass analysis in order to obtain the first indications of the fluorescent compound. The obtained fluorescence also means that the previously postulated pathway, in which the deacylation of the fatty acid is downstream of the complete oxidation in the maturation process, was not verified.

In addition, when measuring the different fractions after different ultracentrifugation steps, the fluorescence that could still be detected in the sample before disappeared in a way that could not be explained. For instance, a distinct fluorescence was detected in the supernatant fraction after ultrasonic disruption, but when this sample was ultracentrifuged again, it could not be detected either in the newly obtained supernatant nor in the pellet. One possible explanation may be that the unidentified fluorescent molecule is simply not as stable and more redox-sensitive as pyoverdine and therefore decays faster and loses its fluorescence. An approach to detect these compounds nonetheless could be the combination of fluorescence detection and mass spectrometry in order to anticipate the disappearance of fluorescence, as established for example in the analysis of redox-sensitive cysteines or the detection of benzo(a)pyrene metabolites (Petrotchenko *et al.* 2006; Harris *et al.* 2020).

The reason for the shift of the fluorescence maxima in the individual measurements of the same sample could already be attributed experimentally to the different pH values in which the fluorescence was measured. The reason for this may be the phenomenon that hydroxyl groups, which also occur in the fluorophore of pyoverdine, are deprotonated as the pH value increases. As a result, the deprotonated fluorophore can take on several resonance forms, which lead to the stabilisation of the excited state. In contrast, the non-deprotonated fluorophore has only one excited state. This leads to the emission spectrum being shifted into higher, lower-energy wavelength ranges in a basic environment (Valeur *et al.* 2012). As has already been shown with the example of quinoline, the fluorescence here depends on the solvent in which the measurement is carried out. Thus, the fluorescence is significantly stronger in polar solutions than in non-polar solutions (Valeur *et al.* 2012). In a non-protonated state, for example, quinoline has only a relatively weak fluorescence, which is due to the fact that the free electron pair of nitrogen can interact with the π -electron system and thus interfere. However, if the nitrogen atom is protonated, the free electron pair is shared with a hydrogen and thus no longer hinders the electrons in the π -electron system (Sauer 2010; Tervola *et al.* 2020). The reason for the shift of the extinction maxima is therefore the increasing difference of pH values that arises over time in the medium when pseudomonads grow and reach a value of pH 8.0 and the pH of the buffer, the cells and various fractions were resuspended.

4.5 Di-methylated EDDHA could facilitate iron release

In the course investigating different proteins for their involvement and function in the synthesis of pyoverdine, it was observed that several strains, after a certain incubation period, were able to grow in iron-depleted medium, although they were no longer able to produce pyoverdine. Initially, it was assumed that *P. fluorescens* A506 first had to adapt to the conditions in the medium and, due to the lack of synthesising pyoverdines, produced a new siderophore that took over the tasks of pyoverdines with regard to iron acquisition. However, a new siderophore was not being detected in the analysis of the medium supernatant. Instead, a modified form of the iron chelator EDDHA was discovered, which was methylated at the two amino groups involved in the complexation of iron. Fractionation of the grown cells and subsequent examination via UPLC-MS showed that the methylated EDDHA was only detectable in the medium, but neither in the cytoplasm nor periplasm of the cells. Since this dimethylated form of EDDHA was not

detected in the control, in which only the medium was incubated under the same conditions, the cause for this modification must be the presence of the bacteria. Due to the methylation of the amino groups, which play a decisive role in the coordination of iron by EDDHA, two of the six binding sites are modified, so that the hexadentate ligand now becomes a tetradentate ligand. As a result, the iron is bound much weaker to EDDHA and can be dissolved more easily. The results of the analysis of the medium and the fraction of the cells suggest that the EDDHA was methylated outside of the cell in the extracellular space. Most likely, the formation of this new EDDHA derivative is due to the action of so-called methyltransferases. These are enzymes that are able to transfer methyl groups to a wide range of different substrates (Bussiere *et al.* 1998). Methylations are common processes that occur throughout nature in both prokaryotes and eukaryotes and play a role in the regulation of proteins, for example, by influencing protein-protein or protein-DNA interactions or the regulation of chromosomal DNA (Adams and Cory 1975; Oliveira and Fang 2021). Prokaryotic epigenetics, i.e., changing gene expression without changing the DNA sequence, is mainly achieved by the methylation of the DNA and it is considered the most frequently occurring form of post-replicative nucleotide modification (Adhikari and Curtis 2016; Jensen *et al.* 2019). Normally, methylation takes place mainly in the cytoplasm of bacteria, as it is primarily DNA and proteins in post-translational modifications that are methylated (Blanc and Richard 2017; Schubert *et al.* 2006). However, since in this case neither in the periplasm nor in the cytoplasm could the dimethylated EDDHA derivative be detected, the methylation must unusually be carried out either by methyltransferases that have been transported into the extracellular space or adhere to the outside of the cell as an outer membrane protein. The various outer membrane proteins characterised as of now belong to 6 different families, including e.g. substrate-specific porins, TonB-dependent receptors, small β -barrel membrane anchors or membrane-integral enzymes (Schubert *et al.* 2006). While methylated outer membrane proteins do exist and can perform a specific function, no protein is yet known that can carry out this methylation outside the cell (Yang *et al.* 2017). Since the known methylation processes, such as the methylation of histones or the N-terminal methylation of proteins, rely on the universal methyl group donor S-adenosyl-methionine, another donor would have to be available for the process taking place here (Wood and Shilatifard 2004; Stock *et al.* 1987; Zhang and Huang 2016). A possible donor for methyl groups would be methionine, which, as an essential amino acid is freely available in the CAA medium, due to the composition of the medium with its main component being an

acid hydrolysate from casein (Obeid 2013). As a methyl group donor, methionine would be demethylated to homocysteine in the course of this reaction (**Figure 52**).

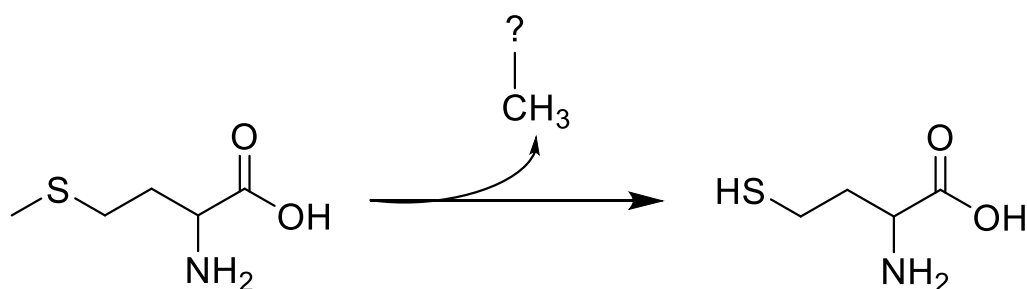


Figure 52: Possible donation of methyl group by methionine. Demethylation of methionine to homocysteine by an unknown methyltransferase.

However, to confirm this, future experiments and detection of the different intermediates are needed, which could possibly be carried out using mass spectroscopy analyses in combination with isotope detection and methionine with methyl groups consisting of ¹³C isotopes, in order to be able to clearly detect the methyl group of methionine being transferred to the demethylated EDDHA.

4.6 Summary and Outlook

In this work, the precise subcellular localisation of PvdM in *P. fluorescens* A506 was determined and it was demonstrated that the unusual N-terminus functions as a signal peptide and mediates translocation via the Sec pathway despite the absence of a hydrophilic carboxyterminal c-region. Furthermore, it was shown that the signal peptide of PvdM, due to the lack of a cleavage site for a periplasmic leader peptidase, also acts as a transmembrane helix for the integration into the cytoplasmic membrane. Why a PvdM variant was not liberated into the periplasm despite a properly processed signal peptide, but was still firmly associated with the membrane, could not be conclusively clarified despite the analysis of the fragments obtained after tryptic digestion via MS/MS. No post-translational modifications of the protein could be detected, but two potential amino acid residues on the surface of the folded protein were identified. These two amino acids could possibly be modified in way that results in a membrane integration of PvdM. Another possible explanation would be the interaction with other membrane-anchored proteins to form a multi-protein complex that ensures that PvdM remains associated with the membrane despite the absence of a signal peptide. A multi-protein complex could next to PvdM consist of PvdP and possibly other essential proteins such as PvdE or PvdO.

Furthermore, it could be shown that PvdM does not take over the task of the still unknown site 1-like peptidase in the periplasmic processing of FpvR and is therefore not involved in the regulatory pathway of pyoverdine synthesis in this manner, but plays an essential role in the maturation of pyoverdines. Mass spectrometric studies have shown that only deacylated ferribactin could be detected in a $\Delta pvdM$ strain. This shows that PvdM is essential for the activity of PvdP *in vivo*, i.e., formation of the characteristic fluorophore through the oxidation of ferribactin to dihydropyoverdine. Two possible functions for PvdM in relation to PvdP were suggested. Firstly, PvdM may facilitate the incorporation of copper into PvdP as a copper chaperone, and secondly, PvdM may be involved in a kind of handover mechanism to deliver the deacylated ferribactin to the active site of PvdP.

Moreover, PvdP was detected for the first time as a full-length protein in the membrane fraction of the natural host, which, in addition to the similarity of the signal peptide to that of the Rieske protein, suggests that it could be a membrane-bound protein and not, as previously assumed, a protein liberated into the periplasm. In order to finally answer this question and also the question about the potential copper chaperone function of PvdM, the purification and solubilisation protocol must be optimised in the future.

In addition, it was finally demonstrated that PvdN catalyses the oxidative conversion of the glutamate residue on pyoverdine to succinamide. At the same time, glutamine was discovered as a new alternative substrate, which will significantly simplify future experiments concerning PvdN. The predicted intermediate bound to PLP, which would prove the postulated reaction mechanism of oxidative decarboxylation under the retention of an amine, could not yet be detected, but two different modified pyoverdines were detected (Ringel *et al.* 2016). These two modified pyoverdines indicate that not only the basic amino acid histidine at position 260 is involved in the catalytic action of PvdN, but also a second basic amino acid in the immediate vicinity of the active site, identified as arginine at position 267. Substitution of both histidine at position 260 and arginine at position 267 in a single PvdN variant could lead to the desired intermediate in the future. It could also be attempted to use glutamine for the conversion by the competing protein PtaA in order to clarify the last open question to which carbonyl compound the excess amino group is transferred.

Furthermore, an attempt was made to determine the substrate of PvdQ, as different opinions exist here. Although fluorescence was detected in a $\Delta pvdQ$ deletion strain in which no deacylation of the pyoverdine precursor ferribactin can take place, no pyoverdine in any possible form modified, could be detected that could have been responsible for this. Instead, another, still unknown compound must be responsible for the detected fluorescence, which needs to be identified in the future.

Lastly, it was also found that, contrary to expectations, growth is possible in a medium depleted with the strong iron chelator EDDHA, although no pyoverdine can be synthesised. Surprisingly, modified EDDHA variants were detected that may impair the binding affinity to iron and thus enable easier release of the metal from the chelator. However, the exact mechanism of this

extracellular methylation of the amino groups by the bacteria remains unknown. This still needs to be determined and elucidated in future experiments.

In summary, this results in the following procedure for the maturation of pyoverdine (**Figure 53**). First, ferribactin is synthesised in the cytoplasm by NRPSs and then transported into the periplasm, most likely by PvdE. This is followed by the deacylation of the myristic or myristoleic acid, both of which were detected as an acyl chain, by PvdQ. Ferribactin is then oxidised to dihydropyoverdine by PvdP in a first step, with the indispensable presence of PvdM, and further oxidised to pyoverdine by PvdO in a second step. This is followed by the modification of the N-terminal glutamate residue by either PvdN or PtaA and the export of the mature pyoverdine to the extracellular space, where it sequesters iron and is subsequently imported into the cell. After the iron is released, the pyoverdine is recycled and exported from the cell for a new cycle of uptake.

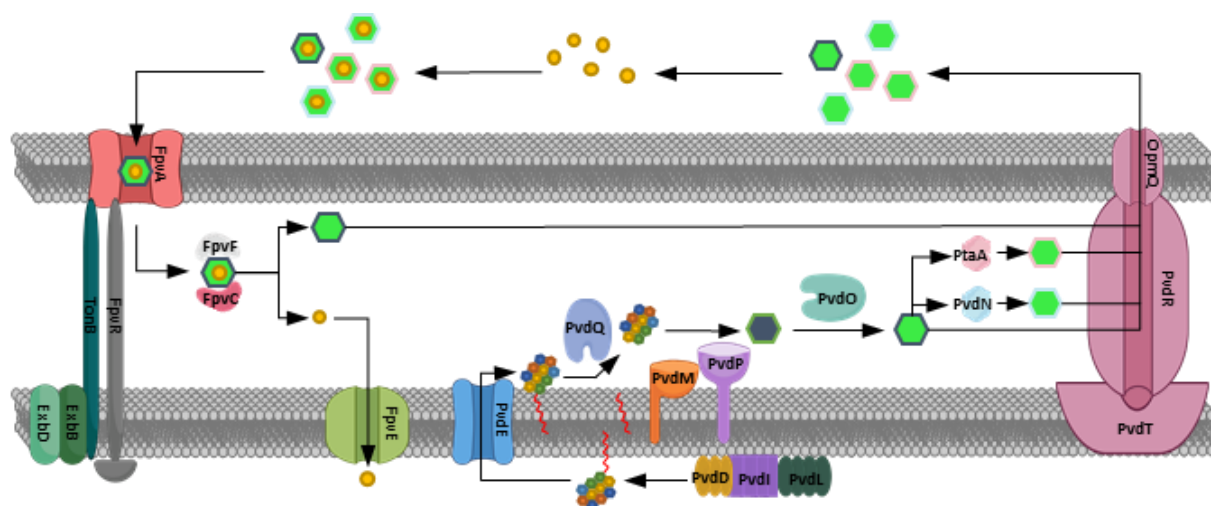


Figure 53: Updated overview of pyoverdine biosynthesis. After the synthesis of acylated ferribactin by the NRPSs PvdL, PvdI, PvdD, it is exported into the periplasm by the ABC transporter PvdE and subsequently deacylated by PvdQ. The deacylated ferribactin is then oxidized by PvdP, in essential interaction with PvdM, and PvdO to pyoverdine, forming the fluorescent chromophore. Additional alternations by either PvdN or PtaA allow for the modification of the glutamic acid side chain. The mature pyoverdine is exported out of the cell by PvdRTOPmQ and other unidentified transport systems for the sequestering of iron. The ferri-pyoverdine is recognised by the outer membrane importer FpvA and is actively imported into the periplasm by the interaction of FpvA and the TonB-ExbB-ExbD-complex. Once imported into the periplasm, the iron is disassociated from the pyoverdine while at the same time being reduced to Fe^{2+} by FpvF and FpvC and other auxiliary enzymes. The ferrous iron is then imported into the cytoplasm by FpvE while the pyoverdine is being regenerated and exported for another cycle of iron chelation.

5 References

- Ackerley, D. F.; Caradoc-Davies, T. T.; Lamont, I. L. (2003): Substrate Specificity of the Nonribosomal Peptide Synthetase PvdD from *Pseudomonas aeruginosa*. In *Journal of Bacteriology* 185 (9), pp. 2848–2855. DOI: 10.1128/JB.185.9.2848-2855.2003.
- Adachi, H.; Katayama, T.; Inuzuka, C.; Oikawa, S.; Tsujimoto, M.; Nakazato, H. (1990a): Identification of membrane anchoring site of human renal dipeptidase and construction and expression of a cDNA for its secretory form. In *Journal of Biological Chemistry* 265 (25), pp. 15341–15345. DOI: 10.1016/S0021-9258(18)77261-X.
- Adachi, H.; Tawaragi, Y.; Inuzuka, C.; Kubota, I.; Tsujimoto, M.; Nishihara, T.; Nakazato, H. (1990b): Primary structure of human microsomal dipeptidase deduced from molecular cloning. In *Journal of Biological Chemistry* 265 (7), pp. 3992–3995. DOI: 10.1016/S0021-9258(19)39692-9.
- Adams, Hendrik; Zeder-Lutz, Gabrielle; Schalk, Isabelle; Pattus, Franc; Celia, Hervé (2006): Interaction of TonB with the outer membrane receptor FpvA of *Pseudomonas aeruginosa*. In *Journal of Bacteriology* 188 (16), pp. 5752–5761. DOI: 10.1128/JB.00435-06.
- Adams, J. M.; Cory, S. (1975): Modified nucleosides and bizarre 5'-termini in mouse myeloma mRNA. In *Nature* 255 (5503), pp. 28–33. DOI: 10.1038/255028a0.
- Adhikari, Satish; Curtis, Patrick D. (2016): DNA methyltransferases and epigenetic regulation in bacteria. In *FEMS Microbiology Reviews* 40 (5), pp. 575–591. DOI: 10.1093/femsre/fuw023.
- Almagro Armenteros, José Juan; Tsirigos, Konstantinos D.; Sønderby, Casper Kaae; Petersen, Thomas Nordahl; Winther, Ole; Brunak, Søren et al. (2019): SignalP 5.0 improves signal peptide predictions using deep neural networks. In *Nature Biotechnology* 37 (4), pp. 420–423. DOI: 10.1038/s41587-019-0036-z.
- Andreini, Claudia; Bertini, Ivano; Cavallaro, Gabriele; Holliday, Gemma L.; Thornton, Janet M. (2008): Metal ions in biological catalysis: from enzyme databases to general principles. In *Journal of Biological Inorganic Chemistry* 13 (8), pp. 1205–1218. DOI: 10.1007/s00775-008-0404-5.

Anraku, Y. (1988): Bacterial electron transport chains. In *Annual Review of Biochemistry* 57 (1), pp. 101–132. DOI: 10.1146/annurev.bi.57.070188.000533.

Archibald, Frederick (1983): *Lactobacillus plantarum*, an organism not requiring iron. In *FEMS Microbiology Letters* 19 (1), pp. 29–32. DOI: 10.1111/j.1574-6968.1983.tb00504.x.

Auld, D. S. (2001): Zinc coordination sphere in biochemical zinc sites. In *Biometals* 14 (3-4), pp. 271–313. DOI: 10.1023/A:1012976615056.

Bachmann, Julie; Bauer, Brigitte; Zwicker, Klaus; Ludwig, Bernd; Anderka, Oliver (2006): The Rieske protein from *Paracoccus denitrificans* is inserted into the cytoplasmic membrane by the twin-arginine translocase. In *FEBS Journal* 273 (21), pp. 4817–4830. DOI: 10.1111/j.1742-4658.2006.05480.x.

Baek, Minkyung; DiMaio, Frank; Anishchenko, Ivan; Dauparas, Justas; Ovchinnikov, Sergey; Lee, Gyu Rie et al. (2021): Accurate prediction of protein structures and interactions using a three-track neural network. In *Science* 373 (6557), pp. 871–876. DOI: 10.1126/science.abj8754.

Bagg, A.; Neilands, J. B. (1987): Ferric uptake regulation protein acts as a repressor, employing iron (II) as a cofactor to bind the operator of an iron transport operon in *Escherichia coli*. In *Biochemistry* 26 (17), pp. 5471–5477.

Beare, Paul A.; For, Raewyn J.; Martin, Lois W.; Lamont, Iain L. (2003): Siderophore-mediated cell signalling in *Pseudomonas aeruginosa*: divergent pathways regulate virulence factor production and siderophore receptor synthesis. In *Molecular Microbiology* 47 (1), pp. 195–207. DOI: 10.1046/j.1365-2958.2003.03288.x.

Begg, Stephanie L.; Eijkelkamp, Bart A.; Luo, Zhenyao; Couñago, Rafael M.; Morey, Jacqueline R.; Maher, Megan J. et al. (2015): Dysregulation of transition metal ion homeostasis is the molecular basis for cadmium toxicity in *Streptococcus pneumoniae*. In *Nature Communications* 6 (1), p. 6418. DOI: 10.1038/ncomms7418.

Behrenfeld; Kolber (1999): Widespread iron limitation of phytoplankton in the south pacific ocean. In *Science (New York, N.Y.)* 283 (5403), pp. 840–843. DOI: 10.1126/science.283.5403.840.

Berks, B. C. (1996): A common export pathway for proteins binding complex redox cofactors? In *Molecular Microbiology* 22 (3), pp. 393–404. DOI: 10.1046/j.1365-2958.1996.00114.x.

Berks, B. C.; Sargent, F.; Palmer, T. (2000): The Tat protein export pathway. In *Molecular Microbiology* 35 (2), pp. 260–274. DOI: 10.1046/j.1365-2958.2000.01719.x.

Berks, Ben C.; Palmer, Tracy; Sargent, Frank (2005): Protein targeting by the bacterial twin-arginine translocation (Tat) pathway. In *Current Opinion in Microbiology* 8 (2), pp. 174–181. DOI: 10.1016/j.mib.2005.02.010.

Bickel, H.; Gaeumann, E.; Keller-Schierlein, W.; Prelog, V.; Vischer, E.; Wettstein, A.; Zaehner, H. (1960): On iron-containing growth factors, sideramines, and their antagonists, the iron-containing antibiotics, sideromycins. In *Experientia* 16, pp. 129–133.

Bishop, Thomas F.; Martin, Lois W.; Lamont, Iain L. (2017): Activation of a Cell Surface Signaling Pathway in *Pseudomonas aeruginosa* Requires ClpP Protease and New Sigma Factor Synthesis. In *Frontiers in Microbiology* 8, p. 2442. DOI: 10.3389/fmicb.2017.02442.

Blanc, Roméo S.; Richard, Stéphane (2017): Arginine Methylation: The Coming of Age. In *Molecular cell* 65 (1), pp. 8–24. DOI: 10.1016/j.molcel.2016.11.003.

Blaudeck, Natascha; Kreutzenbeck, Peter; Freudl, Roland; Sprenger, Georg A. (2003): Genetic analysis of pathway specificity during posttranslational protein translocation across the *Escherichia coli* plasma membrane. In *Journal of Bacteriology* 185 (9), pp. 2811–2819. DOI: 10.1128/JB.185.9.2811-2819.2003.

Bleam, William F. (2011): Chapter 1 - Elements: Their Origin and Abundance. In William F. Bleam (Ed.): *Soil and environmental chemistry*. Amsterdam, Heidelberg: Academic Press, pp. 1–39.

Bokhove, Marcel; Nadal Jimenez, Pol; Quax, Wim J.; Dijkstra, Bauke W. (2010): The quorum-quenching N-acyl homoserine lactone acylase PvdQ is an Ntn-hydrolase with an unusual substrate-binding pocket. In *Proceedings of the National Academy of Sciences of the United States of America* 107 (2), pp. 686–691. DOI: 10.1073/pnas.0911839107.

Bonanno, J. B.; Patskovsky, Y.; Dickey, M.; Bain, K. T.; Mendoza, M.; Fong, R. et al. (2007): Crystal structure of the probable dipeptidase PvdM from *Pseudomonas aeruginosa*. Protein Structure Initiative, New York SGX Research Center for Structural Genomics (NYSGXRC) entry PDB 3B40. DOI: 10.2210/pdb3B40/pdb.

Bonneau, Anne; Roche, Béatrice; Schalk, Isabelle J. (2020): Iron acquisition in *Pseudomonas aeruginosa* by the siderophore pyoverdine: an intricate interacting network including periplasmic and membrane proteins. In *Scientific Reports* 10 (1), p. 120. DOI: 10.1038/s41598-019-56913-x.

Bradford, Marion M. (1976): A rapid and sensitive method for the quantitation of microgram quantities of protein utilizing the principle of protein-dye binding. In *Analytical Biochemistry* 72 (1-2), pp. 248–254. DOI: 10.1016/0003-2697(76)90527-3.

Brakke, Myron K. (1951): Density Gradient Centrifugation: A New Separation Technique 1. In *Journal of the American Chemical Society* 73 (4), pp. 1847–1848. DOI: 10.1021/ja01148a508.

Braud, Armelle; Hoegy, Françoise; Jezequel, Karine; Lebeau, Thierry; Schalk, Isabelle J. (2009): New insights into the metal specificity of the *Pseudomonas aeruginosa* pyoverdine-iron uptake pathway. In *Environmental Microbiology* 11 (5), pp. 1079–1091. DOI: 10.1111/j.1462-2920.2008.01838.x.

Braun, Volkmar; Pramanik, Avijit; Gwinner, Thomas; Köberle, Martin; Bohn, Erwin (2009): Sideromycins: tools and antibiotics. In *BioMetals* 22 (1), pp. 3–13. DOI: 10.1007/s10534-008-9199-7.

Brickman, Edith; Beckwith, Jon (1975): Analysis of the regulation of *Escherichia coli* alkaline phosphatase synthesis using deletions and ϕ 80 transducing phages. In *Journal of Molecular Biology* 96 (2), pp. 307–316. DOI: 10.1016/0022-2836(75)90350-2.

Brillet, Karl; Ruffenach, Frank; Adams, Hendrik; Journet, Laure; Gasser, Véronique; Hoegy, Françoise et al. (2012): An ABC transporter with two periplasmic binding proteins involved in iron acquisition in *Pseudomonas aeruginosa*. In *ACS Chemical Biology* 7 (12), pp. 2036–2045. DOI: 10.1021/cb300330v.

Brüser, Thomas (2007): The twin-arginine translocation system and its capability for protein secretion in biotechnological protein production. In *Applied Microbiology and Biotechnology* 76 (1), pp. 35–45. DOI: 10.1007/s00253-007-0991-z.

Burbidge, E. Margaret; Burbidge, G. R.; Fowler, William A.; Hoyle, F. (1957): Synthesis of the Elements in Stars. In *Reviews of Modern Physics* 29 (4), pp. 547–650. DOI: 10.1103/RevModPhys.29.547.

Burnette, W. Neal (1981): “Western Blotting”. Electrophoretic transfer of proteins from sodium dodecyl sulfate-polyacrylamide gels to unmodified nitrocellulose and radiographic detection with antibody and radioiodinated protein A. In *Analytical Biochemistry* 112 (2), pp. 195–203. DOI: 10.1016/0003-2697(81)90281-5.

Bussiere, D. E.; Muchmore, S. W.; Dealwis, C. G.; Schluckebier, G.; Nienaber, V. L.; Edalji, R. P. et al. (1998): Crystal structure of ErmC', an rRNA methyltransferase which mediates antibiotic resistance in bacteria. In *Biochemistry* 37 (20), pp. 7103–7112. DOI: 10.1021/bi973113c.

Campbell, B. J.; Forrester, L. J.; Zahler, W. L.; Burks, M. (1984): Beta-lactamase activity of purified and partially characterized human renal dipeptidase. In *Journal of Biological Chemistry* 259 (23), pp. 14586–14590. DOI: 10.1016/S0021-9258(17)42642-1.

Campbell, Benedict J.; Di Yuan, Shih; Forrester, Lawrence J.; Zahler, Warren L. (1988): Specificity and inhibition studies of human renal dipeptidase. In *Biochimica et Biophysica Acta (BBA) - Protein Structure and Molecular Enzymology* 956 (2), pp. 110–118. DOI: 10.1016/0167-4838(88)90256-7.

Campbell, Benedict J.; Lin, Yuan-Chuan; Davis, Raymond V.; Ballew, Elizabeth (1966): The purification and properties of a particulate renal dipeptidase. In *Biochimica et Biophysica Acta (BBA) - Enzymology and Biological Oxidation* 118 (2), pp. 371–386. DOI: 10.1016/S0926-6593(66)80046-2.

Casabadan, M. J. (1976): Transposition and fusion of the lac genes to selected promoters in *Escherichia coli* using bacteriophage lambda and Mu. In *Journal of Molecular Biology* 104 (3), pp. 541–555. DOI: 10.1016/0022-2836(76)90119-4.

Chaisson, Eric; McMillan, Stephen (1999): *Astronomy today*. 3rd ed. Upper Saddle River, N.J: Prentice Hall.

Challis, Gregory L.; Naismith, James H. (2004): Structural aspects of non-ribosomal peptide biosynthesis. In *Current Opinion in Structural Biology* 14 (6), pp. 748–756. DOI: 10.1016/j.sbi.2004.10.005.

Chen, L. Y.; Leu, W. M.; Wang, K. T.; Lee, Y. H. (1992): Copper transfer and activation of the *Streptomyces* apotyrosinase are mediated through a complex formation between apotyrosinase and its trans-activator MelC1. In *Journal of Biological Chemistry* 267 (28), pp. 20100–20107. DOI: 10.1016/S0021-9258(19)88671-4.

Claus, Harald; Decker, Heinz (2006): Bacterial tyrosinases. In *Systematic and Applied Microbiology* 29 (1), pp. 3–14. DOI: 10.1016/j.syapm.2005.07.012.

Clément, Emilie; Mesini, Philippe J.; Pattus, Franc; Schalk, Isabelle J. (2004): The binding mechanism of pyoverdinin with the outer membrane receptor FpvA in *Pseudomonas aeruginosa* is dependent on its iron-loaded status. In *Biochemistry* 43 (24), pp. 7954–7965. DOI: 10.1021/BI049768C.

Clevenger, Kenneth D.; Mascarenhas, Romila; Catlin, Daniel; Wu, Rui; Kelleher, Neil L.; Drake, Eric J. et al. (2017): Substrate Trapping in the Siderophore Tailoring Enzyme PvdQ. In *ACS Chemical Biology* 12 (3), pp. 643–647. DOI: 10.1021/acscchembio.7b00031.

Cooley, Richard B.; Arp, Daniel J.; Karplus, P. Andrew (2010): Evolutionary origin of a secondary structure: π -helices as cryptic but widespread insertional variations of α -helices that enhance protein functionality. In *Journal of Molecular Biology* 404 (2), pp. 232–246. DOI: 10.1016/j.jmb.2010.09.034.

Crichton, R. R.; Charleaux-Wauters, M. (1987): Iron transport and storage. In *European journal of biochemistry* 164 (3), pp. 485–506. DOI: 10.1111/j.1432-1033.1987.tb11155.x.

Crisma, Marco; Saviano, Michele; Moretto, Alessandro; Broxterman, Quirinus B.; Kaptein, Bernard; Toniolo, Claudio (2007): Peptide $\alpha/3(10)$ -helix dimorphism in the crystal state. In *Journal of the American Chemical Society* 129 (50), pp. 15471–15473. DOI: 10.1021/ja076656a.

Cristóbal, S.; Gier, J. W. de; Nielsen, H.; Heijne, G. von (1999): Competition between Sec- and TAT-dependent protein translocation in *Escherichia coli*. In *The EMBO Journal* 18 (11), pp. 2982–2990. DOI: 10.1093/emboj/18.11.2982.

Cummings, Jennifer A.; Nguyen, Tinh T.; Fedorov, Alexander A.; Kolb, Peter; Xu, Chengfu; Fedorov, Elena V. et al. (2010): Structure, mechanism, and substrate profile for Sco3058: the closest bacterial homologue to human renal dipeptidase. In *Biochemistry* 49 (3), pp. 611–622. DOI: 10.1021/bi901935y.

Cunliffe, H. E.; Merriman, T. R.; Lamont, I. L. (1995): Cloning and characterization of pvdS, a gene required for pyoverdine synthesis in *Pseudomonas aeruginosa*: PvdS Is Probably an Alternative Sigma Factor. In *Journal of Bacteriology* 177 (10), pp. 2744–2750. DOI: 10.1128/jb.177.10.2744-2750.1995

Dalbey, R. E.; Kuhn, A. (2000): Evolutionarily related insertion pathways of bacterial, mitochondrial, and thylakoid membrane proteins. In *Annual Review of Cell and Developmental Biology* 16 (1), pp. 51–87. DOI: 10.1146/annurev.cellbio.16.1.51.

Deneer, Harry G.; Healey, Vanessa; Boychuk, Irene (1995): Reduction of exogenous ferric iron by a surface-associated ferric reductase of *Listeria* spp. In *Microbiology (Reading)* 141 (Pt 8) (8), pp. 1985–1992. DOI: 10.1099/13500872-141-8-1985.

Dixon, Scott J.; Stockwell, Brent R. (2014): The role of iron and reactive oxygen species in cell death. In *Nature Chemical Biology* 10 (1), pp. 9–17.

Donadio, Stefano; Monciardini, Paolo; Sosio, Margherita (2007): Polyketide synthases and nonribosomal peptide synthetases: the emerging view from bacterial genomics. In *Natural Product Reports* 24 (5), pp. 1073–1109. DOI: 10.1039/B514050C.

Dorrestein, Pieter C.; Poole, Keith; Begley, Tadhg P. (2003): Formation of the chromophore of the pyoverdine siderophores by an oxidative cascade. In *Organic Letters* 5 (13), pp. 2215–2217. DOI: 10.1021/ol034531e.

Drake, Eric J.; Gulick, Andrew M. (2011): Structural characterization and high-throughput screening of inhibitors of PvdQ, an NTN hydrolase involved in pyoverdine synthesis. In *ACS Chemical Biology* 6 (11), pp. 1277–1286. DOI: 10.1021/cb2002973.

Driessen, A. (2001): SecB, a molecular chaperone with two faces. In *Trends in Microbiology* 9 (5), pp. 193–196. DOI: 10.1016/S0966-842X(01)01980-1.

Dyson, Freeman J. (1979): Time without end: Physics and biology in an open universe. In *Reviews of Modern Physics* 51 (3), pp. 447–460. DOI: 10.1103/revmodphys.51.447.

Erbse, A.; Schmidt, R.; Bornemann, T.; Schneider-Mergener, J.; Mogk, A.; Zahn, R. et al. (2006): ClpS is an essential component of the N-end rule pathway in *Escherichia coli*. In *Nature* 439 (7077), pp. 753–756. DOI: 10.1038/nature04412.

Fass, Deborah; Thorpe, Colin (2018): Chemistry and Enzymology of Disulfide Cross-Linking in Proteins. In *Chemical Reviews* 118 (3), pp. 1169–1198. DOI: 10.1021/acs.chemrev.7b00123.

Fewell, M. P. (1995): The atomic nuclide with the highest mean binding energy. In *American Journal of Physics* 63 (7), pp. 653–658. DOI: 10.1119/1.17828.

Frawley, Elaine R.; Fang, Ferric C. (2014): The ins and outs of bacterial iron metabolism. In *Molecular microbiology* 93 (4), pp. 609–616. DOI: 10.1111/mmi.12709.

Frey, Perry A.; Reed, George H. (2012): The ubiquity of iron. In *ACS Chemical Biology* 7 (9), pp. 1477–1481. DOI: 10.1021/cb300323q.

Fröbel, Julia; Rose, Patrick; Lausberg, Frank; Blümmel, Anne-Sophie; Freudl, Roland; Müller, Matthias (2012a): Transmembrane insertion of twin-arginine signal peptides is driven by TatC and regulated by TatB. In *Nature Communications* 3 (1), p. 1311. DOI: 10.1038/ncomms2308.

Fröbel, Julia; Rose, Patrick; Müller, Matthias (2012b): Twin-arginine-dependent translocation of folded proteins. In *Philosophical transactions of the Royal Society of London. Series B, Biological sciences* 367 (1592), pp. 1029–1046. DOI: 10.1098/rstb.2011.0202.

Fromm, Steffanie; Senkler, Jennifer; Eubel, Holger; Peterhänsel, Christoph; Braun, Hans-Peter (2016): Life without complex I: proteome analyses of an *Arabidopsis* mutant lacking the mitochondrial NADH dehydrogenase complex. In *Journal of Experimental Botany* 67 (10), pp. 3079–3093. DOI: 10.1093/jxb/erw165.

Gerwien, Franziska; Safyan, Abu; Wisgott, Stephanie; Brunke, Sascha; Kasper, Lydia; Hube, Bernhard (2017): The Fungal Pathogen *Candida glabrata* Does Not Depend on Surface Ferric Reductases for Iron Acquisition. In *Frontiers in Microbiology* 8, p.1055. DOI: 10.3389/fmicb.2017.01055.

Gómez-Gallego, Mar; Sierra, Miguel A.; Alcázar, Roberto; Ramírez, Pedro; Piñar, Carmen; Mancheño, María José et al. (2002): Synthesis of o,p-EDDHA and its detection as the main impurity in o,o-EDDHA commercial iron chelates. In *Journal of agricultural and food chemistry* 50 (22), pp. 6395–6399. DOI: 10.1021/jf025727g.

González, Jaime; Salvador, Manuel; Özkaya, Özhan; Spick, Matt; Reid, Kate; Costa, Catia et al. (2021): Loss of a pyoverdine secondary receptor in *Pseudomonas aeruginosa* results in a fitter strain suitable for population invasion. In *The ISME Journal* 15 (5), pp. 1330–1343. DOI: 10.1038/s41396-020-00853-2.

Grandchamp, Gabrielle M.; Caro, Lewis; Shank, Elizabeth A. (2017): Pirated Siderophores Promote Sporulation in *Bacillus subtilis*. In *Applied and Environmental Microbiology* 83 (10). DOI: 10.1128/AEM.03293-16.

Greenwald, Jason; Hoegy, Françoise; Nader, Mirella; Journet, Laure; Mislin, Gaëtan L. A.; Graumann, Peter L.; Schalk, Isabelle J. (2007): Real time fluorescent resonance energy transfer visualization of ferric pyoverdine uptake in *Pseudomonas aeruginosa*. A role for ferrous iron. In *Journal of Biological Chemistry*. 282 (5), pp. 2987–2995. DOI: 10.1074/jbc.M609238200.

Greenwald, Jason; Nader, Mirella; Celia, Hervé; Gruffaz, Christelle; Geoffroy, Valérie; Meyer, Jean-Marie et al. (2009): FpvA bound to non-cognate pyoverdines: molecular basis of siderophore recognition by an iron transporter. In *Molecular microbiology* 72 (5), pp. 1246–1259. DOI: 10.1111/j.1365-2958.2009.06721.x.

Gur, Eyal; Biran, Dvora; Ron, Eliora Z. (2011): Regulated proteolysis in Gram-negative bacteria--how and when? In *Nature Reviews Microbiology* 9 (12), pp. 839–848. DOI: 10.1038/nrmicro2669.

Haber, Fritz; Weiss, Joseph (1934): The catalytic decomposition of hydrogen peroxide by iron salts. In *Proceedings of the Royal Society of London A* 147 (861), pp. 332–351. DOI: 10.1098/rspa.1934.0221.

Hannauer, Mélissa; Schäfer, Mathias; Hoegy, Françoise; Gizzi, Patrick; Wehrung, Patrick; Mislin, Gaëtan L. A. et al. (2012): Biosynthesis of the pyoverdine siderophore of *Pseudomonas aeruginosa* involves precursors with a myristic or a myristoleic acid chain. In *FEBS Letters* 586 (1), pp. 96–101. DOI: 10.1016/j.febslet.2011.12.004.

Hannauer, Mélissa; Yeterian, Emilie; Martin, Lois W.; Lamont, Iain L.; Schalk, Isabelle J. (2010): An efflux pump is involved in secretion of newly synthesized siderophore by *Pseudomonas aeruginosa*. In *FEBS Letters* 584 (23), pp. 4751–4755. DOI: 10.1016/j.febslet.2010.10.051.

Harris, Kenneth J.; Subbiah, Seenivasan; Tabatabai, Mohammad; Archibong, Anthony E.; Singh, Kamaleshwar P.; Anderson, Todd A. et al. (2020): Pressurized liquid extraction followed by liquid chromatography coupled to a fluorescence detector and atmospheric pressure chemical ionization mass spectrometry for the determination of benzo(a)pyrene metabolites in liver tissue of an animal model of colon cancer. In *Journal of Chromatography. A* 1622, p. 461126. DOI: 10.1016/j.chroma.2020.461126.

Harrison, Katherine J.; Crécy-Lagard, Valérie de; Zallot, Rémi (2018): Gene Graphics: a genomic neighborhood data visualization web application. In *Bioinformatics* 34 (8), pp. 1406–1408. DOI: 10.1093/bioinformatics/btx793.

Henríquez, Tania; Stein, Nicola Victoria; Jung, Heinrich (2019): PvdRT-OpmQ and MdtABC-OpmB efflux systems are involved in pyoverdine secretion in *Pseudomonas putida* KT2440. In *Environmental microbiology reports* 11 (2), pp. 98–106. DOI: 10.1111/1758-2229.12708.

Hider, Robert C.; Kong, Xiaole (2010): Chemistry and biology of siderophores. In *Natural Product Reports* 27 (5), pp. 637–657. DOI: 10.1039/b9066679a.

Hoffmann, Lena; Suggest, Michael-Frederick; Brüser, Thomas (2021): A tunable anthranilate-inducible gene expression system for *Pseudomonas* species. In *Applied Microbiology and Biotechnology* 105 (1), pp. 247–258. DOI: 10.1007/s00253-020-11034-8.

Hooper, N. M.; Keen, J. N.; Turner, A. J. (1990): Characterization of the glycosyl-phosphatidylinositol-anchored human renal dipeptidase reveals that it is more extensively glycosylated than the pig enzyme. In *Biochemical Journal* 265 (2), pp. 429–433. DOI: 10.1042/bj2650429.

Hu, X.; Boyer, G. L. (1996): Siderophore-Mediated Aluminum Uptake by *Bacillus megaterium* ATCC 19213. In *Applied and environmental microbiology* 62 (11), pp. 4044–4048. DOI: 10.1128/aem.62.11.4044-4048.1996.

Huang, Jean J.; Han, Jong-In; Zhang, Lian-Hui; Leadbetter, Jared R. (2003): Utilization of acyl-homoserine lactone quorum signals for growth by a soil pseudomonad and *Pseudomonas aeruginosa* PAO1. In *Applied and environmental microbiology* 69 (10), pp. 5941–5949. DOI: 10.1128/AEM.69.10.5941-5949.2003.

Huang, Ying; Liu, Xiaodong; Cui, Zheng; Wiegmann, Daniel; Niro, Giuliana; Ducho, Christian et al. (2018): Pyridoxal-5'-phosphate as an oxygenase cofactor: Discovery of a carboxamide-forming, α -amino acid monooxygenase-decarboxylase. In *Proceedings of the National Academy of Sciences of the United States of America* 115 (5), pp. 974–979. DOI: 10.1073/pnas.1718667115.

Huber, M.; Hintermann, G.; Lerch, K. (1985): Primary structure of tyrosinase from *Streptomyces glaucescens*. In *Biochemistry* 24 (22), pp. 6038–6044. DOI: 10.1021/bi00343a003.

Ilbert, Marianne; Bonnefoy, Violaine (2013): Insight into the evolution of the iron oxidation pathways. In *Biochimica et Biophysica Acta* 1827 (2), pp. 161–175. DOI: 10.1016/j.bbabi.2012.10.001.

Imperi, Francesco; Tiburzi, Federica; Visca, Paolo (2009): Molecular basis of pyoverdine siderophore recycling in *Pseudomonas aeruginosa*. In *Proceedings of the National Academy of Sciences of the United States of America* 106 (48), pp. 20440–20445. DOI: 10.1073/pnas.0908760106.

Imperi, Francesco; Visca, Paolo (2013): Subcellular localization of the pyoverdine biogenesis machinery of *Pseudomonas aeruginosa*: a membrane-associated "siderosome". In *FEBS Letters* 587 (21), pp. 3387–3391. DOI: 10.1016/j.febslet.2013.08.039.

Izé, Berengère; Viarre, Véronique; Voulhoux, Romé (2014): Cell fractionation. In *Methods in Molecular Biology* 1149, pp. 185–191. DOI: 10.1007/978-1-4939-0473-0_15.

Jansonius, Johan N. (1998): Structure, evolution and action of vitamin B6-dependent enzymes. In *Current Opinion in Structural Biology* 8 (6), pp. 759–769. DOI: 10.1016/S0959-440X(98)80096-1.

Jeeves, Rose E.; Mason, Robert P.; Woodacre, Alexandra; Cashmore, Annette M. (2011): Ferric reductase genes involved in high-affinity iron uptake are differentially regulated in yeast and hyphae of *Candida albicans*. In *Yeast* 28 (9), pp. 629–644. DOI: 10.1002/yea.1892.

Jensen, Torbjørn Ølshøj; Tellgren-Roth, Christian; Redl, Stephanie; Maury, Jérôme; Jacobsen, Simo Abdessamad Baallal; Pedersen, Lasse Ebdrup; Nielsen, Alex Toftgaard (2019): Genome-wide systematic identification of methyltransferase recognition and modification patterns. In *Nature Communications* 10 (1), p. 3311. DOI: 10.1038/s41467-019-11179-9.

Kahan, F. M.; Kropp, H.; Sundelof, J. G.; Birnbaum, J. (1983): Thienamycin: development of imipenem-cilastatin. In *Journal of Antimicrobial Chemotherapy* 12 Suppl D (suppl D), pp. 1–35. DOI: 10.1093/jac/12.suppl_D.1.

Kang, Donghoon; Revtovich, Alexey V.; Chen, Qingquan; Shah, Kush N.; Cannon, Carolyn L.; Kirienko, Natalia V. (2019): Pyoverdine-Dependent Virulence of *Pseudomonas aeruginosa* Isolates From Cystic Fibrosis Patients. In *Frontiers in Microbiology* 10, p. 2048. DOI: 10.3389/fmicb.2019.02048.

Kang, Donghoon; Revtovich, Alexey V.; Deyanov, Alexander E.; Kirienko, Natalia V. (2021): Pyoverdine Inhibitors and Gallium Nitrate Synergistically Affect *Pseudomonas aeruginosa*. In *mSphere*, e0040121. DOI: 10.1128/mSphere.00401-21.

Kaushik, Manish Singh; Singh, Prashant; Tiwari, Balkrishna; Mishra, Arun Kumar (2016): Ferric Uptake Regulator (FUR) protein: properties and implications in cyanobacteria. In *Annals of Microbiology* 66 (1), pp. 61–75. DOI: 10.1007/s13213-015-1134-x.

Kim, Haeng Soon; Campbell, Benedict J. (1982): β -lactamase activity of renal dipeptidase against N-formimidoyl-thienamycin. In *Biochemical and Biophysical Research Communications* 108 (4), pp. 1638–1642. DOI: 10.1016/S0006-291X(82)80097-1.

Kim, Hayoung; Botelho, Salomé Calado; Park, Kwangjin; Kim, Hyun (2015): Use of carbonate extraction in analyzing moderately hydrophobic transmembrane proteins in the mitochondrial inner membrane. In *Protein Science* 24 (12), pp. 2063–2069. DOI: 10.1002/pro.2817.

Kirienko, Daniel R.; Kang, Donghoon; Kirienko, Natalia V. (2018): Novel Pyoverdine Inhibitors Mitigate *Pseudomonas aeruginosa* Pathogenesis. In *Frontiers in Microbiology* 9, p. 3317. DOI: 10.3389/fmicb.2018.03317.

Kirienko, Daniel R.; Revtovich, Alexey V.; Kirienko, Natalia V. (2016): A High-Content, Phenotypic Screen Identifies Fluorouridine as an Inhibitor of Pyoverdine Biosynthesis and *Pseudomonas aeruginosa* Virulence. In *mSphere* 1 (4). DOI: 10.1128/mSphere.00217-16.

Kleinkauf, H.; Döhren, H. von (1996): A nonribosomal system of peptide biosynthesis. In *European journal of biochemistry* 236 (2), pp. 335–351. DOI: 10.1111/j.1432-1033.1996.00335.x.

Klem-Marciniak, Ewelina; Huculak-Mączka, Marta; Marecka, Kinga; Hoffmann, Krystyna; Hoffmann, Józef (2021): Chemical Stability of the Fertilizer Chelates Fe-EDDHA and Fe-EDDHA over Time. In *Molecules* 26 (7), p. 1933. DOI: 10.3390/molecules26071933.

Knüsel, L. F.; Nüsch, J. (1965): Mechanism of action of sideromycins. In *Nature* 206 (985), pp. 674–676. DOI: 10.1038/206674a0.

Kollef, Marin H.; Bassetti, Matteo; Francois, Bruno; Burnham, Jason; Dimopoulos, George; Garnacho-Montero, Jose et al. (2017): The intensive care medicine research agenda on multidrug-resistant bacteria, antibiotics, and stewardship. In *Intensive Care Medicine* 43 (9), pp. 1187–1197. DOI: 10.1007/s00134-017-4682-7.

Krogh, A.; Larsson, B.; Heijne, G. von; Sonnhammer, E. L. (2001): Predicting transmembrane protein topology with a hidden Markov model: application to complete genomes. In *Journal of Molecular Biology* 305 (3), pp. 567–580. DOI: 10.1006/jmbi.2000.4315.

Kropp, H.; Sundelof, J. G.; Hajdu, R.; Kahan, F. M. (1982): Metabolism of thienamycin and related carbapenem antibiotics by the renal dipeptidase, dehydropeptidase. In *Antimicrobial Agents and Chemotherapy* 22 (1), pp. 62–70. DOI: 10.1128/AAC.22.1.62.

Laemmli, U. K. (1970): Cleavage of structural proteins during the assembly of the head of bacteriophage T4. In *Nature* 227 (5259), pp. 680–685. DOI: 10.1038/227680a0.

Lamont, Iain L.; Beare, Paul A.; Ochsner, Urs; Vasil, Adriana I.; Vasil, Michael L. (2002): Siderophore-mediated signaling regulates virulence factor production in *Pseudomonas aeruginosa*. In *Proceedings of the National Academy of Sciences of the United States of America* 99 (10), pp. 7072–7077. DOI: 10.1073/pnas.092016999.

Lautru, Sylvie; Challis, Gregory L. (2004): Substrate recognition by nonribosomal peptide synthetase multi-enzymes. In *Microbiology (Reading)* 150 (Pt 6), pp. 1629–1636. DOI: 10.1099/mic.0.26837-0.

Lee, Philip A.; Orriss, George L.; Buchanan, Grant; Greene, Nicholas P.; Bond, Peter J.; Punginelli, Claire et al. (2006): Cysteine-scanning mutagenesis and disulfide mapping studies of the conserved domain of the twin-arginine translocase TatB component. In *Journal of Biological Chemistry* 281 (45), pp. 34072–34085. DOI: 10.1074/jbc.M607295200.

Lee, Yan-Hwa Wu; Chen, Bin-Fang; Wu, Shwu-Yuan; Leu, Wei-Ming; Lin, Jin-Jer; Chen, Carton W.; Lo, Szecheng J. (1988): A trans-acting gene is required for the phenotypic expression of a tyrosinase gene in *Streptomyces*. In *Gene* 65 (1), pp. 71–81. DOI: 10.1016/0378-1119(88)90418-0.

Lehoux, Dario E.; Sanschagrín, François; Levesque, Roger C. (2000): Genomics of the 35-kb *pvd* locus and analysis of novel *pvdIJK* genes implicated in pyoverdine biosynthesis in *Pseudomonas aeruginosa*. In *FEMS Microbiology Letters* 190 (1), pp. 141–146. DOI: 10.1111/j.1574-6968.2000.tb09276.x.

Liao, Rong-Zhen; Himo, Fahmi; Yu, Jian-Guo; Liu, Ruo-Zhuang (2010): Dipeptide hydrolysis by the dinuclear zinc enzyme human renal dipeptidase: mechanistic insights from DFT calculations. In *Journal of Inorganic Biochemistry* 104 (1), pp. 37–46. DOI: 10.1016/j.jinorgbio.2009.09.025.

Loper, Joyce E.; Hassan, Karl A.; Mavrodi, Dmitri V.; Davis, Edward W.; Lim, Chee Kent; Shaffer, Brenda T. et al. (2012): Comparative genomics of plant-associated *Pseudomonas* spp.: insights into diversity and inheritance of traits involved in multitrophic interactions. In *PLOS Genetics* 8 (7), e1002784. DOI: 10.1371/journal.pgen.1002784.

Mahmoud, Samar A.; Chien, Peter (2018): Regulated Proteolysis in Bacteria. In *Annual Review of Biochemistry* 87 (1), pp. 677–696. DOI: 10.1146/annurev-biochem-062917-012848.

Manoil, C.; Beckwith, J. (1986): A genetic approach to analyzing membrane protein topology. In *Science* 233 (4771), pp. 1403–1408. DOI: 10.1126/science.3529391.

Manoil, Colin (1991): Chapter 3 Analysis of Membrane Protein Topology Using Alkaline Phosphatase and β -Galactosidase Gene Fusions. In *Methods in Cell Biology* 34, pp. 61–75. DOI: 10.1016/S0091-679X(08)61676-3.

Manting, E. H.; Driessen, A. J. (2000): *Escherichia coli* translocase: the unravelling of a molecular machine. In *Molecular Microbiology* 37 (2), pp. 226–238. DOI: 10.1046/j.1365-2958.2000.01980.x.

Marelja, Zvonimir; Leimkühler, Silke; Missirlis, Fanis (2018): Iron Sulfur and Molybdenum Cofactor Enzymes Regulate the *Drosophila* Life Cycle by Controlling Cell Metabolism. In *Frontiers in Physiology* 9, p. 50. DOI: 10.3389/fphys.2018.00050.

Marvin, Marcus E.; Williams, Peter H.; Cashmore, Annette M. (2003): The *Candida albicans* CTR1 gene encodes a functional copper transporter. In *Microbiology (Reading)* 149 (Pt 6), pp. 1461–1474. DOI: 10.1099/mic.0.26172-0.

McAuliffe, C. A.; Quagliano, J. V.; Vallarino, L. M. (1966): Metal Complexes of the Amino Acid DL-Methionine. In *Inorganic Chemistry* 5 (11), pp. 1996–2003. DOI: 10.1021/ic50045a034.

McMorran, B. J.; Merriman, M. E.; Rombel, I. T.; Lamont, I. L. (1996): Characterisation of the *pvdE* gene which is required for pyoverdine synthesis in *Pseudomonas aeruginosa*. In *Gene* 176 (1-2), pp. 55–59. DOI: 10.1016/0378-1119(96)00209-0.

McMorran, B. J.; Shanta Kumara, H. M.; Sullivan, K.; Lamont, I. L. (2001): Involvement of a transformylase enzyme in siderophore synthesis in *Pseudomonas aeruginosa*. In *Microbiology* 147 (Pt 6), pp. 1517–1524. DOI: 10.1099/00221287-147-6-1517.

Mercer, Andrew C.; Burkart, Michael D. (2007): The ubiquitous carrier protein--a window to metabolite biosynthesis. In *Natural Product Reports* 24 (4), pp. 750–773. DOI: 10.1039/b603921a.

Meyer, J. M.; Neely, A.; Stintzi, A.; Georges, C.; Holder, I. A. (1996): Pyoverdine is essential for virulence of *Pseudomonas aeruginosa*. In *Infection and Immunity* 64 (2), pp. 518–523. DOI: 10.1128/iai.64.2.518-523.1996.

Meyer, J. M.; Stintzi, A.; Vos, D. de; Cornelis, P.; Tappe, R.; Taraz, K.; Budzikiewicz, H. (1997): Use of siderophores to type pseudomonads: the three *Pseudomonas aeruginosa* pyoverdine systems. In *Microbiology (Reading)* 143 (Pt 1), pp. 35–43. DOI: 10.1099/00221287-143-1-35.

Min, Donghong; Josephine, Helen R.; Li, Hongzhi; Lakner, Clemens; MacPherson, Iain S.; Naylor, Gavin J. P. et al. (2008): An enzymatic atavist revealed in dual pathways for water activation. In *PLOS Biology* 6 (8), e206. DOI: 10.1371/journal.pbio.0060206.

Minandri, Fabrizia; Imperi, Francesco; Frangipani, Emanuela; Bonchi, Carlo; Visaggio, Daniela; Facchini, Marcella et al. (2016): Role of Iron Uptake Systems in *Pseudomonas aeruginosa* Virulence and Airway Infection. In *Infection and Immunity* 84 (8), pp. 2324–2335. DOI: 10.1128/IAI.00098-16.

Mislin, Gaëtan L. A.; Schalk, Isabelle J. (2014): Siderophore-dependent iron uptake systems as gates for antibiotic Trojan horse strategies against *Pseudomonas aeruginosa*. In *Metallomics : integrated biometal science* 6 (3), pp. 408–420. DOI: 10.1039/c3mt00359k.

Morgan, J. W.; Anders, E. (1980): Chemical composition of Earth, Venus, and Mercury. In *Proceedings of the National Academy of Sciences of the United States of America* 77 (12), pp. 6973–6977. DOI: 10.1073/pnas.77.12.6973.

Mori, Hiroyuki; Ito, Koreaki (2001): The Sec protein-translocation pathway. In *Trends in Microbiology* 9 (10), pp. 494–500. DOI: 10.1016/S0966-842X(01)02174-6.

Mossialos, Dimitris; Ochsner, Urs; Baysse, Christine; Chablain, Patrice; Pirnay, Jean-Paul; Koedam, Nico et al. (2002): Identification of new, conserved, non-ribosomal peptide synthetases from fluorescent pseudomonads involved in the biosynthesis of the siderophore pyoverdine. In *Molecular Microbiology* 45 (6), pp. 1673–1685. DOI: 10.1046/j.1365-2958.2002.03120.x.

Nadal Jimenez, Pol; Koch, Gudrun; Papaioannou, Evelina; Wahjudi, Mariana; Krzeslak, Joanna; Coenye, Tom et al. (2010): Role of PvdQ in *Pseudomonas aeruginosa* virulence under iron-limiting conditions. In *Microbiology* 156 (Pt 1), pp. 49–59. DOI: 10.1099/mic.0.030973-0.

Nadal-Jimenez, Pol; Koch, Gudrun; Reis, Carlos R.; Muntendam, Remco; Raj, Hans; Jeronimus-Stratingh, C. Margot et al. (2014): PvdP is a tyrosinase that drives maturation of the pyoverdine chromophore in *Pseudomonas aeruginosa*. In *Journal of Bacteriology* 196 (14), pp. 2681–2690. Available online at <http://jb.asm.org/content/196/14/2681.full>.

Nair, Anupa; Juwarkar, Asha A.; Singh, Sanjeev K. (2007): Production and Characterization of Siderophores and its Application in Arsenic Removal from Contaminated Soil. In *Water Air Soil Pollut* 180 (1-4), pp. 199–212. DOI: 10.1007/s11270-006-9263-2.

Nairz, Manfred; Schroll, Andrea; Sonnweber, Thomas; Weiss, Günter (2010): The struggle for iron - a metal at the host-pathogen interface. In *Cellular microbiology* 12 (12), pp. 1691–1702. DOI: 10.1111/j.1462-5822.2010.01529.x.

Nitanai, Yasushi; Satow, Yoshinori; Adachi, Hideki; Tsujimoto, Masafumi (2002): Crystal Structure of Human Renal Dipeptidase Involved in β -Lactam Hydrolysis. In *Journal of Molecular Biology* 321 (2), pp. 177–184. DOI: 10.1016/S0022-2836(02)00632-0.

Noinaj, Nicholas; Guillier, Maude; Barnard, Travis J.; Buchanan, Susan K. (2010): TonB-dependent transporters: regulation, structure, and function. In *Annual Review of Microbiology* 64 (1), pp. 43–60. DOI: 10.1146/annurev.micro.112408.134247.

Obeid, Rima (2013): The metabolic burden of methyl donor deficiency with focus on the betaine homocysteine methyltransferase pathway. In *Nutrients* 5 (9), pp. 3481–3495. DOI: 10.3390/nu5093481.

Ochsner, U. A.; Johnson, Z.; Lamont, I. L.; Cunliffe, H. E.; Vasil, M. L. (1996): Exotoxin A production in *Pseudomonas aeruginosa* requires the iron-regulated *pvdS* gene encoding an alternative sigma factor. In *Molecular Microbiology* 21 (5), pp. 1019–1028. DOI: 10.1046/j.1365-2958.1996.481425.x.

Ochsner, U. A.; Vasil, A. I.; Vasil, M. L. (1995): Role of the ferric uptake regulator of *Pseudomonas aeruginosa* in the regulation of siderophores and exotoxin A expression: purification and activity on iron-regulated promoters. In *Journal of Bacteriology* 177 (24), pp. 7194–7201. DOI: 10.1128/jb.177.24.7194-7201.1995.

Olivares, Adrian O.; Baker, Tania A.; Sauer, Robert T. (2016): Mechanistic insights into bacterial AAA+ proteases and protein-remodelling machines. In *Nature Reviews Microbiology* 14 (1), pp. 33–44. DOI: 10.1038/nrmicro.2015.4.

Oliveira, Pedro H.; Fang, Gang (2021): Conserved DNA Methyltransferases: A Window into Fundamental Mechanisms of Epigenetic Regulation in Bacteria. In *Trends in Microbiology* 29 (1), pp. 28–40. DOI: 10.1016/j.tim.2020.04.007.

Paetzel, Mark; Karla, Andrew; Strynadka, Natalie C. J.; Dalbey, Ross E. (2002): Signal peptidases. In *Chemical Reviews* 102 (12), pp. 4549–4580. DOI: 10.1021/cr010166y.

Palmer, Ira; Wingfield, Paul T. (2004): Preparation and extraction of insoluble (inclusion-body) proteins from *Escherichia coli*. In *Current protocols in protein science / editorial board, John E. Coligan ... [et al.]* Chapter 6, Unit 6.3. DOI: 10.1002/0471140864.ps0603s38.

Palmer, Tracy; Sargent, Frank; Berks, Ben C. (2005): Export of complex cofactor-containing proteins by the bacterial Tat pathway. In *Trends in Microbiology* 13 (4), pp. 175–180. DOI: 10.1016/j.tim.2005.02.002.

Papaloukas, Costas; Granseth, Erik; Viklund, Håkan; Elofsson, Arne (2008): Estimating the length of transmembrane helices using Z-coordinate predictions. In *Protein Science* 17 (2), pp. 271–278. DOI: 10.1110/ps.073036108.

Paulick, Margot G.; Bertozzi, Carolyn R. (2008): The glycosylphosphatidylinositol anchor: a complex membrane-anchoring structure for proteins. In *Biochemistry* 47 (27), pp. 6991–7000. DOI: 10.1021/bi8006324.

Petrotchenko, Evgeniy V.; Pasek, Dan; Elms, Phillip; Dokholyan, Nikolay V.; Meissner, Gerhard; Borchers, Christoph H. (2006): Combining fluorescence detection and mass spectrometric analysis for comprehensive and quantitative analysis of redox-sensitive cysteines in native membrane proteins. In *Analytical Chemistry* 78 (23), pp. 7959–7966. DOI: 10.1021/ac060238r.

Poole, K.; Heinrichs, D. E.; Neshat, S. (1993a): Cloning and sequence analysis of an EnvCD homologue in *Pseudomonas aeruginosa*: regulation by iron and possible involvement in the secretion of the siderophore pyoverdine. In *Molecular Microbiology* 10 (3), pp. 529–544. DOI: 10.1111/j.1365-2958.1993.tb00925.x.

Poole, K.; Neshat, S.; Krebs, K.; Heinrichs, D. E. (1993b): Cloning and nucleotide sequence analysis of the ferripyoverdine receptor gene *fpvA* of *Pseudomonas aeruginosa*. In *Journal of Bacteriology* 175 (15), pp. 4597–4604.

Poppe, Juliane; Reichelt, Joachim; Blankenfeldt, Wulf (2018): *Pseudomonas aeruginosa* pyoverdine maturation enzyme PvdP has a noncanonical domain architecture and affords insight into a new subclass of tyrosinases. In *The Journal of biological chemistry* 293 (38), pp. 14926–14936. DOI: 10.1074/jbc.RA118.002560.

Porcelli, Ida; Leeuw, Erik de; Wallis, Russell; van den Brink-van der Laan, Els; Kruijff, Ben de; Wallace, B. A. et al. (2002): Characterization and membrane assembly of the TatA component of the *Escherichia coli* twin-arginine protein transport system. In *Biochemistry* 41 (46), pp. 13690–13697. DOI: 10.1021/bi026142i.

Raju, T. Shantha (Ed.) (2019): Co- and post-translational modifications of therapeutic antibodies and proteins. Hoboken, NJ: John Wiley & Sons.

Rausch, Christian; Hoof, Ilka; Weber, Tilmann; Wohlleben, Wolfgang; Huson, Daniel H. (2007): Phylogenetic analysis of condensation domains in NRPS sheds light on their functional evolution. In *BMC Evolutionary Biology* 7 (1), p. 78. DOI: 10.1186/1471-2148-7-78.

Rédly, Gyula Alan; Poole, Keith (2003): Pyoverdine-mediated regulation of FpvA synthesis in *Pseudomonas aeruginosa*: involvement of a probable extracytoplasmic-function sigma factor,

FpvI. In *Journal of Bacteriology* 185 (4), pp. 1261–1265. DOI: 10.1128/JB.185.4.1261-1265.2003.

Rédly, Gyula Alan; Poole, Keith (2005): FpvIR control of fpvA ferric pyoverdine receptor gene expression in *Pseudomonas aeruginosa*: demonstration of an interaction between FpvI and FpvR and identification of mutations in each compromising this interaction. In *Journal of Bacteriology* 187 (16), pp. 5648–5657. DOI: 10.1128/JB.187.16.5648-5657.2005.

Rensing, Christopher; Grass, Gregor (2003): *Escherichia coli* mechanisms of copper homeostasis in a changing environment. In *FEMS Microbiology Reviews* 27 (2-3), pp. 197–213. DOI: 10.1016/S0168-6445(03)00049-4.

Rieske, John S.; MacLennan, David H.; Coleman, Roger (1964): Isolation and properties of an iron-protein from the (reduced coenzyme Q)-cytochrome C reductase complex of the respiratory chain. In *Biochemical and Biophysical Research Communications* 15 (4), pp. 338–344. DOI: 10.1016/0006-291X(64)90171-8.

Ringel, Michael T.; Brüser, Thomas (2018): The biosynthesis of pyoverdines. In *Microbial cell (Graz, Austria)* 5 (10), pp. 424–437. DOI: 10.15698/mic2018.10.649.

Ringel, Michael T.; Dräger, Gerald; Brüser, Thomas (2016): PvdN Enzyme Catalyzes a Periplasmic Pyoverdine Modification. In *Journal of Biological Chemistry* 291 (46), pp. 23929–23938. DOI: 10.1074/jbc.M116.755611.

Ringel, Michael T.; Dräger, Gerald; Brüser, Thomas (2017): The periplasmic transaminase PtaA of *Pseudomonas fluorescens* converts the glutamic acid residue at the pyoverdine fluorophore to α -ketoglutaric acid. In *Journal of Biological Chemistry* 292 (45), pp. 18660–18671. DOI: 10.1074/jbc.M117.812545.

Ringel, Michael T.; Dräger, Gerald; Brüser, Thomas (2018): PvdO is required for the oxidation of dihydropyoverdine as the last step of fluorophore formation in *Pseudomonas fluorescens*. In *Journal of Biological Chemistry* 293 (7), pp. 2330–2341. DOI: 10.1074/jbc.RA117.000121.

Ringel, Michael Thomas (2018): Enzymology of the periplasmic pyoverdine maturation. Hannover : Institutionelles Repositorium der Leibniz Universität Hannover. Available online at <https://www.repo.uni-hannover.de/handle/123456789/3437>.

Romero, Antonia María; Martínez-Pastor, María Teresa; Puig, Sergi (2021): Iron in Translation: From the Beginning to the End. In *Microorganisms* 9 (5). DOI: 10.3390/microorganisms9051058.

Ryan, Colm J.; Krogan, Nevan J.; Cunningham, Pádraig; Cagney, Gerard (2013): All or nothing: protein complexes flip essentiality between distantly related eukaryotes. In *Genome Biology and Evolution* 5 (6), pp. 1049–1059. DOI: 10.1093/gbe/evt074.

Sauer, Markus (2010): Handbook of Fluorescence Spectroscopy and Imaging. From Ensemble to Single Molecules. With assistance of Johan Hofkens, Jörg Enderlein. 1st ed. Weinheim: John Wiley & Sons Incorporated.

Schalk, I. J.; Kyslik, P.; Prome, D.; van Dorsselaer, A.; Poole, K.; ABDALLAH, M. A.; Pattus, F. (1999): Copurification of the FpvA ferric pyoverdine receptor of *Pseudomonas aeruginosa* with its iron-free ligand: implications for siderophore-mediated iron transport. In *Biochemistry* 38 (29), pp. 9357–9365. DOI: 10.1021/bi990421x.

Schalk, Isabelle J.; Guillon, Laurent (2013): Pyoverdine biosynthesis and secretion in *Pseudomonas aeruginosa*: implications for metal homeostasis. In *Environmental Microbiology* 15 (6), pp. 1661–1673. DOI: 10.1111/1462-2920.12013.

Schenkeveld, W. D. C.; Reichwein, A. M.; Temminghoff, E. J. M.; van Riemsdijk, W. H. (2007): The behaviour of EDDHA isomers in soils as influenced by soil properties. In *Plant Soil* 290 (1-2), pp. 85–102. DOI: 10.1007/s11104-006-9135-y.

Schramm, Frederic D.; Schroeder, Kristen; Jonas, Kristina (2020): Protein aggregation in bacteria. In *FEMS Microbiology Reviews* 44 (1), pp. 54–72. DOI: 10.1093/femsre/fuz026.

Schrödinger, L.; DeLano, W. (2020): PyMol. Version 2.4.0. Available online at <http://www.pymol.org/pymol>.

Schubert, Heidi L.; Blumenthal, Robert M.; Cheng, Xiaodong (2006): Protein Methyltransferases: Their Distribution Among the Five Structural Classes of AdoMet-Dependent Methyltransferases. In Steven G. Clarke, Fuyuhiko Tamanoi (Eds.): *The Enzymes : Protein Methyltransferases*, vol. 24: Academic Press, pp. 3–28.

Schuenemann, Verena J.; Kralik, Stephanie M.; Albrecht, Reinhard; Spall, Sukhdeep K.; Truscott, Kaye N.; Dougan, David A.; Zeth, Kornelius (2009): Structural basis of N-end rule substrate recognition in *Escherichia coli* by the ClpAP adaptor protein ClpS. In *EMBO Reports* 10 (5), pp. 508–514. DOI: 10.1038/embor.2009.62.

Schwarzer, D.; Marahiel, M. A. (2001): Multimodular biocatalysts for natural product assembly. In *Naturwissenschaften* 88 (3), pp. 93–101. DOI: 10.1007/s001140100211.

Shen, Jiang-Sheng; Geoffroy, Valérie; Neshat, Shadi; Jia, Zongchao; Meldrum, Allison; Meyer, Jean-Marie; Poole, Keith (2005): FpvA-mediated ferric pyoverdine uptake in *Pseudomonas aeruginosa*: identification of aromatic residues in FpvA implicated in ferric pyoverdine binding and transport. In *Journal of Bacteriology* 187 (24), pp. 8511–8515. DOI: 10.1128/JB.187.24.8511-8515.2005.

Singh, Surinder Mohan; Panda, Amulya Kumar (2005): Solubilization and refolding of bacterial inclusion body proteins. In *Journal of Bioscience and Bioengineering* 99 (4), pp. 303–310. DOI: 10.1263/jbb.99.303.

Sonnhammer, E. L.; Heijne, G. von; Krogh, A. (1998): A hidden Markov model for predicting transmembrane helices in protein sequences. In *Proceedings. International Conference on Intelligent Systems for Molecular Biology* 6, pp. 175–182.

Stachelhaus, T.; Marahiel, M. A. (1995): Modular structure of peptide synthetases revealed by dissection of the multifunctional enzyme GrsA. In *Journal of Biological Chemistry* 270 (11), pp. 6163–6169. DOI: 10.1074/jbc.270.11.6163.

Stock, Ann; Clarke, Steven; Clarke, Catherine; Stock, Jeff (1987): N-terminal methylation of proteins: Structure, function and specificity. In *FEBS Letters* 220 (1), pp. 8–14. DOI: 10.1016/0014-5793(87)80866-9.

Stolle, Patrick; Hou, Bo; Brüser, Thomas (2016): The Tat Substrate CueO Is Transported in an Incomplete Folding State. In *Journal of Biological Chemistry* 291 (26), pp. 13520–13528. DOI: 10.1074/jbc.M116.729103.

Sun, S.; Zabinski, R. F.; Toney, M. D. (1998): Reactions of alternate substrates demonstrate stereoelectronic control of reactivity in dialkylglycine decarboxylase. In *Biochemistry* 37 (11), pp. 3865–3875. DOI: 10.1021/bi972055s.

Swingle, Bryan; Thete, Deepti; Moll, Monica; Myers, Christopher R.; Schneider, David J.; Cartinhour, Samuel (2008): Characterization of the PvdS-regulated promoter motif in *Pseudomonas syringae* pv. *tomato* DC3000 reveals regulon members and insights regarding PvdS function in other pseudomonads. In *Molecular microbiology* 68 (4), pp. 871–889. DOI: 10.1111/j.1365-2958.2008.06209.x.

Tervola, Essi; Truong, Khai-Nghi; Ward, Jas S.; Priimagi, Arri; Rissanen, Kari (2020): Fluorescence enhancement of quinolines by protonation. In *RSC Advances* 10 (49), pp. 29385–29393. DOI: 10.1039/D0RA04691D.

Thal, Beate; Braun, Hans-Peter; Eubel, Holger (2018): Proteomic analysis dissects the impact of nodulation and biological nitrogen fixation on *Vicia faba* root nodule physiology. In *Plant Molecular Biology* 97 (3), pp. 233–251. DOI: 10.1007/s11103-018-0736-7.

Tobias, J. W.; Shrader, T. E.; Rocap, G.; Varshavsky, A. (1991): The N-end rule in bacteria. In *Science* 254 (5036), pp. 1374–1377. DOI: 10.1126/science.1962196.

Toney, M. D.; Kirsch, J. F. (1993): Lysine 258 in aspartate aminotransferase: enforcer of the Circe effect for amino acid substrates and general-base catalyst for the 1,3-prototropic shift. In *Biochemistry* 32 (6), pp. 1471–1479. DOI: 10.1021/bi00057a010.

Toney, Michael D. (2014): Aspartate aminotransferase: an old dog teaches new tricks. In *Archives of Biochemistry and Biophysics* 544, pp. 119–127. DOI: 10.1016/j.abb.2013.10.002.

Towbin, H.; Staehelin, T.; Gordon, J. (1979): Electrophoretic transfer of proteins from polyacrylamide gels to nitrocellulose sheets: procedure and some applications. In *Proceedings of the National Academy of Sciences of the United States of America* 76 (9), pp. 4350–4354.

Trakhanov, S.; Kreimer, D. I.; Parkin, S.; Ames, G. F.; Rupp, B. (1998): Cadmium-induced crystallization of proteins: II. Crystallization of the *Salmonella typhimurium* histidine-binding protein in complex with L-histidine, L-arginine, or L-lysine. In *Protein Science* 7 (3), pp. 600–604. DOI: 10.1002/pro.5560070308.

Traxler, Matthew F.; Watrous, Jeramie D.; Alexandrov, Theodore; Dorrestein, Pieter C.; Kolter, Roberto (2013): Interspecies interactions stimulate diversification of the *Streptomyces coelicolor* secreted metabolome. In *mBio* 4 (4). DOI: 10.1128/mbio.00459-13.

Troxell, Bryan; Hassan, Hosni M. (2013): Transcriptional regulation by Ferric Uptake Regulator (Fur) in pathogenic bacteria. In *Frontiers in Cellular and Infection Microbiology* 3, p. 59. DOI: 10.3389/fcimb.2013.00059.

Valeur, Bernard; Berberan-Santos, Mário Nuno; Berberan-Santos, Mario N. (2012): Molecular fluorescence. Principles and applications. 2. ed. Weinheim: Wiley-VCH.

Valko, Marian; Leibfritz, Dieter; Moncol, Jan; Cronin, Mark T. D.; Mazur, Milan; Telser, Joshua (2007): Free radicals and antioxidants in normal physiological functions and human disease. In *The International Journal of Biochemistry & Cell Biology* 39 (1), pp. 44–84. DOI: 10.1016/j.biocel.2006.07.001.

Vandenende, Chris S.; Vlasschaert, Matthew; Seah, Stephen Y. K. (2004): Functional Characterization of an Aminotransferase Required for Pyoverdine Siderophore Biosynthesis in *Pseudomonas aeruginosa* PAO1. In *Journal of Bacteriology* 186 (17), pp. 5596–5602. DOI: 10.1128/JB.186.17.5596-5602.2004.

Vasil, M. L.; Ochsner, U. A.; Johnson, Z.; Colmer, J. A.; Hamood, A. N. (1998): The fur-regulated gene encoding the alternative sigma factor PvdS is required for iron-dependent expression of the LysR-type regulator ptxR in *Pseudomonas aeruginosa*. In *Journal of Bacteriology* 180 (24), pp. 6784–6788. DOI: 10.1128/JB.180.24.6784-6788.1998.

Visca, P. (2004): Iron Regulation and Siderophore Signalling in Virulence by *Pseudomonas Aeruginosa*. In Juan-Luis Ramos (Ed.): *Pseudomonas. Virulence and Gene Regulation*. New York, NY: Kluwer Acad./Plenum Publ, pp. 69–123.

Visca, P.; Ciervo, A.; Orsi, N. (1994): Cloning and nucleotide sequence of the pvdA gene encoding the pyoverdine biosynthetic enzyme L-ornithine N5-oxygenase in *Pseudomonas aeruginosa*. In *Journal of Bacteriology* 176 (4), pp. 1128–1140. DOI: 10.1128/jb.176.4.1128-1140.1994.

Visca, Paolo; Imperi, Francesco; Lamont, Iain L. (2007a): Pyoverdine siderophores: from biogenesis to biosignificance. In *Trends in Microbiology* 15 (1), pp. 22–30. DOI: 10.1016/j.tim.2006.11.004.

Visca, Paolo; Imperi, Francesco; Lamont, Iain L. (2007b): Pyoverdine Synthesis and its Regulation in Fluorescent *Pseudomonads*. In Ajit Varma, Sudhir B. Chincholkar (Eds.): *Microbial Siderophores*, Vol. 12. Berlin, Heidelberg: Springer Berlin Heidelberg (Soil Biology), pp. 135–163.

Voulhoux, R.; Filloux, A.; Schalk, I. J. (2006): Role of the TAT System in the Pyoverdine-Mediated Iron Acquisition in *Pseudomonas aeruginosa*. In *Journal of Bacteriology* 188, pp. 3317–3323. DOI: 10.1128/JB.188.9.3317-3323.2006.

Saurin, W., Hofnung, M., & Dassa, E. (1999). Getting in or out: Early segregation between importers and exporters in the evolution of ATP-binding cassette (ABC) transporters. In *Journal of molecular evolution*, 48 (1), pp. 22–41. DOI:10.1007/pl00006442.

Wagoner, Robert V.; Fowler, William A.; Hoyle, F. (1967): On the Synthesis of Elements at Very High Temperatures. In *The Astrophysical Journal* 148, p. 3. DOI: 10.1086/149126.

Wang, Min; Zhao, Qunfei; Zhang, Qinglin; Liu, Wen (2016): Differences in PLP-dependent cysteinyl processing lead to diverse S-functionalization of lincosamide antibiotics. In *Journal of the American Chemical Society* 138 (20), pp. 6348–6351. DOI: 10.1021/jacs.6b01751.

Wibowo, Joko P.; Batista, Fernando A.; van Oosterwijk, Niels; Groves, Matthew R.; Dekker, Frank J.; Quax, Wim J. (2020): A novel mechanism of inhibition by phenylthiourea on PvdP, a tyrosinase synthesizing pyoverdine of *Pseudomonas aeruginosa*. In *International journal of biological macromolecules* 146, pp. 212–221. DOI: 10.1016/j.ijbiomac.2019.12.252.

Wilderman, P. J.; Vasil, A. I.; Johnson, Z.; Wilson, M. J.; Cunliffe, H. E.; Lamont, I. L.; Vasil, M. L. (2001): Characterization of an endoprotease (PrpL) encoded by a PvdS-regulated gene in *Pseudomonas aeruginosa*. In *Infection and immunity* 69 (9), pp. 5385–5394. DOI: 10.1128/IAI.69.9.5385-5394.2001.

Wilson, M. J.; Lamont, I. L. (2000): Characterization of an ECF sigma factor protein from *Pseudomonas aeruginosa*. In *Biochemical and Biophysical Research Communications* 273 (2), pp. 578–583. DOI: 10.1006/bbrc.2000.2996.

Winkelmann, G. (1991): Handbook of Microbial Iron Chelates. 1st edition: CRC Press.

Wood, Adam; Shilatifard, Ali (2004): Posttranslational Modifications of Histones by Methylation. In *Advances in Protein Chemistry* 67, pp. 201–222. DOI: 10.1016/S0065-3233(04)67008-2.

Xiao, R.; Kisaalita, W. S. (1997): Iron acquisition from transferrin and lactoferrin by *Pseudomonas aeruginosa* pyoverdin. In *Microbiology (Reading)* 143 (Pt 7), pp. 2497–2507. DOI: 10.1099/00221287-143-7-2509.

Yang, David C. H.; Abeykoon, Amila H.; Choi, Bok-Eum; Ching, Wei-Mei; Chock, P. Boon (2017): Outer Membrane Protein OmpB Methylation May Mediate Bacterial Virulence. In *Trends in biochemical sciences* 42 (12), pp. 936–945. DOI: 10.1016/j.tibs.2017.09.005.

Ye, Lumeng; Matthijs, Sandra; Bodilis, Josselin; Hildebrand, Falk; Raes, Jeroen; Cornelis, Pierre (2014): Analysis of the draft genome of *Pseudomonas fluorescens* ATCC17400 indicates a capacity to take up iron from a wide range of sources, including different exogenous pyoverdines. In *BioMetals* 27 (4), pp. 633–644. DOI: 10.1007/s10534-014-9734-7.

Yeterian, Emilie; Martin, Lois W.; Guillon, Laurent; Journet, Laure; Lamont, Iain L.; Schalk, Isabelle J. (2010): Synthesis of the siderophore pyoverdine in *Pseudomonas aeruginosa* involves a periplasmic maturation. In *Amino Acids* 38 (5), pp. 1447–1459. DOI: 10.1007/s00726-009-0358-0.

Zaman, M.; Kleineidam, K.; Bakken, L.; Berendt, J.; Bracken, C.; Butterbach-Bahl, K. et al. (2021): Automated Laboratory and Field Techniques to Determine Greenhouse Gas Emissions. In Mohammad Zaman, Lee Heng, Christoph Müller (Eds.): *Measuring Emission of Agricultural Greenhouse Gases and Developing Mitigation Options using Nuclear and Related Techniques*. Cham: Springer International Publishing, pp. 109–139.

Zhang, Gang; Huang, Rong (2016): Facile synthesis of SAM-peptide conjugates through alkyl linkers targeting protein N-terminal methyltransferase 1. In *RSC advances* 6 (8), pp. 6768–6771. DOI: 10.1039/C5RA20625A.

6 Supplement

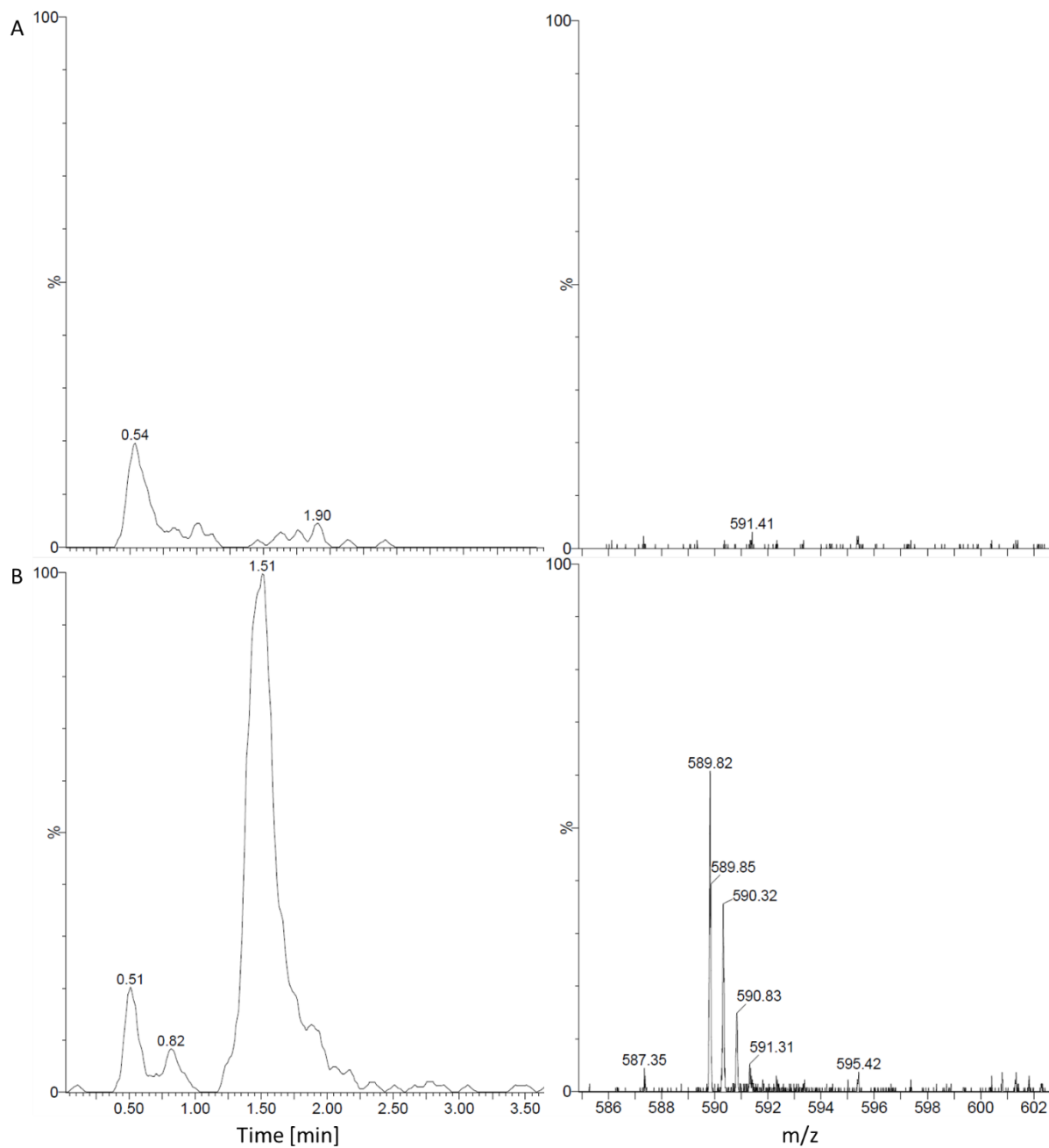


Figure S1: UPLC-MS analyses of medium supernatant. Detection of ferribactin in (A) a *P. fluorescens* A506 Δ *pvdL* strain and a (B) *P. fluorescens* A506 Δ *pvdM* strain.

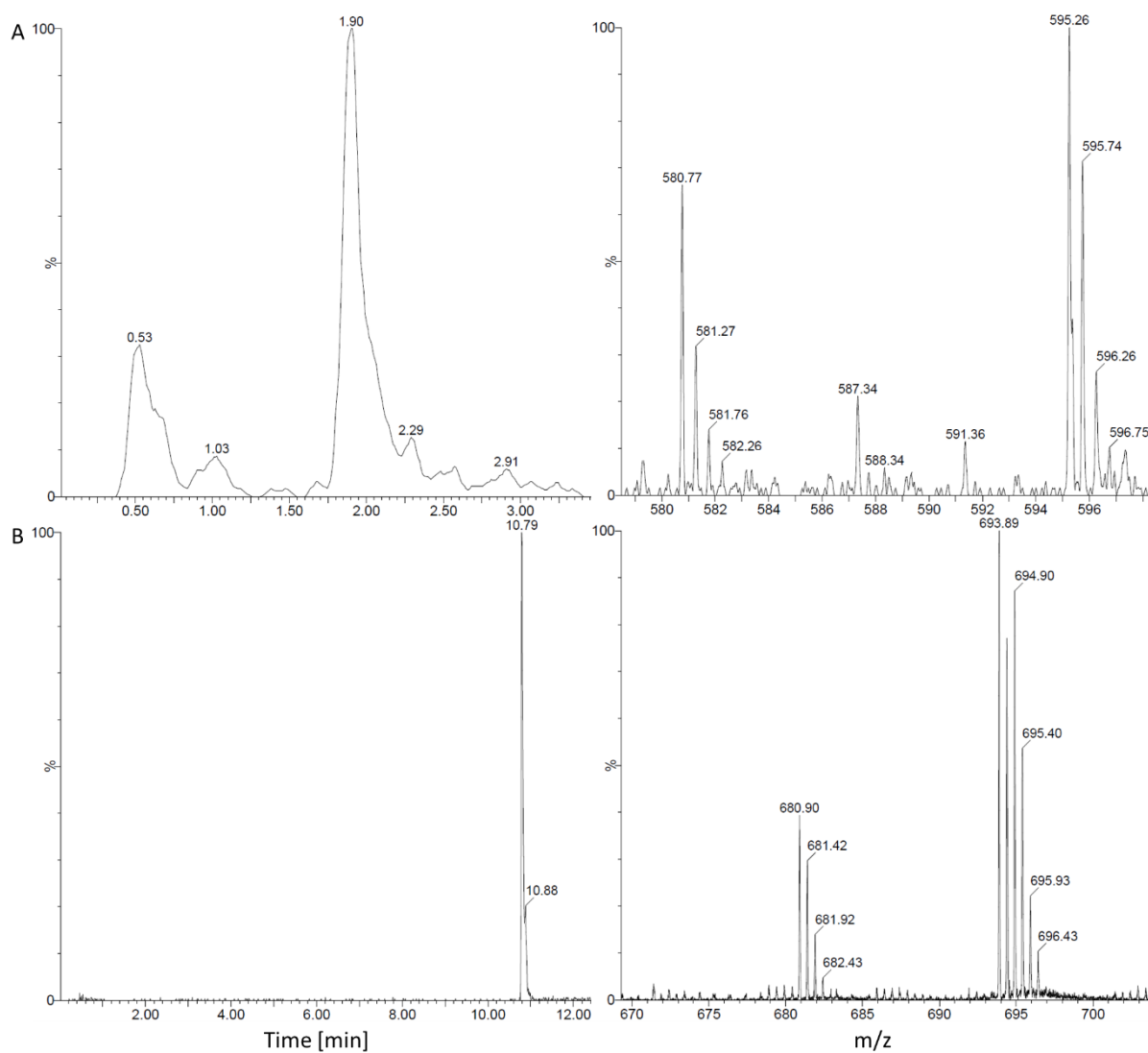


Figure S2: UPLC-MS analyses of medium supernatant. Detection of ferribactin in (A) a *P. fluorescens* A506 $\Delta pvdM$ strain and a (B) *P. fluorescens* A506 wild-type strain.

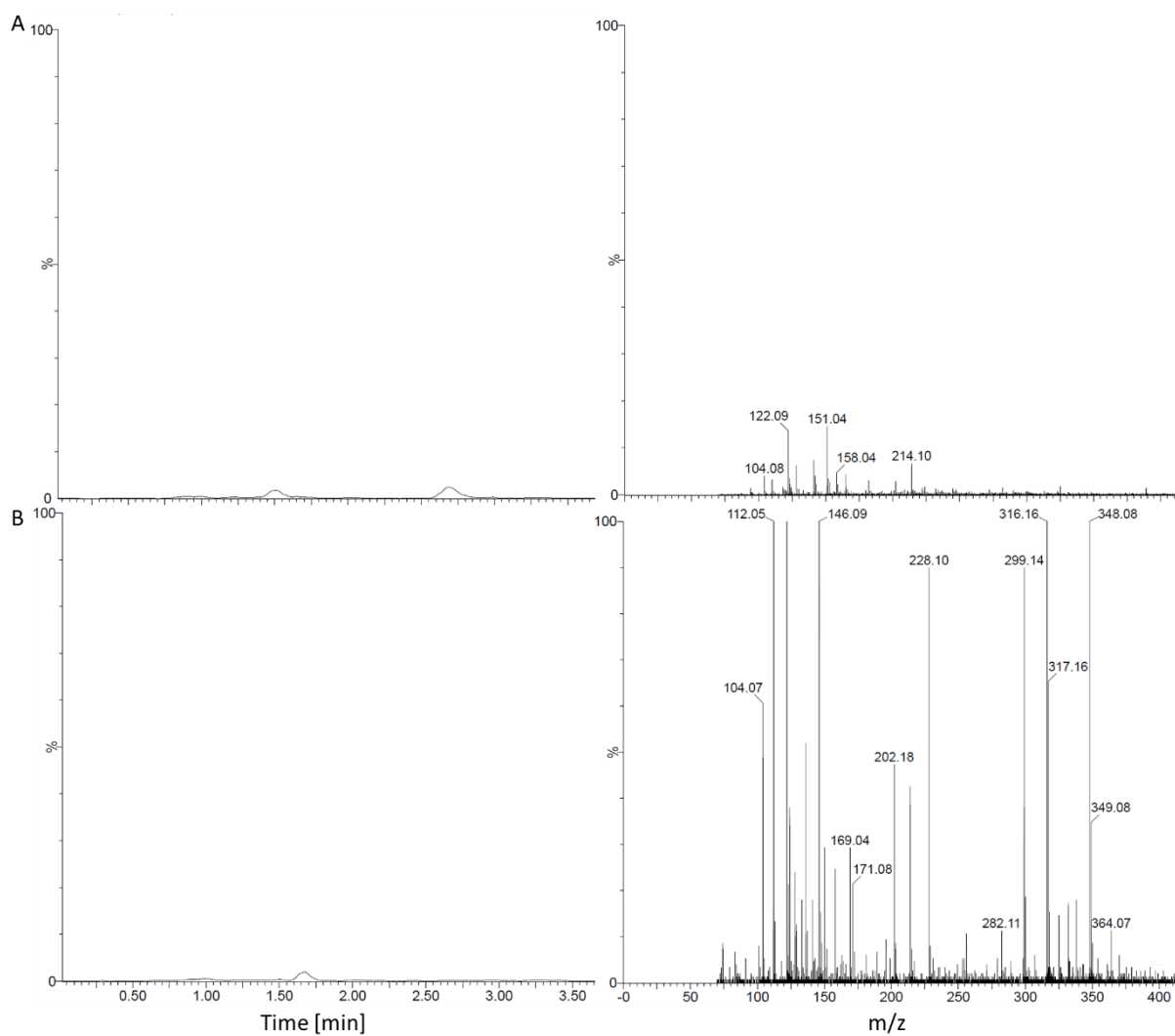


Figure S3: UPLC-MS analyses of subcellular fractions. Detection of dimethylated EDDHA in (A) the periplasmic fraction of a *P. fluorescens* A506 $\Delta pvdL$ strain and (B) the cytoplasmic fraction of a *P. fluorescens* A506 $\Delta pvdL$ strain.

7 Acknowledgements

Zunächst möchte ich mich ganz herzlich bei meinem Doktorvater Prof. Dr. Thomas Brüser für die Möglichkeit bedanken, meine Dissertation über dieses knifflige und gerade deshalb so spannende Thema am Institut für Mikrobiologie anzufertigen. Gleichzeitig bedanke ich mich für die gute Betreuung und die stetige Bereitschaft, neue Ergebnisse ausführlich zu diskutieren.

Des Weiteren gilt mein Dank Prof. Dr. Marcus Horn für die Übernahme des zweiten Gutachtens und für die interessanten Diskurse während der montäglichen Seminare.

Prof. Dr. Jens Boch danke ich ganz herzlich für die Übernahme des Prüfungsvorsitzes.

Bei Sybille Traupe, Dr. Denise Mehner-Breitfeld und Dr. Lena Hoffmann möchte ich für die tolle Atmosphäre in Labor 1 bedanken. Sybille Traupe danke ich weiterhin ganz besonders für die stetige Hilfsbereitschaft bei Experimenten, vor allem in den frühen Morgenstunden. Eike Schniete, Dr. Hendrik Geise, Dr. Heinrich Schäfer und Dr. Ingo Hantke danke ich für die erfrischenden Persona(a)lversammlungen und die währenddessen häufig beiläufig gegebenen Tipps und Hinweise. Dr. Patrick Stolle danke ich herzlich sowohl für die Beschaffung aller möglichen, zum Teil seltensten Chemikalien, ohne die diese Arbeit nicht hätte durchgeführt werden können, als auch für die frühzeitige Koordination aller organisatorischen Hürden, die im Laufe der Promotion angefallen sind. Dr. Katrin Gunka danke ich vielmals für die tatkräftige Unterstützung an mittlerweile drei unterschiedlichen Mikroskopen mit ihren jeweiligen unergründlichen Tücken. Bei Tobias Spanner bedanke ich mich für die tatkräftige Unterstützung bei den Messungen im Institut für Bodenkunde und die gegenseitige Motivation, die jeweiligen Arbeiten einigermaßen zeitnah erfolgreich abzuschließen. Dr. Holger Eubel vom Institut für Pflanzengenetik danke ich für die Hilfe bei der Analyse von PvdM und die Zeit, die Ergebnisse in aller Ruhe zu besprechen. Bei Ali Burdur und Katharina Franke möchte ich mich für die Durchführung von Experimenten im Rahmen ihrer Masterarbeiten bedanken, deren Ergebnisse dieser Arbeit eine große Hilfe waren. Eike Schniete danke ich für die konstruktiven Hinweise beim Korrekturlesen dieser Arbeit.

Besonderer Dank gilt an dieser Stelle Dr. Gerald Dräger für die immerwährende Bereitschaft, Pyoverdine und andere unbekannte Substanzen auch kurzfristig am Institut für Organische Chemie zu analysieren und die Zeit, die Ergebnisse in Ruhe zu diskutieren.

Acknowledgements

Großer Dank gilt neben allen aktuellen und ehemaligen Kolleginnen und Kollegen der Arbeitsgruppe Brüser natürlich auch den Mitgliedern des Instituts für Mikrobiologie aus den Arbeitsgruppen Turgay, Horn und Tschowri, dem Sekretariat und dem technischen Personal, für die durchgehend gute Stimmung und das nette Arbeitsklima am Institut.

Meinen Eltern danke ich für die stetige Unterstützung in allen möglichen Bereichen, die sich nun schon seit der schulischen Ausbildung bis zur Promotion zieht, für die Care-Pakete und das einfach immer da sein. Meinen Geschwistern Lea und Merlin danke ich vor allem für die wichtigen Pausen und die Zeit, neben der Promotion ein bisschen zu entspannen und neue Kraft zu sammeln.

Mein größter Dank gilt Annabelle Behnke, die mich während der gesamten Promotionszeit mit viel Verständnis und Geduld, auch für Arbeiten am Wochenende, unterstützt und mir stets Mut zugesprochen und geholfen hat, nicht den Fokus zu verlieren. Vielen Dank für deine manchmal mahnenden, aber immer herzlichen Worte, vor allem in der letzten Phase dieser Arbeit. Ohne deine Unterstützung hätte ich diese Arbeit so nicht anfertigen können.

8 Curriculum vitae

Michael-Frederick Sugue

Geb.: 05.03.1992 in Berlin

01/2018 – 03/2022	<p>Leibniz-Universität Hannover</p> <p>Promotionsstudium Biologie am Institut für Mikrobiologie</p>
10/2015 – 09/2017	<p>Philipps-Universität Marburg, M.Sc. Molecular and Cellular Biology</p> <p>„Untersuchung des initialen Schrittes im anaeroben Abbau langkettiger Kohlenwasserstoffe des Sulfatreduzierers <i>Desulfococcus oleovorans</i> Hxd3 und Vergleich zweier Thiolasen des denitrifizierenden Bakteriums <i>Aromatoleum aromaticum</i> EbN1“</p>
10/2012 – 09/2015	<p>Philipps-Universität Marburg, B.Sc. Biologie</p> <p>„Konstruktion eines Fusionsproteins zur Aufnahme und Aktivierung von Benzoat und mikrobielle Produktion von 3,5-Dihydroxybipheny“</p>
09/2002 – 06/2011	<p>Canisius Kolleg Berlin, Abitur</p>

9 List of publications

Hoffmann, Lena; Suge, Michael-Frederick; Brüser, Thomas (2021): A tunable anthranilate-inducible gene expression system for *Pseudomonas* species. In: *Applied genetics and molecular biotechnology* 105 (1), S. 247–258. DOI: 10.1007/s00253-020-11034-8.

Suge, Michael-Frederick; Burdur, Ali Nazmi; Ringel, Michael T.; Dräger, Gerald; Brüser, Thomas (2022): PvdM is required for the oxidation of ferribactin by PvdP in periplasmic pyoverdine maturation. (Submitted in *Journal of Biological Chemistry*)